

Functional and Structural Studies of DNA Assembled Oligochromophores

Inauguraldissertation

der Philosophisch-naturwissenschaftlichen Fakultät

der Universität Bern

vorgelegt von

Markus Probst

von Langnau i.E. BE

Leiter der Arbeit:

Prof. Dr. Robert Häner

Departement für Chemie und Biochemie der Universität Bern

Functional and Structural Studies of DNA Assembled Oligochromophores

Inauguraldissertation

der Philosophisch-naturwissenschaftlichen Fakultät

der Universität Bern

vorgelegt von

Markus Probst

von Langnau i.E. BE

Leiter der Arbeit:

Prof. Dr. Robert Häner

Departement für Chemie und Biochemie der Universität Bern

Von der Philosophisch-naturwissenschaftlichen Fakultät angenommen.

Der Dekan:

Bern, 13.06.2016

Prof. Dr. G. Colangelo

Acknowledgments

I sincerely thank Robert for the scientific freedom he gave me during the past 4 years.

My thanks indeed go to Prof. U. Baumann to act as external Co-Referee. And I'm thankful that Prof. P. Renaud agreed to be Chairman of my PhD defense.

Of course, Chapter 7 was only possible due to the help of Achim Stocker. Thank you.

I'm grateful for the challenge - but also the help for my own work - to supervise the two Master Students:

Katarzyna Anikiej (2013) and Thi Thu Hang Chau (2015).

Last but not least, Simon Langenegger and the rest of THE research group,

thank you all!

For the man who wasn't there

Table of Contents

Summary	1
Chapter 1 – Nucleic Acid	3
Chapter 2 – Structural Aspects of the DNA	6
Chapter 3 – Alteration of the DNA	10
Chapter 4 – The DNA Three-Way Junction as a tool for Chromophore Assembly	14
Aim of the Work:	14
Introduction.....	14
Results and Discussion.....	15
Conclusions	21
Experimental Section	21
Chapter 5 – A modular LHC built on the DNA Three-Way Junction	22
Aim of the Work:	22
Introduction.....	23
Chapter 5a - A modular LHC built on the DNA Three-Way Junction	24
Results and Discussion.....	24
Conclusions	30
Experimental Section	31
Chapter 5b - A modular LHC built on the DNA 3WJ with an “always-on” Exciplex	32
Results and Discussion.....	32
Conclusions	39
Experimental Section	40
Chapter 6 – A modified DNA bis-3WJ as a scaffold for a LHC	41
Aim of the Work	41
Introduction.....	41
Results and Discussion.....	42
Conclusions	46
Experimental Section	47
Chapter 7 – Crystal structures of modified DNA	48
Aim of the Work:	48
Introduction.....	48
Materials and Methods.....	50
Results and Discussion.....	53
Conclusions	67
Chapter 8 – Outlook	68

References Chapter 1	69
References Chapter 2	73
References Chapter 3	76
References Chapter 4	80
References Chapter 5	82
References Chapter 6	85
References Chapter 7	87
Appendix A	89
Synthetic and analytical procedure	89
Overview three-way junctions	90
Temperature dependent UV/Vis measurements	91
Fluorescence measurements: emission spectra	95
Appendix B	98
Synthetic and analytical procedure	98
Investigated oligonucleotides and masses	99
T _m values and thermal denaturation profiles.....	104
UV/Vis spectra	108
Fluorescence spectra.....	112
Excitation spectra	116
Polyacrylamide gels	118
Quantum yield determination	119
Calculation of Förster radius (phenanthrene excimer – Cy).....	120
Appendix C	121
Synthetic and analytical procedure	121
Overview three-way junctions	122
UV/Vis spectra	123
Fluorescence spectra.....	125
T _m values and thermal denaturation profiles.....	126
Polyacrylamide gels	126
Erklärung	127
Lebenslauf	128

Summary

The core of this work can be divided into two major projects: Chapters 4 to 6 include the development of a light-harvesting complex (LHC) based on the DNA three-way junction (3WJ). It is demonstrated that a stack of light-absorbing non-nucleosidic chromophores covalently linked to natural DNA strands act as a light-harvesting antenna. Furthermore, the experiments show that an energy transfer takes place to an acceptor chromophore in close proximity to the light-harvesting part. The design of these DNA-based systems can be varied in several ways and is interchangeable in terms of the complementarity of the strands.

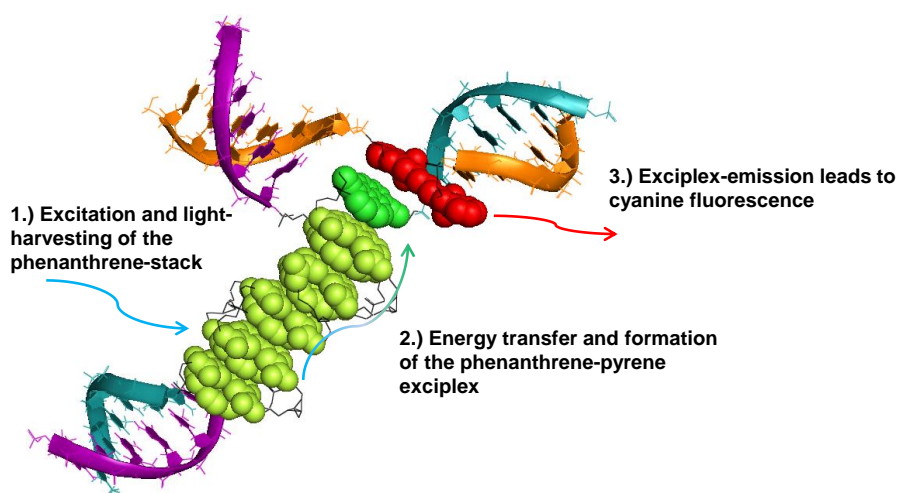
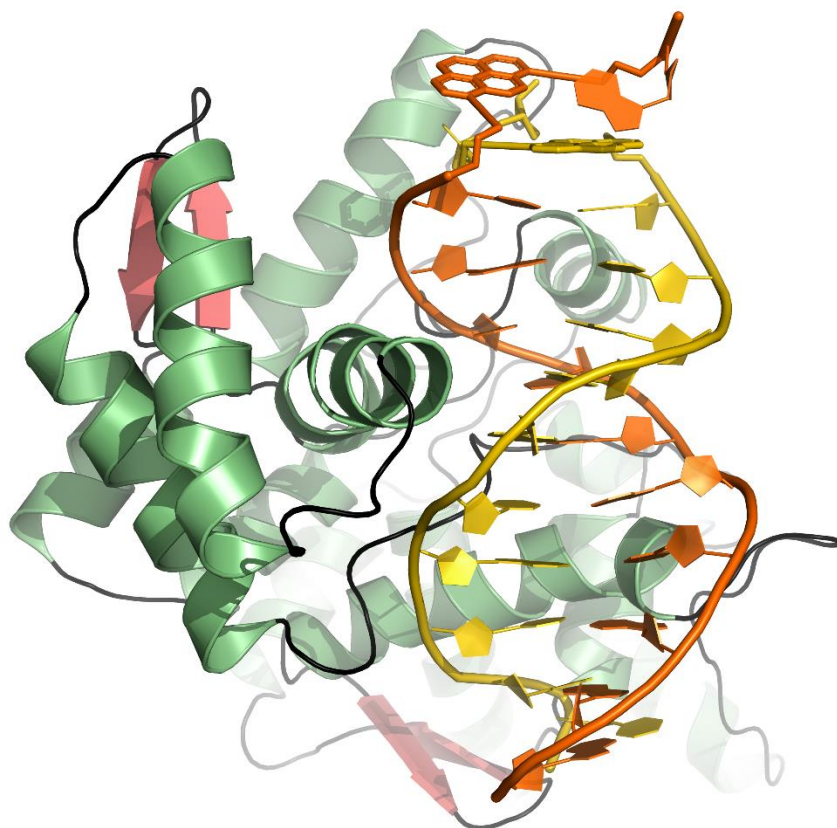


Illustration of an example of a DNA-based light-harvesting complex.

Parts of these results are published in:

Markus Probst, Simon M. Langenegger and Robert Häner. A modular LHC built on the DNA three-way junction. *Chem. Commun.*, **2014**, 50, 159-161.

The second project described in this thesis (Chapter 7) addresses the work that was carried out in order to get a crystal structure of modified DNA strands, preferably in a duplex with at least two chromophores. The chromophores are non-nucleosidic building blocks, incorporated into the sugar-phosphate backbone of the DNA. The modified DNA strands also contain a recognition sequence for an endonuclease binding domain. By co-crystallization of the protein-DNA complexes, a total of 3 structures were solved (one of which is shown below):



Representation of the 3D structure of modified DNA strands (yellow and orange, the two pyrene modifications are located in the terminal region on the top), bound to the binding domain of the restriction endonuclease BpuJ1. The amino acids are represented and coloured according to their secondary structure.

The structures are deposited in the RCSB PDB, entries:

5HLT (**Complex1**), 5HNF (**Complex2**) and 5HNH (**Complex3**)

Chapter 1 – Nucleic Acid

DNA, Deoxyribonucleic acid, today a term quite popular to many of us. But this fascinating molecule wasn't just born yesterday nor was it discovered (or what others may claim, invented) by Watson and Crick (we come to that later). It is noteworthy to mention that after the formation of Earth, approximately 4.54 billion years ago, some early form of life started to exist roughly 1 billion years after this meaningful event.^[1,2,3] The building blocks for these creatures were probably born in a great primordial ocean in an iron-sulfur based chemistry ("iron-sulfur world theory") with or without the help of pumice.^[4,5] Or somewhere before the process of the replication-first approach called "RNA world hypothesis".^[6] Certainly there are other highly speculative theories including the explanation for the development of the evolution of pre-cellular life to protocells and the development of metabolism and the origin of the cell membrane.^[7-10] Whether or not through the process of transition of an ancient RNA (ribonucleic acid) cell to a cell carrying DNA as genetic material, most likely multiple steps and intermediates were necessary.^[11,12] One way or another, from the beginning of a "last universal cellular ancestor", the three domains of life and the moment when the Tree of Life began to spread, today's nucleobases were formed and became part of one of nature's most successful principle: The DNA.^[13,14,15]

Its existence was first described in 1869 by Friedrich Miescher as a substance in the nuclei of cells.^[16,17] However, it took half a century until it became clearer what the key components of this substance were: a base, a sugar and a phosphate group.^[18,19,20]

Within the next 33 years researchers like Nikolai Koltsov to Frederick Griffith to Alfred Hershey and Martha Chase tried to identify the biological role of this material, when finally in 1952 there was no doubt left that DNA and DNA only serves as the carrier of hereditary information.^[21-27] Then in 1953, through a series of events involving the findings of Erwin Chargaff, Rosalind Franklin and Raymond Gosling as well as Maurice Wilkins, James Watson and Francis Crick proposed the nowadays accepted correct 3D structure of the DNA double helix.^[28-34] The formal crystallographic proof of the structure, however, was accomplished 26 years later in the year 1979.^[35,36]

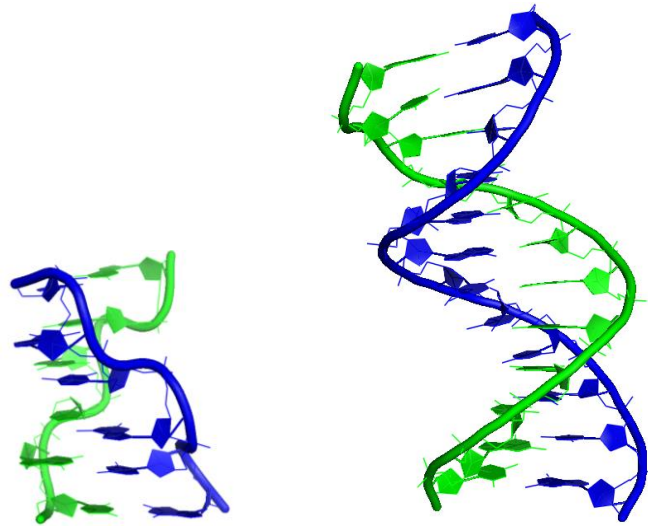


Figure 1.1. Crystal structure of a left-handed double helical DNA fragment (left) and a self-complementary dodecamer sequence of right-handed B-DNA (right).^[37] Images adapted from RCSB PDB entries 2DCG and 1BNA.

A few years earlier however, the first ever crystal structure of nucleic acid was determined. It was the yeast phenylalanine transfer RNA (tRNA).^[38]

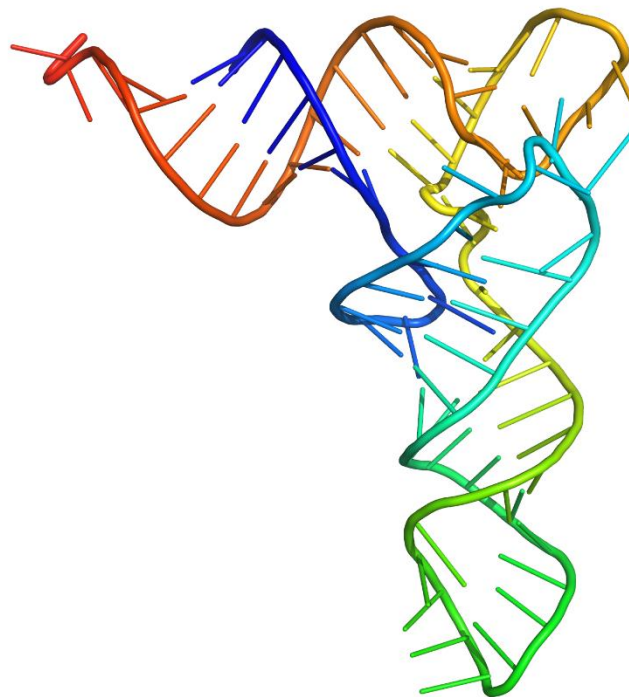


Figure 1.2. Crystal structure of the yeast PHE tRNA (improved model; based on the original deposit by Kim et al.). Adapted from RCSB PDB entry 6TNA.

The idea and confirmation of the central dogma of molecular biology and cracking the genetic code are other highlights on the way to modern life sciences.^[39,40] Sequencing technologies as well as the synthesis of DNA strands fall in the same category and were viable for the herein presented work in particular.^[41-50]

Especially the solid-phase synthesis of DNA deserves to be mentioned in more detail. More specific the phosphoramidite method pioneered by Marvin Caruthers. The basic steps include: Deprotection of the first nucleoside linked to the solid support (or the last that was coupled to the growing chain); addition and coupling of the activated second nucleoside phosphoramidite (or the next one); oxidation of the phosphite-triester to the phosphotriester.^[51]

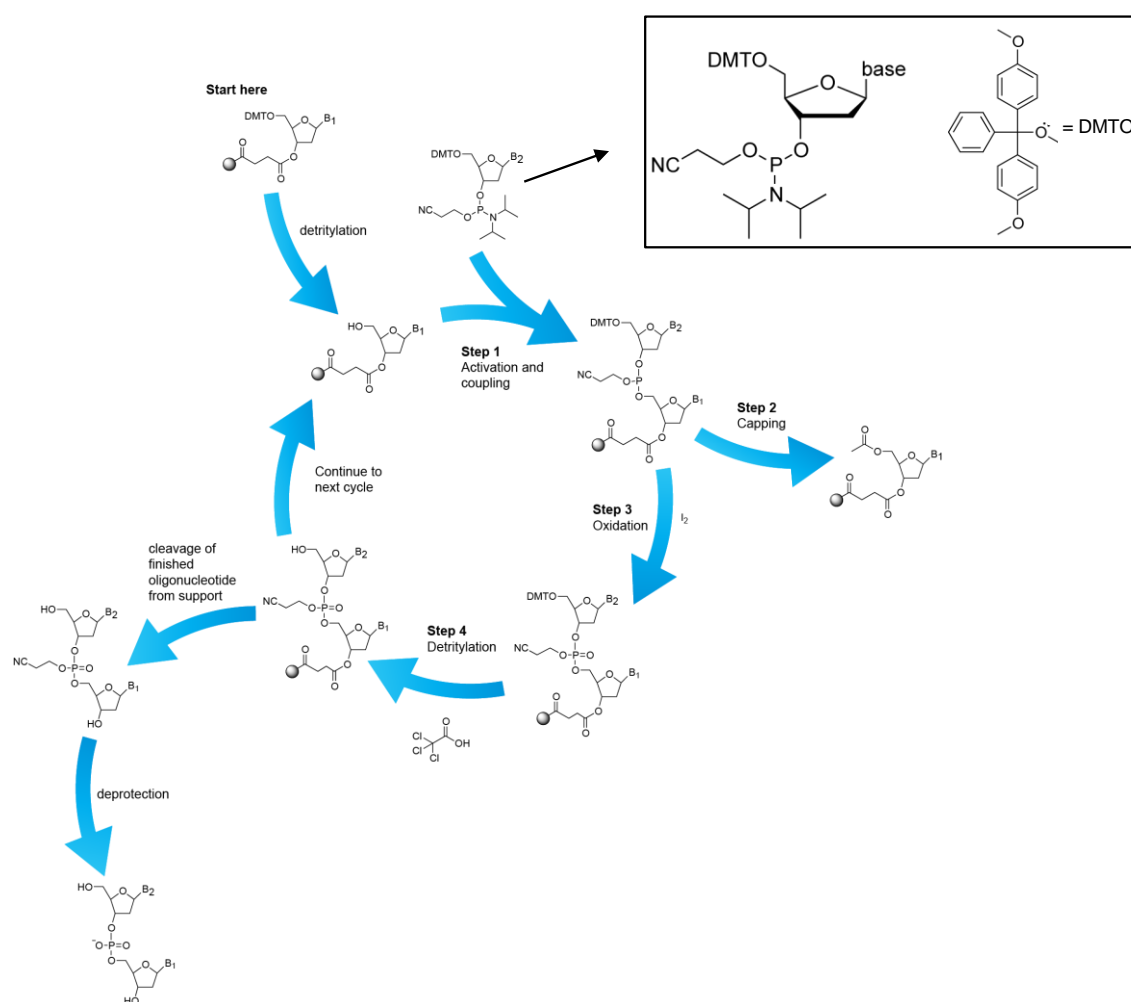


Figure 1.3. Cycle of the solid-phase oligonucleotide synthesis. The final product results after the two steps shown at the bottom left (cleavage and deprotection). The monomers for the ongoing synthesis of a strand always carry a dimethoxytrityl group at the 5'-position and a 2-cyanoethyl diisopropylaminophosphonite at the 3'-position.^[51]

Chapter 2 – Structural Aspects of the DNA

As already briefly mentioned in Chapter 1, the DNA consists of repetitive units (nucleotides) built from a base (nucleobases: adenine A, cytosine C, guanine G and thymine T), a sugar (pentose 2-deoxyribose) and a phosphate group.^[1-4] Two complementary DNA strands hybridize in an antiparallel fashion in order to form the double helix. This process of nucleation and propagation is mainly driven by base stacking and the hydrophobic effect.^[5-8] The hybridization of two strands leads to a specific pattern of what's called base pairing. In two fully complementary strands every A is paired with a T, and C with G (Watson-Crick base pairs). Hydrogen bonds between the bases A – T, and C – G are responsible for the specificity of the base pairing. There is no need for fully complementary sequences, nor is it necessary to have a balanced amount of A – T, and C – G in order to hybridize two strands. However, these factors do contribute to the overall stability of the formed construct. Amongst other, the influence of the environment in which the DNA strands are is of high importance too. In an aqueous environment (physiological conditions) complementary DNA sequences form B-DNA (some of its features are presented in the images below).^[1-8]

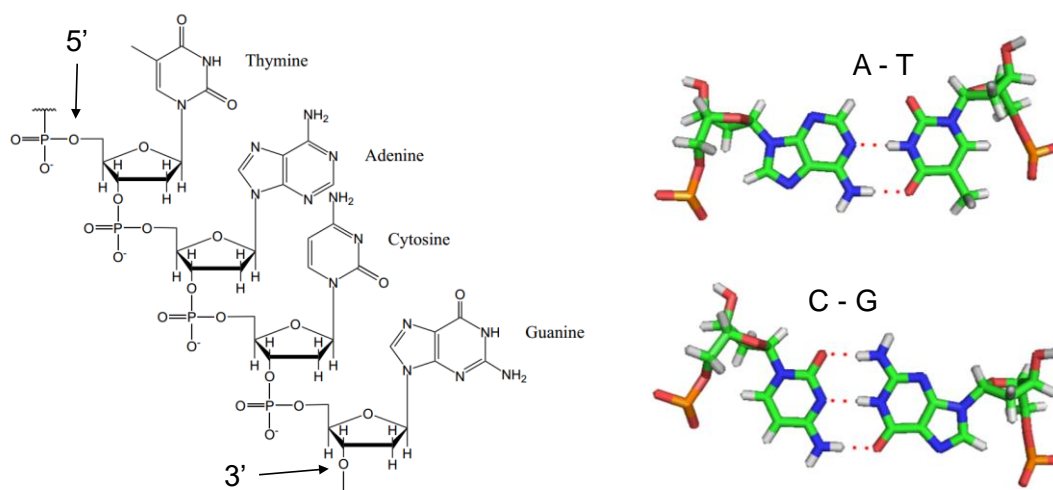


Figure 2.1. The four canonical nucleotides of the DNA, indicated is the 5' – 3' direction of the strand (left) and the naturally occurring Watson-Crick base pairs illustrating the number of H-bonds between A – T (2), and C – G (3) (right).^[9,10,11]

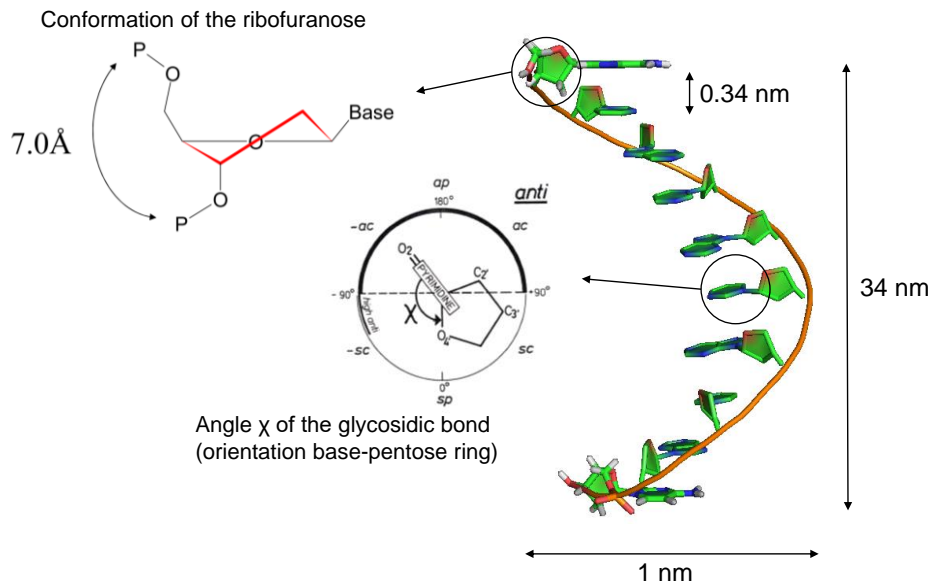


Figure 2.2. A representation of one DNA strand of the double helix where some of the key features are highlighted: the sugar pucker (C2'-endo or S) and the angle χ of the glycosidic bond (*anti*), as well as the helical diameter, the pitch and the axial rise per residue.).^[1,11-13]

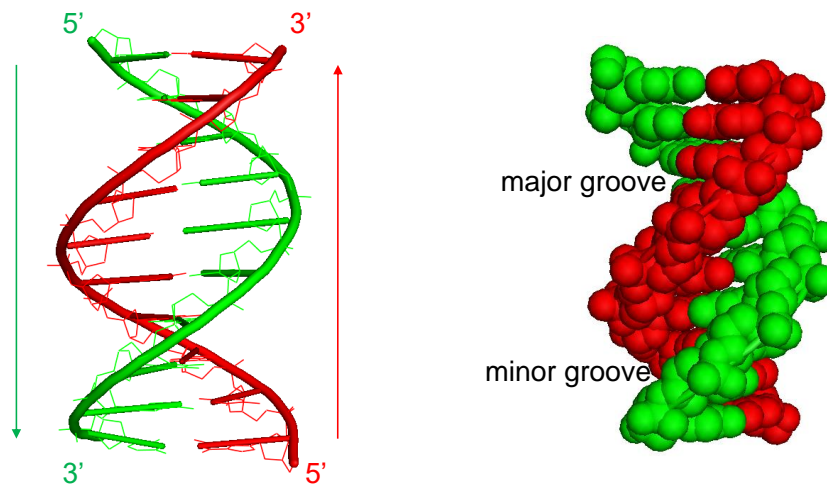


Figure 2.3. The DNA double helix with the two strands aligned in an antiparallel fashion (left) and the calotte model illustrating the accessibility of the two grooves (right).^[11,12,13]

In addition, the DNA does not necessary always fold into a “perfectly paired” double helix. Other secondary or tertiary structures do exist, either natural or artificial ones.^[14-24] Some of these structural elements are given below.

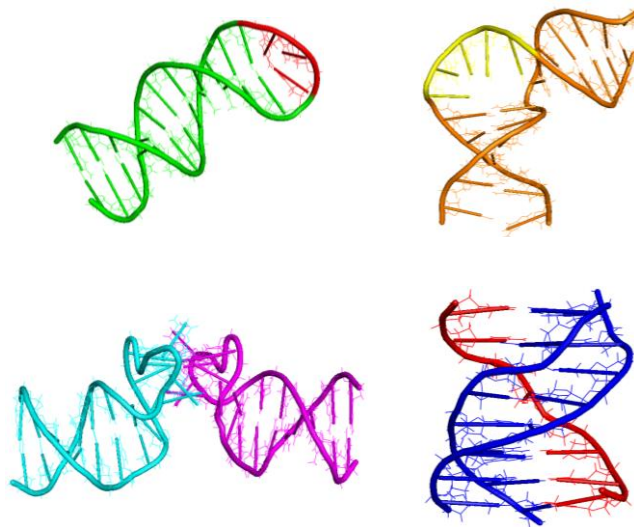


Figure 2.4. Structure of a hairpin loop with the GAA loop sequence colored red (top left). Structure with a five-adenine bulge loop, yellow highlighted (top right). A DNA kissing complex built from two hairpins (bottom left). And a DNA triple helix where the third strand – red – is linked via Hoogsteen base pairs (bottom right). Images adapted from RCSB PDB entries 1JVE, 1QSK, 1JU0 and 1D3X.

Besides the structure of the DNA there are especially two properties that are important for working with this material:

- Complementary DNA strands (in solution) will pair and form a double helix, even at low single strand concentration. The stability of a DNA double helix underlies a series of parameters like: presence of cations, the sequence (base composition and length) and the concentration of the DNA strands itself. Taken together, a double helix of about 20 bp length at physiological conditions and a single strand concentration down to the nanomolar range, is still stable...^[25]
- ...Stability of a DNA duplex can be expressed as its melting temperature (T_m). The melting temperature can be measured by increasing the temperature of the sample and simultaneously recording the change in the UV absorption. Due to the fact that the duplex has a lower absorption than the corresponding single strands, the absorbance increases once the duplex is denatured (hyperchromicity). Based on the UV melting curve, the T_m is then calculated as the temperature at which half of the material is melted (mid-point of the transition).^[1,26]

As mentioned above, there are natural DNA structures that do not form a double helix, for example the G-quadruplexes (G-tetrads) formed at the end of the telomers.^[1,14,27] Other structures don't occur in nature, like the DNA three-way junction. This artificial secondary structural element has an approximately Y-shaped, pyramidal geometry with variable flexibility. There are no stacking interactions between the helical arms, though that depends on whether or not there are additional unpaired bases at the branch point.^[28-32] The dynamics and the relative stabilities of constructs on the basis of the three-way junction are sequence-dependant and are affected by the salt concentration.^[33-45]

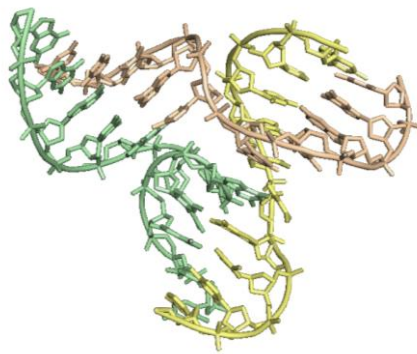


Figure 2.5. NMR structure of a 3WJ having two unpaired bases at the branch point of the junction. Image adapted from RCSB PDB entry 1EKW.

Investigations on the local and global structure of the DNA three-way junction revealed that despite the full complementarity of the three arms, it is most likely that the bases adjacent to the branch point are unpaired. This allows for the formation of a nanoscale cavity at the center of the junction.^[46]

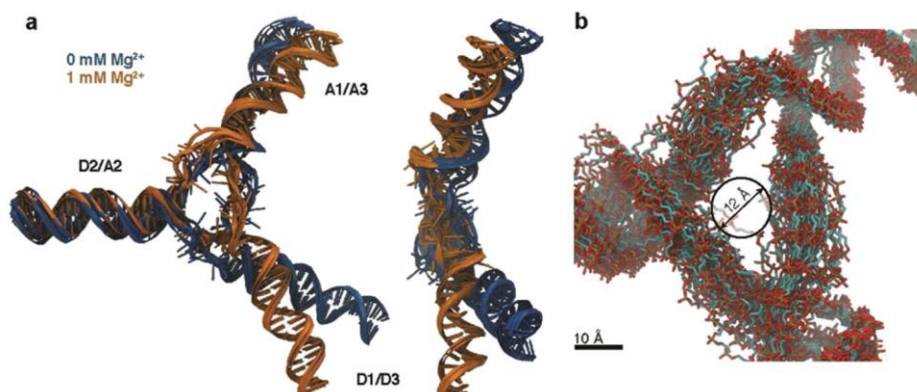


Figure 2.6. Structure of the three-way junction based on SM-FRET distance restraints and MD simulations (a). The branch point area of the three-way junction shows the cavity (b).^[46]

Chapter 3 – Alteration of the DNA

Once the molecular structure of DNA was established, procedures to modify this biopolymer were developed. There are sugar-phosphate backbone and base analogues. The first category includes changes derived from considerations regarding the origin and evolution of nucleic acids, as well as diagnostic and therapeutic applications.^[1-4] The other category, novel bases, led to fluorescent conjugates (fluorophore-base) or fluorescent non-canonical bases.^[5-17] Also, unnatural base pairs or base pairs with special properties belong in the same category.^[18-31]

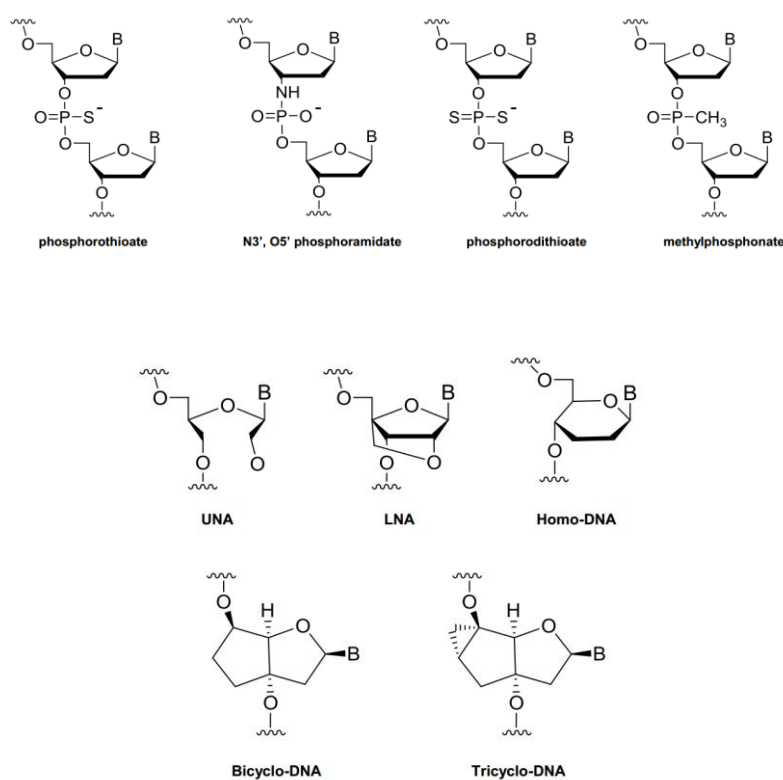


Figure 3.1. Examples of phosphate backbone (upper row) and sugar modifications (lower rows).^[32,33]

In particular for antisense applications various chemically modified oligonucleotides were synthesized. Hexitol nucleic acid (HNA) is one of them. While the bases remain the same as in the DNA, the sugar units are altered (phosphorylated 1',5'-anhydrohexitol backbone). The high-resolution structure given below shows that the Watson-Crick base pairing is maintained for a HNA duplex.^[34] Another type of sugar

modification, introduced to enhance the bio- and thermostability, is the Locked nucleic acid (LNA). The structure below shows a duplex with all modified β -D-2'-O-4'-C-methylene ribofuranose nucleotides.^[35]

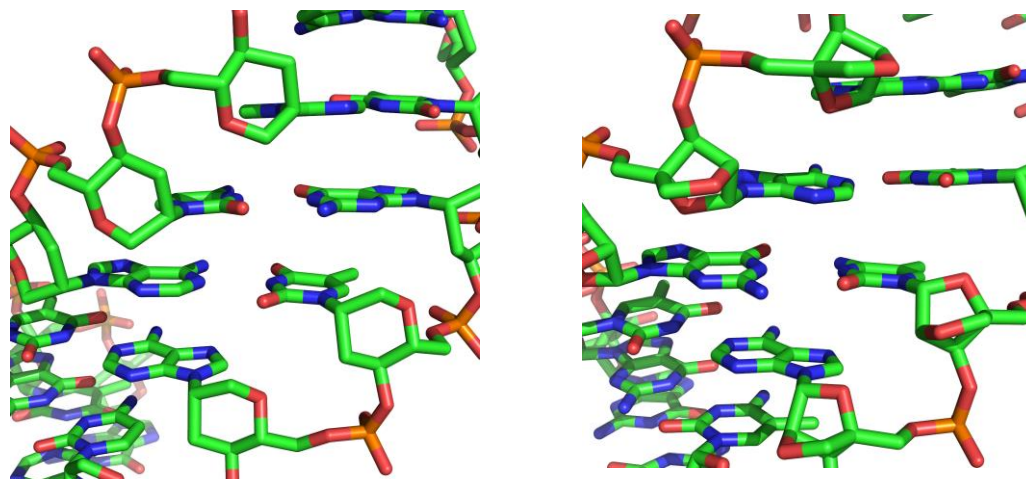


Figure 3.2. Crystal structures of a HNA duplex based on RCSB PDB entry 481D (on the left) and a LNA duplex based on RCSB PDB entry 2X2Q (on the right).

Since the modifications are not limited to the sugar-phosphate backbone, the exchange or addition of artificial nucleobases is for example of interest to extend the genetic code. The d5SICS – dNaM pair lacks the ability to form hydrogen bonds and its pairing is mediated by hydrophobic and packing forces.^[36] In contrast the Z – P pair, another nonstandard base pair, are joined by rearranged hydrogen bond donor and acceptor groups.^[37]

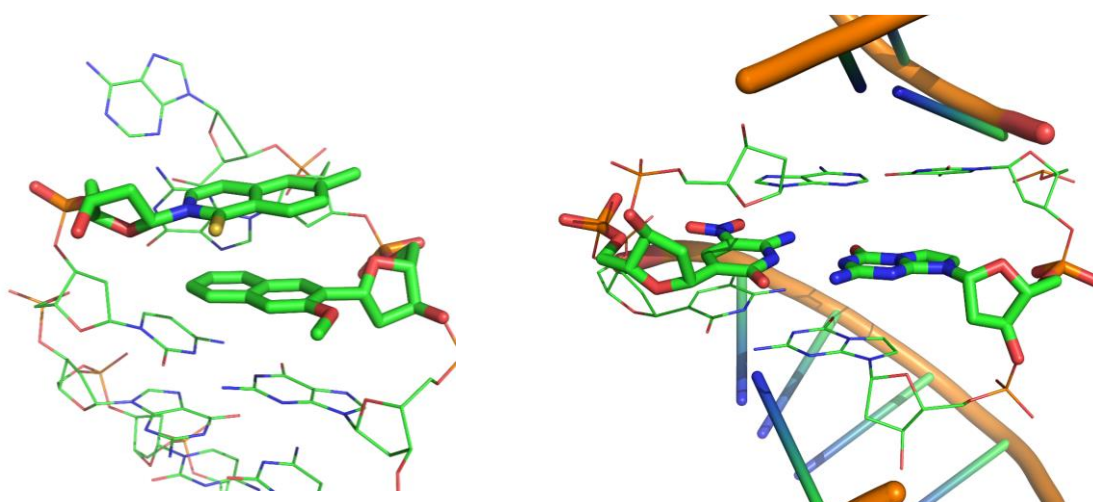


Figure 3.3. The artificial base pair dNaM-d5SICS (left, PDB entry 4C8L) and the Z:P pair (right, PDB entry 4XNO).

One group of modifications eliminates the sugar and base completely, the non-nucleosidic building blocks.^[38,39] These molecules are linked via phosphate groups to the rest of the DNA strand and can be incorporated either at the termini or internally. Some examples are given below.

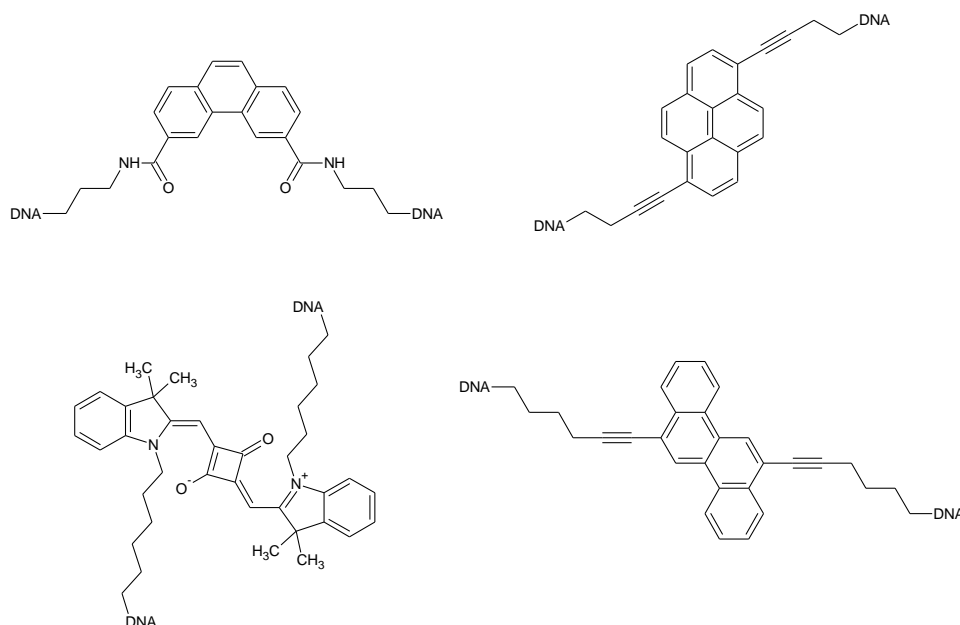


Figure 3.4. Non-nucleosidic, fluorescent building blocks: Phenanthrene^[40] (top left), pyrene^[41] (top right), squaraine^[42] (bottom left) and chrysenes^[43] (bottom right).

As mentioned in the last chapter, DNA has an inherent ability to form a double helix in case of complementary sequences. The hybridization does also work in case of modified strands, allowing the assembly of molecules that otherwise require a higher concentration and / or organic solvents. Therefore, the nucleic acid-guided assembly of aromatic chromophores in DNA hybrids makes the (spectroscopic) properties easily accessible.^[38] Two examples are given below (Figures 3.5 and 3.6).

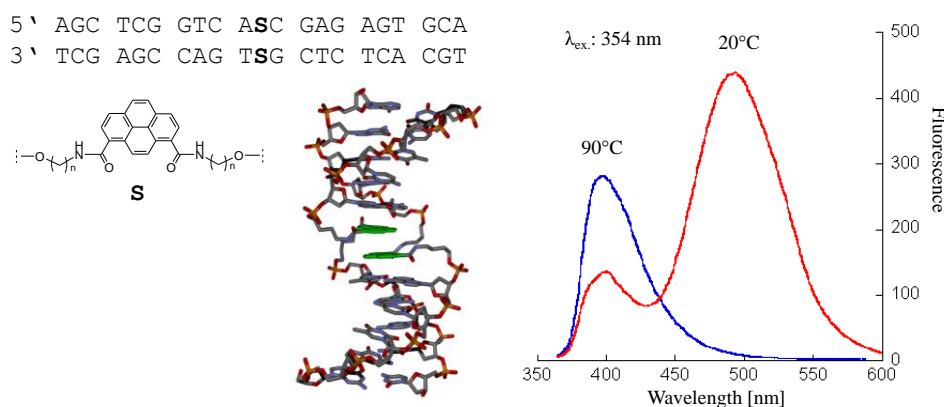


Figure 3.5. Excimer formation by interstrand stacked pyrenes.^[44]

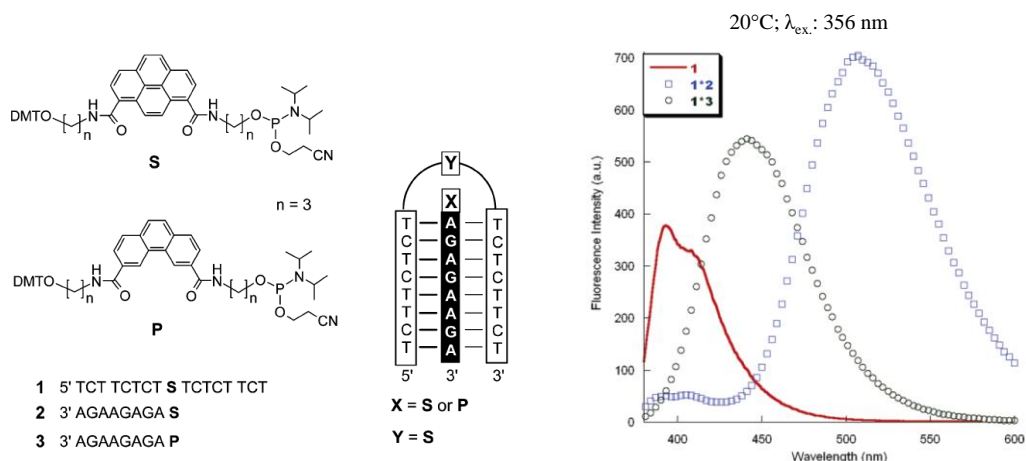


Figure 3.6. Triple-Helix Mediated Excimer and Exciplex Formation.^[45]

Using the DNA as a scaffold for chromophore assembly is not limited to one incorporation per strand. Hybrids with more than a total of two chromophores were successfully assembled as well (see Figure 3.7). These multichromophoric constructs have often more pronounced features (compared to a single modification), but still show a DNA-like behaviour. However this is only valid as long as the number of artificial building blocks does not exceed to a point where the nature of the hybrid is controlled exclusively by the chromophores.

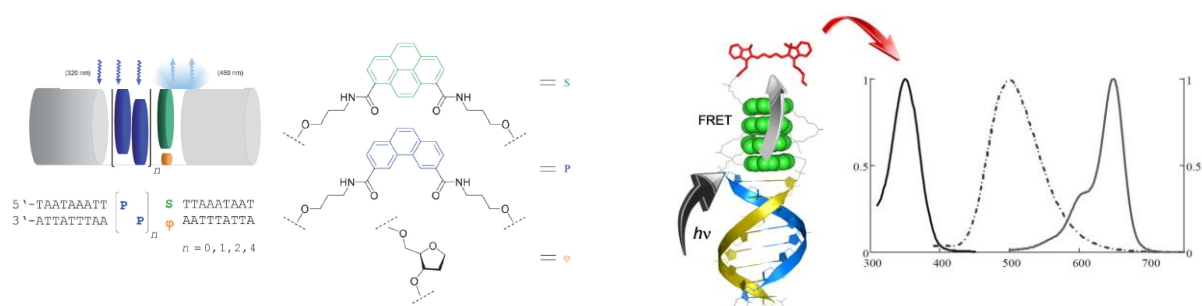


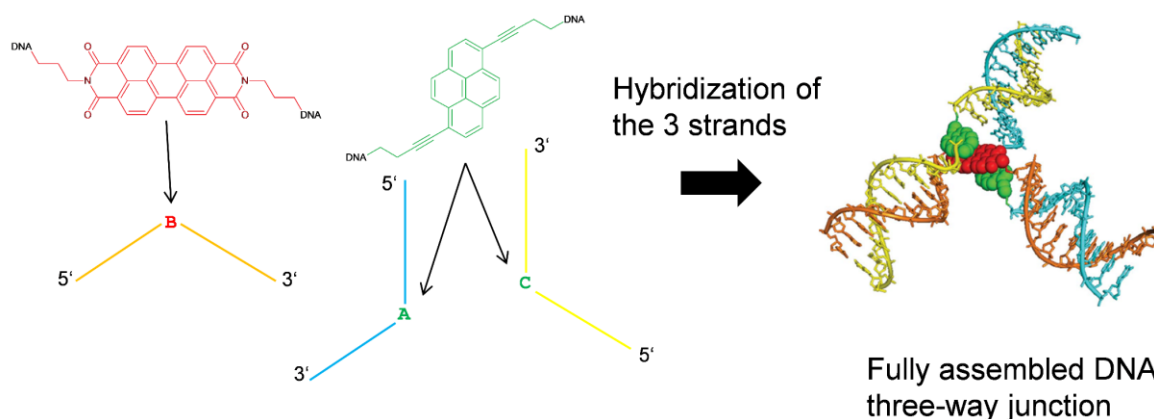
Figure 3.7. A DNA-based light-harvesting antenna (on the right) where a stack of phenanthrenes (blue) act as light-harvester, forming an exciplex with the pyrene (green, opposite of an abasic site).^[46] On the left: photon harvesting occurs through excimer-forming pyrenes (green) which then excite a terminal cyanine dye.^[47]

Chapter 4 – The DNA Three-Way Junction as a tool for Chromophore Assembly

Aim of the Work:

The DNA three-way junction (3WJ) serves as a scaffold for the molecular organization of individual non-nucleosidic chromophores. These building blocks are covalently attached to the DNA strands and are assembled in the branch point region of the structure (an example is given below). The distinct spectroscopic properties of the tripartite constructs are described in this chapter.

DNA sequences with non-nucleosidic chromophore modification (A and C are modified with a pyrene unit; B is modified with a PDI)

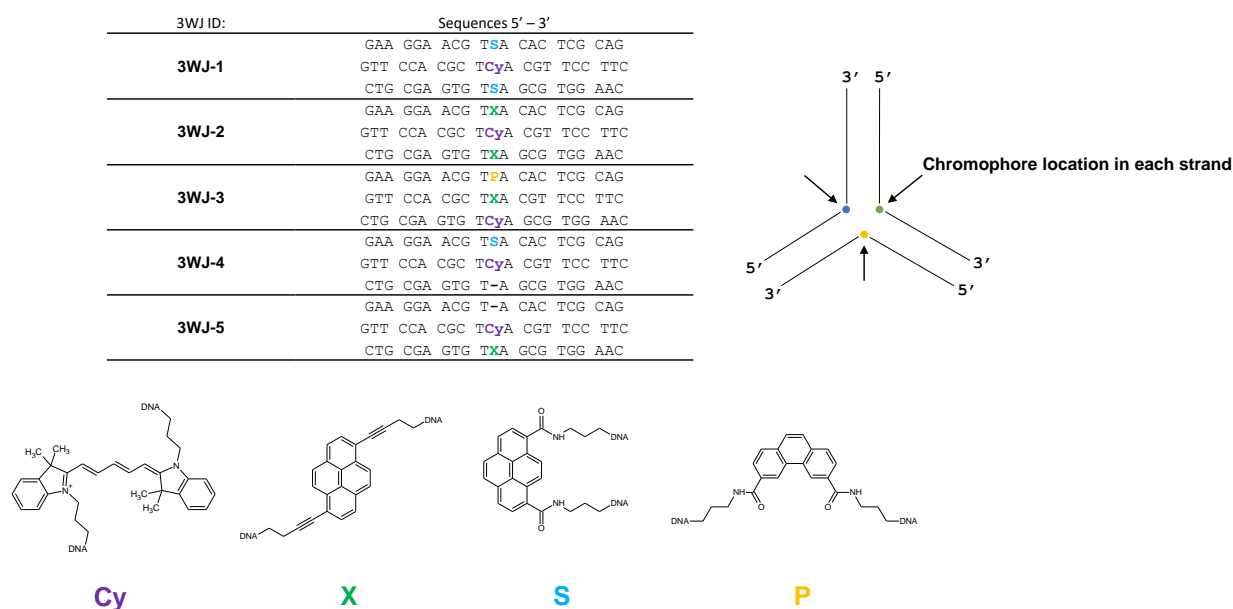


Introduction

In order to control the arrangement of functional molecules as well as expanding the diversity of such functionality itself, DNA guided assembly has become an essential instrument.^[1] Apart from using non-nucleosidic building blocks^[2] for diagnostic applications^[3] and artificial light-harvesting systems,^[4] we wanted to implement this type of modified DNA into higher-order DNA structures. In terms of simplicity and handling, the DNA three-way junction is the most prominent one among all the other branched structures.^[5] Although lacking of a natural counterpart the DNA 3WJ can be found as a subject matter in structural studies,^[6] biophysical assays for junction-specific small-molecules,^[7] electrochemical sensors,^[8] and even as part of sensitive a RNA detection mechanism.^[9]

Results and Discussion

This work is a follow-up of previous studies with the goal to use the DNA three-way junction as a mould for tripartite chromophore assembly.^[10] The design of the study is illustrated in Scheme 4.1. The 3WJ is formed by three oligodeoxynucleotides that are partially complementary in a pairwise fashion. The phenanthrene (P), pyrenes (S and X) and cyanine (Cy) building blocks are positioned in the middle of the oligomers so that they are located at the branch point of the formed 3WJ. In addition to those four chromophores, other non-nucleosidic building blocks were incorporated into DNA strands as well (see Appendix A). The sequences were designed to ensure that a maximum of combinations of possible arrangements resulted. **3WJ-1** to **3WJ-5** are shown in Scheme 4.1. Length and nucleotide sequence of the oligomers were chosen with help of the UNAFold software^[11,12] to ensure sufficient stability of the tripartite hybrids at room temperature and avoiding the formation of other, unwanted secondary structures. Additionally, direct neighboring guanine nucleotides next to the modification were avoided in order to minimize fluorescence quenching by this base.



Scheme 4.1. Schematic illustration of the 3WJs investigated (**3WJ-1** to **3WJ-5**) and structures of the non-nucleosidic building blocks 3,6-dicarboxamide phenanthrene (P), 1,8-dicarboxamide pyrene (S), 1,6-dialkynylpyrene (X) and cyanine dye Cy5 (Cy).

UV/Vis spectroscopy was carried out in order to verify the presence of all chromophores inside the samples and their main absorption peaks. An overview of these spectra is given in Figure 4.1. For clarification of the respective peaks of each sample especially in the absorption range of the phenanthrene and pyrene chromophores, an enlargement is given in Figure 4.2.

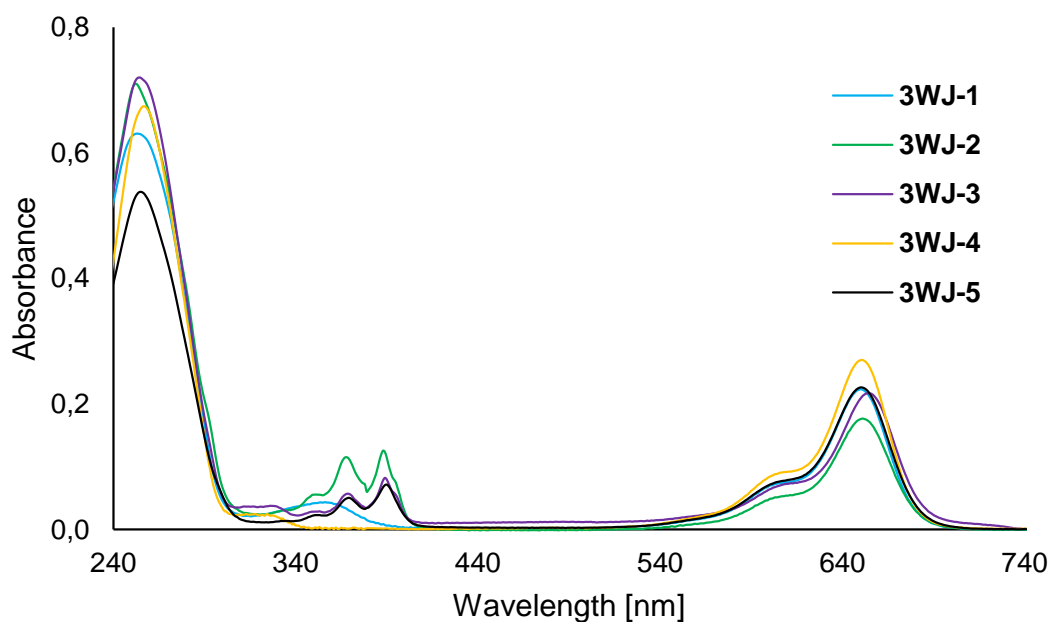


Figure 4.1. UV/Vis spectra of **3WJ-1** to **3WJ-5**. An enlargement of the region between 280 nm to 440 nm is given in Figure 4.2. Since all samples contain a strand with a cyanine dye, the characteristic peak around 650 nm which corresponds to the absorption of the cyanine is present. Conditions: 1 μM single strand concentration, 20°C, 100 mM NaCl, 10 mM sodium phosphate buffer, pH 7.0.

All the expected absorption peaks of the chromophores were present in the UV/Vis spectra, namely: for the 3,6-dicarboxamide phenanthrene (P): λ_{abs} 320 – 330 nm; for 1,8-dicarboxamide pyrene (S): λ_{abs} 350 – 360 nm; for 1,6-dialkynylpyrene (X): λ_{abs} 350 – 390 nm; and for the cyanine dye (Cy): λ_{abs} 600 – 650 nm.^[4,10,13] Although each sample contains only one cyanine (and the concentration of the strands was kept the same – of course within the pipetting errors), there are slight differences in the peak's intensity and shift (peaks of the Cy dye at around 650 nm). This may indicate the change in the

“environment” of the cyanine from one sample to the other one (e.g. structural changes and / or change of the nearest neighbour base or chromophore).

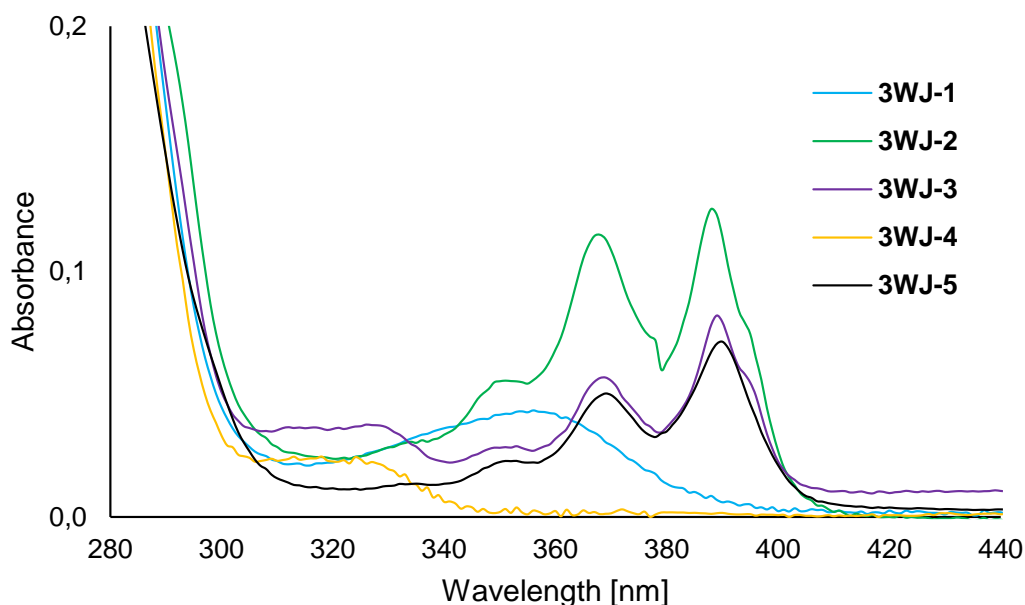


Figure 4.2. Enlargement of the UV/Vis spectra shown in Figure 4.1 (range 280 nm to 440 nm) of **3WJ-1** to **3WJ-5**. Conditions: see Figure 4.1.

In contrast to previous studies, the aggregation behaviour of the alkynylpyrenes in the present case (illustrated by **3WJ-2**, see Figure 4.2) is not observed. I.e. the changes in the vibronic band intensities that are characteristic for alkynylpyrene aggregation (330-410 nm region) are not noticeable.^[13] Therefore, no information on the interactions between the individual chromophores was obtained from UV/Vis spectroscopy. All samples that contain at least one alkynylpyrene unit (**3WJ-2**, **3WJ-3** and **3WJ-5**) show the same absorption band pattern at 20°C: the $A_0 \rightarrow 1$ transition (370 nm) is of lower intensity than the $A_0 \rightarrow 0$ transition (390 nm).

Next, the fluorescence properties for the two hybrids containing two pyrene derivatives, **3WJ-1** and **3WJ-2**, along with a cyanine dye in the third strand were investigated (see Figure 4.3). Upon excitation of the pyrenes, both samples show a peak at around 670 nm which corresponds to the emission of the cyanine dye. Hence, energy transfer

takes place between the pyrenes and the cyanine (since the cyanine does not or only negligible emit when excited at these wavelengths).

Relative to this peak, blue-shifted at about 520 nm is the (remaining) excimer emission of the alkynylpyrenes detectable (less pronounced in case of the excimer signal of the carboxamidepyrenes in **3WJ-1** which is expected at around 500 nm). The formation of pyrene excimers is, thus, enabled by bringing together the individual pyrene residues at the branch point of the 3WJ. At shorter wavelengths (380 – 450 nm) the monomer emission of the pyrenes is observed.^[14-24]

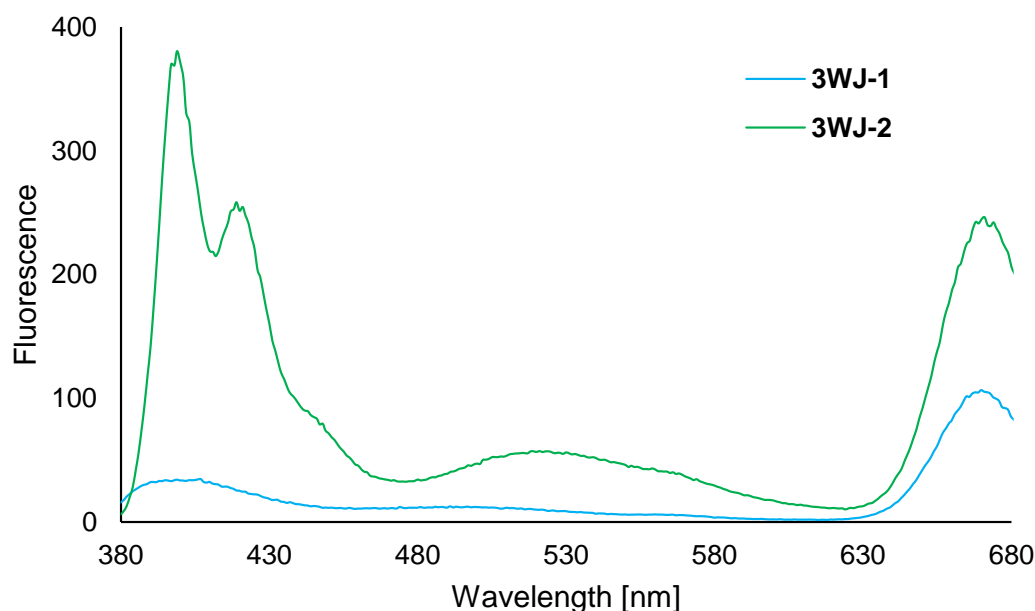


Figure 4.3. Fluorescence spectra of **3WJ-1** and **3WJ-2**, both contain two pyrene units. Conditions: see Figure 4.1. Instrumental set-up: excitation wavelength: 350 nm (for **3WJ-1**) and 370 nm (for **3WJ-2**), excitation slit width: 5 nm; emission slit width: 5 nm; PMT voltage: 600 V.

In addition to the three-way junctions with two pyrene moieties (**3WJ-1** and **3WJ-2**), an approach with a phenanthrene-pyrene-cyanine system (**3WJ-3**) was investigated. Instead of the before mentioned pyrene excimer emission, here the formation of an exciplex between the phenanthrene and pyrene can lead to excitation of the cyanine dye (through emission of the exciplex). The temperature-dependent fluorescence spectra are given in Figure 4.4.

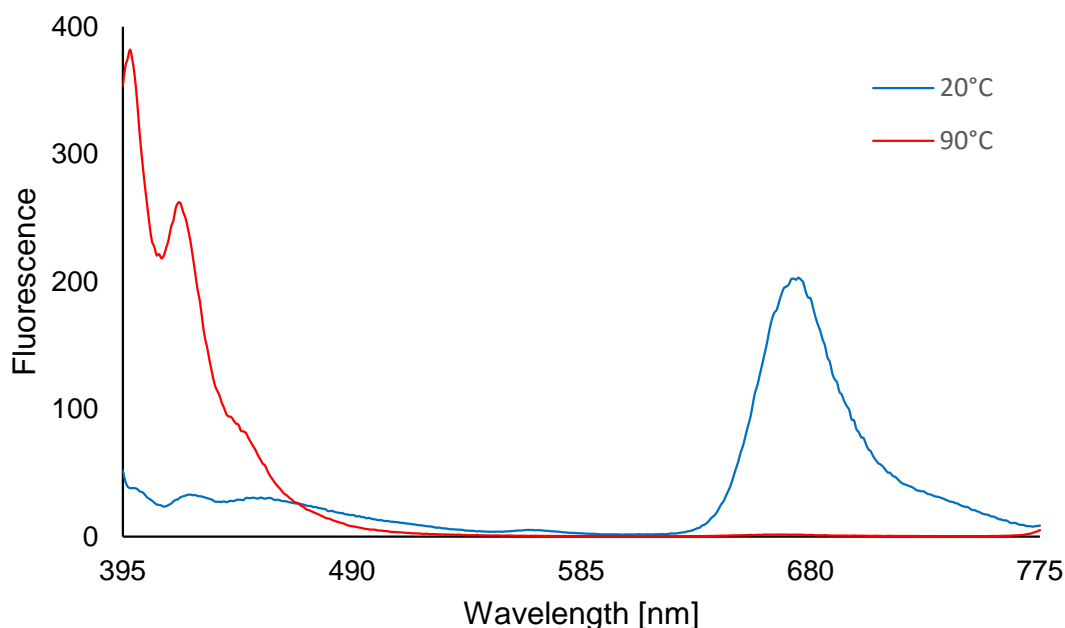


Figure 4.4. Temperature-dependent fluorescence spectra of **3WJ-3** containing phenanthrene, pyrene and cyanine. Conditions: see Figure 4.1. Instrumental set-up: see Figure 4.3, except for the excitation wavelength: 390 nm.

Based on the data shown in Figure 4.4, the emission of the phenanthrene-pyrene exciplex (peaked at around 450 nm) as well as the pyrene monomer emission (400 – 420 nm) are relatively weak in comparison with the emission originating from the cyanine dye (670 nm). The thermally induced “aggregation-deaggregation” process observed in the fluorescence spectrum simply demonstrates that at 90°C monomer emission is observed exclusively, that is due to the spatial separation of the chromophores.

Although the idea was to use primarily the excimer emission to excite the cyanine, it is noteworthy to mention that with or without the formation of an excimer (i.e. the requirement of two pyrenes) or exciplex (i.e. phenanthrene-pyrene) similar results are obtained. As demonstrated with **3WJ-4** and **3WJ-5**, both containing one pyrene, one cyanine and an “empty” third strand, energy is transferred “directly” from the excited pyrene to the cyanine. The corresponding fluorescence emission spectra are shown in Figure 4.5.

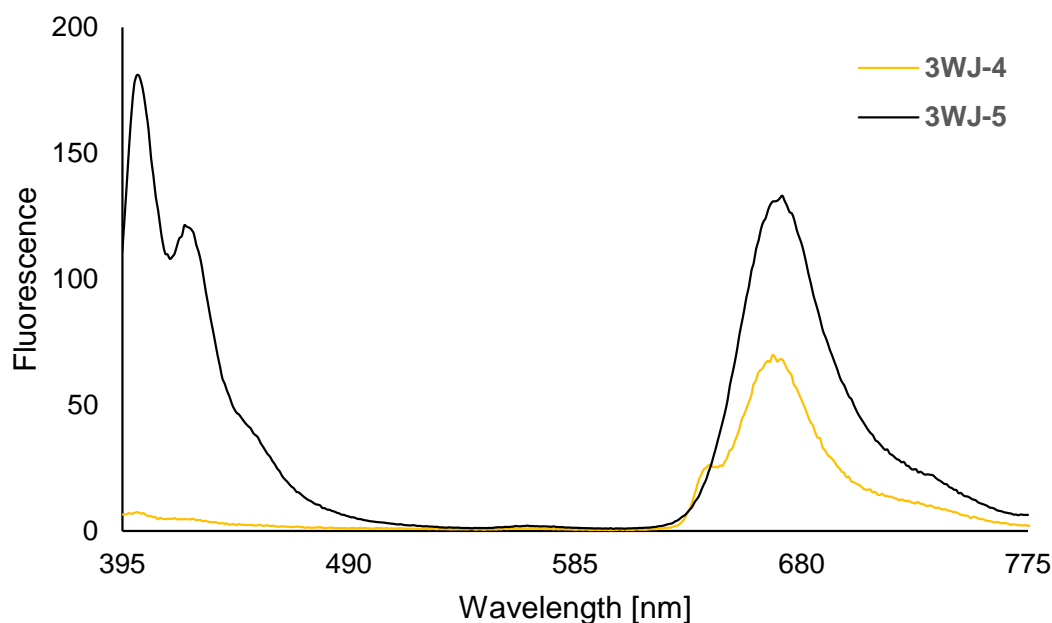


Figure 4.5. Fluorescence spectra of **3WJ-4** and **3WJ-5**. Conditions and instrumental set-up: see Figure 4.3, except for the excitation wavelength: 320 nm (for **3WJ-4**) and 390 nm (for **3WJ-5**). The small shoulder at 640 nm in case of **3WJ-4** results from artifacts caused by the second order transmission of the monochromator.

Taking the evidence provided by the experiments described above together, the following points can be stated: i) the DNA three-way junction provides indeed a framework for assembling non-nucleosidic chromophoric building blocks; ii) as for the 3WJs with two pyrenes (**3WJ-1** and **3WJ-2**) and phenanthrene-pyrene (**3WJ-3**) the introduction of a cyanine dye does have an impact on the pyrene excimer or phenanthrene-pyrene exciplex formation, similar to systems presumably to form a donor-acceptor-donor (D-A-D) complex.^[25-29] This may go in parallel with the absence of any changes in the vibronic band ratios in the UV/Vis spectra upon thermal denaturation (see Appendix A), in contrast to observations made with related compounds associated with aggregation behaviour;^[30-37] iii) the exact nature of the chromophore arrangement in the present 3WJs remains unknown, the collected data is to “diverse” for that to be answered; iv) energy transfer between the excited entity and the cyanine dye is shown to occur, whether with (**3WJ-1** to **3WJ-3**) or without (**3WJ-4** and **3WJ-5**) the help of an excimer / exciplex.

Conclusions

The present study shows that the DNA 3WJ serves as a suitable scaffold for the assembly of non-nucleosidic chromophores. Furthermore, the aggregates exhibit spectroscopic properties that are controlled by the choice of the chromophore combination. The data demonstrate the value of higher order DNA structures for the molecular assembly of functional molecules.

In addition and with regard to all the arrangements that were formed (i.e. the 3WJs given in the Appendix A) the following point has to be considered as well: a permutation of the chromophores in the respective sample does not lead to a severe change in the spectroscopic properties (there are slight quantitative differences though).

Experimental Section

The modified oligomers were synthesized by automated oligonucleotide synthesis using an adapted synthetic procedure on a 394-DNA/RNA synthesizer (Applied Biosystems) and previously described protocols for the phosphoramidite building blocks. Purification was performed by RP-HPLC. Oligonucleotide masses were determined by LC-MS.

UV/Vis spectra were taken on a Varian Cary-100 Bio-UV/Vis spectrophotometer equipped with a Varian Cary-block temperature controller and processed with Varian WinUV software. The concentration of the single strands was adjusted to 1 μM . Additionally, each solution contained 10 mM sodium phosphate buffer, pH 7.0 and 100 mM NaCl.

Fluorescence spectroscopy involved the use of a Varian Cary Eclipse fluorescence spectrophotometer equipped with a Varian Cary-block temperature controller with 1 cm x 1 cm quartz cuvettes and Varian Eclipse software. Conditions and instrumental setups for fluorescence emission spectra: see description figures in the main text.

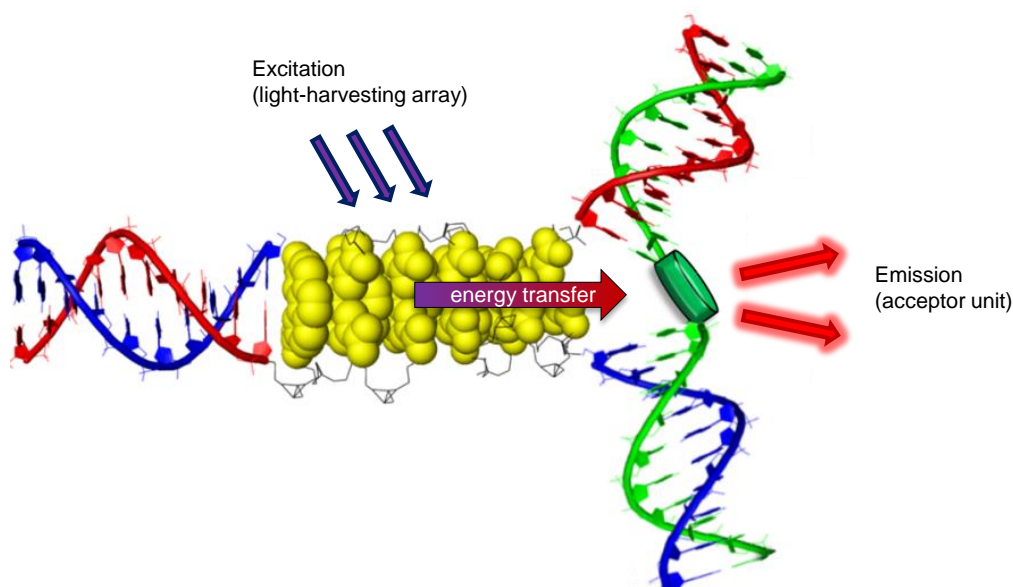
For a full description see Appendix A.

Chapter 5 – A modular LHC built on the DNA Three-Way Junction

Aim of the Work:

The suitability of the DNA three-way junction (3WJ) as a versatile scaffold for the modular construction of an artificial light-harvesting complex (LHC) is investigated. In contrast to the 3WJs in the previous chapter, the constructs in this chapter consist of a light-harvesting, π -stacked multichromophoric part (“stem”) and an acceptor unit which is variable. The close proximity of the two entities allows for an efficient energy transfer.

Initially, we started with two different approaches for the LHC. The first one is presented in **Chapter 5a**, the second, slightly different, design is separately discussed in **Chapter 5b**.



(The scheme shown above does apply to the work presented in Chapter 5a. For a schematic illustration of the approach given in Chapter 5b, see the corresponding “Results and Discussion” part).

Introduction

DNA Nanoarchitectonics (the terms DNA Nanotechnology and DNA Origami are often used in this context too) evolved into a major playground for all kinds of DNA-based applications controlled by this smart self-assembling biopolymer.^[1,2] The range of these developments is as diverse as the field from which they emerge: genetics, medicine, nanoelectronics and biophysics.^[3,4]

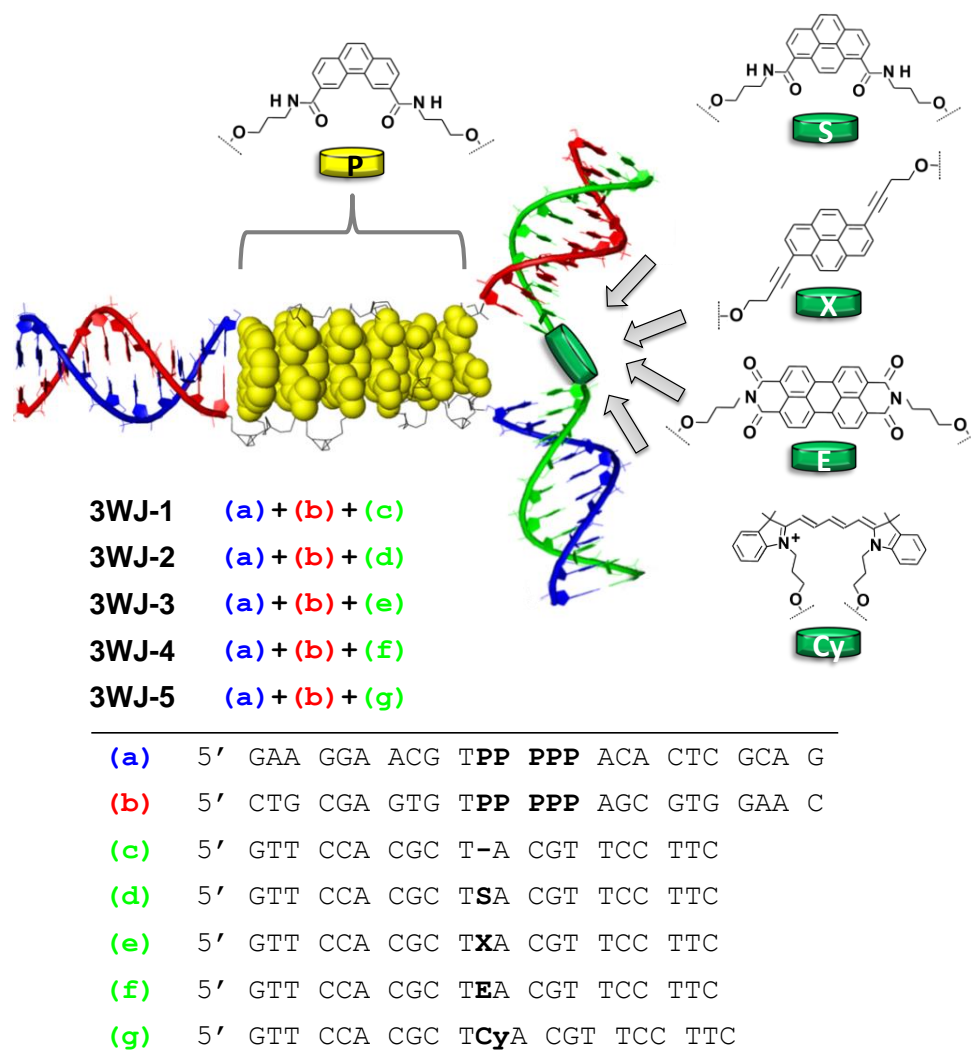
In particular: Addressable DNA Nanoconstructs via orthogonal Click Chemistry,^[5] programmable DNA Nanocircles^[6] or light-driven conformational regulation of G-quadruplex DNA,^[7] to name only a few of them. To expand the potential of such DNA-based molecular systems^[8] even further, novel functional molecules^[9–12] or conjugates are required.^[13,14] As a result, Energy-transfer paths on DNA Origami,^[15] Photonic wires,^[16] an Artificial photosynthetic reaction center^[17] and Light-harvesting antenna systems were realized.^[18–22]

Amongst other intra- and intermolecular secondary DNA structures, branched DNA motifs and more precisely the DNA three-way junction (3WJ) became the topic of interest over the past few years. The nature of this higher-order DNA structure was investigated in thermodynamic studies and 3D global structural analysis.^[23–25] The influence of small-molecules binding to the three-way junction,^[26,27] the use in detection systems^[28,29] and even in electrochemical sensors was tested as well.^[30,31] Moreover, the construction of Y-shaped DNA to supramolecular assemblies using Click Chemistry^[32] and the controlled energy transfer along a DNA three-way junction,^[33–35] underline the versatility this structural element.

Chapter 5a - A modular LHC built on the DNA Three-Way Junction

Results and Discussion

The design of the light-harvesting complex, the sequences it is built on and the chromophores are shown in Scheme 5.1. Additional data (LHCs with other acceptor dyes) are listed in the Appendix B.



Scheme 5.1. Schematic illustration of the light harvesting 3WJ, the chromophores used and the corresponding sequences.

In **3WJ-2**, **-3**, **-4** and **-5**, the LHC is composed of a phenanthrene (P) stack, the light absorbing antenna (strands **a** and **b**), and an exchangeable acceptor chromophore (strands **d-g**). **3WJ-1** serves as a control bearing no acceptor dye in the third strand (**c**). The formation of the 3WJs was demonstrated by polyacrylamide gel

electrophoresis (Appendix B). The thermal denaturation experiments showed for all 3WJs a single transition. Melting temperature (T_M) values are ranging from 57-63 °C and are listed in Table 5.1. UV/Vis spectra of the different 3WJs are given in Figure 5.1 and show the long-wavelength absorptions of the various chromophores: P ($\lambda_{\max} = 316$ nm); S ($\lambda_{\max} = 353$ nm); X ($\lambda_{\max} = 391$ nm); E ($\lambda_{\max} = 561$ nm) and Cy ($\lambda_{\max} = 652$ nm).

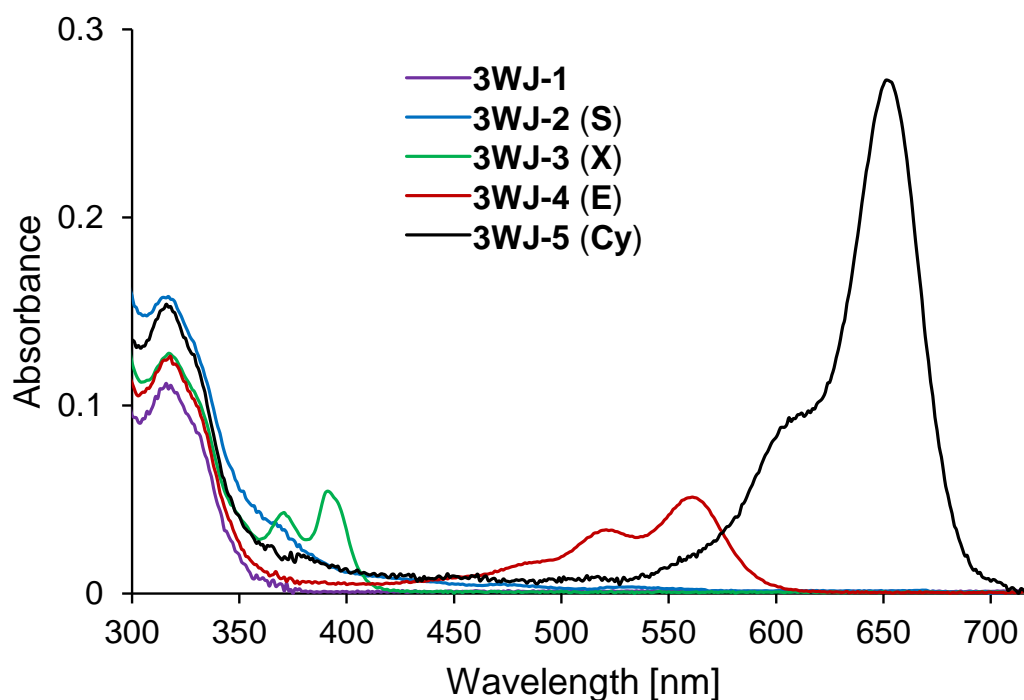


Figure 5.1. UV/Vis spectra of the investigated three-way junctions. Conditions: 1 μ M single strand, 20°C; 100 mM NaCl, 10 mM sodium phosphate buffer, pH 7.0; acceptors are given in brackets.

The effectiveness of the 3WJs as LHCs was investigated by fluorescence spectroscopy. Figure 5.2 shows the emission spectra of **3WJ-1** to **3WJ-4** after phenanthrene excitation at 320 nm. **3WJ-2** and **3WJ-3**, both of which contain a pyrene derivative as acceptor dye, exhibit strong exciplex emission ($\lambda_{\max} = 435$ and 455 nm, respectively). The slight differences are attributed to changes in the linkers, i.e. carboxamide- vs. alkynyl-substituents. This is in agreement with the observation made previously with a duplex containing a phenanthrene antenna containing a covalently attached pyrene (S).^[36] In the present case, however, the acceptor dye is brought into proximity of the phenanthrene antenna in a non-covalent fashion.

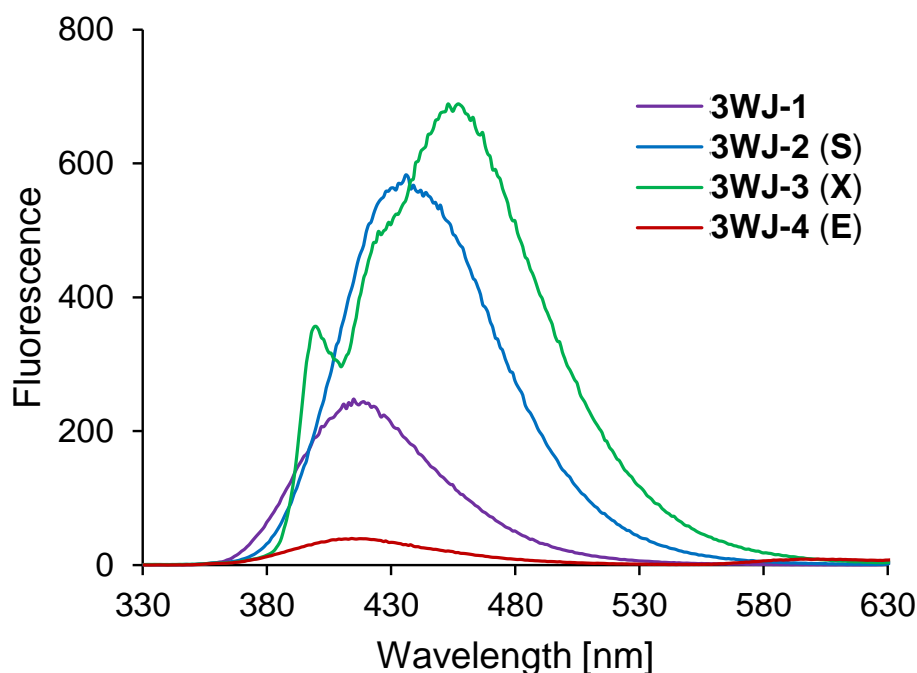


Figure 5.2. Fluorescence emission spectra of **3WJ-1**, **3WJ-2**, **3WJ-3** and **3WJ-4**. Conditions: see Figure 5.1; λ_{ex} : 320 nm; ex./em. slit: 5 nm. PMT voltage: 580 V.

A quantum yield of 0.21 (Table 5.1) is obtained for **3WJ-2**. Similar results are obtained with **3WJ-3**. However, some pyrene monomer fluorescence (peak at 400 nm and shoulder around 425 nm) is evident in addition to the exciplex emission. The total quantum yield for the 3WJ with the 1,6-dialkynylpyrene as acceptor dye is 0.32.

Table 5.1. T_M values and fluorescence quantum yields (Φ_F)^[a] of 3WJs.^[b]

	3WJ-1	3WJ-2	3WJ-3	3WJ-4	3WJ-5
Acceptor:	-	S	X	E	Cy
T_M (°C):	57	59	58	63	59
Φ_F ^[c]	0.10	0.21	0.32	0.02	0.06 ^[d]

[a] Standard: 2-aminopyridine; Appendix B for details.

[b] Conditions as in Figure 5.1.

[c] Phenanthrene excitation (320 nm).

[d] total Φ_F (1.5% from phenanthrene and 4.9% from Cy emission).

Irradiation of the control **3WJ-1**, which contains the phenanthrene stack but no acceptor chromophore, at 320 nm results in a broad, unstructured emission band centred around 415 nm, which is assigned to phenanthrene excimer fluorescence.^[37-40] Φ_F for **3WJ-1** was 0.10 (Table 5.1). This is considerably less than the values found for **3WJ-2** and **-3** (0.21 and 0.32) that contain a terminal pyrene chromophore.

In three-way junction **3WJ-4**, a perylenediimide unit is used in strand **c**. This chromophore quenches the phenanthrene excimer fluorescence to a considerable extent (Φ_F 0.02). The quenching effect^[41,42] is strong, but not as pronounced as in the case of pyrene excimer quenching by the same perylenediimide derivative.^[43] The reduced effect can be rationalized by a smaller spectral overlap in the present case (phenanthrene-perylenediimide) than between pyrene and perylenediimide.^[43]

The emission spectra obtained by direct excitation of the two pyrene acceptor dyes (S or X) are shown in Figure 5.3. Excitation was carried out at 370 nm, at which wavelength both pyrene derivatives absorb and phenanthrene excitation is negligible. Two aspects are noteworthy: i) the fluorescence intensities are significantly lower than after excitation of phenanthrene, which shows that the phenanthrene-pyrene 3WJ functions as a LHC; and ii) the fraction of monomer emission in **3WJ-3** is somewhat larger than after phenanthrene excitation (for comparison see Figure 5.2). Furthermore, direct excitation of control **3WJ-1** at 370 nm (Figure 5.3) results in no significant fluorescence.

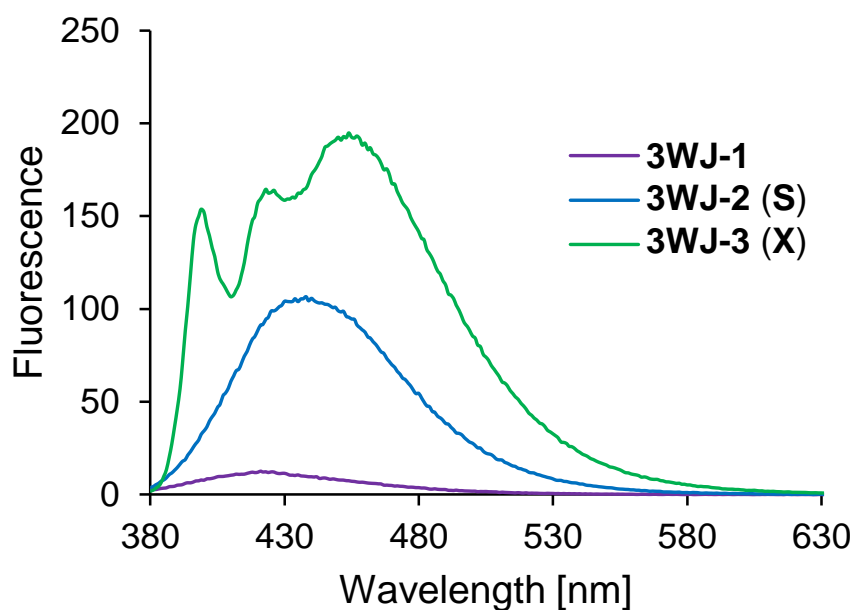


Figure 5.3. Fluorescence spectra of **3WJ-1**, **3WJ-2** and **3WJ-3**. Conditions: see Figure 5.1. Instrumental set-up as in Figure 5.2 (except for λ_{ex} : 370 nm).

Energy transfer is also observed from phenanthrenes to Cy. Figure 5.4 shows the effect of a stepwise build-up of **3WJ-5**. In this experiment, the phenanthrene antenna (i.e. a 1:1-mixture of strands **a** and **b**) is added stepwise to the acceptor dye (strand **g**). A gradual increase in Cy fluorescence is observed until antenna and acceptor are present in equimolar concentrations. Phenanthrene excimer emission is also present and grows parallel to Cy fluorescence. Further addition of the antenna beyond the 1:1-ratio does not result in additional growth of Cy fluorescence, while phenanthrene fluorescence grows proportionally. The quantum yields for P and Cy emission amount to 0.015 and 0.049, respectively (Table 5.1). Cy has no significant absorbance (see Appendix C) at the irradiation wavelength (320 nm) nor in the region of phenanthrene emission (360 – 530 nm).

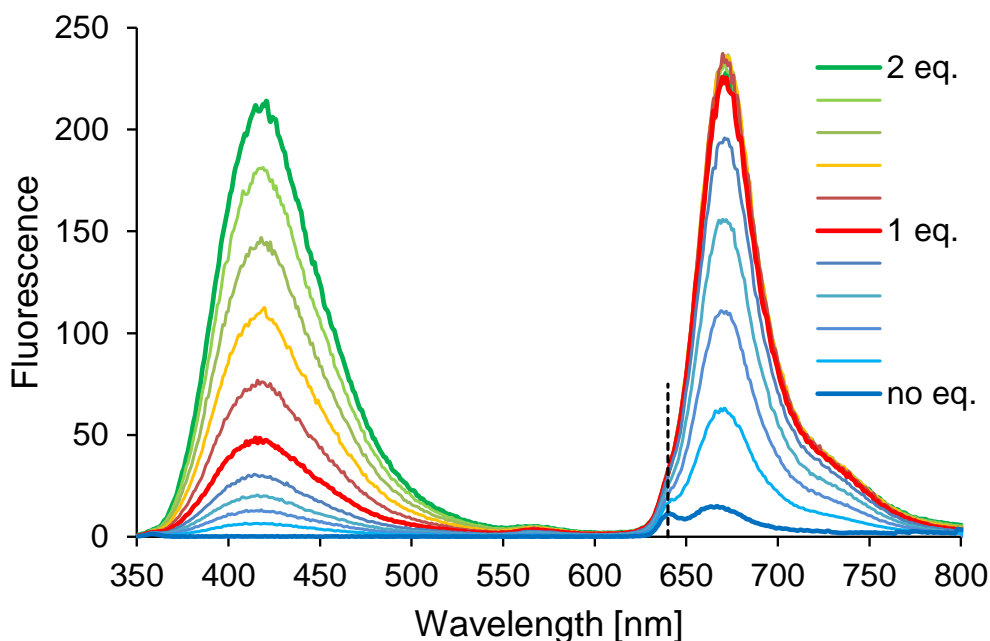


Figure 5.4. Build-up of **3WJ-5**: fluorescence spectra after stepwise addition of strands **a** and **b** (1:1-mixture) to single strand **g**. The two strands were pre-annealed and added in 0.2 molar equivalents; 5 minutes equilibration time was given before recording the spectrum; other conditions were as in Figure 5.2. Dashed marker indicates artefacts caused by the second order transmission of the monochromator.

As shown by the corresponding excitation spectra (Figure 5.5), phenanthrene excitation (320 nm) leads to Cy emission only in **3WJ-5** but not in single strand **g**.

These experiments demonstrate that Cy fluorescence in **3WJ-5** is due to energy transfer from the phenanthrenes.^[44] A Förster radius of ~ 26 Å is calculated (see Appendix C). Considering the dimensions of a typical 3WJ (~ 12 Å)^[45] as well as its inherent flexibility,^[45,46] energy transfer via FRET is, thus, possible. On the other hand, molecular contact between donor and acceptor is also feasible (as e.g. shown by exciplex formation in **3WJ-2** and **-3**) rendering also excitation transfer via Dexter electron exchange a plausible mechanism.^[41,47]

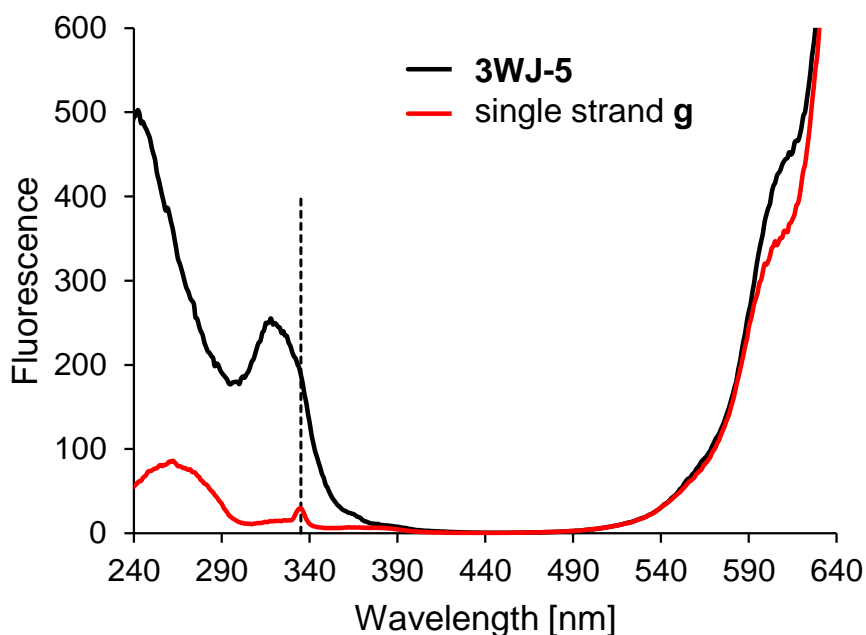


Figure 5.5. Fluorescence excitation spectra of **3WJ-5** and single strand **g**. Conditions: Figure 5.1; instrumental set-up: Figure 5.2, except for λ_{em} : 670 nm; dashed marker: see Figure 5.4.

Conclusions

The construction of LHCs on the basis of the DNA three-way junction resulted in stable, modular assemblies with programmable spectroscopic properties. The LHC is based on a modular construction in which a phenanthrene antenna is located in one of the three stems of the 3WJ and the acceptor is brought into proximity of the antenna through the annealing of the third strand. Phenanthrene excitation (320 nm) is followed by energy transfer to pyrene, perylenediimide or a cyanine dye. In case of pyrene, exciplex fluorescence is observed, whereas perylenediimide acts as a quencher. In the case of cyanine, energy transfer leads to cyanine fluorescence.

Experimental Section

For additional data and details see Appendix B.

Oligonucleotide-synthesis was performed by an automated oligonucleotide synthesis on a 394-DNA/RNA synthesizer (*Applied Biosystems*), based on phosphoramidite chemistry. The building blocks of the pyrene derivatives were synthesized according to previously described protocols^[48] as well as the phenanthrene^[49] and PDI^[50]. Cleavage from the solid support and final deprotection was done by an overnight treatment with 30% NH₄OH solution at 55°C. The Cy-phosphoramidite was obtained from *GlenResearch* (Sterling, USA), incorporation, cleavage and deprotection followed the *UltraMILD* procedure (*GlenResearch*). All unmodified strands were commercially obtained from *Microsynth* (Balgach, Switzerland).

Reversed-phase HPLC purification of the modified oligonucleotides was carried out on a LC-20AT system (*Shimadzu*, Kyoto, Japan) using a LiChrospher 100 RP18, 5 μ m column (*Dr. Maisch GmbH*, Ammerbuch, Germany) and a gradient consisting of eluent A (0.1 M triethylamine / acetic acid) and B (acetonitrile) with 5-50% B within 20 minutes.

Molecular mass of the synthesized oligonucleotides was determined by LC-MS (LC-20AT, SPD-M20A, LCMS-2010EV, all *Shimadzu*), with a C18 3.5 μ m 2.1x100 mm column (*XTerra MS*, *Waters*, Milford, USA) and an applied gradient of 100% A (50 mM ammonium formate) to 50% B (acetonitrile) over 10 minutes.

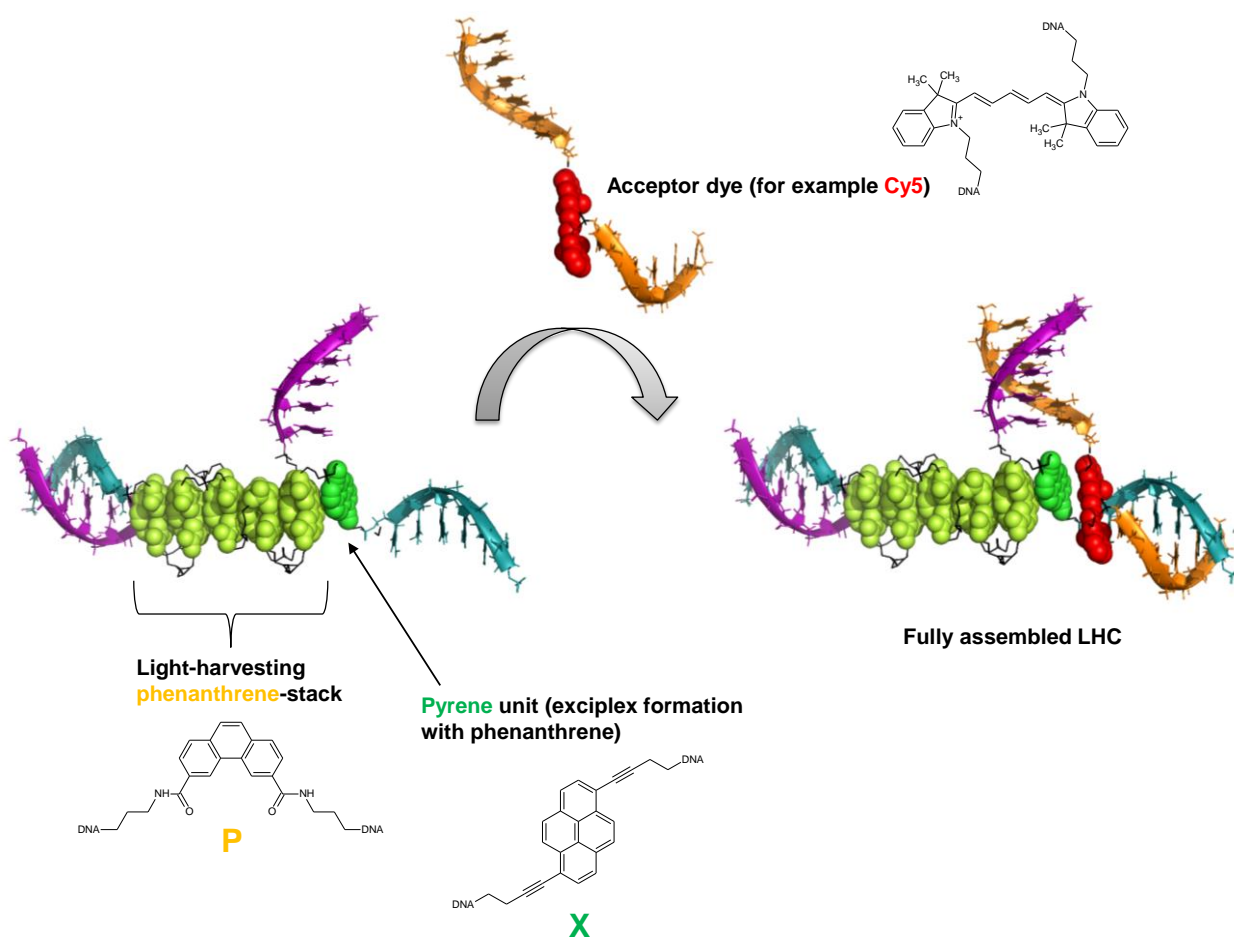
UV-Vis spectra were collected on a Varian Cary-100 Bio-UV / Visible spectrophotometer equipped with a Varian Cary-block temperature controller, 1 cm quartz cuvettes and processed with Varian WinUV software. Experiments were performed with samples prepared from 1 μ M single strand concentration in *Milli-Q* H₂O containing 100 mM NaCl and 10 mM sodium phosphate buffer (pH 7.0).

Fluorescence spectra were acquired on a Varian Cary Eclipse fluorescence spectrophotometer equipped with a Varian Cary-block temperature controller with 1 cm x 1 cm quartz cuvettes and Varian Eclipse software. Instrumental setups for fluorescence emission and excitation spectra were: $\lambda_{ex} / \lambda_{em}$: according to description in the corresponding figure; excitation slit width: 5 nm; emission slit width: 5 nm; PMT voltage: 580 V. Samples treated as mentioned above.

Chapter 5b - A modular LHC built on the DNA 3WJ with an “always-on” Exciplex

Results and Discussion

In contrast to the design of the LHC described in Chapter 5a, here a light-harvesting phenanthrene-stack and a pyrene with the ability to form an exciplex with a phenanthrene upon excitation (of either of the chromophores), form the “stem” of the LHC (Scheme 5.2).



Scheme 5.2. Two strands of the three-way junction form the light-harvesting part (phenanthrenes) and attached to one of them is the pyrene. The exciplex is formed between an excited phenanthrene and the pyrene (or vice versa). Upon hybridization of the third strand (containing an acceptor chromophore), the energy of the exciplex can be transferred to the acceptor and its corresponding emission is observed.

Table 5.2. Summary of the samples that were investigated. For the chemical structures of the chromophores and the letter code, see Scheme 5.1 (Chapter 5a) and Scheme 5.2.

Light-harvesting stem	Acceptor	Sample
	GTT CCA CGC T-A CGT TCC TTC	3WJ-6
GAA GGA ACG T PP PPP ACA CTC GCA G	GTT CCA CGC T X A CGT TCC TTC	3WJ-7
CTG CGA GTG T PP PPP X AG CGT GGA AC	GTT CCA CGC T Cy A CGT TCC TTC	3WJ-8
	GTT CCA CGC T E A CGT TCC TTC	3WJ-9

3WJ-6 contains an “empty” third strand and is the basic construct of the LHC. In contrast, **3WJ-7** carries an additional alkynylpyrene (X) in the third strand (acceptor strand). The absorption pattern of these two samples is shown in Figure 5.6. The influence of the second alkynylpyrene in **3WJ-7** is noticeable in the range of 240 – 280 nm (i.e. the area of the nucleobases) and between 340 – 400 nm (the characteristic vibronic bands of alkynylpyrene)^[48]. The absorption range of the phenanthrenes (300 – 340 nm) is for both samples almost identical since the pyrenes are not active in this area.

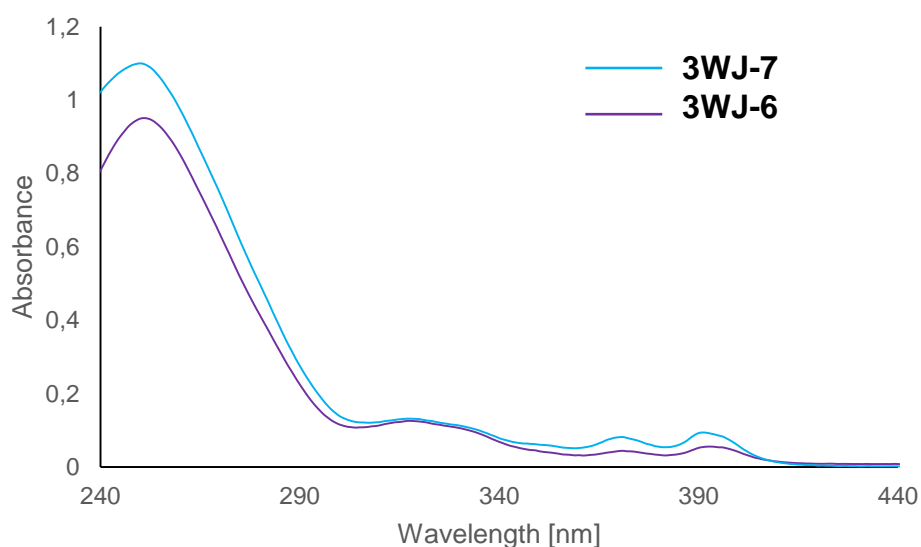


Figure 5.6. UV/Vis spectra of **3WJ-6** and **3WJ-7**. Conditions: 1 μ M single strand concentration, 20°C, 100 mM NaCl, 10 mM sodium phosphate buffer, pH 7.0.

Excitation of **3WJ-6** and **3WJ-7** at 320 nm (phenanthrenes) leads in both cases to strong exciplex emission (with a maximum λ_{em} around 450 nm).

The similar construct discussed in Chapter 5a (3WJ-3) shows the same behavior. The excitation spectra for **3WJ-6** and **3WJ-7** is given in Figure 5.7. The exciplex emission results from both phenanthrene and pyrene excitation.

In addition, the comparison of the two spectra demonstrates the impact of the second alkynylpyrene (**3WJ-7**) attached to the LHC. By exciting the phenanthrenes in **3WJ-7** the exciplex emission is lower than for **3WJ-6**, however, excitation of the pyrenes (**3WJ-7**) produces a slightly higher signal. This is somehow unexpected based on the assumption that the two pyrenes are in close range and the pyrene in the acceptor strand is further away from the phenanthrene stack than the other one. Therefore, the two pyrenes may form an excimer in case of pyrene excitation.^[48]

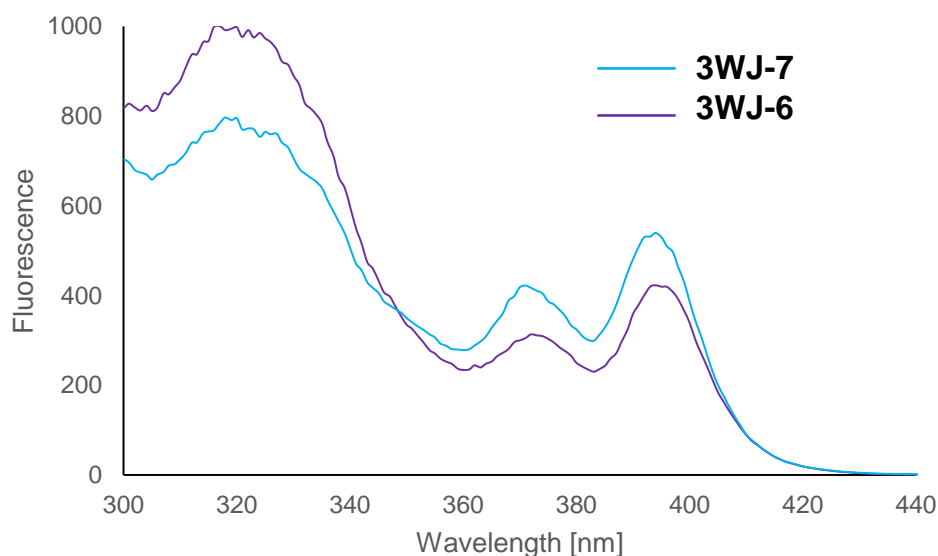


Figure 5.7. Fluorescence excitation spectra of **3WJ-6** and **3WJ-7**. Conditions: see Figure 5.6; instrumental set-up: emission wavelength: 450 nm, excitation slit width: 5 nm; emission slit width: 5 nm; PMT voltage: 600 V.

Though a closer look at the fluorescence emission spectra of **3WJ-7** (Figure 5.8) does not show a major peak at 520 nm (expected λ_{em} of pyrene excimer). In fact, excitation at 320 nm (phenanthrenes) or 390 nm (pyrenes) leads to an almost identical shape of the peak that corresponds to the exciplex emission.

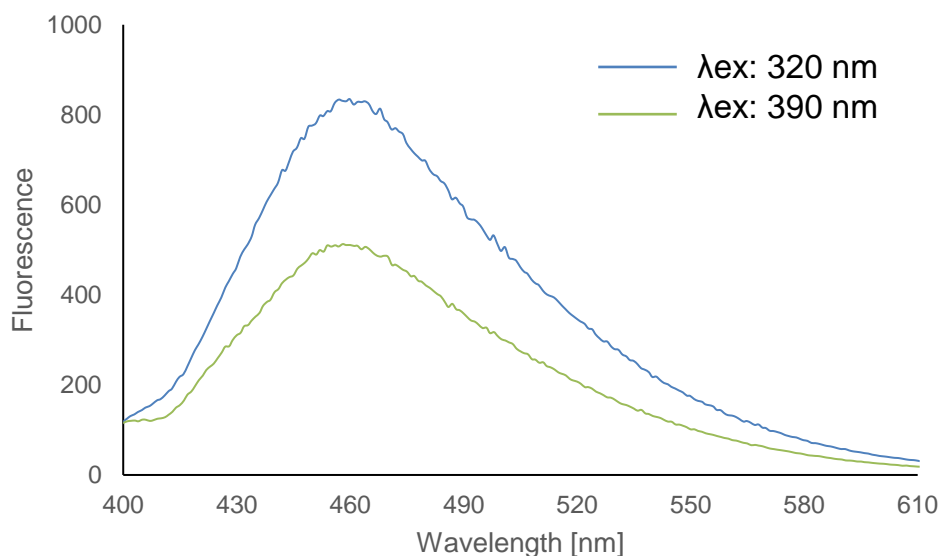


Figure 5.8. Fluorescence emission spectra of **3WJ-7**. Conditions: see Figure 5.6; instrumental set-up: excitation wavelength: see legend, excitation slit width: 5 nm; emission slit width: 5 nm; PMT voltage: 600 V.

Furthermore, a comparison between **3WJ-6** and **3WJ-7** both excited at 390 nm (λ_{abs} of pyrene) reveals a shoulder at 420 nm in the emission spectrum of **3WJ-6** originating from pyrene monomer emission (Figure 5.9). Overall it seems: i) that the introduction of a second pyrene (**3WJ-7**) through the hybridization of the third (acceptor) does only enhance the exciplex formation if direct excitation of the pyrenes occurs; ii) no clear evidence of pyrene excimer formation is present.

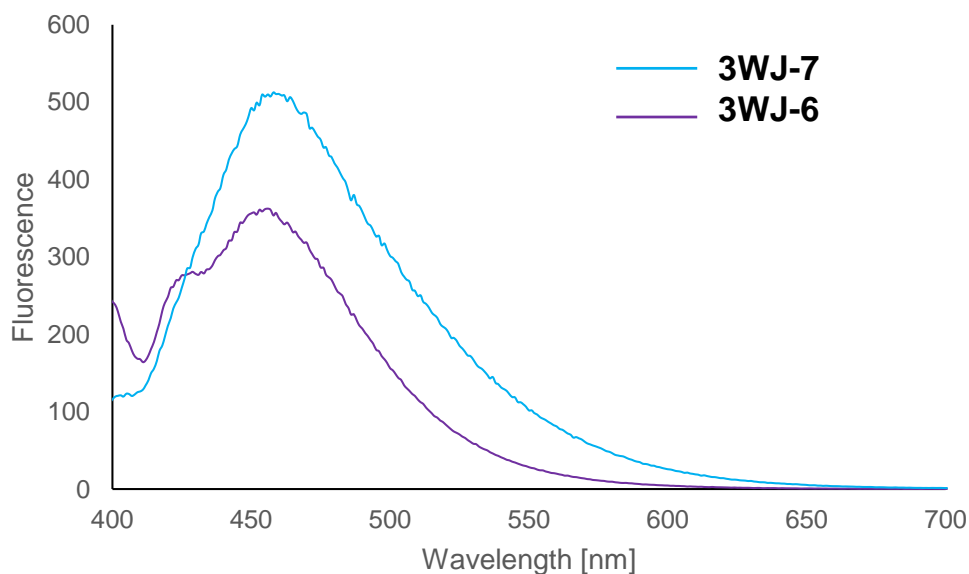


Figure 5.9. Fluorescence emission spectra of **3WJ-6** and **3WJ-7**. Conditions: see Figure 5.6; instrumental set-up: see Figure 5.8, except for λ_{ex} : 390 nm.

Changing the subject to the last two 3WJs presented here, **3WJ-8** and **3WJ-9**, we observe the presence of all chromophores in the UV/Vis absorption spectrum (Figure 5.10): the phenanthrenes (max. λ_{abs} : 320 nm), the alkynylpyrene (max. λ_{abs} : 390 nm), perylenediimide (PDI or E, λ_{max} around 560 nm) and the cyanine (Cy, λ_{max} around 650 nm).

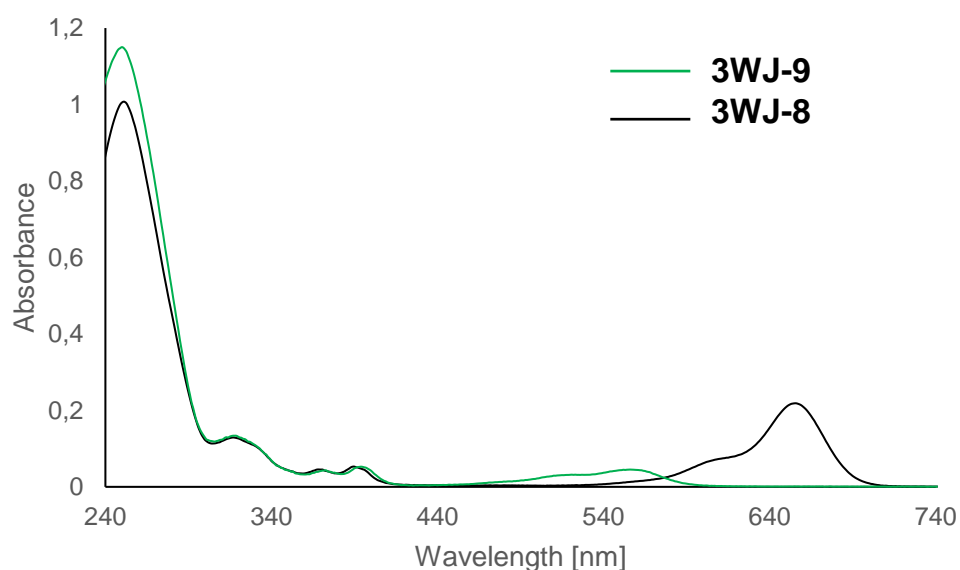


Figure 5.10. UV/Vis spectra of **3WJ-8** and **3WJ-9**. Conditions: see Figure 5.6.

As shown in the fluorescence emission spectra (Figure 5.11), excitation / emission of the cyanine is either possible via excitation of the phenanthrenes or the pyrene. Either way the result looks similar to 3WJ-5 of Chapter 5a (Figure 5.4). Except that for **3WJ-8** remaining phenanthrene-pyrene exciplex emission (around 450 nm) is observed instead of phenanthrene excimer emission.

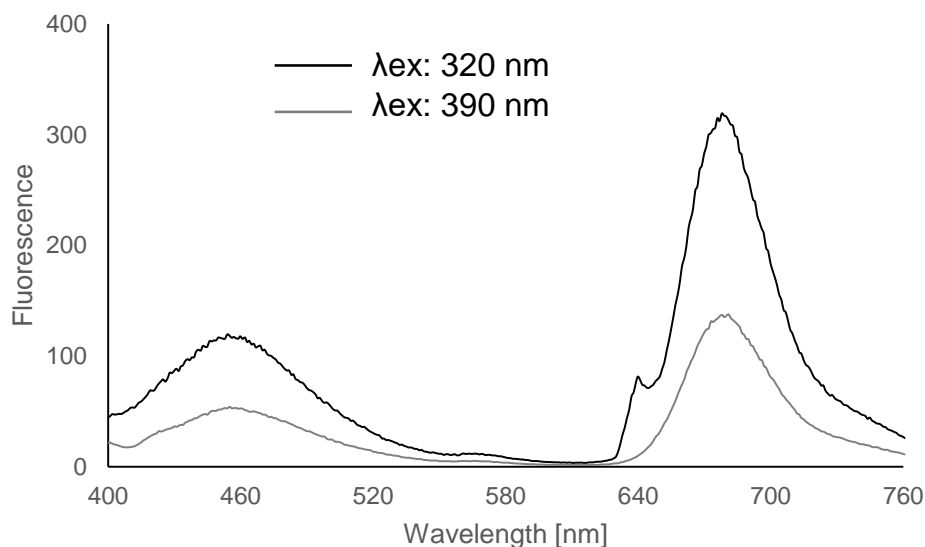


Figure 5.11. Fluorescence emission spectra of **3WJ-8**. Sharp peak at 640 nm ($\lambda_{ex}: 320$ nm) indicates artefacts caused by the second order transmission of the monochromator. Conditions: see Figure 5.6; instrumental set-up: see Figure 5.8, except for λ_{ex} : see legend.

A comparison between the two cyanine containing 3WJs 3WJ-5 (from Chapter 5a) and **3WJ-8** was made (Figure 5.12). Interestingly, a shift of the maximum λ_{em} of cyanine takes place as shown in Figure 5.12. As for other chromophores, this may be a result of a change in the molecular environment of the chromophore (e.g. change in orientation / aggregation).^[51]

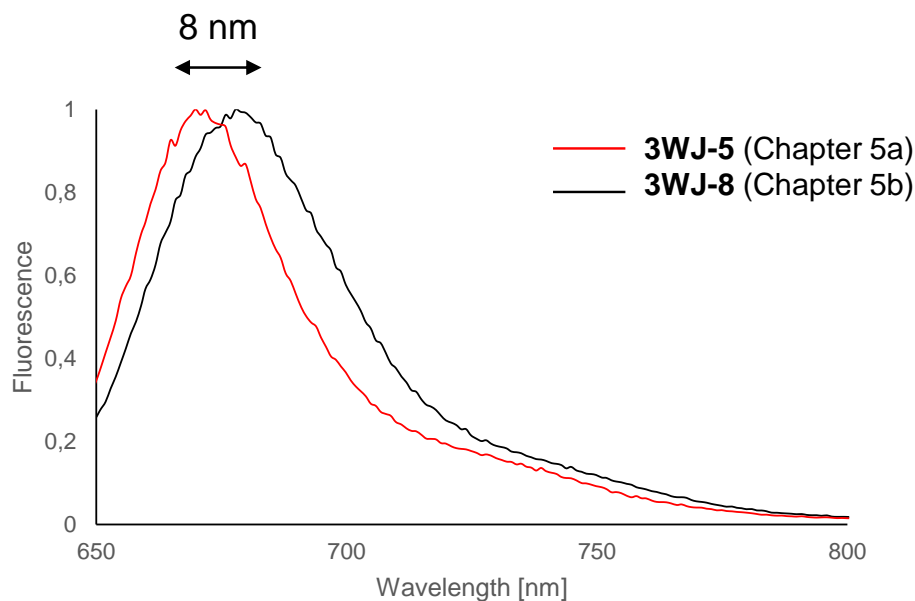


Figure 5.12. Fluorescence emission spectra of 3WJ-5 (Chapter 5a) and **3WJ-8** (Chapter 5b) normalized at max. λ_{em} of the cyanine dye. Conditions: see Figure 5.6; instrumental set-up: see Figure 5.8, except for λ_{ex} : 320 nm.

Since the cyanine dye can be excited by the phenanthrenes only (Chapter 5a) without the need of an additional pyrene as it is present in case of **3WJ-8**, an energy transfer from the excited phenanthrenes directly to the cyanine, or via phenanthrene-pyrene exciplex is at the same time possible.

An energy transfer is possible for both **3WJ-8** and **3WJ-9** and reduces the exciplex emission dramatically (Figure 5.13). As noted in Chapter 5a, perylenediimide acts as quencher, this is also the case in **3WJ-9**. Because of the red-shift of the phenanthrene-excimer compared to the phenanthrene excimer (see Chapter 5a), the emission of the exciplex ranges overall closer to the absorption area of the perylenediimide. Thus, a more severe quenching effect was expected to happen. A direct comparison between 3WJ-4 (Chapter 5a) and **3WJ-9** may be rather difficult to interpret, but the ratio of the remaining excimer emission of 3WJ-4 and 3WJ-5 (both Chapter 5a) and the remaining exciplex emission of **3WJ-8** and **3WJ-9** may be of help. In the first case (3WJ-5 compared to 3WJ-4) a decrease of the excimer emission of about 1.2fold is observed, whereas for the exciplex in **3WJ-9** compared to **3WJ-8** a decrease of 2.2fold is calculated. Taken together, this may be hint for the rather unfavorable arrangement

(for an energy transfer that leads to fluorescence emission) of the acceptor chromophore present in **3WJ-8** and **3WJ-9**.

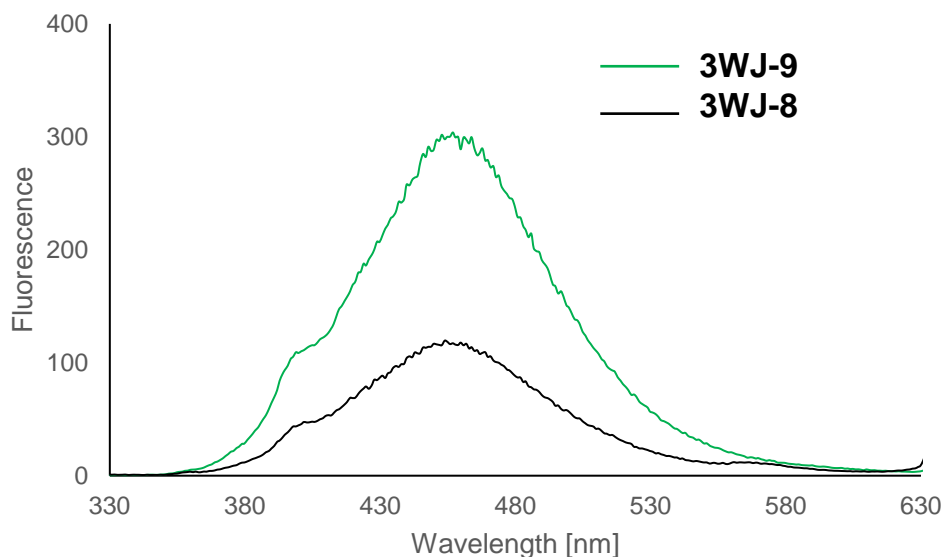


Figure 5.13. Fluorescence emission spectra of **3WJ-8** and **3WJ-9**. Conditions: see Figure 5.6; instrumental set-up: see Figure 5.8, except for λ_{ex} : 320 nm.

Conclusions

The formation of the phenanthrene-pyrene exciplex (**3WJ-6**) was expected since the units are covalently linked to each other. There is also evidence that the acceptor chromophore, introduced in the third strand, interact with the other chromophores of the LHC (e.g. energy transfer) due to the overall change of the spectroscopic outcome. Yet it is unclear how the strands (more importantly the chromophores they contain) are arranged, because the data provided here are not sufficient to help clarify this question. Pyrene excimer emission seems to be almost inexistent (**3WJ-7**); energy transfer from the phenanthrenes-pyrene to the cyanine is observed (**3WJ-8**) yet can be achieved with or without the pyrene; and quenching by the perylenediimide is not as pronounced as expected. As a consequence of these results, the use of the LHC design described in Chapter 5a is more promising.

Experimental Section

Oligonucleotide-synthesis was performed by an automated oligonucleotide synthesis on a 394-DNA/RNA synthesizer (*Applied Biosystems*), based on phosphoramidite chemistry. The building blocks of the pyrene derivative was synthesized according to previously described protocol^[48] as well as the phenanthrene^[49] and PDI^[50]. Cleavage from the solid support and final deprotection was done by an overnight treatment with 30% NH₄OH solution at 55°C. The Cy-phosphoramidite was obtained from *GlenResearch* (Sterling, USA), incorporation, cleavage and deprotection followed the *UltraMILD* procedure (*GlenResearch*). All unmodified strands were commercially obtained from *Microsynth* (Balgach, Switzerland).

Reversed-phase HPLC purification of the modified oligonucleotides was carried out on a LC-20AT system (*Shimadzu*, Kyoto, Japan) using a LiChrospher 100 RP18, 5 μm column (*Dr. Maisch GmbH*, Ammerbuch, Germany) and a gradient consisting of eluent A (0.1 M triethylamine / acetic acid) and B (acetonitrile) with 5-50% B within 20 minutes.

Molecular mass of the synthesized oligonucleotides was determined by LC-MS (LC-20AT, SPD-M20A, LCMS-2010EV, all *Shimadzu*), with a C18 3.5 μm 2.1x100 mm column (XTerra MS, *Waters*, Milford, USA) and an applied gradient of 100% A (50 mM ammonium formate) to 50% B (acetonitrile) over 10 minutes.

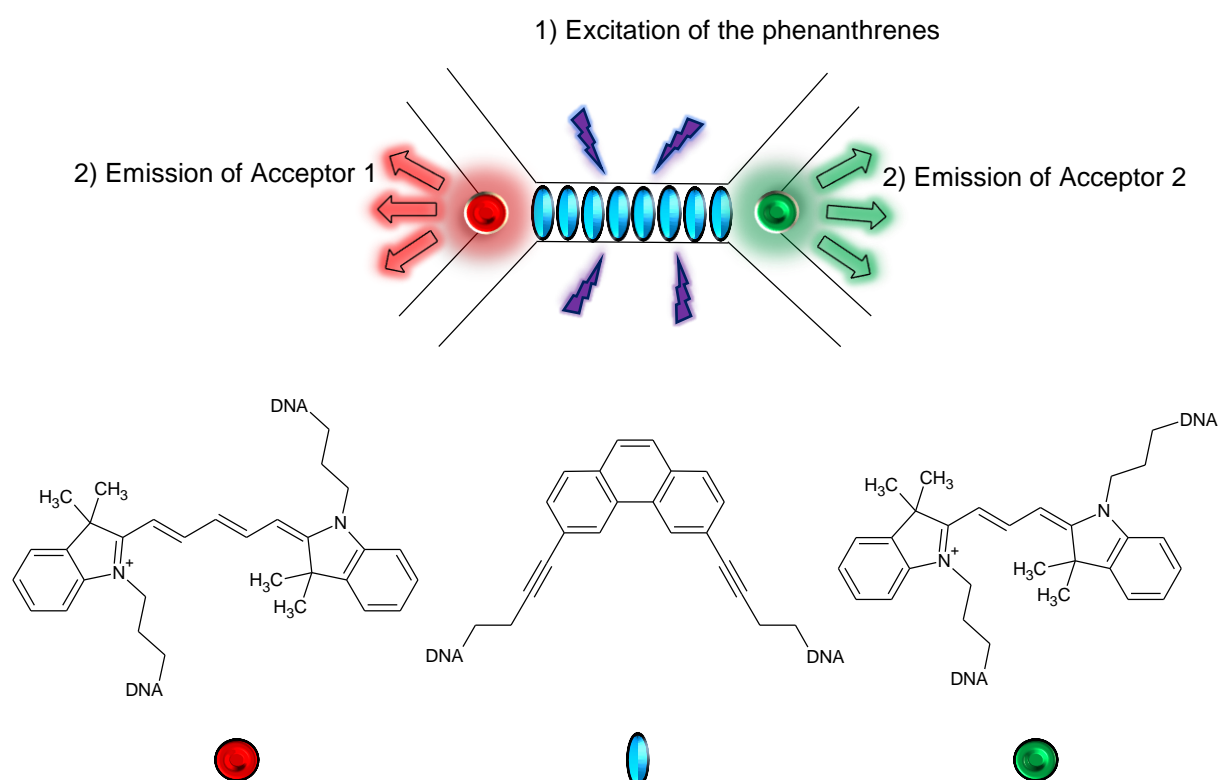
UV-Vis spectra were collected on a Varian Cary-100 Bio-UV / Visible spectrophotometer equipped with a Varian Cary-block temperature controller, 1 cm quartz cuvettes and processed with Varian WinUV software. Experiments were performed with samples prepared from 1 μM single strand concentration in *Milli-Q* H₂O containing 100 mM NaCl and 10 mM sodium phosphate buffer (pH 7.0).

Fluorescence spectra were acquired on a Varian Cary Eclipse fluorescence spectrophotometer equipped with a Varian Cary-block temperature controller with 1 cm x 1 cm quartz cuvettes and Varian Eclipse software. Instrumental setups for fluorescence emission and excitation spectra were: $\lambda_{\text{ex}} / \lambda_{\text{em}}$: according to description in the corresponding figure; excitation slit width: 5 nm; emission slit width: 5 nm; PMT voltage: 600 V. Samples treated as mentioned above.

Chapter 6 – A modified DNA bis-3WJ as a scaffold for a LHC

Aim of the Work

The goal of this study is to form an H-shaped DNA structure (basically a “paired” three-way junction or bis-3WJ) that contains an array of light-absorbing phenanthrenes in the part connecting the two junctions. The design of the sequences allow the controlled hybridization of two different acceptor-strands.

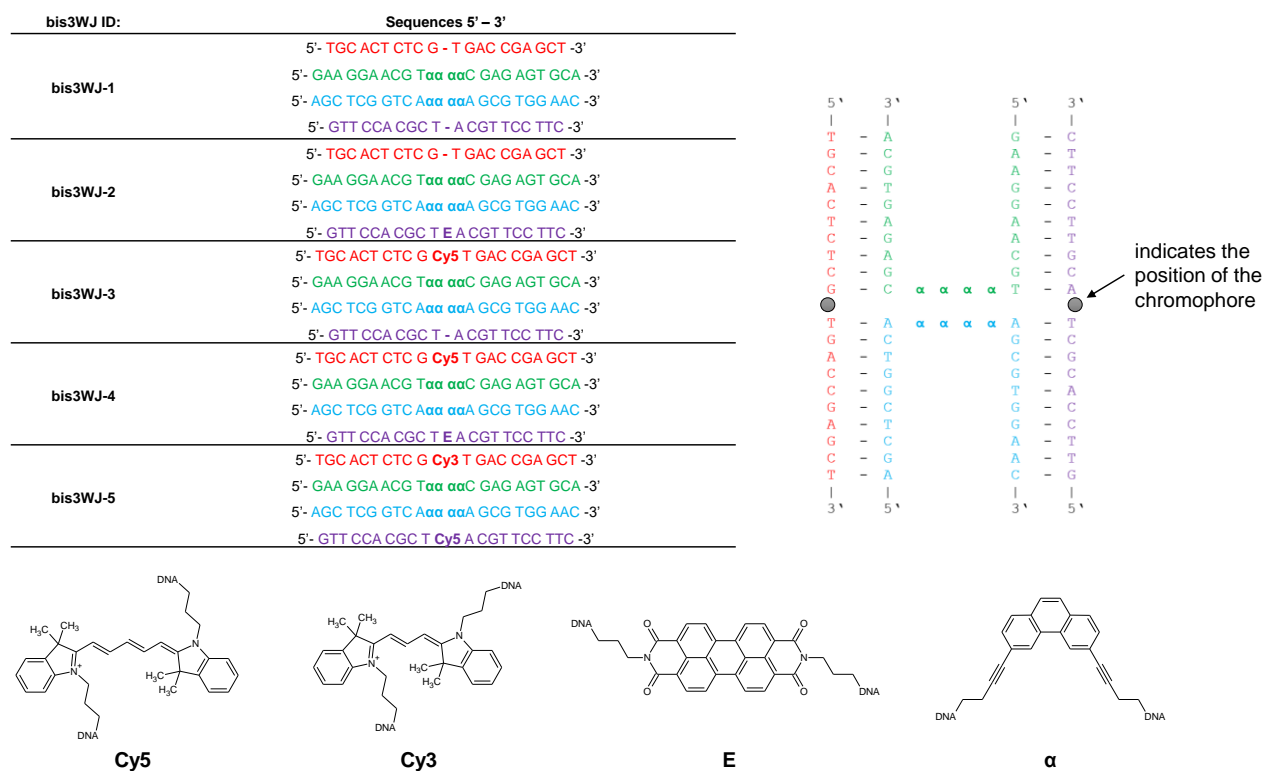


Introduction

Except for the design and the use of a different phenanthrene derivative as light-harvester, the underlying concept of this work is the same as in Chapter 5 and similar to published work, which all can be summarized as “DNA-Based Oligochromophores as Light-Harvesting Systems”.^[1-5] However, initial thoughts included the idea to use the system as a “tunnel” to transfer energy from a donor to the phenanthrenes and then to the acceptor or furthermore to drive a chemical reaction.^[6,7] This was not achieved due to the lack of a suitable donor-acceptor pair. In its current state the system described in this chapter is a multichromophoric acceptor-donor-acceptor complex.^[8-11]

Results and Discussion

The design of the sequences, the building blocks and the samples of this chapter are shown in Scheme 6.1.



Scheme 6.1. The bis-3WJs and their corresponding strands are given on the left, the predicted hybridization of the strands is shown on the right and the chromophores are listed below.

The first sample, **bis3WJ-1** contains the strands that form the basic construct of the light-harvesting part (modified with α , the bisalkynylphenanthrenes) and two additional unmodified DNA strands. The lowest energy bands visible in the UV/Vis spectrum of this bis-3-way junction are between 300 – 340 nm. These bands are characteristic for alkynylphenanthrene and are present in all samples, as shown in Figure 6.1.^[12] The influence of the additional perylene-3,4,9,10-tetracarboxylic diimide (PDI, E) in **bis3WJ-2** and **bis3WJ-4** on the absorption spectra (range of 460 – 590 nm) is noticeable as well.^[4] And there is the prominent peak arising from the cyanine dye (Cy5) with a λ_{\max} of 660 nm, in **bis3WJ-3** and **bis3WJ-4**.^[13,14]

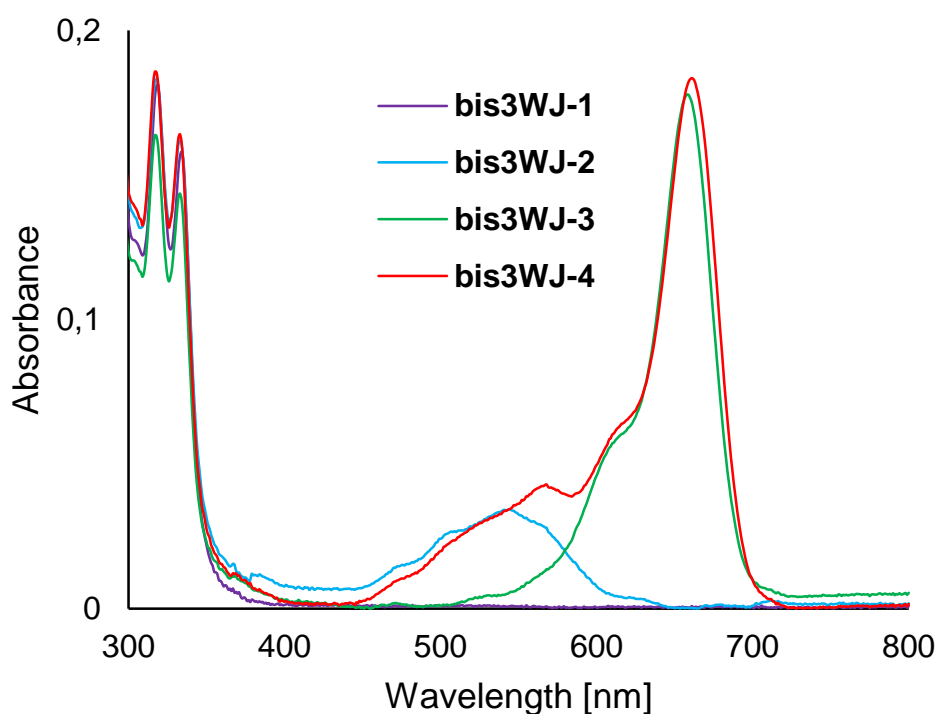


Figure 6.1. UV/Vis spectra of **bis3WJ-1** to **bis3WJ-4**. Not shown is the absorption-range below 300 nm. Conditions: 1 μM single strand concentration, 20°C, 100 mM NaCl, 10 mM sodium phosphate buffer, pH 7.0.

Based on the UV/Vis data a wavelength of 320 nm was chosen to excite the phenanthrenes in all samples. This leads, in case of **bis3WJ-1**, to emission of the phenanthrenes with a maximum λ_{em} of 400 nm. This emission is significantly higher than for **bis3WJ-2**, which contains a PDI in one of the “acceptor” strands (see Figure 6.2). This may be well explained by the fact that PDI is known to quench fluorescence in similar environments as in the present case.^[15,16]

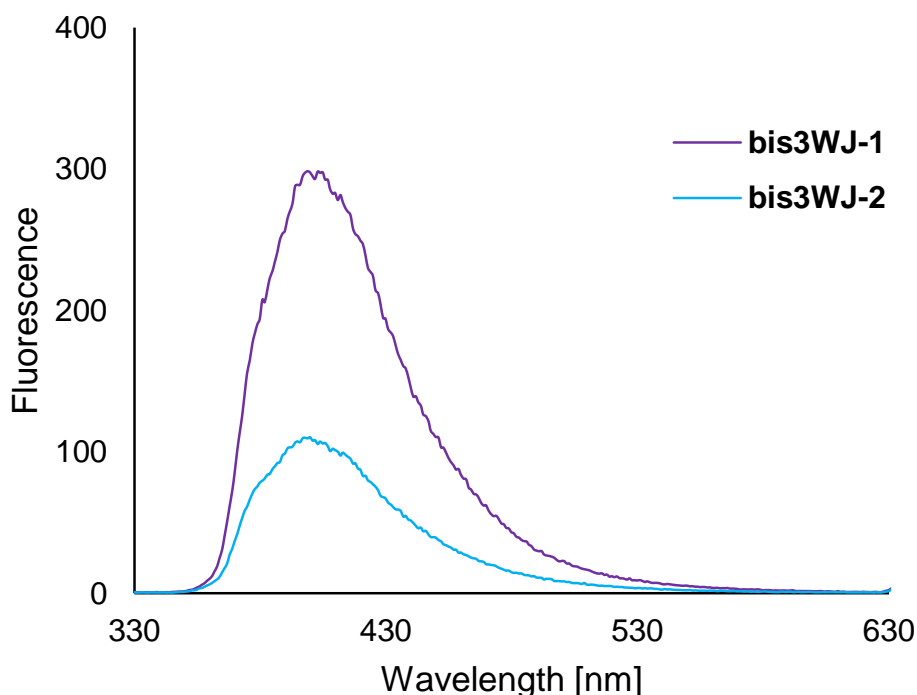


Figure 6.2. Fluorescence spectra of **bis3WJ-1** and **bis3WJ-2**. Conditions: see Figure 6.1; instrumental set-up: excitation wavelength: 320 nm, excitation slit width: 5 nm; emission slit width: 5 nm; PMT voltage: 600 V.

Instead of a quencher molecule as in **bis3WJ-2**, in **bis3WJ-3** a cyanine dye takes the role of the acceptor. Although the gap between the phenanthrene emission around 400 nm and the absorption range of the cyanine (above 500 nm) is rather large compared to common FRET Donor/Acceptor pairs,^[17,18] there is evidently an energy transfer from the phenanthrenes to the cyanine (see Figure 6.3).^[4] It has to be mentioned that the exact mechanism that finally leads to emission of the cyanine is not known and FRET may be the wrong explanation here. The same goes for **bis3WJ-4** that is the first example in this chapter of a modified DNA bis-three-way junction containing two acceptors separated through an array of phenanthrenes. One acceptor is the PDI and the other one the cyanine (Cy5). As shown in Figure 6.3, the direct comparison between **bis3WJ-4** (PDI and Cy5 as acceptors) and **3WJ-3** (only Cy5 as acceptor) reveals the influence of the quencher (PDI) on the fluorescence outcome. The residual emission from the phenanthrenes (λ_{max} : 400 nm) is in both samples of similar intensity, whereas the emission of the cyanine is considerably reduced in case of **bis3WJ-4**.

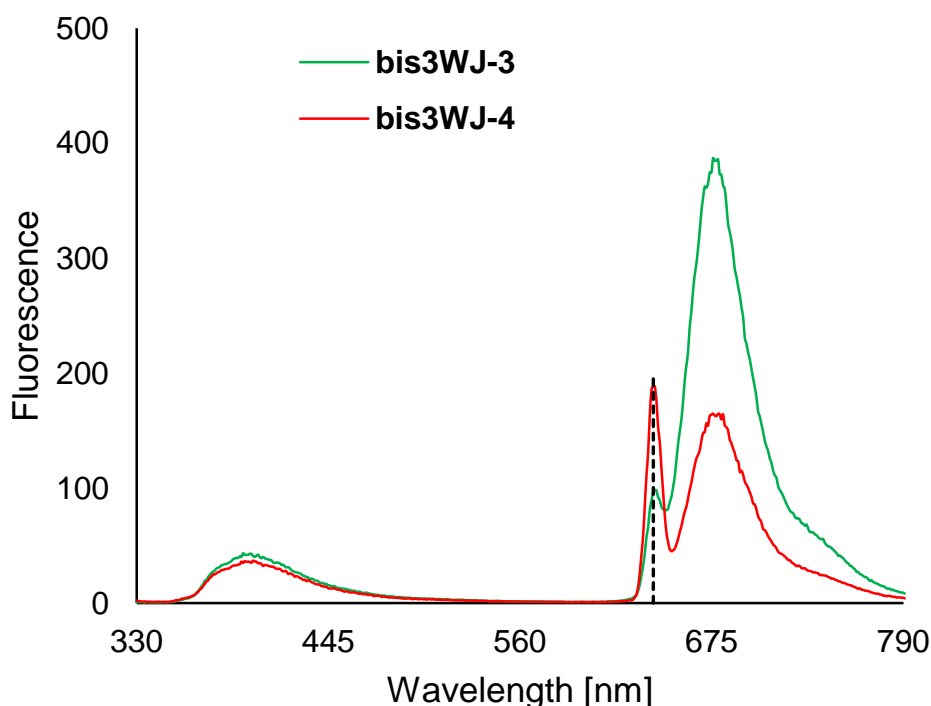


Figure 6.3. Fluorescence spectra of **bis3WJ-3** and **bis3WJ-4**. Conditions: see Figure 6.1; instrumental set-up: see Figure 6.2. The dashed line at 640 nm indicates artefacts caused by the second order transmission of the monochromator.

The last bis-3-way junction herein presented is **bis3WJ-5**. This construct does also contain two acceptors (Cy3 and Cy5) in their respective strands that are also known to be a suitable FRET pair.^[17,18] The normalized UV/Vis and fluorescence emission spectra are given in Figure 6.4. In addition to the absorption peaks of the phenanthrenes and Cy5 mentioned before, the Cy3 in **bis3WJ-5** shows its presence with a peak at 500 – 550 nm.^[17,18] The fluorescence spectrum of the same sample on the other hand, results in strong emission of both cyanine dyes (λ_{\max} of Cy3: 570 nm and λ_{\max} of Cy5: 680 nm). Although there was the probability that an excited Cy3 may lead to further emission of the Cy5 (via FRET), the intensity of the Cy5 emission in case of **bis3WJ-3** (that contains only a Cy5) is about the same as for **bis3WJ-5** (see Appendix C). Direct excitation of Cy3 (**bis3WJ-5**) does not alter the emission of the Cy5 severely (though it results in a slightly higher signal, see Appendix C).

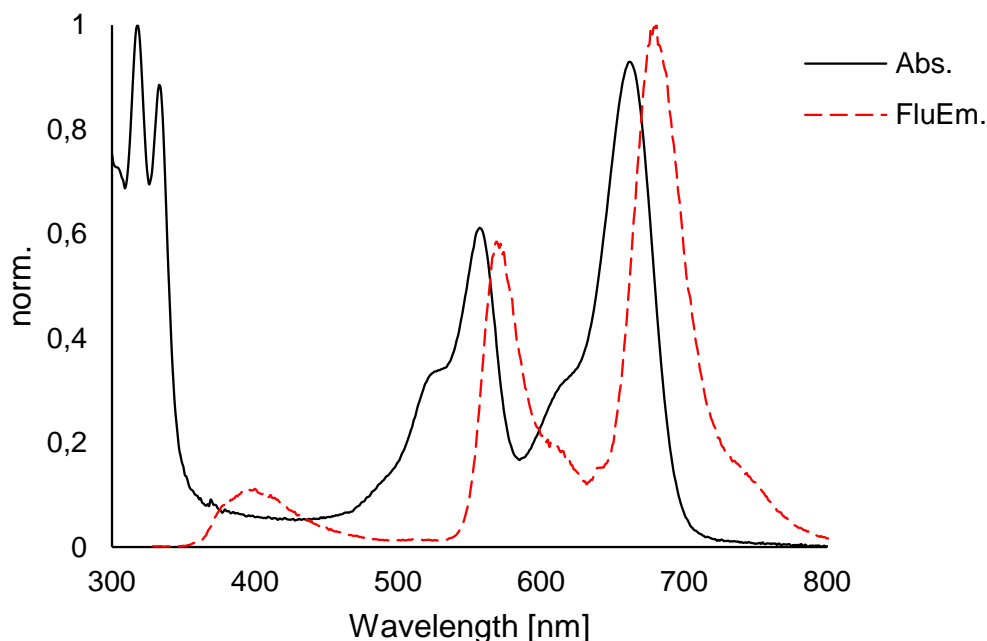


Figure 6.4. Normalized (highest peak set to 1.0) absorption and fluorescence spectra of **bis3WJ-5**. Conditions: see Figure 6.1; instrumental set-up: see Figure 6.2.

Interestingly, the incorporation of chromophores into the “acceptor” strands (compared to “empty” ones) and the subsequent formation of the corresponding bis3WJ results in major stabilization of the structure. Therefore, for **bis3WJ-1** a melting temperature of about 48°C is determined, whereas for both **bis3WJ-4** and **bis3WJ-5** an increase of approximately +12°C is measured (melting curves, see Appendix C).

Conclusions

The modified DNA bis-3way junctions discussed in this chapter consist of a central structure built around two DNA strands containing non-nucleosidic, alkynylphenanthrenes. Due to complementary base pairing the hybridization of two strands that can contain additional chromophores results in formation of the complete structure (the bis3WJ). In this study perylenediimide and cyanine dyes (Cy3 and Cy5) were used as acceptor chromophores. Excitation of the phenanthrenes was followed by energy transfer to the attached acceptors. The use of a DNA-based bis-three-way junction as the structural design of the light-harvesting complexes (or multichromophoric donor/acceptor assemblies) proofed to be a useful tool for the formation of stable constructs containing two separate acceptor chromophores.

Experimental Section

For details and additional data see Appendix C.

The modified oligomers were synthesized by automated oligonucleotide synthesis using an adapted synthetic procedure on a 394-DNA/RNA synthesizer (*Applied Biosystems*) and previously described protocols for the phosphoramidite building blocks. The Cy-phosphoramidites were obtained from *GlenResearch* (Sterling, USA), incorporation, cleavage and deprotection followed the *UltraMILD* procedure (*GlenResearch*). Purification was performed by RP-HPLC. Oligonucleotide masses were determined by LC-MS. All unmodified strands were commercially obtained from *Microsynth* (Balgach, Switzerland).

UV-Vis spectra were collected on a Varian Cary-100 Bio-UV / Visible spectrophotometer equipped with a Varian Cary-block temperature controller, 1 cm quartz cuvettes and processed with Varian WinUV software. Experiments were performed with samples prepared from 1 μM single strand concentration in *Milli-Q* H₂O containing 100 mM NaCl and 10 mM sodium phosphate buffer (pH 7.0).

Thermal denaturation curves were recorded on the same device (same conditions), the absorption at 260 nm was monitored for three ramps (cooling-heating-cooling cycles in the temperature range of 20°C – 90°C; gradient of 0.5°C/min).

Fluorescence spectra were acquired on a Varian Cary Eclipse fluorescence spectrophotometer equipped with a Varian Cary-block temperature controller with 1 cm x 1 cm quartz cuvettes and Varian Eclipse software. Instrumental setups for fluorescence emission spectra were: λ_{ex} : according to description in the corresponding figure; excitation slit width: 5 nm; emission slit width: 5 nm; PMT voltage: 600 V. Samples treated as mentioned above.

Chapter 7 – Crystal structures of modified DNA

Aim of the Work:

Modified DNA strands alter the properties of natural nucleic acids in unique ways as shown in the previous chapters. The Incorporation of non-nucleosidic dialkynylpyrenes and phenanthrenes into oligonucleotides, resulting in highly fluorescent constructs, are such examples. In this chapter does the DNA not only serve as a scaffold for the molecular organization of the chromophores, but it also provides a recognition site for the binding of an endonuclease.

The goal of this study is to solve the structure of modified DNA strands containing non-nucleosidic building blocks. To do so, the synthetic DNA duplexes have to be recognized and bound by the recombinant binding domain of a selected restriction enzyme. Co-crystallization and X-ray structural analysis should then reveal the spatial arrangement of the chromophores.

Introduction

As mentioned in Chapter 3, there are several ways to modify DNA (as for nucleic acids in general). The 3D molecular structure of modified DNA strands is especially of interest to explain their physical, chemical and biological properties. Unfortunately these crystal structures or NMR solution structures are usually limited to natural (or unnatural) base modifications or alterations of the sugar ring.^[1-4] To gain insights into the mechanism of enzymes and their DNA substrates, solved by co-crystallization and X-Ray Diffraction (which is still the method of choice for that matter), is another field where structural information about (modified) nucleic acids is obtained.^[5-9] Though there are examples of NMR and crystal structures of pyrene and phenanthrene derivatives covalently attached to the DNA, they do not compare well with the non-nucleosidic building blocks described in the previous chapters.^[10]

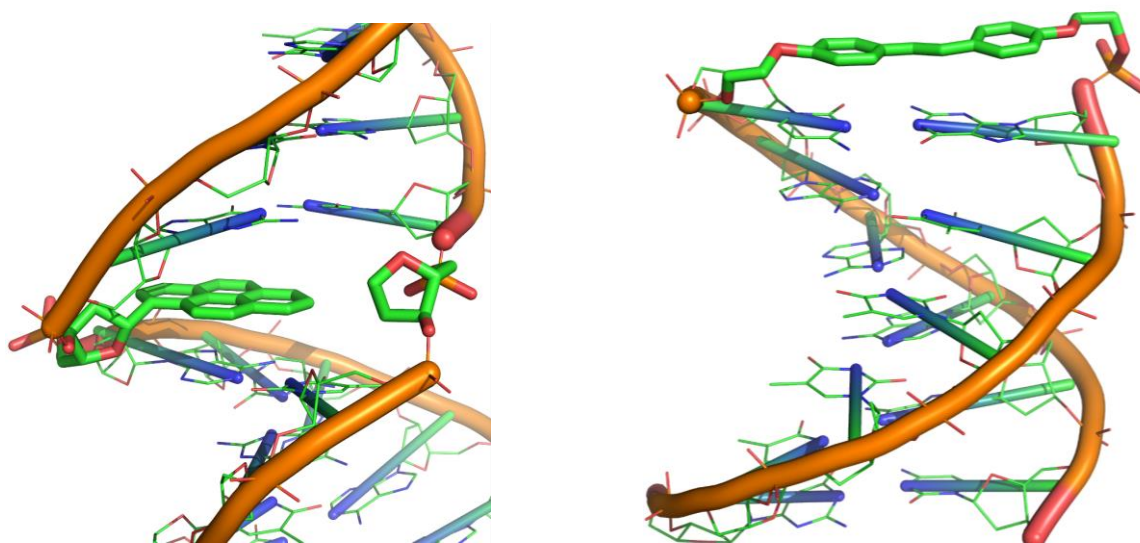


Figure 7.1. NMR structure of a DNA with a pyrene molecule opposite of an abasic site (left, based on RCSB PDB entry 1FZL) and crystal structure of a DNA hairpin with a stilbenediether linker (right, based on RCSB PDB entry 1PUY).

The successful crystallization required the careful choice of a suitable DNA-binding protein. For that matter, the RCSB Protein Data Bank was searched for mixed protein-DNA type polymers.^[5] The two most prominent classes are: the transferases (e.g. DNA polymerases) and the hydrolases (e.g. restriction endonucleases). The examples found in the category of enzymes transferring functional groups tend to have a much higher mass (i.e. more residues) than the ones catalysing the hydrolysis of bonds. This was one of the reasons why we chose an endonuclease as our protein of interest. Another reason for this decision concerned the overall difficulty of the protocol describing the expression and processing of the protein. And at last, the expression organism and the resolution of the published structure were taken into account. In the end, the decision was made to use the binding domain of the restriction endonuclease BpuJ1, for which a high-resolution structure was previously published.^[11] Only a few changes to the original protocol had to be done in order to obtain the protein-DNA complex containing the modified DNA strands.

Materials and Methods

Cloning of the BpuJ1 binding domain The amino acid sequence of the N-terminal DNA BpuJ1 restriction endonuclease binding domain (residues 1 – 285) was obtained from the UniProt server.^[12] The amino acid sequence was back-translated and optimized for codon usage in *E. coli* with the help of the EMBOSS Backtranseq application.^[13] In addition, an Nde1 (N-terminal) and an Xho1 (C-terminal) restriction site were introduced as well as a stop codon (TAA). The designed sequence was ordered from a commercial supplier (Bio Basic Canada Inc., Ontario, Canada). This synthetic sequence was delivered in the pUC57 cloning vector, which is not suitable for protein expression. In order to obtain high yields of the binding domain, the sequence had to be cloned into the pET28a expression vector. The successful restriction digestion (Nde1 / Xho1), the isolation of the linear fragment, and the correct ligation were monitored and controlled with agarose gels (gel electrophoresis). The final construct was sent for sequencing (Microsynth, Balgach, Switzerland). The sequence was verified including its N-terminal His-tag / thrombin configuration.

Synthesis of the modified oligonucleotides The synthesis of the pyrene and phenanthrene phosphoramidites and their incorporation into DNA oligonucleotides is described in the literature, as well as the standard procedures for purification and characterization of the strands.^[14,15] Three DNA duplexes were prepared with the single strands (5'-3'): GYT ACC CGT GGA (**ON1**); TCC ACG GGT AYC (**ON2**); GYA CCC GTG GA (**ON3**); TCC ACG GGT α C (**ON4**); TCC ACG GGT YYC (**ON5**); where **Y** = 1,8-dialkynypyrene and α = 3,6-dialkynylphenanthrene.

The DNA duplexes and the structures of the building blocks are given in Table 7.1.

ID	Sequence
ON1	5' - GYT ACC CGT GGA -3'
ON2	3' - CYA TGG GCA CCT -5'
ON3	5' - GYA CCC GTG GA -3'
ON4	3' - C α T GGG CAC CT -5'
ON3	5' - GYA CCC GTG GA -3'
ON5	3' - CYY TGG GCA CCT -5'

Y =

α =

Table 7.1. List of the sequences of the single strands, the corresponding duplexes and the structures of the non-nucleosidic building blocks.

Expression and loading of the BpuJ1 DNA binding domain The recombinant protein was expressed in *E. coli* (transformed BL21 DE3) using ZYP-5052 rich medium for auto-induction. The cells were harvested by centrifugation at 10'000 g and resuspended in lysis buffer (10 mM K-phosphate buffer pH 7.4; 300 mM NaCl; 15 mM Imidazole; 0.025% Triton X-100). The cells were disrupted by French Press, centrifuged at 30'000 g and the supernatant was loaded onto a Ni-NTA-column (affinity chromatography). The subsequent washing (lysis buffer, except for Imidazole → 40 mM) and elution (lysis buffer, except for Imidazole → 200 mM) steps were performed at 4 °C. The retained flow through (eluate) contained usually about 0.5 – 0.6 mg protein per ml. Based on the respective concentration of these solutions a 1.1 molar excess of the corresponding DNA duplex was added. The DNA duplexes consisted of either **ON1 + ON2**, **ON3 + ON4** or **ON3 + ON5**. Shortly before adding to the protein, these modified single strands were prepared and annealed in an aqueous solution containing 100 mM NaCl and 10 mM Na-phosphate buffer (pH 7.4). Finally, thrombin was added to the samples and cleavage of the His-tag occurred overnight at 4 °C.

Purification and crystallization screens The samples were concentrated to a smaller volume and subjected to gel filtration (Superdex 200 10/300 GL; buffer A: 10 mM Tris-HCl pH 7.5; 0.1 mM EDTA; 1 mM DTT; 0.02% NaN₃). All samples showed two major peaks in the chromatogram. Only the fractions emerging from the first peak were pooled and concentrated to a final concentration of 5 mg complex per ml (for **ON1*ON2, Complex1**), 6 mg complex per ml (for **ON3*ON4, Complex2**) and 10 mg complex per ml (for **ON3*ON5, Complex3**). Crystallization was carried out by the sitting-drop method using PEG/Ion and PEG/Ion 2 screens from Hampton Research. For **Complex1**, containing **ON1** and **ON2**, the best crystals were grown in drops consisting of 1 µl complex in buffer A and 1 µl of the reservoir solution (0.2 M Magnesium acetate tetrahydrate; 20% w/v Polyethylene glycol 3,350). In case of **Complex2**, containing **ON3** and **ON4**, the best crystals were obtained from 2 µl complex in buffer A and 1 µl reservoir solution (0.2 M Ammonium citrate tribasic 7.0; 20% w/v Polyethylene glycol 3,350). And for **Complex3 (ON3*ON5)**, the best crystals arose from a 2:1 drop of the solution containing the complex and the reservoir solution (8% v/v Tacsimate 6.0; 20% w/v Polyethylene glycol 3,350). Cryo-protection was achieved by adding 20% w/v glycerol to the corresponding reservoir solution.

Data collection and structure determination Diffraction data sets were collected at the X06DA beamline at the Swiss Light Source (SLS, Paul Scherrer Institut, Villigen, Switzerland). Data was processed using XDS.^[16] The PHENIX software suite and WinCoot were used for model building and refinement.^[17,18] First, Phaser-MR and AutoBuild were used in order to create an initial model of the structure, based on the existing PDB entry 2VLA. The natural nucleotides that were not present in our oligonucleotide sequences were removed from the initial model and replaced stepwise with the non-nucleosidic pyrene and phenanthrene components. Data files containing the geometry restraints of these molecules were generated using the PRODRG Server.^[19] An additional file describing the bonds between artificial and natural building blocks had to be written and included in the refinement process.

UV-Vis spectra were collected on a Varian Cary-100 Bio-UV / Visible spectrophotometer equipped with a Varian Cary-block temperature controller, 1 cm quartz cuvettes and processed with Varian WinUV software.

Fluorescence spectra were acquired on a Varian Cary Eclipse fluorescence spectrophotometer equipped with a Varian Cary-block temperature controller with 1 cm x 1 cm quartz cuvettes and Varian Eclipse software. Instrumental setups for fluorescence emission spectra were: λ_{ex} : according to description in the corresponding figure; excitation slit width: 5 nm; emission slit width: 5 nm; PMT voltage: 600 V.

Results and Discussion

X-ray structures of the protein-DNA complexes

In case of **Complex1** (containing **ON1** and **ON2**): The crystallographic details are listed below (see Table 7.2) including the final refinement results (Table 7.3). The crystals had orthorhombic symmetry and data was collected at a resolution of 2.67 Å. The asymmetric unit contains two complete protein-DNA complexes. Regarding the rather low resolution the main effort was put into the structure determination of the modified DNA duplex rather than the surrounding protein. For both covalently attached pyrene molecules density was found on top of the natural base stack (Figure 7.4). One unit “sitting” right on top of the last Watson-Crick base pair. Due to the relative high density of the phosphate groups the remaining pyrene and bases were placed by following the backbone of the strands. Figures 7.2 and 7.3 show the complete protein-DNA complex.

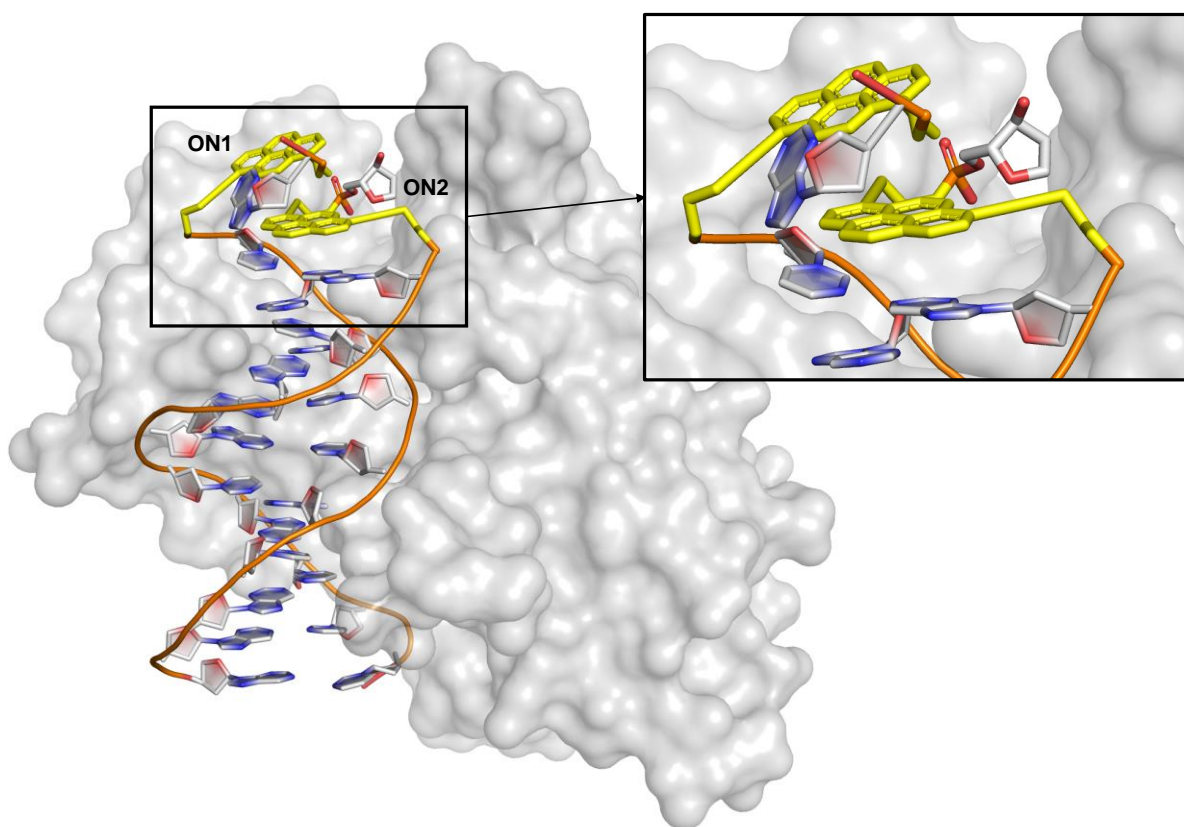


Figure 7.2. X-ray crystallographic structure of the protein-DNA complex (**Complex1**). The protein is represented as grey surface. The phosphate backbone of the DNA, shown as cartoon tubes, is linked to the pyrene modifications (yellow sticks). The terminal region is shown as an enlargement top right.

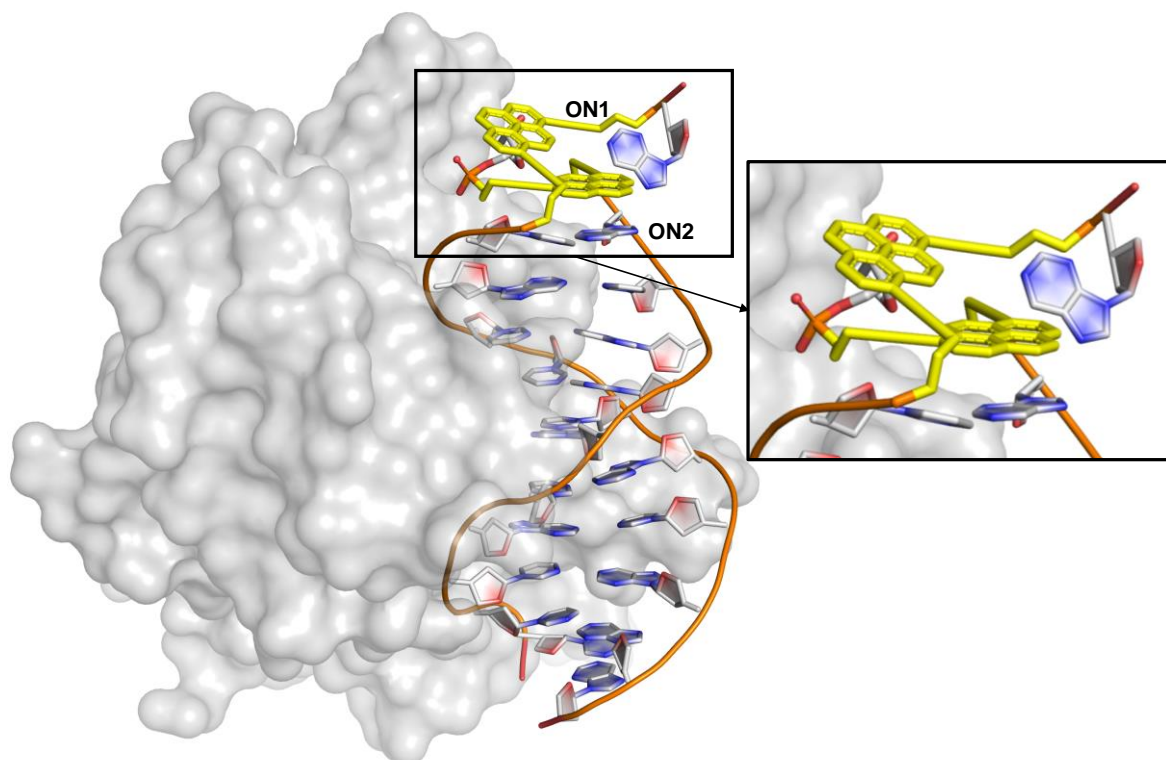


Figure 7.3. Crystal structure of the protein-DNA complex (**Complex1**). The structure was slightly rotated compared to Figure 7.2, so that the pyrene modification of **ON1** is turned towards the viewer.

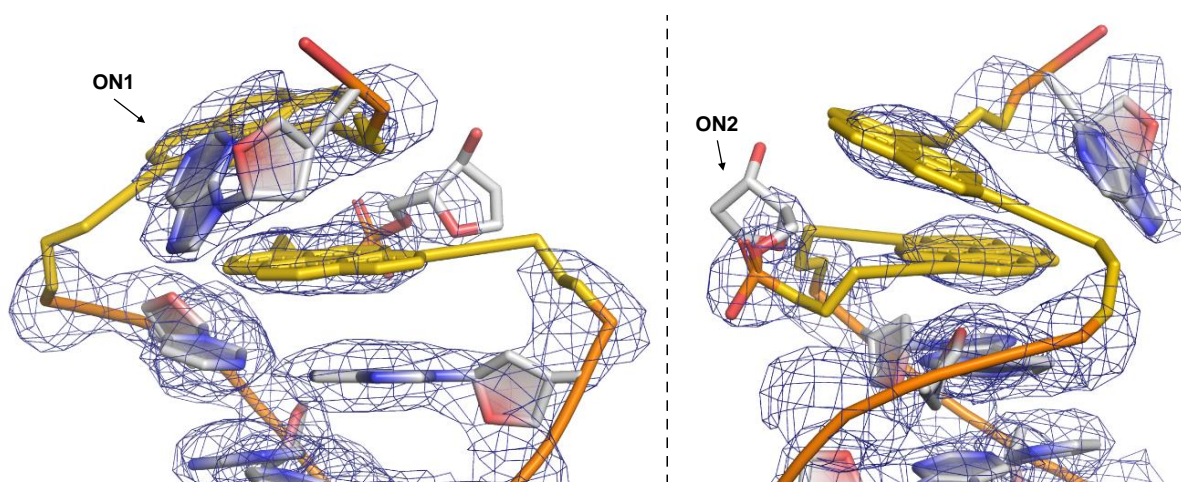


Figure 7.4. The experimental electron density map of **Complex1** (protein not shown) is given as a blue mesh contoured at 1σ . In contrast to the aromatic core of the pyrenes, none or almost no density was found around the alkyne linkers that make the connection to the phosphate groups. For better visualization, the structure was rotated (left vs. right image).

Almost all of the duplex (**ON1*ON2**) was built into the available density, however the last cytidine (3' end of **ON2**) and especially its nucleobase (cytosine) remained difficult to be positioned since there was almost no density allowing for fitting in this part of the strand (therefore only the deoxyribose was introduced).

For **ON3** and **ON4 (Complex2)**: In comparison to the previous data set, here a pyrene-phenanthrene hybrid was the matter of interest. In addition to this more obvious change, the duplex was also shortened by one base pair. Crystals showed a monoclinic symmetry with one complete complex in the asymmetric unit (Figures 7.5 / 7.6). The details about the experimental data and final refinement are summarized below (Tables 7.2 / 7.3). The resolution of 1.55 Å allowed for a more detailed structure determination of the complex. Most of the natural nucleotides and the phenanthrene chromophore were easily assigned in the corresponding electron density map (Figure 7.7). Unfortunately, things were more complicated for the pyrene unit as its position in the crystal was rather undefined. Only by trial and error (i.e. variants with different XYZ parameters for pyrene) a final structure was found to be acceptable.

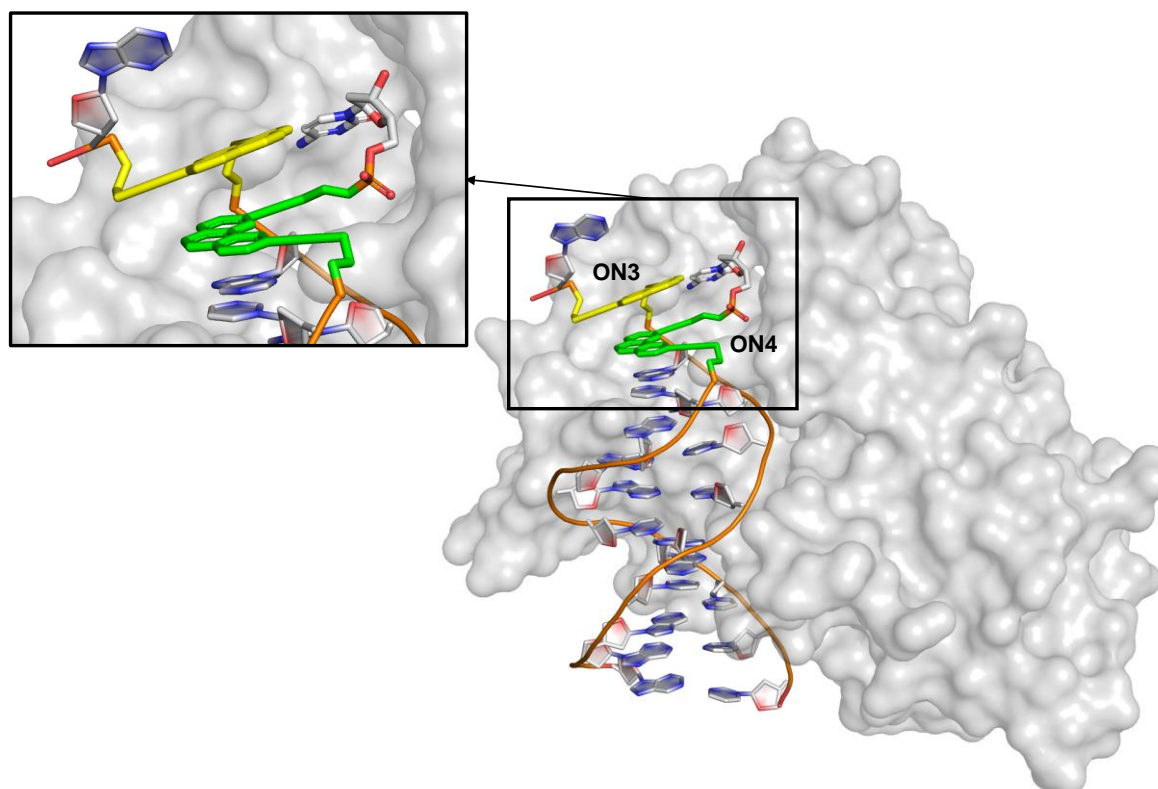


Figure 7.5. 3D structure of **Complex2** (enlargement of the terminal region is shown top left). The phosphate backbone of the DNA, shown as cartoon tubes, is linked to the pyrene (yellow sticks) and phenanthrene (green sticks) modifications.

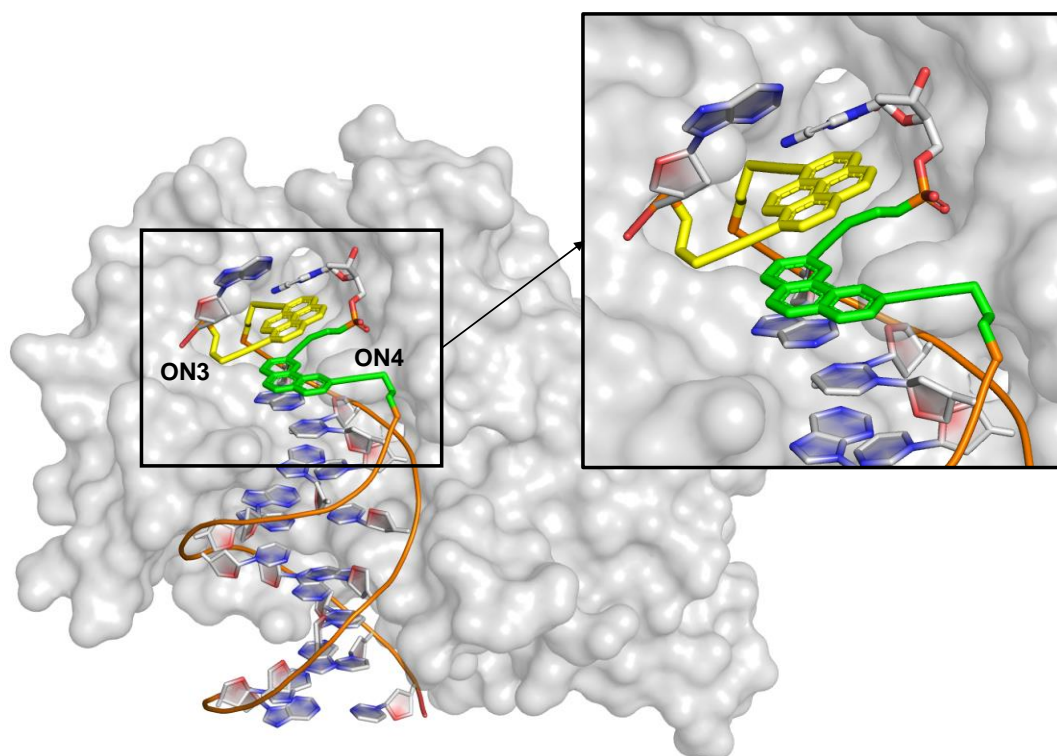


Figure 7.6. X-ray structure of the protein-DNA complex (**Complex2**). The structure was slightly turned compared to Figure 7.5, so that the pyrene modification of **ON3** is in focus.

The phenanthrene molecule, including its alkynyl linkers, and the connecting phosphate groups fit well into the available density. The adjacent nucleotide (3'-C) was placed in extension of the phosphate backbone, resulting in an arrangement where the base is pointing away from the helical axis towards the surface of the protein. As already indicated, finding the link between the natural nucleotide and the pyrene as well as the exact location of the pyrene itself was not that simple. Variations of different positions around the last well resolved phosphate group of that strand, each refined several times, turned up one solution that seems to be preferable. The remaining 5'-terminal guanosine was therefore placed in the "free" space around the top of the duplex. In addition, a sodium ion was found in close proximity of the pyrene and the next complex in the crystal lattice. Based on the structures of **Complex1** and **Complex2**, the following similarity was found: regardless of the length of the duplex and the type of chromophore, the one chromophore that is attached to the 3' end of

the last nucleotide in the natural base stack is also positioned on top of the base stack. This does make sense in a structural perspective where the “packing” of the units depends on the length of their linkers. The structures also reveal antiparallel-displaced “stacking” of the two chromophores (either pyrene-pyrene or phenanthrene-pyrene).

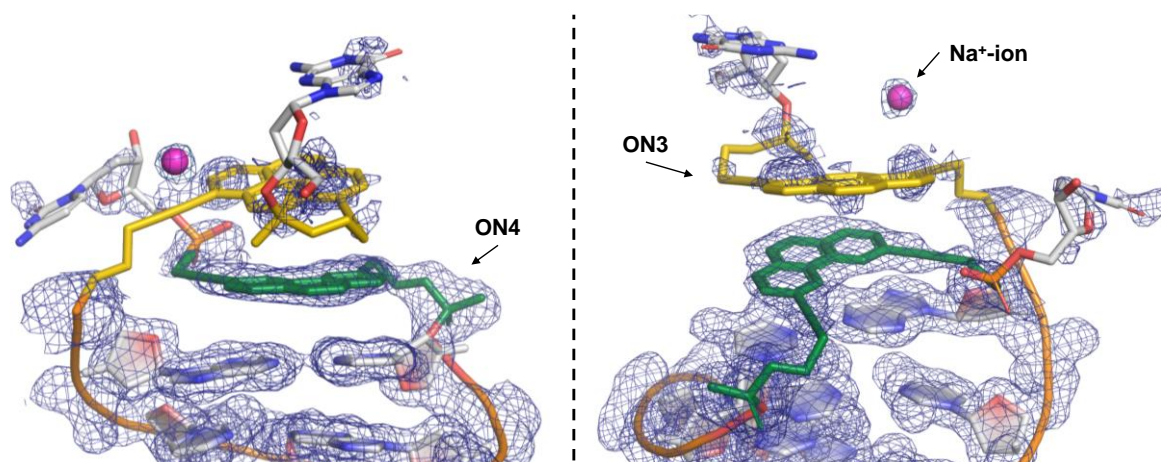


Figure 7.7. The experimental electron density map of **Complex2** is shown as a blue mesh contoured at 1σ (the pyrene unit and the 5'-G of **ON3** are set at 0.8σ). The phenanthrene unit (green sticks) stacks on the adjacent base pair (T-A). The pyrene (yellow sticks) is located on top of the phenanthrene, although only residual density was found. The last nucleotide of **ON4** (3'-C) provided even less density.

For **ON3** and **ON5** (**Complex3**): This sample contains a total of three pyrene moieties. One strand (**ON3**, one pyrene unit) is the same as in the previous complex, the other one, **ON5**, has two pyrene incorporations. As a result, the structure shows stacking of the pyrenes of the same strand (**ON5**), rather than an “intercalation” of the pyrene of **ON3**. The structures are given in Figures 7.8 and 7.9. The fact that the two pyrenes of **ON5** are part of the helical stack and therefore “fixed” on their position is reflected by the disk-like density spheres on top of the natural base stack (see Figure 7.10). In contrast, the pyrene of **ON3** is almost inexistent in the present density map, which may be of no surprise based on its location. This pyrene and the last nucleotide of the same strand (5'-G) are positioned in a way that allows for a certain degree of flexibility. In regard to the stacking of the two pyrenes of **ON5**, a parallel-displaced alignment is observed.

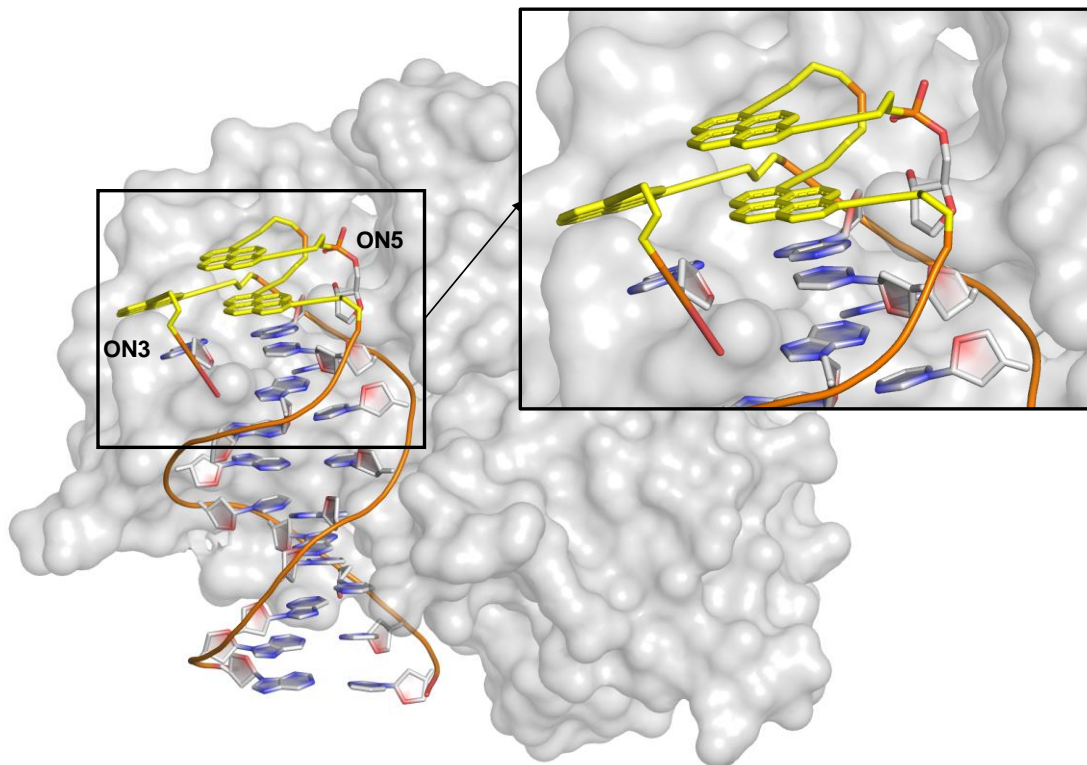


Figure 7.8. X-ray crystallographic structure of the protein-DNA **Complex3**. The two pyrenes of **ON5** (yellow sticks) are tilted towards the viewer.

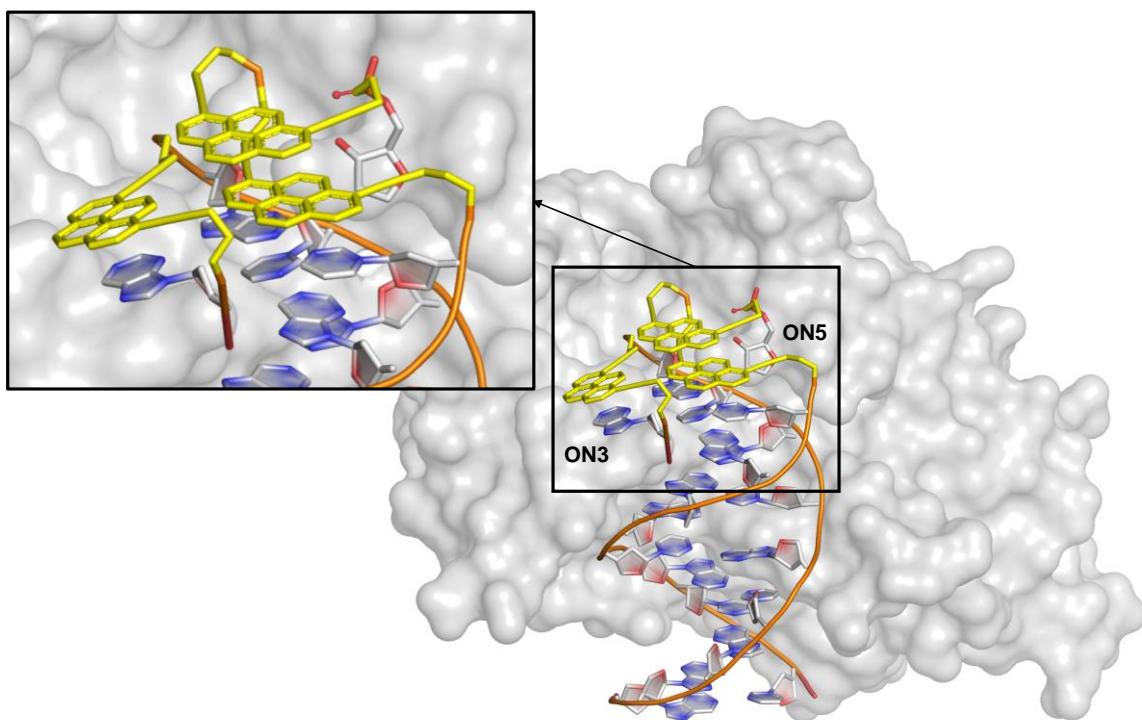


Figure 7.9. The X-ray structure of the protein-DNA **Complex3**. The pyrene of **ON3** (yellow sticks) is now turned to the right compared to Figure 7.8.

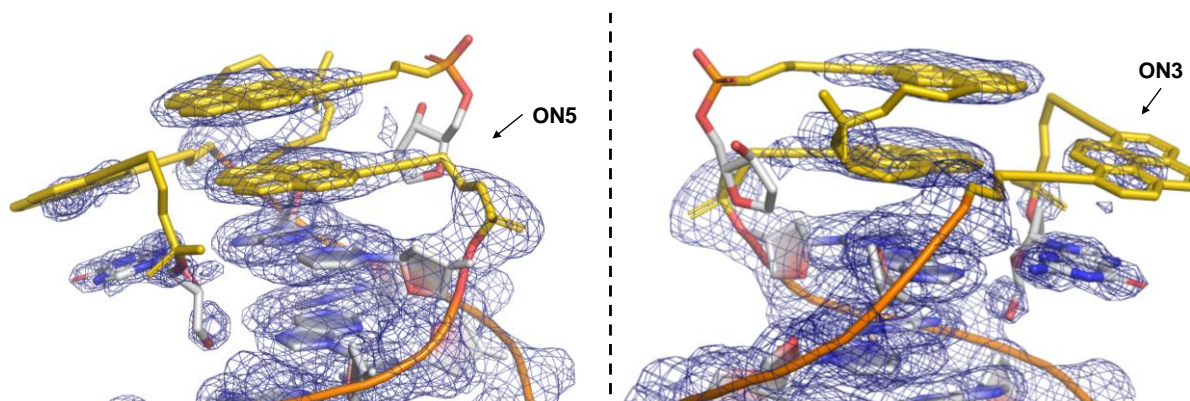


Figure 7.10. The experimental electron density map of **Complex3** is shown as a blue mesh contoured at 1σ (for the pyrene of **ON3** and the 5'-G of the same strand at 0.8σ). The density from the pyrenes (**ON5**) within the stack is evidently present in the crystal, whereas the single pyrene unit from **ON3** is located outside the stack and its density is relatively weak.

Table 7.2. Data collection statistics for the 3 structures.

	Complex1:	Complex2:	Complex3:
Temperature (K) was 100 and X-ray wavelength (Å) was 1.000.			
Number of reflections (total):	71'798	193'861	115'743
Cell constants (Å):			
A	77.87	165.72	44.03
B	85.50	59.28	59.67
C	115.90	44.05	164.40
Resolution range (Å):	2.67 – 47.97	1.55 – 43.93	1.88 – 48.29
Space group:	P 21 21 21 (19)	C 1 2 1 (5)	P 21 21 2 (18)
Completeness of data (total):	94.5%	98.0%	97.3%
I/Sigma (total):	12.8	16.70	14.14
R-meas (total):	6.6%	5.5%	5.6%
CC(1/2) (total):	99.8	99.9	99.9

Table 7.3. Refinement statistics of the 3 structures.

	Complex1:	Complex2:	Complex3:
Resolution range used for refinement (Å):	2.67 – 46.49	1.55 – 43.93	1.88 – 48.29
Number of reflections (non-anomalous):	22'202	61'042	35'452
R-factor:	0.2076	0.1711	0.1619
Free R-factor (free R value test set size):	0.2477 (4.97%)	0.1998 (5.00%)	0.2021 (4.99%)
Number of non-hydrogen atoms:			
Protein/DNA	5255	2800	2777
Solvent	46	532	233
Ligand/Ion	104	1	-
	(the pyrenes in this structure were counted as ligands)		
Average B (all atoms) (Å ²):	63.0	25.0	44.0
r.m.s. deviations from ideal values:			
Bonds (Å)	0.004	0.011	0.015
Angles (°)	0.631	1.258	1.352
Ramachandran analysis:			
Most favored (%)	97.63	97.15	97.85
Allowed (%)	2.19	2.85	2.15

Spectroscopic properties of the protein-DNA complexes

A small amount of the purified binding domain in complex with **ON1** and **ON2** was diluted (1:100, approx. 1 μM final conc. of the complex) and used for UV/Vis and fluorescence measurements. The absorbance spectrum shows the well-characterized vibronic band pattern in the area of 320 – 420 nm, indicating the aggregation of the pyrene moieties (see Figure 7.11). That is, the transition $A_0 \rightarrow 1$ at 370 nm is of similar intensity than the $A_0 \rightarrow 0$ at 390 nm (for comparison, see the monomer-like absorption peaks of the next sample, Figure 7.13). The fluorescence readout of the same sample shows a major peak around 520 nm when excited at 370 nm (Figure 7.12). This corresponds to the pyrene excimer fluorescence and clearly demonstrates the interaction between the two units. The two smaller peaks ranging from 380 – 450 nm match the monomer emission of pyrene.^[15] All the measurements were carried out at 18 °C within 24 hours after purification of the complex.

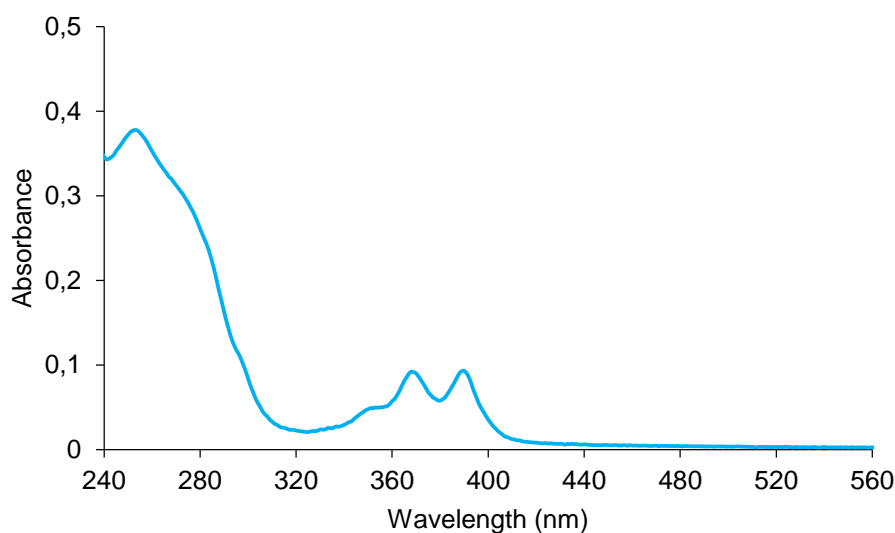


Figure 7.11. UV/Vis spectrum of the protein-DNA **Complex1** (approx. 1 μM conc. of the complex; 18 °C; buffer A, see Materials and Methods).

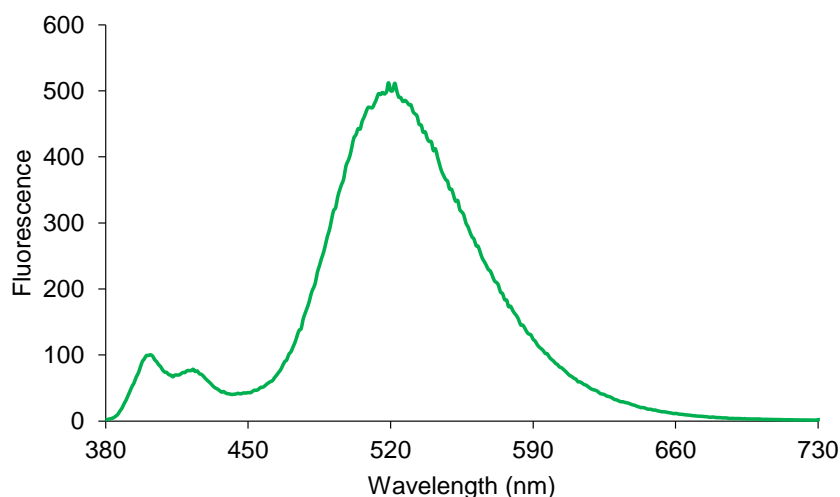


Figure 7.12. Fluorescence emission spectrum of the protein-DNA **Complex1** (λ_{ex} : 370 nm; approx. 1 μM conc. of the complex; 18 °C; buffer A, see Materials and Methods).

The same measurements were performed with the protein-DNA **Complex2**, containing **ON3** and **ON4**. UV/Vis absorption reflects the presence of the two chromophores as two separate peak areas are seen (Figure 7.13). One ranging from 310 – 340 nm, i.e. the alkynylphenanthrene, the other one from 350 – 400 nm that are the distinct absorption bands of alkynylpyrene. Fluorescence emission of the sample originates most likely from pyrene monomer as described recently (Figure 7.14).^[14]

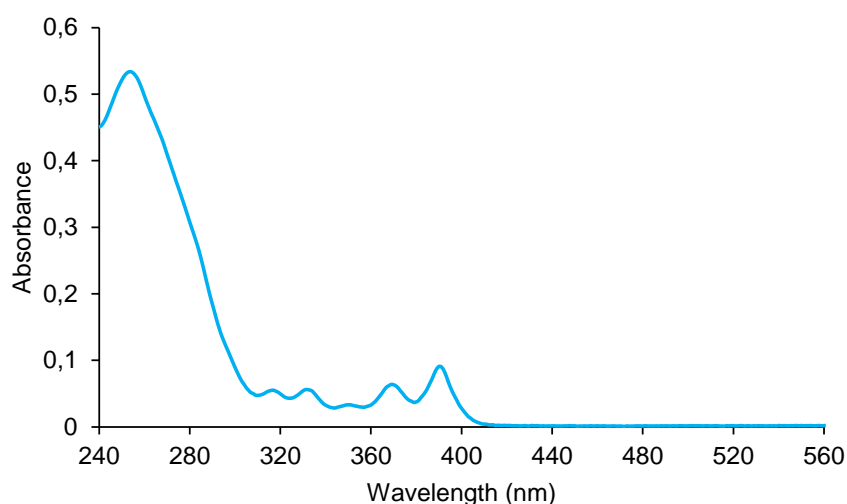


Figure 7.13. UV/Vis spectrum of the protein-DNA **Complex2** (approx. 1 μM conc. of the complex; 18 °C; buffer A, see Materials and Methods).

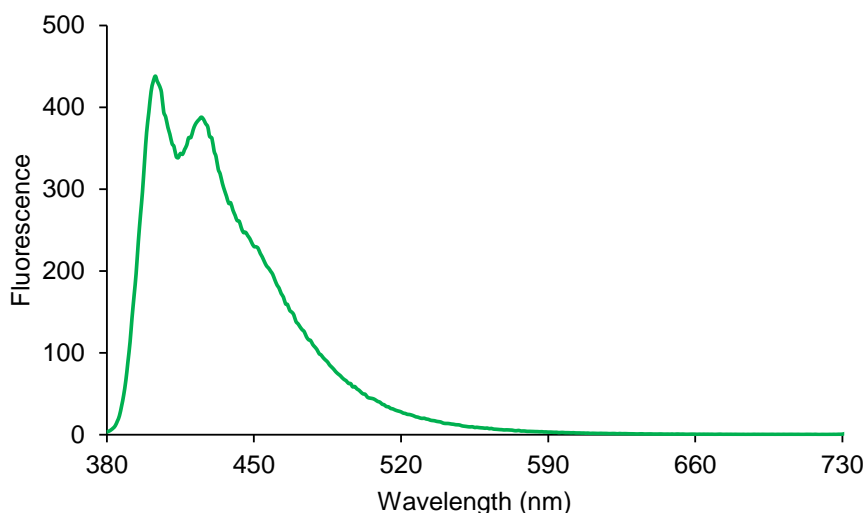


Figure 7.14. Fluorescence emission spectrum of the protein-DNA **Complex2** (λ_{ex} : 370 nm; approx. 1 μM conc. of the complex; 18 °C; buffer A, see Materials and Methods).

The absorption and the fluorescence spectra of **Complex3** (containing **ON3** and **ON5**) show similarities to the results of **Complex1**. In case of the UV/Vis spectrum, the ratio of the vibronic band intensity of 370 nm vs. 390 nm suggests pyrene aggregation (Figure 7.15). Excitation of the pyrenes (at 370 nm) leads to strong excimer emission at 520 nm with little monomer emission left (see Figure 7.16).

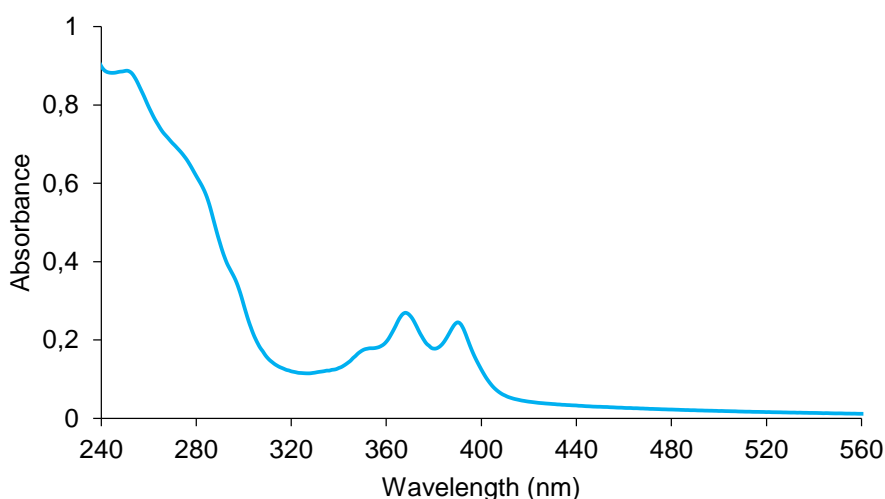


Figure 7.15. UV/Vis spectrum of the protein-DNA **Complex3** (approx. 2 μM conc. of the complex; 18 °C; buffer A, see Materials and Methods).

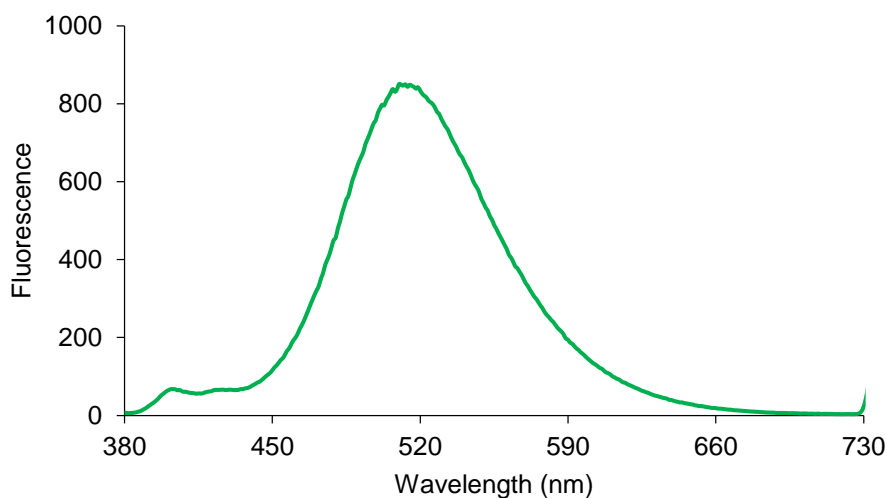


Figure 7.16. Fluorescence emission spectrum of the protein-DNA **Complex3** (λ_{ex} : 370 nm; approx. 2 μM conc. of the complex; 18 $^{\circ}\text{C}$; buffer A, see Materials and Methods).

Taken the structural and spectroscopic evidence together: For **Complex1**, the two pyrenes are in close contact with each other. This goes along with the observed excimer fluorescence in solution that is distance and flexibility dependent as described in several reports.^[20] While most of the natural base stack is intact resulting in B-DNA, the two bases separated by the pyrene incorporations are not paired. Based on the arrangement of the modifications (and in particular how their alkynyl linkers are aligned), it is difficult to imagine the formation of this last Watson-Crick base pair. Changing the chromophore (in one case) and the length of the sequences (as in **Complex2**), results in a similar construct (relative orientation of the chromophores) but with a different crystal packing (see below). Finally, **Complex3** shows a crystal structure in which intrastrand stacking of the pyrenes takes place. The interactions between the individual chromophores are well illustrated by their UV/Vis and fluorescence behavior (at least a correlation between the crystal structure and the results obtained in solution is possible).

The modified duplexes in the crystal lattice

In regard to the crystal, it is interesting to see how one protein-DNA complex is in contact with the surrounding complexes. And of course whether or not the modifications seem to influence the packing (or vice versa, how is the duplex affected). Starting again from **Complex1**, an almost linear array in a head-to-tail fashion of the modified duplexes is present (see Figure 7.17). In addition, it seems as if the pyrene of **ON1** (at the end of the duplex) mediates the crystal contacts to the next complex (or more precise to the duplex of the next complex).

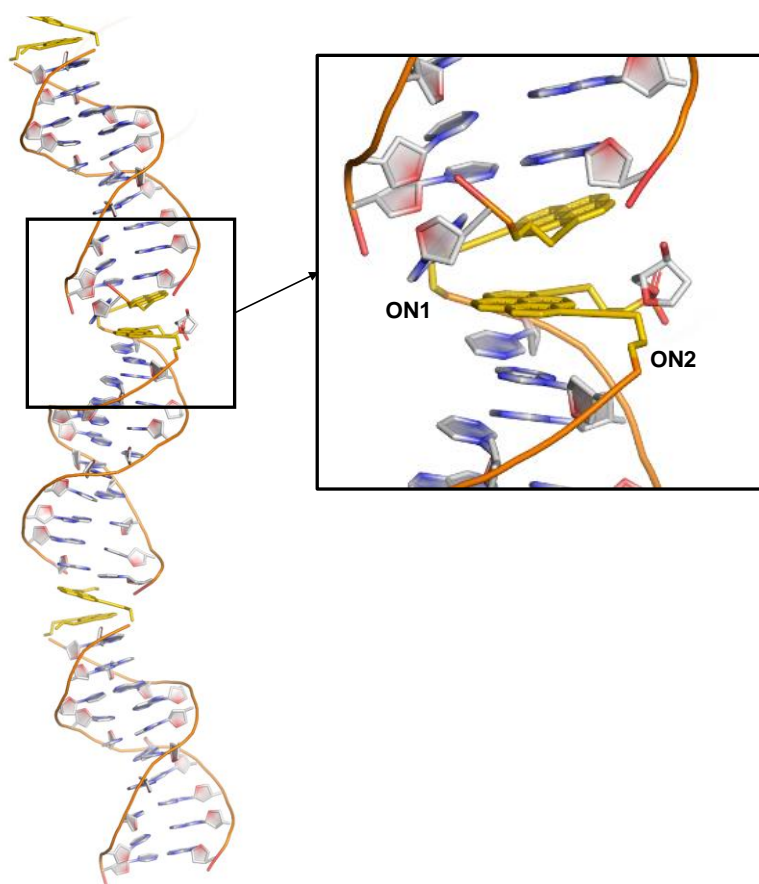


Figure 7.17. Repetition of the duplex throughout the crystal lattice of **Complex1** in a continuous way (generating the symmetry mates). In this structure, the 5'-T / 3'-A base pair of one complex stacks on top of the terminating pyrene (of **ON1**) of the adjoining complex.

In contrast, the complex containing **ON3** and **ON4** (**Complex2**) did end up with a head-to-head positioning of the chromophores (i.e. the modified strands) within the crystal (see Figure 7.18). Here, a sodium cation lies in the plane of mirror symmetry, close to the pyrenes and the present phosphate groups. This, together with the shortening of the sequences (compared to the previous sample), may be responsible for the completely different way of how the complex crystallized.

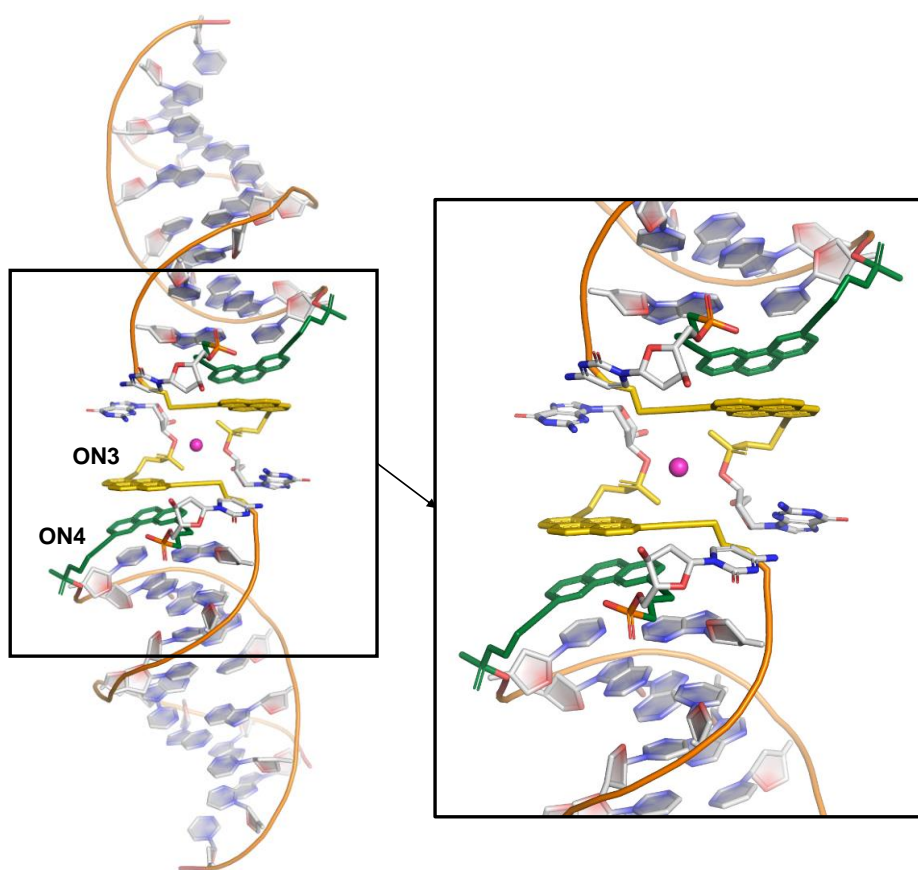


Figure 7.18. Repetition of the duplex throughout the crystal lattice in case of **Complex2**. The crystal contacts seem to be mediated by a sodium ion (magenta).

Following the same pattern, a head-to-head stacking of the chromophores from one complex on the adjoining one is also found for **Complex3** (see Figure 7.19). In the crystal, the two pyrenes of **ON5** (one from each complex) stack almost perfectly antiparallel cofacial. Plus, this is something that all structures do have in common: the non-natural building blocks are somehow involved in the contact(s) between the complexes.

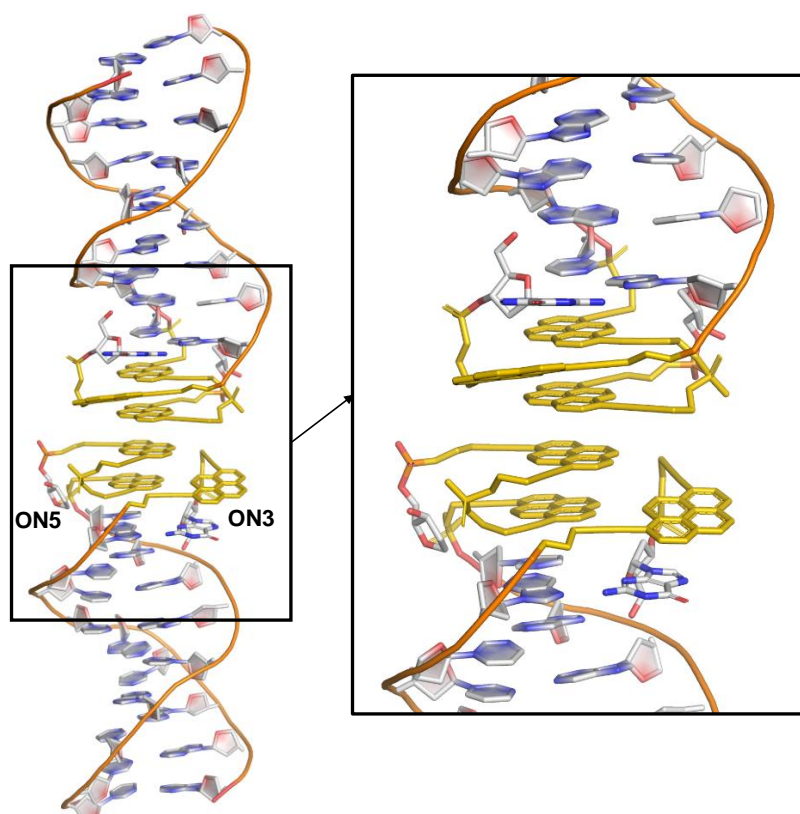


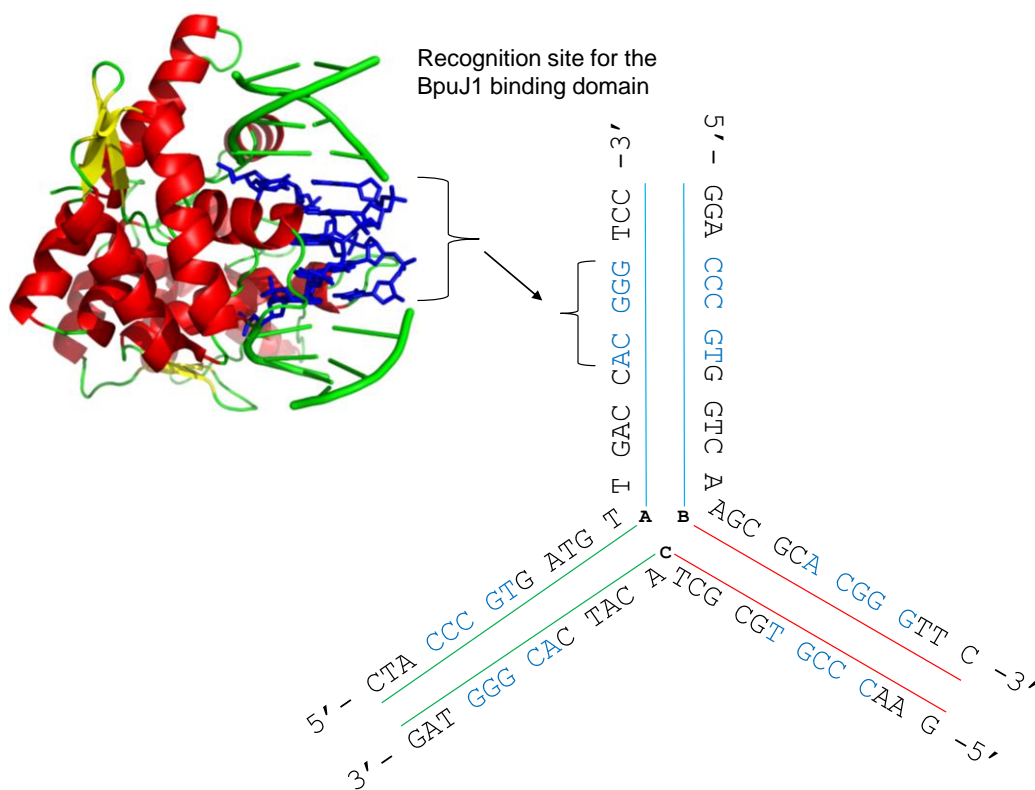
Figure 7.19. Repetition of the duplex throughout the crystal lattice in case of **Complex3**. The most distinct feature of this structure is the stack of a total of 4 pyrene units (two from each complex).

Conclusions

Co-crystallization of the pyrene- and phenanthrene-modified DNA and the BpuJ1 endonuclease binding domain worked according to the method that was applied. The obtained crystal structures of the three complexes revealed the spatial arrangement of the chromophores as well as other structural features resulting from the incorporation of the chromophores (e.g. the chromophore unit on top of the base stack is linked via 3' to the nucleotide in the helical stack; there is no Watson-Crick base pair formation between the terminal bases next to the modifications). The observations made herein go along with the spectroscopic properties of the complexes in solution. Also, most of the DNA remains B-DNA (perfectly paired, right-handed double helix with its standard parameters) and the target site and the binding region (along with the rest of the protein) are no different to the original RCSB PDB entry 2VLA.

Chapter 8 – Outlook

Throughout this thesis a lot of work was dedicated to the DNA three-way junctions, but there was never an attempt to solve the 3D molecular structure of these constructs. In regard to the last chapter, one possibility is to follow the same approach with a therefore designed three-way junction:



The core of the 3WJ may be modified in order to understand the arrangement inside the junction. The approach may also include the use of more than one target sequence (5'-**CCCGT**) to help “stabilize” the whole construct.

As for the crystal structures itself, all of the examples have the common feature that the chromophores are located “on top” of the structure which of course has to do with the sequences that were used. Although there were trials with modified DNA strands with chromophores closer to the recognition site or at least closer to it than in the examples shown above, there were no or no useful crystals obtained from these experiments. To search for an alternative protein or to mutate the existing one in order to get crystals that will show the structure of a modified sequence with internal incorporations of the non-nucleosidic building blocks is an option.

References Chapter 1

- [1] **G. Brent Dalrymple**. The age of the Earth in the twentieth century: a problem (mostly) solved. *Geological Society, London, Special Publications*, **2001**, 190, 205-221.
- [2] **University of California Museum of Paleontology**. History of life through time. Online: <http://www.ucmp.berkeley.edu/exhibits/historyoflife.php> (19.11.2015).
- [3] **David Wacey, Matt R. Kilburn, Martin Saunders, John Cliff and Martin D. Brasier**. Microfossils of sulphur-metabolizing cells in 3.4-billion-year-old rocks of Western Australia. *Nature Geoscience*, **2011**, 4, 698–702.
- [4] **G Wächtershäuser**. From volcanic origins of chemoautotrophic life to Bacteria, Archaea and Eukarya. *Philos Trans R Soc Lond B Biol Sci.*, **2006**, 361, 1787–1806.
- [5] **Martin D. Brasier, Richard Matthewman, Sean McMahon, David Wacey**. Pumice as a Remarkable Substrate for the Origin of Life. *Astrobiology*, **2011**, 11, 725–735.
- [6] **Thomas R. Cech**. The RNA Worlds in Context. Cold Spring Harbor Laboratory Press. *Cold Spring Harb Perspect Biol*, **2011**, doi: 10.1101/cshperspect.a006742.
- [7] **Overview**: English site of Wikipedia, the free encyclopedia: https://en.wikipedia.org/wiki/Main_Page Articles: DNA, RNA world hypothesis, Abiogenesis, Life, Primordial sandwich, Iron–sulfur world theory. Online: <https://en.wikipedia.org/wiki/Abiogenesis> (19.11.2015).
- [8] **Martin M. Hanczyc**. Metabolism and motility in prebiotic structures. *Phil. Trans. R. Soc. B.*, **2011**, 366, 2885-2893.
- [9] **Norman H. Sleep, Dennis K. Bird, Emily C. Pope**. Serpentinite and the dawn of life. *Phil. Trans. R. Soc. B.*, **2011**, 366, 2857-2869.
- [10] **David M. J. Lilley, John Sutherland**. The chemical origins of life and its early evolution: an introduction. *Phil. Trans. R. Soc. B.*, **2011**, 366, 2853-2856.
- [11] **Patrick Forterre**. The origin of DNA genomes and DNA replication proteins. *Current Opinion in Microbiology*, **2002**, 5, 525–532.
- [12] **Anthony Poole, David Penny, Britt-Marie Sjöberg**. Methyl-RNA: an evolutionary bridge between RNA and DNA?. *Chemistry & Biology*, **2000**, 7, 12, R207-R216.
- [13] **Robert Shapiro**. Prebiotic cytosine synthesis: A critical analysis and implications for the origin of life. *Proc. Natl. Acad. Sci.*, **1999**, 96, 4396–4401.
- [14] **Michael P. Callahan, Karen E. Smith, H. James Cleaves II, Josef Ruzicka, Jennifer C. Stern, Daniel P. Glavin, Christopher H. House, Jason P. Dworkin**. Carbonaceous meteorites contain a wide range of extraterrestrial nucleobases. *PNAS*, **2011**, 108, 34, 13995–13998.

- [15] **Patrick Forterre**. The origin of DNA genomes and DNA replication proteins. *Current Opinion in Microbiology*, **2002**, 5, 525–532.
- [16] **Friedrich Miescher**. Über die chemische Zusammensetzung der Eiterzellen. *Medicinischemische Untersuchungen*, **1871**, 4, 441–460.
- [17] **R. Dahm**. Discovering DNA: Friedrich Miescher and the early years of nucleic acid research. *Hum. Genet.*, **2008**, 122, 6, 565–81.
- [18] **Albrecht Kossel**. *Zeitschrift für physiologische Chemie*, **1879**, 3, 284-291. **1880**, 4, 290-295. **1881**, 5, 267-271. **1882**, 6, 422-431. **1883**, 7, 7-22. **1886**, 10, 248-264.
- [19] **M.E. Jones**. Albrecht Kossel, A Biographical Sketch. *Yale Journal of Biology and Medicine*, **1953**, 26, 1, 80–97.
- [20] **P. Levene**. The structure of yeast nucleic acid. *J. Biol. Chem.*, **1919**, 40, 2, 415–24.
- [21] **W. T. Astbury and Florence O. Bell**. Some recent developments in the X-ray study of proteins and related structures. *Cold Spring Harbor Symposia on Quantitative Biology*, **1938**, 6, 109-121. **W. T. Astbury**. X-ray studies of nucleic acids. *Symposia of the Society for Experimental Biology*, **1947**, 1, 66-76.
- [22] **Nikolaj K. Koltzoff**. Physikalisch-chemische Grundlagen der Morphologie. *Biologisches Zentralblatt*, **1928**, 48, 6, 345-369.
- [23] **N. K. Koltzoff**. The structure of the chromosomes in the salivary glands of *Drosophila*. *Science*, **1934**, 80, 2075, 312-313.
- [24] **V. N. Soyfer**. The consequences of political dictatorship for Russian science. *Nature Reviews Genetics*, **2001**, 2, 9, 723–729.
- [25] **F. Griffith**. The significance of pneumococcal types. *The Journal of Hygiene*, **1928**, 27, 2, 113–59.
- [26] **M. G. Lorenz, W. Wackernagel**. Bacterial gene transfer by natural genetic transformation in the environment. *Microbiol. Rev.*, **1994**, 58, 3, 563–602.
- [27] **O. T. Avery, C. M. Macleod, M. McCarty**. Studies on the Chemical Nature of the Substance Inducing Transformation of Pneumococcal Types: Induction of Transformation by a Desoxyribonucleic Acid Fraction Isolated from *Pneumococcus* Type Iii. *J. Exp. Med.*, **1944**, 79, 2, 137–158.
- [28] **A. D. Hershey, M. Chase**. Independent Functions of Viral Protein and Nucleic Acid in Growth of Bacteriophage. *J. Gen. Physiol.*, **1952**, 36, 1, 39–56.
- [29] **J. D. Watson, F. H. Crick**. A Structure for Deoxyribose Nucleic Acid. *Nature*, **1953**, 171, 4356, 737–738.
- [30] **J. D. Watson and F. H. C. Crick**. *Nature*, **1953**, 171, 737-738. **M. H. F. Wilkins, A. R. Stokes A. R. and H. R. Wilson**. *Nature*, **1953**, 171, 738-740. **R. Franklin and R. G. Gosling**. *Nature*, **1953**, 171,

- 740-741. **J. D. Watson and F. H. C. Crick.** *Nature*, **1953**, 171, 964-967. **R. Franklin and R. G. Gosling.** *Nature*, **1953**, 172, 156-157. **O. T. Avery, C. M. MacLeod C. M. and M. McCarty.** *J. Exp. Med.*, **1944**, 79, 137-159.
- [31] **R. E. Franklin, R. G. Gosling.** Molecular Configuration in Sodium Thymonucleate. *Nature*, **1953**, 171, 4356, 740–1.
- [32] **M. H. Wilkins, A. R. Stokes, H. R. Wilson.** Molecular Structure of Deoxypentose Nucleic Acids. *Nature*, **1953**, 171, 4356, 738–740.
- [33] **B. Maddox.** The double helix and the 'wronged heroine'. *Nature*, **2003**, 421, 6921, 407–408.
- [34] **Erwin Chargaff, Stephen Zamenhof, Charlotte Green.** Composition of human desoxypentose nucleic acid. *Nature*, **1950**, 165, 4202, 756–7.
- [35] **Angela K. Eggleston.** Probing the molecular heart of life. *Nature Milestones | Crystallography*, **2014**, doi: 10.1038/nature13370. Online: <http://www.nature.com/milestones/milecrystal/full/milecrystal23.html> (23.11.2015).
- [36] **Aaron Klug.** The Discovery of the DNA Double Helix. *J. Mol. Biol.*, **2004**, 335, 3–26.
- [37] **A. H. Wang, et al.** Molecular structure of a left-handed double helical DNA fragment at atomic resolution. *Nature*, **1979**, 282, 680–686. **R. Wing, et al.** Crystal structure analysis of a complete turn of B-DNA. *Nature*, **1980**, 287, 755–758. **H. R. Drew, R. M. Wing, T. Takano, C. Broka, S. Tanaka, K. Itakura, R. E. Dickerson.** Structure of a B-DNA dodecamer: conformation and dynamics. *Proc. Natl. Acad. Sci. USA*. **1981**, 78, 2179-2183.
- [38] **Source:** Research Collaboratory for Structural Bioinformatics (RCSB) Protein Data Bank (PDB). About the PDB Archive and the RCSB PDB. Online: http://www.rcsb.org/pdb/static.do?p=general_information/about_pdb/index.html (30.01.2016).
- [39] **M. Meselson, F. W. Stahl.** The replication of DNA in *Escherichia coli*. *Proc. Natl. Acad. Sci.*, **1958**, 44, 7, 671–82.
- [40] **Har Gobind Khorana, Robert W. Holley and Marshall Warren Nirenberg** received The Nobel Prize in Physiology or Medicine in 1968 “for their interpretation of the genetic code and its function in protein synthesis”.
- [41] **R. W. Holley, J. Apgar, G. A. Everett, J. T. Madison, M. Marquisee, S. H. Merrill, J. R. Penswick, A. Zamir.** Structure of a Ribonucleic Acid. *Science*, **1965**, 147, 3664, 1462–1465.
- [42] **F. Sanger, A. R. Coulson.** A rapid method for determining sequences in DNA by primed synthesis with DNA polymerase. *Journal of Molecular Biology*, **1975**, 94, 3, 441–448.
- [43] **F. Sanger, G. M. Air, B. G. Barrell, N. L. Brown, A. R. Coulson, C. A. Fiddes, C. A. Hutchinson, P. M. Slocombe, M. Smith.** Nucleotide sequence of bacteriophage ϕ X174 DNA. *Nature*, **1977**, 265, 5596, 687–695.

[44] **F. Sanger, S. Nicklen, A. R. Coulson.** DNA sequencing with chain-terminating inhibitors. *Proceedings of the National Academy of Sciences USA*, **1977**, 74, 12, 5463–5467.

[45] **Paul Berg, Walter Gilbert, Frederick Sanger** received The Nobel Prize in Chemistry 1980 "for his fundamental studies of the biochemistry of nucleic acids, with particular regard to recombinant-DNA" (Paul Berg) and "for their contributions concerning the determination of base sequences in nucleic acids" (Walter Gilbert and Frederick Sanger).

[46] **A. M. Michelson, A. R. Todd.** Nucleotides part XXXII. Synthesis of a dithymidine dinucleotide containing a 3': 5'-internucleotidic linkage. *J. Chem. Soc.*, **1955**, 2632.

[47] **P. T. Gilham, H. G. Khorana.** Studies on Polynucleotides. I. A New and General Method for the Chemical Synthesis of the C5'-C3' Internucleotidic Linkage. Syntheses of Deoxyribo-dinucleotides. *J. Amer. Chem. Soc.*, **1958**, 80, 23, 6212.

[48] **R. L. Letsinger, K. K. Ogilvie.** Nucleotide chemistry. XIII. Synthesis of oligothymidylates via phosphotriester intermediates. *J. Amer. Chem. Soc.*, **1969**, 91, 12, 3350.

[49] **S. L. Beaucage, M. H. Caruthers.** Deoxynucleoside phosphoramidites—A new class of key intermediates for deoxypolynucleotide synthesis. *Tetrahedron Lett.*, **1981**, 22, 20, 1859.

[50] **Overview:** English site of Wikipedia, the free encyclopedia:

https://en.wikipedia.org/wiki/Main_Page Articles: DNA sequencing, Oligonucleotide synthesis, Artificial gene synthesis. Online: https://en.wikipedia.org/wiki/Oligonucleotide_synthesis (24.11.2015).

[51] **Source:** ATDBio. Solid-phase oligonucleotide synthesis. Online:

<http://www.atdbio.com/content/17/Solid-phase-oligonucleotide-synthesis#Tritylation> (31.01.2016).

References Chapter 2

- [1] **Overview:** From the lecture “*Principles of nucleic acids*”, by Prof. Dr. R. Häner, **2009**, Department of Chemistry and Biochemistry, University of Bern, Freiestrasse 3, CH-3012 Bern, Switzerland.
- [2] **J. D. Watson, F. H. C. Crick.** Molecular Structure of Nucleic Acids: A Structure for Deoxyribose Nucleic Acid. *Nature*, **1953**, 171, 737 - 738.
- [3] **Richard Wing, Horace Drew, Tsunehiro Takano, Chris Broka, Shoji Tanaka, Keiichi Itakura, Richard E. Dickerson.** Crystal structure analysis of a complete turn of B-DNA. *Nature*, **1980**, 287, 755 – 758.
- [4] **Marshal Mandelkern, John G. Elias, Don Eden, Donald M. Crothers.** The dimensions of DNA in solution. *Journal of Molecular Biology*, **1981**, 152, 1, 153-161.
- [5] **Peter Yakovchuk, Ekaterina Protozanova, Maxim D. Frank-Kamenetskii.** Base-stacking and base-pairing contributions into thermal stability of the DNA double helix. *Nucleic Acids Research*, **2006**, 34, 2, 564–574.
- [6] **A. Ghosh, M. Bansal.** A glossary of DNA structures from A to Z. *Acta Cryst.*, **2003**, D59, 620-626.
- [7] **G. Bonner and A. M. Klibanov.** Structural stability of DNA in nonaqueous solvents. *Biotechnology and Bioengineering*, **2000**, 68, 3, 339–344.
- [8] **R. R. Sinden, C. E. Pearson, V. N. Potaman and D. W. Ussery.** DNA: structure and function. *Advances in genome biology*, **1998**, 5, 1–141.
- [9] **A. Klug.** The discovery of the DNA double helix. *DNA: Changing Science and Society*, **2004**, 17, 5.
- [10] **Aaron Klug.** The Discovery of the DNA Double Helix. *J. Mol. Biol.*, **2004**, 335, 3–26.
- [11] Model: Abalone - Biomolecular Modelling, Version 1.8.28, Copyright (C) 2006-2011 Agile Molecule. Rendering: PyMOL(TM) Educational Product, Version 1.3, Copyright (C) 2010 Schrodinger, LLC.
- [12] **W. Saenger.** Principles of nucleic acid structure. *Springer-Verlag New York*, **1984**, 7.
- [13] **The University of California Museum of Paleontology**, Berkeley, and the Regents of the University of California. The structure of DNA: Cooperation and competition. Online: <http://undsci.berkeley.edu/> (28.11.2015).
- [14] **Sarah Burge, Gary N. Parkinson, Pascale Hazel, Alan K. Todd, Stephen Neidle.** Quadruplex DNA: sequence, topology and structure. *Nucleic Acids Research*, **2006**, 34, 19, 5402–5415.
- [15] **Yougen Li, Yolanda D. Tseng, Sang Y. Kwon, Leo D'Espaux, J. Scott Bunch, Paul L. Mceuen, Dan Luo.** Controlled assembly of dendrimer-like DNA. *Nature Materials*, **2004**, 3, 38-42.
- [16] **U. Dornberger, A. Hillisch, F. A. Gollmick, H. Fritzsche, S. Diekmann.** Solution structure of a five-adenine bulge loop within a DNA duplex. *Biochemistry*, **1999**, 38, 12860-12868.

- [17] **N. B. Ulyanov, W. R. Bauer, T. L. James.** High-resolution NMR structure of an AT-rich DNA sequence. *J. Biomol. NMR*, **2002**, 22, 265-280.
- [18] **F. Barbault, T. Huynh-Dinh, J. Paoletti, G. Lancelotti.** A new peculiar DNA structure: NMR solution structure of a DNA kissing complex. *J. Biomol. Struct. Dyn.*, **2002**, 19, 649-658.
- [19] **M. Tarkoy, A. K. Phipps, P. Schultze, J. Feigon.** Solution structure of an intramolecular DNA triplex linked by hexakis(ethylene glycol) units: d(AGAGAGAA-(EG)₆-TTCTCTCT-(EG)₆-TCTCTCTT). *Biochemistry*, **1998**, 37, 5810-5819.
- [20] **Nadrian C. Seeman.** DNA in a material world. *Nature*, **2003**, 421, 427-431.
- [21] **Leroy Hood, David Galas.** The digital code of DNA. *Nature*, **2003**, 421, 444-448.
- [22] **Gary Felsenfeld, Mark Groudine.** Controlling the double helix. *Nature*, **2003**, 421, 448-453.
- [23] **Young Hoon Roh, Roanna C. H. Ruiz, Songming Peng, Jong Bum Lee, Dan Luo.** Engineering DNA-based functional materials. *Chem. Soc. Rev.*, **2011**, 40, 5730-5744.
- [24] **Ronald R. Breaker.** Natural and engineered nucleic acids as tools to explore biology. *Nature*, **2004**, 432, 838-845.
- [25] *Bioinformatics*, **2005**, 21, 711-722. *Nucleic Acids Research*, **2005**, 33, 570-572. *Biochemistry*, **1996**, 35, 3555-3562. *Biochemistry*, **2008**, 47, 5336-5353.
- [26] ATDBio. DNA duplex stability. Online: <http://www.atdbio.com/content/53/DNA-duplex-stability> (31.01.2016).
- [27] Wikipedia The Free Encyclopedia. G-quadruplex. Online: <https://en.wikipedia.org/wiki/G-quadruplex> (31.01.2016).
- [28] **N. C. Seeman, N. R. Kallenbach.** DNA Branched Junctions. *Annual Review of Biophysics and Biomolecular Structure*, **1994**, 23, 53-86.
- [29] **V. Thiviyathan, B. A. Luxon, N. B. Leontis, N. Illangasekare, D. G. Donne, D. G. Gorenstein.** Hybrid-hybrid matrix structural refinement of a DNA three-way junction from 3D NOESY-NOESY. *J. Biomol. NMR*, **1999**, 14, 209-221.
- [30] **T. Minagawa, A. Murakami, Y. Ryo, H. Yamagishi.** Structural features of very fast sedimenting DNA formed by gene 49 defective T4. *Virology*, **1983**, 15, 126, 1, 183-93.
- [31] **Frank Jensch, Borries Kemper.** Endonuclease VII resolves Y-junctions in branched DNA in vitro. *The EMBO Journal*, **1986**, 5, 1, 181 -189.
- [32] **Martin R. Singleton, Sarah Scaife, Dale B. Wigley.** Structural Analysis of DNA Replication Fork Reversal by RecG. *Cell*, **2001**, 107, 79-89.
- [33] **Derek R. Duckett, David M. J. Lilley.** The three-way DNA junction is a Y-shaped molecule in which there is no helix helix stacking. *The EMBO Journal*, **1990**, 9, 5, 1659 - 1664.

- [34] **Mengsu Yang, David P. Millar.** Conformational Flexibility of Three-Way DNA Junctions Containing Unpaired Nucleotides. *Biochemistry*, **1996**, 35, 7959-7967.
- [35] **Frank Stühmeier, Jonathan B. Welch, Alastair I. H. Murchie, David M. J. Lilley, Robert M. Clegg.** Global Structure of Three-Way DNA Junctions with and without Additional Unpaired Bases: A Fluorescence Resonance Energy Transfer Analysis. *Biochemistry*, **1997**, 36, 13530-13538.
- [36] **L. S. Shlyakhtenko, V. N. Potaman, R. R. Sinden, A. A. Gall, Y. L. Lyubchenko.** Structure and dynamics of three-way DNA junctions: atomic force microscopy studies. *Nucleic Acids Res.*, **2000**, 28, 18, 3472-7.
- [37] **René Assenberg, Anthony Weston, Don L. N. Cardy, Keith R. Fox.** Sequence-dependent folding of DNA three-way junctions. *Nucleic Acids Research*, **2002**, 30, 23, 5142-5150.
- [38] **Bin Wu, Frederic Girard, Bernd van Buuren, Jürgen Schleucher, Marco Tessari, Sybren Wijmenga.** Global structure of a DNA three-way junction by solution NMR: towards prediction of 3H fold. *Nucleic Acids Research*, **2004**, 32, 10, 3228–3239.
- [39] **Tara Sabir, Gunnar F. Schröder, Anita Toulmin, Peter McGlynn, Steven W. Magennis.** Global Structure of Forked DNA in Solution Revealed by High-Resolution Single-Molecule FRET. *J. Am. Chem. Soc.*, **2011**, 133, 1188–1191.
- [40] **Julie L. Kadmas, Amy J. Ravin, Neocles B. Leontis.** Relative stabilities of DNA three-way, four-way and five-way junctions (multi-helix junction loops): unpaired nucleotides can be stabilizing or destabilizing. *Nucleic Acids Research*, **1995**, 23, 12, 2212-2222.
- [41] **Milan N. Stojanovic, Tilla S. Worgall.** Detecting hydrophobic molecules with nucleic acid-based receptors. *Current Opinion in Chemical Biology*, **2010**, 14, 751–757.
- [42] **Sophie Vuong, Loïc Stefan, Pauline Lejault, Yoann Rousselin, Franck Denat, David Monchaud.** Identifying three-way DNA junction-specific small-molecules. *Biochimie*, **2012**, 94, 2, 442–450.
- [43] **Lucia Cardo, Victoria Sadovnikova, Siriporn Phongtongpasuk, Nikolas J. Hodges, Michael J. Hannon.** Arginine conjugates of metallo-supramolecular cylinders prescribe helicity and enhance DNA junction binding and cellular activity. *ChemComm.*, **2011**, 47, 23, 6575-7.
- [44] **Margit Haahr Hansen, Peter Blakskjær, Lars Kolster Petersen, Tara Heitner Hansen, Jonas Westergaard Højfeldt, Kurt Vesterager Gothelf, Nils Jakob Vest Hansen.** A Yoctoliter-Scale DNA Reactor for Small-Molecule Evolution. *J. Am. Chem. Soc.*, **2009**, 131, 1322–1327.
- [45] **Isabelle T. Seemann, Vijay Singh, Mykhailo Azarkh, Malte Drescher, Jörg S. Hartig.** Small-Molecule-Triggered Manipulation of DNA Three-Way Junctions. *J. Am. Chem. Soc.*, **2011**, 133, 4706–4709.
- [46] **T. Sabir, A. Toulmin, L. Ma, A. C. Jones, P. McGlynn, G. F. Schröder, S. W. Magennis.** *J. Am. Chem. Soc.*, **2012**, 134, 6280 –6285.

References Chapter 3

- [1] **B. Petersson, et al.** Crystal structure of a partly self-complementary peptide nucleic acid (PNA) oligomer showing a duplex-triplex network. *J Am Chem Soc.*, **2005**, 127, 5, 1424–30.
- [2] **J. Summerton, D. Weller.** Morpholino Antisense Oligomers: Design, Preparation and Properties. *Antisense & Nucleic Acid Drug Development*, **1997**, 7, 187–195.
- [3] **J. Summerton.** Morpholino Antisense Oligomers: The Case for an RNase-H Independent Structural Type. *Biochimica et Biophysica Acta*, **1999**, 1489, 141–158.
- [4] **Denis A. Malyshev, Kirandeep Dhani, Thomas Lavergne, Tingjian Chen, Nan Dai, Jeremy M. Foster, Ivan R. Corrêa, Floyd E. Romesberg.** A semi-synthetic organism with an expanded genetic alphabet. *Nature*, **2014**, 509, 385–388.
- [5] **Ward, et al.** Fluorescence Studies of Nucleotides and Polynucleotides I. Formycin 2-Aminopurine Riboside 2,6-Diaminopurine Riboside and Their Derivatives. *J. Biol. Chem.*, **1969**, 244, 1228–37.
- [6] **Hawkins.** Fluorescent pteridine nucleoside analogs - A window on DNA interactions. *Cell Biochem. Biophys.*, **2001**, 34, 257–81.
- [7] **Berry, et al.** Pyrrolo-dC and pyrrolo-C: fluorescent analogs of cytidine and 2'-deoxycytidine for the study of oligonucleotides. *Tetrahedron Lett.*, **2004**, 45, 2457–61.
- [8] **Wojciechowski, et al.** Fluorescence and hybridization properties of peptide nucleic acid containing a substituted phenylpyrrolo-cytosine designed to engage guanine with an additional H-bond. *J. Am. Chem. Soc.*, **2008**, 130, 12574–12575.
- [9] **Greco, et al.** Simple fluorescent pyrimidine analogues detect the presence of DNA abasic sites. *J. Am. Chem. Soc.*, **2005**, 127, 10784–85.
- [10] **Rist, et al.** Fluorescent nucleotide base analogs as probes of nucleic acid structure, dynamics and interactions. *Curr. Org. Chem.*, **2002**, 6 775–93.
- [11] **Wilson, et al.** Fluorescent DNA base replacements: reporters and sensors for biological systems. *Org. Biomol. Chem.*, **2006**, 4, 4265–74.
- [12] **Wilhelmsson.** Fluorescent nucleic acid base analogues. *Q. Rev. Biophys.*, **2010**, 43, 2, 159–183.
- [13] **Sinkeldam, et al.** Fluorescent analogs of Biomolecular Building Blocks: Design, properties and applications. *Chem. Rev.*, **2010**, 110, 5, 2579–2619.
- [14] **Wilhelmsson, et al.** A highly fluorescent DNA base analogue that forms Watson-Crick base pairs with guanine. *J. Am. Chem. Soc.*, **2001**, 123, 2434–35.
- [15] **Sandin, et al.** Fluorescent properties of DNA base analogue tC upon incorporation into DNA - negligible influence of neighbouring bases on fluorescence quantum yield. *Nucleic Acids Res.*, **2005**, 33, 5019–25.

- [16] Sandin, et al. Characterization and use of an unprecedentedly bright and structurally non-perturbing fluorescent DNA base analogue. *Nucleic Acids Res.*, **2008**, 36, 157–67.
- [17] Börjesson, et al. Nucleic acid base analog FRET-pair facilitating detailed structural measurements in nucleic acid containing systems. *J. Am. Chem. Soc.*, **2009**, 131, 4288–93.
- [18] M. D. Kirnos, I. Y. Khudyakov, N. I. Alexandrushkina, B. F. Vanyushin. 2-aminoadenine is an adenine substituting for a base in S-2L cyanophage DNA. *Nature*, **1977**, 270, 5635, 369–70.
- [19] S. C. Johnson, et al. A third base pair for the polymerase chain reaction: inserting isoC and isoG. *Nucleic Acids Res.*, **2004**, 29, 32, 6, 1937–41.
- [20] Y. Taniguchi, E. T. Kool. Nonpolar isosteres of damaged DNA bases: effective mimicry of mutagenic properties of 8-oxopurines. *J. Am. Chem. Soc.*, **2007**, 129, 28, 8836–44.
- [21] G. T. Hwang, F. E. Romesberg. Unnatural Substrate Repertoire of A, B, and X Family DNA Polymerases. *J. Am. Chem. Soc.*, **2008**, 130, 14872–14882.
- [22] M. Kimoto, et al. Fluorescent probing for RNA molecules by an unnatural base-pair system. *Nucleic Acids Res.*, **2007**, 35, 16, 5360–9.
- [23] N. Zimmermann, et al. A second-generation copper(II)-mediated metallo-DNA-base pair. *Bioorg. Chem.*, **2004**, 32, 1, 13–25.
- [24] H. Liu, et al. A four-base paired genetic helix with expanded size. *Science*, **2003**, 302, 5646, 868–71.
- [25] H. Zhang, A. Calzolari, R. Di Felice. On the Magnetic Alignment of Metal Ions in a DNA-Mimic Double Helix. *J. Phys. Chem. B*, **2005**, 109, 15345–15348.
- [26] A. Ono, H. Togashi. Highly Selective Oligonucleotide-Based Sensor for Mercury(II) in Aqueous Solutions. *Angew. Chem.*, **2004**, 43, 4300–4302.
- [27] Denis A. Malyshev, Kirandeep Dhani, Henry T. Quach, Thomas Lavergne, Phillip Ordoukhanian. Efficient and sequence-independent replication of DNA containing a third base pair establishes a functional six-letter genetic alphabet. *Proceedings of the National Academy of Sciences of the United States of America*, **2012**, 109, 30, 12005–12010.
- [28] I. Hirao, et al. An unnatural base pair for incorporating amino acid analogs into proteins. *Nat. Biotechnol.*, **2002**, 20, 177–182.
- [29] I. Hirao, et al. An unnatural hydrophobic base pair system: site-specific incorporation of nucleotide analogs into DNA and RNA. *Nat. Methods*, **2006**, 6, 729–735.
- [30] M. Kimoto, et al. Generation of high-affinity DNA aptamers using an expanded genetic alphabet. *Nat. Biotechnol.*, **2013**, 31, 453–457.
- [31] P. Herdewijn, P. Marlière. Toward safe genetically modified organisms through the chemical diversification of nucleic acids. *Chem. Biodivers.*, **2009**, 6, 6, 791–808.

- [32] E. Uhlmann, A. Peyman. *Chemical Reviews*, **1990**, 90, 543. A. Demesmaeker, R. Häner, P. Martin, H. E. Moser. *Accounts of Chemical Research*, **1995**, 28, 366. S. M. Freier, K. H. Altmann. *Nucleic Acids Research*, **1997**, 25, 4429. K. H. Altmann, N. M. Dean, D. Fabbro, S. M. Freier, T. Geiger, R. Häner. D. Husken, P. Martin, B. P. Monia, M. Muller, F. Natt, P. Nicklin, J. Phillips, U. Pieleas, H. Sasmor, H. E. Moser. *Chimia*, **1996**, 50, 168. M. Matteucci, K. Y. Lin, S. Butcher, C. Moulds. *Journal of the American Chemical Society*, **1991**, 113, 7767. C. A. Stein, Y. C. Cheng. *Science*, **1993**, 261, 1004.
- [33] N. Langkjaer, A. Pasternak, J. Wengel. *Bioorganic & Medicinal Chemistry*, **2009**, 17, 5420. M. A. Campbell, J. Wengel. *Chemical Society Reviews*, **2011**, 40, 5680. A. A. Koshkin, S. K. Singh, P. Nielsen, V. K. Rajwansi, R. Kumar, M. Meldgaard, C. E. Olsen, J. Wengel. *Tetrahedron*, **1998**, 54, 3607. S. K. Singh, P. Nielsen, A. A. Koshkin, J. Wengel. *Chemical Communications*, **1998**, 455. M. Bohringer, H. J. Roth, J. Hunziker, M. Gobel, R. Krishnan, A. Giger, B. Schweizer, J. Schreiber, C. Leumann, A. Eschenmoser. *Helvetica Chimica Acta*, **1992**, 75, 1416. M. Tarkoy, M. Bolli, B. Schweizer, C. Leumann. *Helvetica Chimica Acta*, **1993**, 76, 481. M. Tarkoy, M. Bolli, C. Leumann. *Helvetica Chimica Acta*, **1994**, 77, 716. S. P. Scheidegger, C. J. Leumann. *Chemistry - a European Journal*, **2006**, 12, 8014.
- [34] R. Declercq, A. Van Aerschot, R. J. Read, P. Herdewijn, L. Van Meervelt. *J. Am. Chem. Soc.*, **2002**, 124, 928-933.
- [35] A. Eichert, K. Behling, C. Betzel, V. A. Erdmann, J. P. Furste, C. Forster. *Nucleic Acids Res.*, **2010**, 38, 6729-6736.
- [36] K. Betz, D. A. Malyshev, T. Laverigne, W. Welte, K. Diederichs, F. E. Romesberg, A. Marx. *J. Am. Chem. Soc.*, **2013**, 135, 18637.
- [37] Millie M. Georgiadis, Isha Singh, Whitney F. Kellett, Shuichi Hoshika, Steven A. Benner, Nigel G. J. Richards. *J. Am. Chem. Soc.*, **2015**, 137, 6947–6955.
- [38] V. L. Malinovskii, D. Wenger, R. Haener. *Chemical Society Reviews*, **2010**, 39, 410.
- [39] Y. Zheng, H. Long, G. C. Schatz, F. D. Lewis. *Chemical Communications*, **2005**, 4795. H. Kashida, M. Tanaka, S. Baba, T. Sakamoto, G. Kawai, H. Asanuma, M. Komiyama. *Chemistry - a European Journal*, **2006**, 12, 777. R. L. Letsinger, T. F. Wu. *Journal of the American Chemical Society*, **1995**, 117, 7323. U. B. Christensen, E. B. Pedersen. *Nucleic Acids Research*, **2002**, 30, 4918. K. Berlin, R. K. Jain, M. D. Simon, C. Richert. *Journal of Organic Chemistry*, **1998**, 63, 1527.
- [40] S. M. Langenegger and R. Häner. *ChemBioChem*, **2005**, 6, 848–851. S. M. Langenegger and R. Häner. *Chem. Commun.*, **2004**, 2792–2793. S. M. Langenegger, R. Häner. *Helv. Chim. Acta*, **2002**, 3414-3421.
- [41] H. Bittermann, D. Siegemund, V. L. Malinovskii and R. Häner. *J. Am. Chem. Soc.*, **2008**, 130, 15285–15287.
- [42] Larysa I. Markova, Vladimir L. Malinovskii, Leonid D. Patsenker and Robert Häner. *Org. Biomol. Chem.*, **2012**, 10, 8944-8947.

[43] Oleg Khorev, Caroline D. Bösch, Markus Probst and Robert Häner. *Chem. Sci.*, **2014**, 5, 1506-1512.

[44] S. M. Langenegger, R. Häner. *Chem. Commun.*, **2004**, 2792-2793.

[45] I. Trkulja, R. Häner. *Bioconjugate Chem.*, **2007**, 18, 289-292.

[46] F. Garo, R. Häner. *Angew. Chem. Int. Ed.*, **2012**, 51, 916–919.

[47] O. O. Adeyemi, V. L. Malinovskii, S. M. Biner, G. Calzaferri, R. Häner. *Chem. Comm.*, **2012**, 48, 9589-9591.

References Chapter 4

- [1] **Yashveer Singh, Pierre Murat, Eric Defrancq.** Recent developments in oligonucleotide conjugation. *Chem. Soc. Rev.*, **2010**, 39, 2054–2070.
- [2] **Vladimir L. Malinovskii, Daniel Wenger, Robert Häner.** Nucleic acid-guided assembly of aromatic chromophores. *Chem. Soc. Rev.*, **2010**, 39, 410–422.
- [3] **R. Häner, S. M. Biner, S. M. Langenegger, T. Meng, V. L. Malinovskii.** A highly sensitive, excimer-controlled molecular beacon. *Angew. Chem. Int. Ed.*, **2010**, 49, 1227-1230.
- [4] **F. Garo, R. Häner.** A DNA-Based Light Harvesting Antenna. *Angew. Chem. Int. Ed.*, **2012**, 51, 916-919.
- [5] **N. C. Seeman, N. R. Kallenbach.** DNA Branched Junctions. *Annual Review of Biophysics and Biomolecular Structure*, **1994**, 23, 53-86.
- [6] **Tara Sabir, Anita Toulmin, Long Ma, Anita C. Jones, Peter McGlynn, Gunnar F. Schröder, Steven W. Magennis.** Branchpoint Expansion in a Fully Complementary Three-Way DNA Junction. *J. Am. Chem. Soc.*, **2012**, 134, 6280–6285.
- [7] **Sophie Vuong, Loïc Stefan, Pauline Lejault, Yoann Rousselin, Franck Denat, David Monchaud.** Identifying three-way DNA junction-specific small-molecules. *Biochimie*, **2012**, 94, 442-450.
- [8] **Lingyan Feng, Chuanqi Zhao, Yi Xiao, Li Wu, Jinsong Ren, Xiaogang Qu.** Electrochemical DNA three-way junction based sensor for distinguishing chiral metallo-supramolecular complexes. *Chem. Commun.*, **2012**, 48, 6900–6902.
- [9] **Taku Murakami, Jun Sumaoka, Makoto Komiyama.** Sensitive RNA detection by combining three-way junction formation and primer generation-rolling circle amplification. *Nucleic Acids Research*, **2012**, 40, 3.
- [10] **M. Probst, D. Wenger, S.M. Biner, R. Häner.** The DNA three-way junction as a mould for tripartite chromophore assembly. *Org. Biomol. Chem.*, **2012**, 10, 755–759.
- [11] **N. R. Markham, M. Zuker.** UNAFold - Software for nucleic acid folding and hybridization, **2008**.
- [12] **N. R. Markham, M. Zuker.** *Nucl. Acids Res.*, **2005**, 33, W577-W581.
- [13] **H. Bittermann, D. Siegemund, V. L. Malinovskii, R. Häner.** *J. Am. Chem. Soc.*, **2008**, 130, 15285-15287.
- [14] **M. Masuko, H. Ohtani, K. Ebata, A. Shimadzu.** *Nucl. Acids Res.*, **1998**, 26, 5409-5416.
- [15] **P. L. Paris, J. M. Langenhan, E. T. Kool.** *Nucl. Acids Res.*, **1998**, 26, 3789-3793.
- [16] **K. Yamana, T. Iwai, Y. Ohtani, S. Sato, M. Nakamura, H. Nakano.** *Bioconjug. Chem.*, **2002**, 13, 1266-1273.

- [17] U. B. Christensen, E. B. Pedersen. *Nucl. Acids Res.*, **2002**, 30, 4918-4925.
- [18] S. M. Langenegger, R. Häner. *Chem. Commun.*, **2004**, 2792-2793.
- [19] K. Fujimoto, H. Shimizu, M. Inouye. *J. Org. Chem.*, **2004**, 69, 3271-3275.
- [20] P. J. Hrdlicka, B. R. Babu, M. D. Sorensen, J. Wengel. *Chem. Commun.*, **2004**, 1478-1479.
- [21] I. Trkulja, R. Häner. *Bioconjug. Chem.*, **2007**, 18, 289-292.
- [22] I. Trkulja, R. Häner. *J. Am. Chem. Soc.*, **2007**, 129, 7982-7989.
- [23] I. V. Astakhova, V. A. Korshun, J. Wengel. *Chem. Eur. J.*, **2008**, 14, 11010-11026.
- [24] S. Shirai, S. Iwata, T. Tani, S. Inagaki. *J. Phys. Chem. A*, **2011**, 115, 7687-7699.
- [25] S. M. Biner, D. Kummer, V. L. Malinovskii, R. Häner. *Org. Biomol. Chem.*, **2011**, 9, 2628-2633.
- [26] C. A. Hunter, J. K. M. Sanders. *J. Am. Chem. Soc.*, **1990**, 112, 5525-5534.
- [27] R. S. Lokey, B. L. Iverson. *Nature*, **1995**, 375, 303-305.
- [28] A. L. Sisson, N. Sakai, N. Banerji, A. Furstenberg, E. Vauthey, S. Matile. *Angew. Chem. Int. Ed.*, **2008**, 47, 3727-3729.
- [29] A. Pitto-Barry, N. P. E. Barry, O. Zava, R. Deschenaux, B. Therrien. *Chem. Asian J.*, **2011**, 6, 1595-1603.
- [30] H. Langhals. *Helv. Chim. Acta*, **2005**, 88, 1309-1343.
- [31] F. Würthner. *Chem. Commun.*, **2004**, 1564-1579.
- [32] S. Ghosh, X. Q. Li, V. Stepanenko, F. Würthner. *Chem. Eur. J.*, **2008**, 14, 11343-11357.
- [33] A. D. Q. Li, W. Wang, L. Q. Wang. *Chem. Eur. J.*, **2003**, 9, 4594-4601.
- [34] Y. Zheng, H. Long, G. C. Schatz, F. D. Lewis. *Chem. Commun.*, **2005**, 4795-4797.
- [35] D. Baumstark, H. A. Wagenknecht. *Chem. Eur. J.*, **2008**, 14, 6640-6645.
- [36] J. Wang, A. Kulago, W. R. Browne, B. L. Feringa. *J. Am. Chem. Soc.*, **2010**, 132, 4191-4196.
- [37] N. Rahe, C. Rinn, T. Carell. *Chem. Commun.*, **2003**, 2119-2121.

References Chapter 5

- [1] Zahid et al. *Nanoscale Research Letters*, **2013**, 8, 119.
- [2] Stefan Howorka. *Langmuir*, **2013**, 29, 7344–7353.
- [3] Buckhout-White et al. *ACS Nano*, **2012**, 6, 2, 1026–1043.
- [4] Jinglin Fu, Minghui Liu, Yan Liu, Hao Yan. *Accounts of Chemical Research*, **2012**, 45, 8, 1215–1226.
- [5] Gerrard et al. *ACS Nano*, **2012**, 6, 10, 9221–9228.
- [6] Tao Li, Michael Famulok. *J. Am. Chem. Soc.*, **2013**, 135, 1593–1599.
- [7] Xiwen Xing, Xiaoling Wang, Liang Xu, Yang Tai, Luyang Dai, Xiaolong Zheng, Wuxiang Mao, Xiaowei Xu, Xiang Zhou. *Org. Biomol. Chem.*, **2011**, 9, 6639.
- [8] Toshihiro Ihara, Yusuke Kitamura. *Journal of Photochemistry and Photobiology C: Photochemistry Reviews*, **2012**, 13, 148–167.
- [9] Kristmann Gislason, Dnyaneshwar B. Gophane, Snorri Th. Sigurdsson. *Org. Biomol. Chem.*, **2013**, 11, 149.
- [10] Ulrike Wenge, Thomas Ehenschwender, Hans-Achim Wagenknecht. *Bioconjugate Chem.*, **2013**, 24, 301–304.
- [11] Takeshi Maeda, Tatsuya Tsukamoto, Ayaka Seto, Shigeyuki Yagi, Hiroyuki Nakazumi. *Macromol. Chem. Phys.*, **2012**, 213, 2590–2597.
- [12] Karl J. Thorley, Frank Würthner. *Org. Lett.*, **2012**, 14, 24.
- [13] Bing Wang, Qiong Yang, Libing Liu, Shu Wang. *Colloids and Surfaces B: Biointerfaces*, **2011**, 85, 8–11.
- [14] Shenliang Wang, Jia Guo, Toshikazu Ono, Eric T. Kool. *Angew. Chem. Int. Ed.*, **2012**, 51, 7176–7180.
- [15] Ingo H. Stein, Christian Steinhauer, Philip Tinnefeld. *J. Am. Chem. Soc.*, **2011**, 133, 4193–4195.
- [16] Spillmann et al. *ACS Nano*, **2013**, 7, 8, 7101–7118.
- [17] Vikas Garg, Gerdenis Kodis, Paul A. Liddell, Yuichi Terazono, Thomas A. Moore, Ana L. Moore, Devens Gust. *J. Phys. Chem. B*, **2013**, 117, 38, 11299–11308.
- [18] Hyeonuk Yeo, Kazuo Tanaka, Yoshiki Chujo. *Macromolecules*, **2013**, 46, 2599–2605.
- [19] Bo Albinsson, Jonas K. Hannestad, Karl Börjesson. *Coordination Chemistry Reviews*, **2012**, 256, 2399–2413.
- [20] Palash K. Dutta, Reji Varghese, Jeanette Nangreave, Su Lin, Hao Yan, Yan Liu. *J. Am. Chem. Soc.*, **2011**, 133, 11985–11993.
- [21] Jakob G. Woller, Jonas K. Hannestad, Bo Albinsson. *J. Am. Chem. Soc.*, **2013**, 135, 2759–2768.
- [22] Núria Sancho Oltra, Wesley R. Browne, Gerard Roelfes. *Chem. Eur. J.*, **2013**, 19, 2457–2461.
- [23] S. Maiti et al. *Biophysical Chemistry*, **2011**, 159, 162–171.
- [24] Tod A. Pascal, William A. Goddard, Prabal K. Maiti, Nagarajan Vaidehi. *J. Phys. Chem. B*, **2012**, 116, 12159–12167.
- [25] Tara Sabir, Anita Toulmin, Long Ma, Anita C. Jones, Peter McGlynn, Gunnar F. Schröder,

- Steven W. Magennis. *J. Am. Chem. Soc.*, **2012**, 134, 6280–6285.
- [26] Oren Reinstein, Miguel A. D. Neves, Makbul Saad, Sherry N. Boodram, Stephanie Lombardo, Simone A. Beckham, Jason Brouwer, Gerald F. Audette, Patrick Groves, Matthew C. J. Wilce, Philip E. Johnson. *Biochemistry*, **2011**, 50, 9368–9376.
- [27] S. Vuong et al. *Biochimie*, **2012**, 442–450.
- [28] Yunfeng Xia, Siwen Gan, Qinghao Xu, Xiaowen Qiu, Peiyi Gao, Shasheng Huang. *Biosensors and Bioelectronics*, **2013**, 39, 250–254.
- [29] Shurong Tang, Ping Tong, Heng Li, Fang Gu, Lan Zhang. *Biosensors and Bioelectronics*, **2013**, 41, 397–402.
- [30] Lingyan Feng, Chuanqi Zhao, Yi Xiao, Li Wu, Jinsong Rena, Xiaogang Qu. *Chem. Commun.*, **2012**, 48, 6900–6902.
- [31] Jason M. Thomas, Hua-Zhong Yu, Dipankar Sen. *J. Am. Chem. Soc.*, **2012**, 134, 13738–13748.
- [32] Hai Xiong, Peter Leonard, Frank Seela. *Bioconjugate Chem.*, **2012**, 23, 856–870.
- [33] Wu Su, Clive R. Bagshaw, Glenn A. Burley. *Scientific Reports*, **2013**, 3, 1883.
- [34] Pawan Kumar, Khalil I. Shaikh, Anna S. Jørgensen, Surender Kumar, Poul Nielsen. *J. Org. Chem.*, **2012**, 77, 9562–9573.
- [35] Jean-Louis H. A. Duprey, Yusuke Takezawa, Mitsuhiko Shionoya. *Angew. Chem. Int. Ed.*, **2013**, 52, 1212–1216.
- [36] F. Garo, R. Häner. *Angew. Chem. Int. Ed.*, **2012**, 51, 916–919.
- [37] Y. Nakamura, T. Yamazaki, J. Nishimura. *Org. Lett.*, **2005**, 7, 3259–3262.
- [38] F. D. Lewis, E. L. Burch. *J. Photochem. Photobiol. A - Chem.*, **1996**, 96, 19–23.
- [39] J. B. Birks. in *The Exciplex*, Eds.: M. Gordon, W. R. Ware, Academic Press Inc., New York 1975, pp. 39–73.
- [40] F. M. Winnik, *Chem. Rev.*, **1993**, 93, 587–614.
- [41] P. Ceroni, V. Balzani. in *The Exploration of Supramolecular Systems and Nanostructures by Photochemical Techniques*, 78, Ed.: P. Ceroni, Springer, 2012, pp. 21–38.
- [42] J. R. Lakowicz. *Principles of Fluorescence Spectroscopy*, 3rd ed. Springer, Singapore, 2006.
- [43] N. Bouquin, V. L. Malinovskii, R. Häner. *Chem. Commun.*, **2008**, 1974–1976.
- [44] D. Pevenage, M. Van der Auweraer, F. C. De Schryver. *Chem. Phys. Lett.*, **2000**, 319, 512–520.
- [45] T. Sabir, A. Toulmin, L. Ma, A. C. Jones, P. McGlynn, G. F. Schröder, S. W. Magennis. *J. Am. Chem. Soc.*, **2012**, 134, 6280–6285.
- [46] D. M. J. Lilley. *Q. Rev. Biophys.*, **2000**, 33, 109–159.
- [47] D. L. Dexter. *J. Chem. Phys.*, **1953**, 21, 836–850.
- [48] H. Bittermann, D. Siegemund, V. L. Malinovskii, R. Häner. *J. Am. Chem. Soc.*, **2008**, 130, 15285–15287. S. M. Langenegger, R. Häner. *Chem. Commun.*, **2004**, 2792–2793.

[49] S. M. Langenegger, R. Häner. *Helv. Chim. Acta*, **2002**, 3414-3421. S. M. Langenegger, R. Häner. *ChemBioChem*, **2005**, 6, 848-851.

[50] N. Rahe, C. Rinn, T. Carell. *Chem. Commun.*, **2003**, 2119-2121.

[51] M. Shimomura, R. Ando and T. Kunitake. *Ber. Bunsenges. Phys. Chem.*, **1983**, 87, 1134-1143.

References Chapter 6

- [1] **F. Garo, R. Häner.** A DNA-Based Light Harvesting Antenna. *Angew. Chem. Int. Ed.*, **2012**, 51, 916-919.
- [2] **O. O. Adeyemi, V. L. Malinovskii, S. M. Biner, G. Calzaferri, R. Häner.** Photon Harvesting by Excimer-Forming Multichromophores. *Chem. Comm.*, **2012**, 48, 9589-9591.
- [3] **Philipp Ensslen and Hans-Achim Wagenknecht.** One-Dimensional Multichromophor Arrays Based on DNA: From Self-Assembly to Light-Harvesting. *Acc. Chem. Res.*, **2015**, 48 (10), 2724–2733.
- [4] **M. Probst, S. M. Langenegger, R. Häner.** A modular LHC built on the DNA three-way junction. *Chem. Commun.*, **2014**, 50, 159-161.
- [5] **Philipp Ensslen, Fabian Brandl, Sabrina Sezi, Reji Varghese, Roger-Jan Kutta, Bernhard Dick, Hans-Achim Wagenknecht.** DNA-Based Oligochromophores as Light-Harvesting Systems. *Chem. Eur. J.*, **2015**, 21, 9349–9354.
- [6] **P. Röthlisberger, F. Wojciechowski, C. J. Leumann.** Enhancement of excess electron transfer efficiency in DNA containing a phenothiazine donor and multiple stable phenanthrenyl base pairs. *Chemistry - A European Journal*, **2013**, 35, 11518-11521.
- [7] **Palash K. Dutta, Symon Levenberg, Andrey Loskutov, Daniel Jun, Rafael Saer, J. Thomas Beatty, Su Lin, Yan Liu, Neal W. Woodbury and Hao Yan.** A DNA-Directed Light-Harvesting/Reaction Center System. *J. Am. Chem. Soc.*, **2014**, 136 (47), 16618–16625.
- [8] **F. Garo, R. Häner.** Influence of a GC base pair on excitation energy transfer in DNA-assembled phenanthrene π -stacks. *Bioconjug. Chem.*, **2012**, 23, 2105-2113.
- [9] **Susan Buckhout-White, Jonathan C. Claussen, Joseph S. Melinger, Zaire Dunningham, Mario G. Ancona, Ellen R. Goldman and Igor L. Medintz.** A triangular three-dye DNA switch capable of reconfigurable molecular logic. *RSC Adv.*, **2014**, 4, 48860-48871.
- [10] **Philipp Ensslen, Yannic Fritza, Hans-Achim Wagenknecht.** Mixed non-covalent assemblies of ethynyl nile red and ethynyl pyrene along oligonucleotide templates. *Org. Biomol. Chem.*, **2015**, 13, 487-492.
- [11] **Christopher M. Spillmann, Susan Buckhout-White, Eunkeu Oh, Ellen R. Goldman, Mario G. Ancona and Igor L. Medintz.** Extending FRET cascades on linear DNA photonic wires. *Chem. Commun.*, **2014**, 50, 7246-7249.
- [12] **C.B. Winiger, S. Li, G.R. Kumar, S.M. Langenegger, R. Häner.** Long Distance EET in Light-Harvesting Supramolecular Polymers. *Angew. Chem. Int. Ed.*, **2014**, 53, 13609-13613.
- [13] **L. I. Markova, V. L. Malinovskii, L. D. Patsenker, R. Häner.** J- vs. H-type assembly: pentamethine cyanine (Cy5) as near-IR chiroptical reporter. *Chem. Commun.*, **2013**, 49, 5298-5300.

[14] L. I. Markova, V. L. Malinovskii, L. D. Patsenker, R. Häner. Synthesis and Properties of Squaraine-Modified DNA. *Org. Biomol. Chem.*, **2012**, 10, 8944-8947.

[15] N. Bouquin, V. L. Malinovskii, R. Häner. Highly efficient quenching of excimer fluorescence by perylene diimide in DNA. *Chem. Commun.*, **2008**, 1974-1976.

[16] R. Häner, S. M. Biner, S. M. Langenegger, T. Meng, V. L. Malinovskii. A highly sensitive, excimer-controlled molecular beacon. *Angew. Chem. Int. Ed.*, **2010**, 49, 1227-1230.

[17] **Source:** The European Advanced Light Microscopy Network (EAMNET). Teaching module: Fluorescence Resonance Energy Transfer (FRET). Online:

http://www.embl.de/eamnet/downloads/modules/FRET_teaching_module.pdf (31.03.2016).

[18] **Source:** Glen Research Corporation. Cyanine Labelling. Online:

<http://www.glenresearch.com/Catalog/catalog.php?page=labelling#cyanine> (31.03.2016).

References Chapter 7

- [1] D. Renciuik, O. Blacque, M. Vorlickova, B. Spingler. *Nucl. Acids Res.*, **2013**, *41*, 9891-9900.
- [2] K. Robeyns, P. Herdewijn, L. Van Meervelt. *PNA & XNA*, **2010**, *1*, 2-8.
- [3] M. M. Georgiadis, I. Singh, W. F. Kellett, S. Hoshika, S. A. Benner, N. G. J. Richards. *J. Am. Chem. Soc.*, **2015**, *137*, 21, 6947–6955.
- [4] A. R. Hernandez, Y. Shao, S. Hoshika, Z. Yang, S. A. Shelke, J. Herrou, H.-J. Kim, M.-J. Kim, J. A. Piccirilli, S. A. Benner. *Angew. Chem. Int. Ed.*, **2015**, *54*, 9853–9856.
- [5] Source: RCSB Protein Data Bank. Online: <http://www.rcsb.org/pdb/home/home.do> (04.01.2016).
- [6] M. Sokolowska, M. Kaus-Drobek, H. Czapinska, G. Tamulaitis, R. H. Szczepanowski, C. Urbanke, V. Siksnys, M. Bochtler. *Journal of Molecular Biology*, **2007**, *369*, 3, 722–734.
- [7] A. D. Gelinas, D. R. Davies, T. E. Edwards, J. C. Rohloff, J. D. Carter, C. Zhang, S. Gupta, Y. Ishikawa, M. Hirota, Y. Nakaishi, T. C. Jarvis, N. Janjic. *The Journal of Biological Chemistry*, **2014**, *289*, 12, 8720–8734.
- [8] D. Renciuik, O. Blacque, M. Vorlickova, B. Spingler. *Nucleic Acids Research*, **2013**, *41*, 21, 9891–9900.
- [9] M. Tsunoda, N. Karino, Y. Ueno, A. Matsuda, A. Takenaka. *Acta Cryst*, **2001**, D57, 345-348.
- [10] Wang et al., *Chem. Res. Toxicol.*, **2008**, *21*, 1348–1358. Lin et al., *J. Mol. Biol.*, **2001**, *306*, 1059-1080. Rodriguez et al., *Biochemistry*, **2014**, *53*, 1827–1841. Hsu et al., *The Journal of Biological Chemistry*, **2005**, *280*, 5, 3764–3770. Zhang et al., *J. Mol. Biol.*, **2005**, *346*, 951–965. Tang et al., *Biochemistry*, **2012**, *51*, 9751–9762. Gu et al., *Biochemistry*, **2003**, *42*, 917-921.
- [11] R. Sukackaite, S. Grazulis, M. Bochtler, V. Siksnys. *J. Mol. Biol.*, **2008**, *378*, 1084–1093.
- [12] The Universal Protein Resource (UniProt). URL: <http://www.uniprot.org/uniprot/A3FMN7> (17.01.2016)
- [13] The European Bioinformatics Institute. URL: http://www.ebi.ac.uk/Tools/st/emboss_backtranseq/ (17.01.2016)
- [14] C. B. Winiger, S. Li, G. R. Kumar, S. M. Langenegger, R. Häner., *Angew. Chem. Int. Ed.*, **2014**, *53*, 13609-13613.
- [15] H. Bittermann, D. Siegemund, V. L. Malinovskii, R. Häner. *J. Am. Chem. Soc.*, **2008**, *130*, 15285-15287.
- [16] W. Kabsch. XDS. *Acta Cryst*. **2010**, D66, 125-132.
- [17] P. D. Adams, P. V. Afonine, G. Bunkóczi, V. B. Chen, I. W. Davis, N. Echols, J. J. Headd, L.-W. Hung, G. J. Kapral, R. W. Grosse-Kunstleve, A. J. McCoy, N. W. Moriarty, R. Oeffner, R. J. Read, D. C. Richardson, J. S. Richardson, T. C. Terwilliger and P. H. Zwart. *Acta Cryst*. **2010**, D66, 213-221. A. J. McCoy, R. W. Grosse-Kunstleve, P. D. Adams, M. D. Winn, L. C. Storoni, and R.J. Read. *J Appl Crystallogr*, **2007**, *40*, 658-674. P. V. Afonine, R. W. Grosse-Kunstleve, N. Echols, J. J. Headd, N. W. Moriarty, M. Mustyakimov, T. C. Terwilliger, A. Urzhumtsev, P. H. Zwart, and P. D. Adams. *Acta Crystallogr D Biol Crystallogr*, **2012**, *68*, 352-67. N. Echols, N. W. Moriarty, H. E. Klei, P. V. Afonine, G. Bunkóczi, J. J. Headd, A. J. McCoy, R. D. Oeffner, R. J. Read, T. C. Terwilliger, and P. D. Adams. *Acta Crystallogr D Biol Crystallogr*, **2014**, *70*, 144-54. N.

Echols, R. W. Grosse-Kunstleve, P. V. Afonine, G. Bunkóczi, V. B. Chen, J. J. Headd, A. J. McCoy, N. W. Moriarty, R. J. Read, D. C. Richardson, J. S. Richardson, T. C. Terwilliger, and P. D. Adams. *J. Appl. Cryst.*, **2012**, 45, 581-586.

[18] P. Emsley, B. Lohkamp, W. Scott, K. Cowtan. *Acta Crystallographica Section D - Biological Crystallography*, **2010**, 66, 486-501.

[19] A. W. Schüttelkopf and D. M. F. van Aalten. *Acta Crystallogr.*, **2004**, D60, 1355–1363.

[20] Crawford et al., *J. Am. Chem. Soc.*, **2011**, 133, 13349–13362. **Masuko et al.,** *Nucleic Acids Research*, **1998**, 26, 23, 5409–5416. **Bains et al.,** *Biochemistry*, **2012**, 51, 6207–6219. **Fujii et al.,** *Bioconjugate Chem.*, **2015**, 26, 537–548. **Smirnov et al.,** *Nucleic Acids Research*, **2002**, 30, 24, 5561-5569.

Appendix A

Synthetic and analytical procedure

The synthesis of the building blocks is described: **P** (phenanthrene), **S** (pyrene, bisamidepyrene),^[1,2,3] **X** (pyrene, 1,6-dialkynylpyrene), **Y** (pyrene, 1,8-dialkynylpyrene),^[4] **E** (peryleneimide, PDI),^[5] **Cy5** (commercially available, see below).

Oligonucleotide-synthesis was performed by an automated oligonucleotide synthesis on a 394-DNA/RNA synthesizer (*Applied Biosystems*), based on phosphoramidite chemistry. Cleavage from the solid support and final deprotection was done by an overnight treatment with 30% NH₄OH solution at 55°C. The Cy5-phosphoramidite was obtained from *GlenResearch* (Sterling, USA), incorporation, cleavage and deprotection followed the *UltraMILD* procedure (*GlenResearch*). All unmodified strands were commercially obtained from *Microsynth* (Balgach, Switzerland).

Reversed-phase HPLC purification of the modified oligonucleotides was carried out on a LC-20AT or LC-10ATvp or LC-10ADvp system (*Shimadzu*, Kyoto, Japan) using a LiChrospher 100 RP18, 5 μm column (*Dr. Maisch GmbH*, Ammerbuch, Germany) and a gradient consisting of eluent A (0.1 M triethylamine / acetic acid) and B (acetonitrile) with 5-50% B within 20 minutes. The temperature of the column was set to 40°C in a CTO-20A oven (*Shimadzu*).

Molecular mass of the synthesized oligonucleotides was either determined by LC-MS (LC-20AT, SPD-M20A, LCMS-2010EV, all *Shimadzu*), with a C18 3.5 μm 2.1x100 mm column (XTerra MS, *Waters*, Milford, USA) and an applied gradient of 100% A (50 mM ammonium formate) to 50% B (acetonitrile) over 10 minutes. Or by a LC-MS (negative ion mode, acetonitrile/H₂O/triethylamine) system on a Sciex QTrap (*Applied Biosystems*).

[1] S. M. Langenegger and R. Häner. *ChemBioChem*, **2005**, 6, 848–851.

[2] S. M. Langenegger and R. Häner. *Chem. Commun.*, **2004**, 2792–2793.

[3] S. M. Langenegger, R. Häner. *Helv. Chim. Acta*, **2002**, 3414-3421.

[4] H. Bittermann, D. Siegemund, V. L. Malinovskii and R. Häner. *J. Am. Chem. Soc.*, **2008**, 130, 15285–15287.

[5] N. Rahe, C. Rinn and T. Carell. *Chem. Commun.*, **2003**, 2119–2121.

UV-Vis spectra were collected on a Varian Cary-100 Bio-UV / Visible spectrophotometer or a Varian Cary 300 Scan UV-Visible Spectrophotometer equipped with a Varian Cary-block temperature controller, 1 cm quartz cuvettes and processed with Varian WinUV software. Experiments were performed with samples prepared from 1 μM single strand concentration in *Milli-Q* H_2O containing 100 mM NaCl and 10 mM sodium phosphate buffer (pH 7.0).

Fluorescence spectra were acquired on a Varian Cary Eclipse fluorescence spectrophotometer equipped with a Varian Cary-block temperature controller with 1 cm x 1 cm quartz cuvettes and Varian Eclipse software. Instrumental setups for fluorescence emission spectra were: λ_{ex} according to description in the corresponding figure; excitation slit width: 5 nm; emission slit width: 5 nm; PMT voltage: 600 V. Samples treated as mentioned above.

Overview three-way junctions

Table A4.1: Summary and abbreviations of all the samples.

3WJ ID:	Sequences 5' – 3'		
3WJ-20	GAA GGA ACG T5A CAC TCG CAG		
	GTT CCA CGC T5A CGT TCC TTC		
	CTG CGA GTG T5A GCG TGG AAC		
3WJ-21	GAA GGA ACG TTA CAC TCG CAG		
	GTT CCA CGC T5A CGT TCC TTC		
	CTG CGA GTG T5A GCG TGG AAC		
3WJ-22	GAA GGA ACG T5A CAC TCG CAG		
	GTT CCA CGC T5A CGT TCC TTC		
	CTG CGA GTG T-A GCG TGG AAC		
3WJ-23	GAA GGA ACG T-A CAC TCG CAG		
	GTT CCA CGC T5A CGT TCC TTC		
	CTG CGA GTG T5A GCG TGG AAC		
3WJ-24	GAA GGA ACG T5A CAC TCG CAG		
	GTT CCA CGC T5A CGT TCC TTC		
	CTG CGA GTG T5A GCG TGG AAC		
3WJ-25	GAA GGA ACG T5A CAC TCG CAG		
	GTT CCA CGC T5A CGT TCC TTC		
	CTG CGA GTG T5A GCG TGG AAC		
3WJ-26	GAA GGA ACG TYA CAC TCG CAG		
	GTT CCA CGC T5A CGT TCC TTC		
	CTG CGA GTG TYA GCG TGG AAC		
3WJ-27	GAA GGA ACG T5A CAC TCG CAG		
	GTT CCA CGC T5A CGT TCC TTC		
	CTG CGA GTG T5A GCG TGG AAC		
3WJ-28	GAA GGA ACG TPA CAC TCG CAG		
	GTT CCA CGC T5A CGT TCC TTC		
	CTG CGA GTG T5A GCG TGG AAC		
3WJ-29	GAA GGA ACG TPA CAC TCG CAG		
	GTT CCA CGC T5A CGT TCC TTC		
	CTG CGA GTG T5A GCG TGG AAC		
3WJ-30	GAA GGA ACG TPA CAC TCG CAG		
	GTT CCA CGC T5A CGT TCC TTC		
	CTG CGA GTG T5A GCG TGG AAC		
3WJ-31	GAA GGA ACG TPA CAC TCG CAG		
	GTT CCA CGC T5A CGT TCC TTC		
	CTG CGA GTG T5A GCG TGG AAC		
3WJ-32	GAA GGA ACG TPA CAC TCG CAG		
	GTT CCA CGC T5A CGT TCC TTC		
	CTG CGA GTG T5A GCG TGG AAC		
3WJ-33	GAA GGA ACG TPA CAC TCG CAG		
	GTT CCA CGC T5A CGT TCC TTC		
	CTG CGA GTG T5A GCG TGG AAC		
3WJ-34	GAA GGA ACG TPA CAC TCG CAG		
	GTT CCA CGC T5A CGT TCC TTC		
	CTG CGA GTG T5A GCG TGG AAC		

Temperature dependent UV/Vis measurements

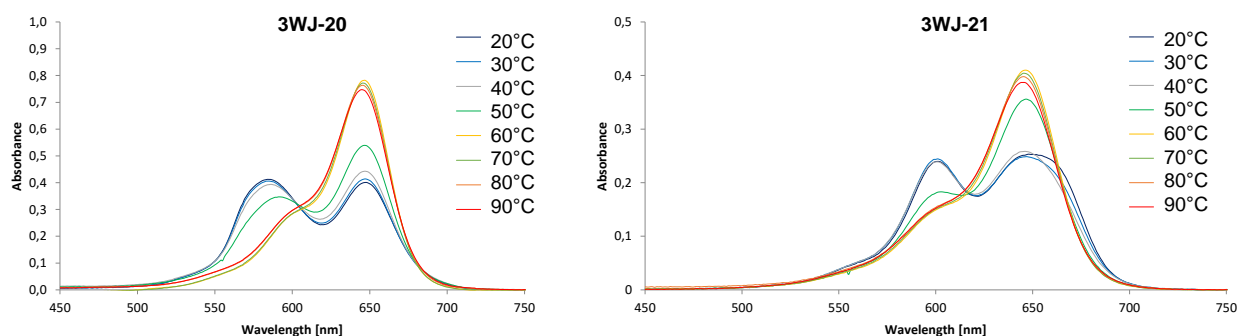


Fig. A4.1. Temperature dependent absorbance spectra. Conditions: Concentration of the samples: 1.0 μM , 10 mM phosphate buffer pH 7.0 and 100 mM NaCl. Samples were cooled down to 20°C and then heated up to 90°C in steps of 10°C (each time an equilibration time of 5 min was chosen).

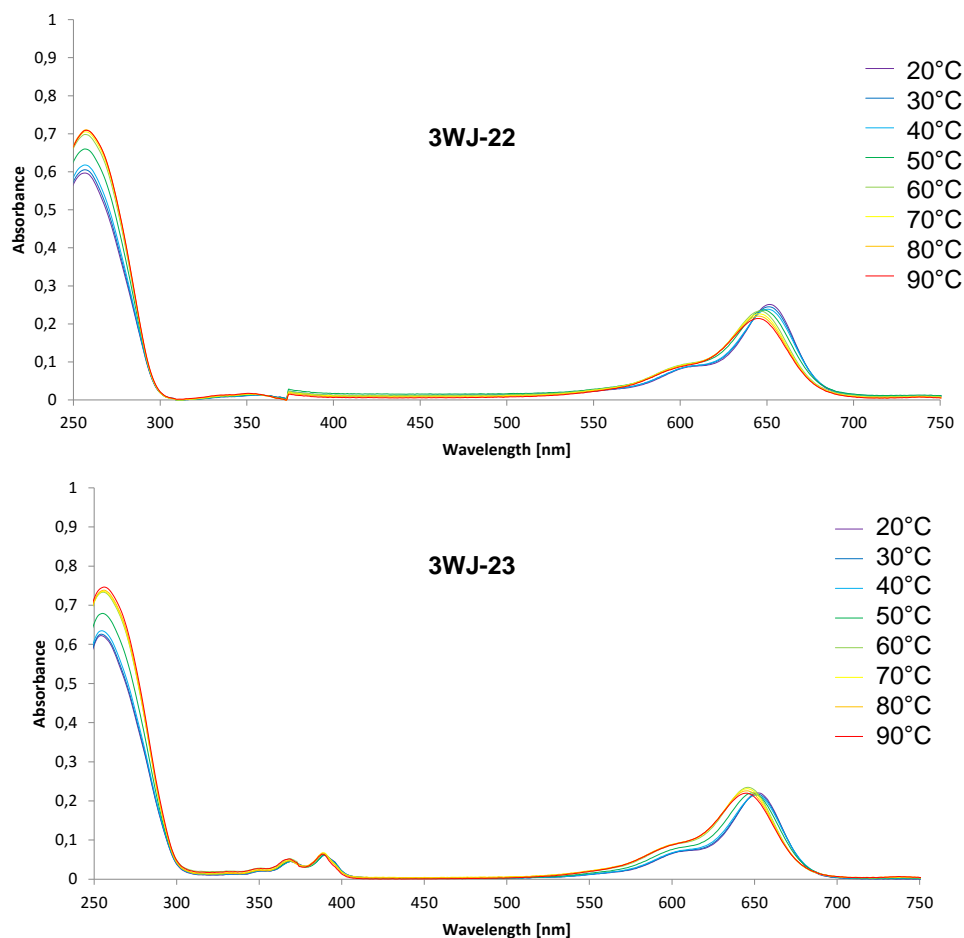


Fig. A4.2. Temperature dependent absorbance spectra. Conditions: see Fig. A4.1; Sample treatment: see Fig. A4.1.

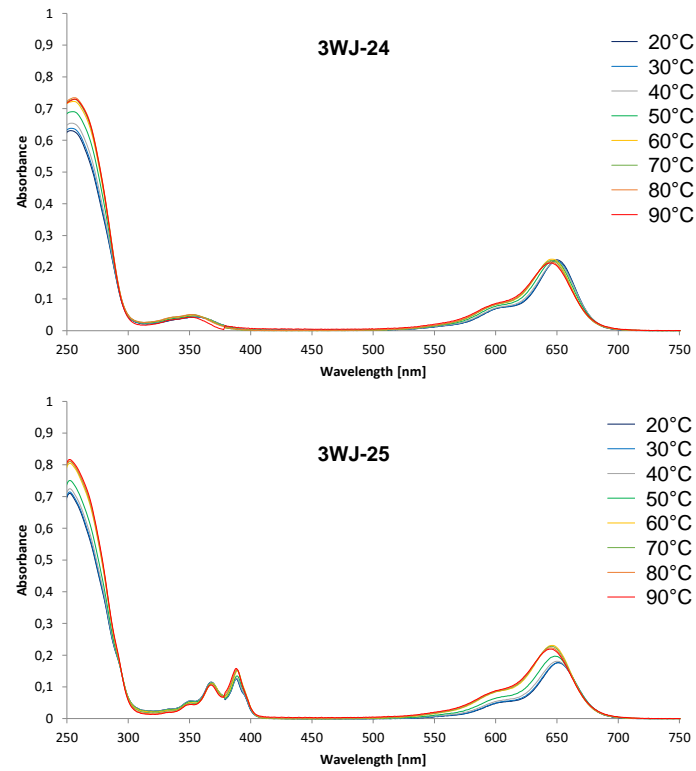


Fig. A4.3. Temperature dependent absorbance spectra. Conditions: see Fig. A4.1; Sample treatment: see Fig. A4.1.

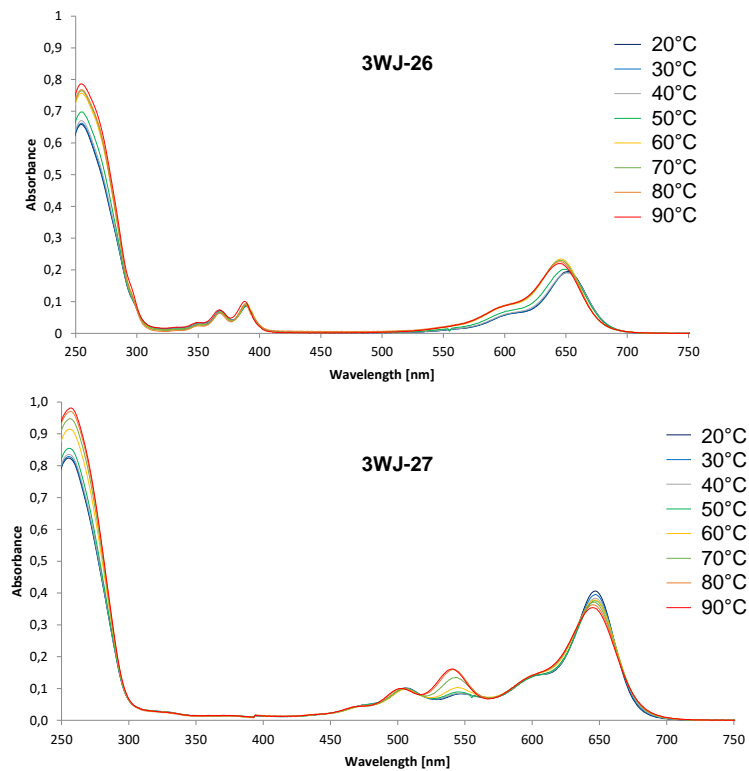


Fig. A4.4. Temperature dependent absorbance spectra. Conditions: see Fig. A4.1; Sample treatment: see Fig. A4.1.

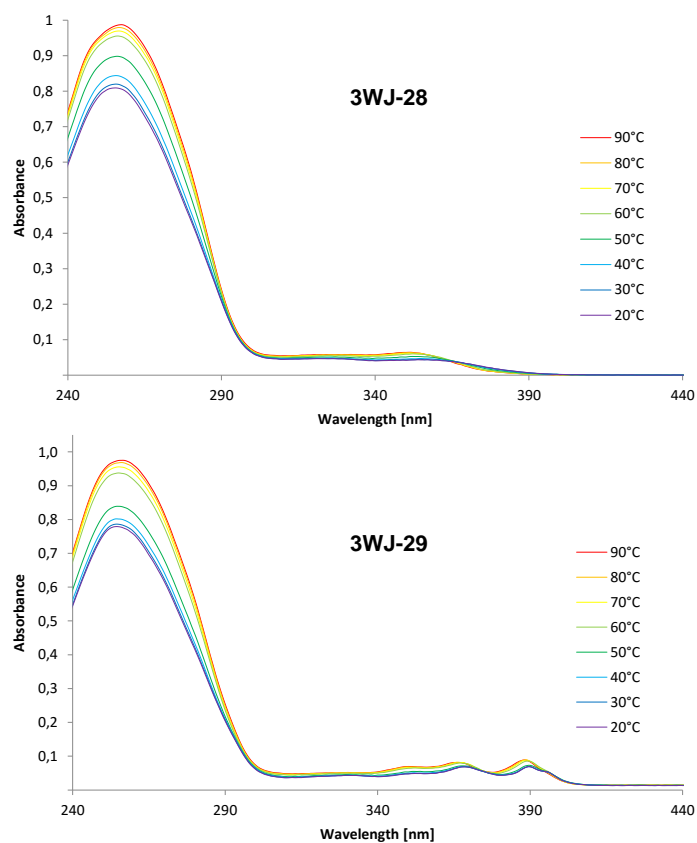


Fig. A4.5. Temperature dependent absorbance spectra. Conditions: see Fig. A4.1; Sample treatment: see Fig. A4.1.

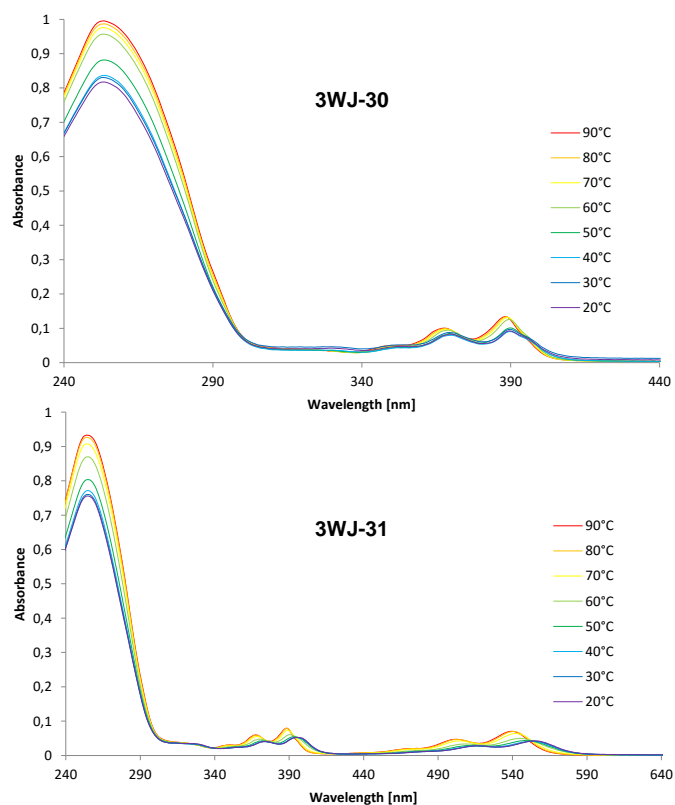


Fig. A4.6. Temperature dependent absorbance spectra. Conditions: see Fig. A4.1; Sample treatment: see Fig. A4.1.

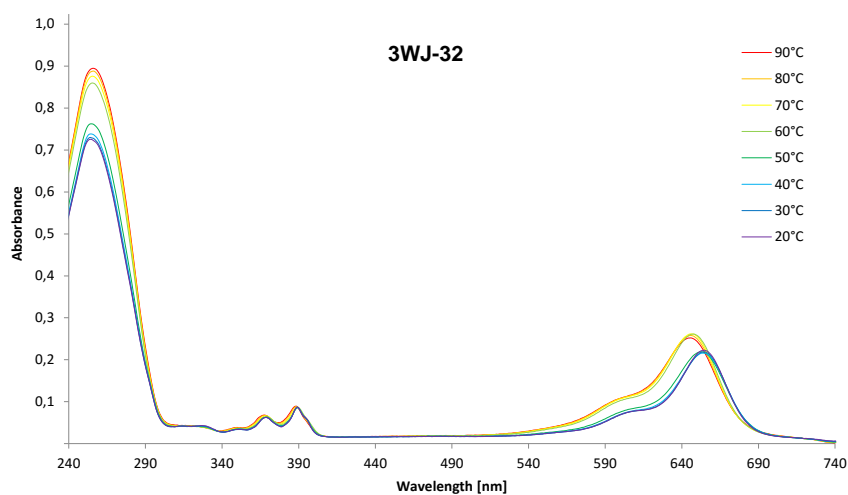


Fig. A4.7. Temperature dependent absorbance spectra. Conditions: see Fig. A4.1; Sample treatment: see Fig. A4.1.

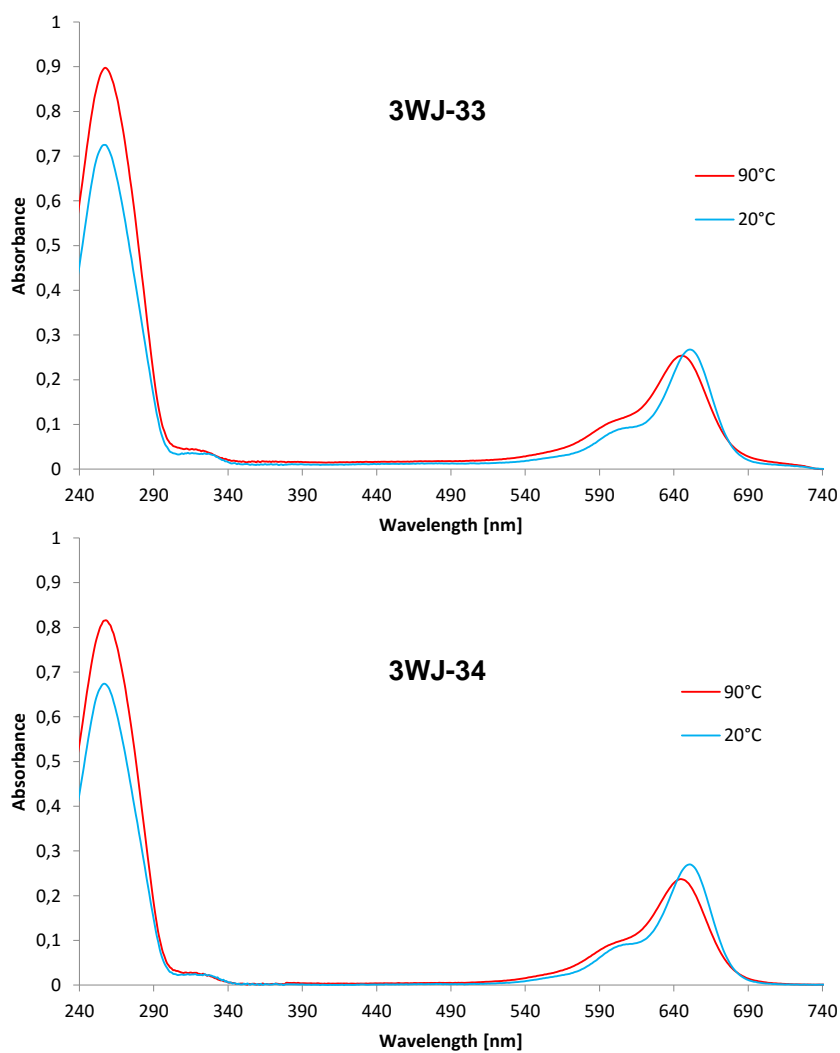


Fig. A4.8. Temperature dependent absorbance spectra. Conditions: see Fig. A4.1; Sample treatment: see Fig. A4.1.

Fluorescence measurements: emission spectra

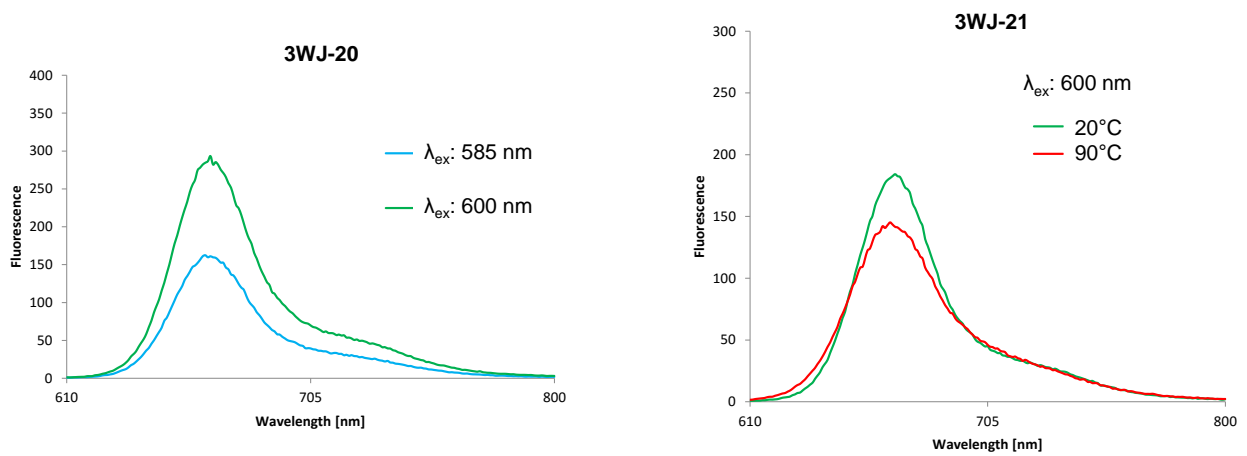


Fig. A4.9. Fluorescence spectra. Conditions: 1.0 μM ; 10 mM phosphate buffer pH 7.0 and 100 mM NaCl; temperature: 20°C (if nothing else stated in the legend); excitation wavelength: see legend. Instrumental set-up: excitation slit width: 5 nm, emission slit width: 5 nm and PMT voltage: 600 V.

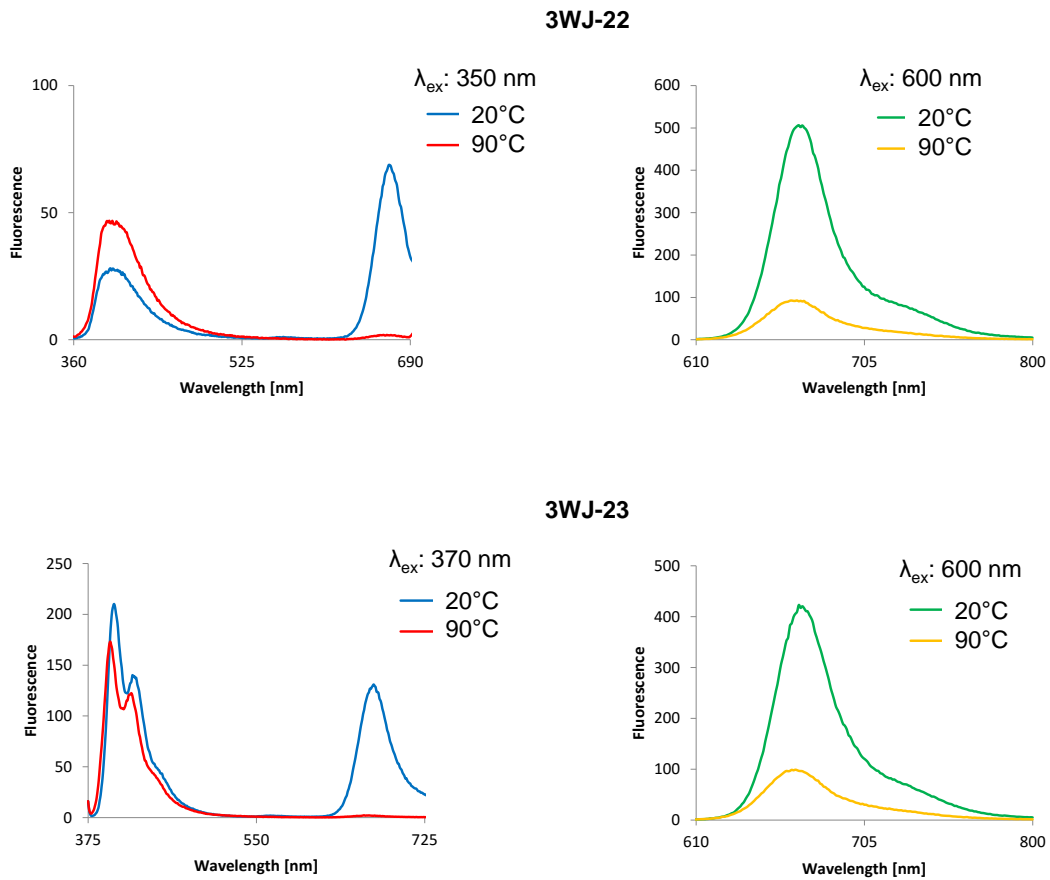


Fig. A4.10. Fluorescence spectra. Conditions: see Fig. A4.9. Excitation wavelength: see legend; instrumental set-up: see Fig. A4.9.

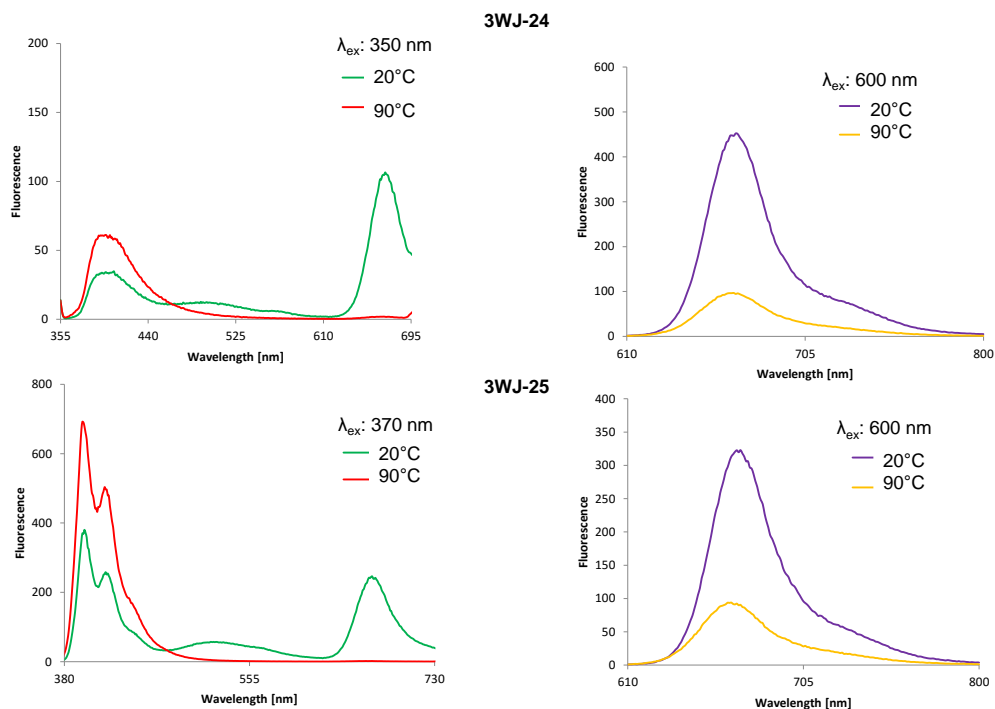


Fig. A4.11. Fluorescence spectra. Conditions: see Fig. A4.9. Excitation wavelength: see legend; instrumental set-up: see Fig. A4.9.

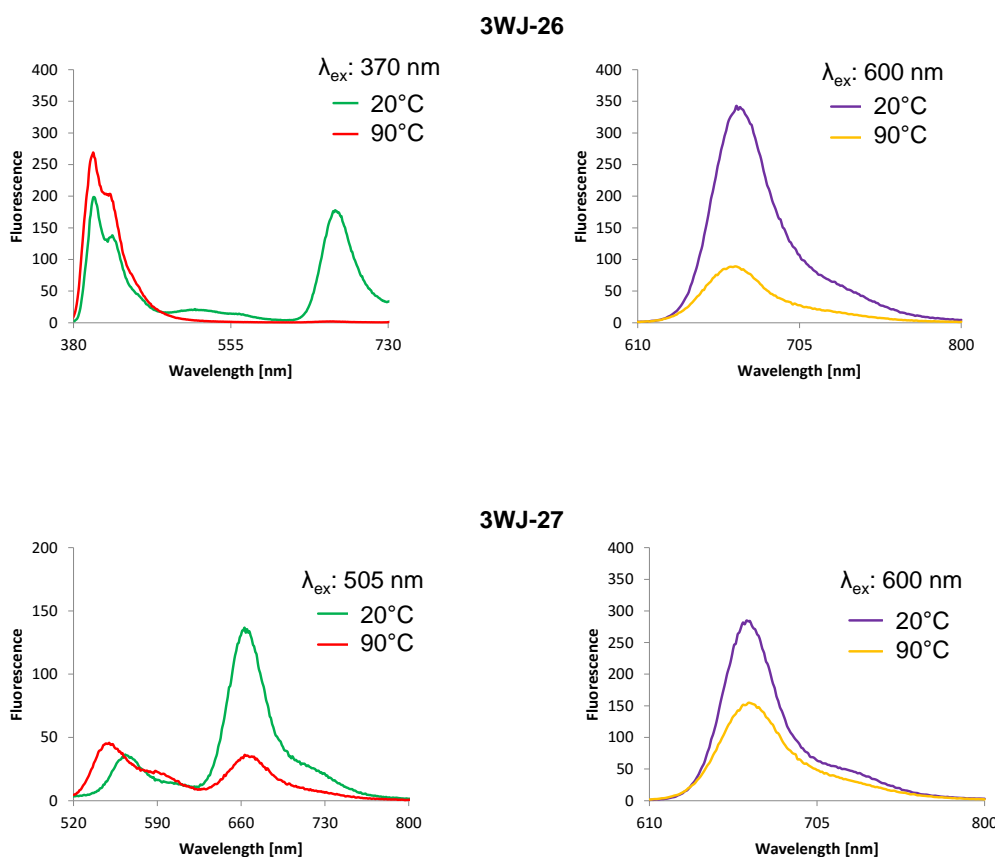


Fig. A4.12. Fluorescence spectra. Conditions: see Fig. A4.9. Excitation wavelength: see legend; instrumental set-up: see Fig. A4.9.

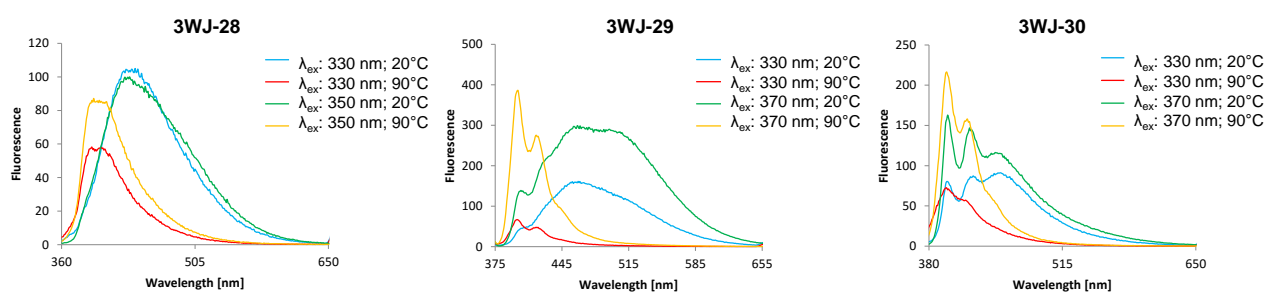


Fig. A4.13. Fluorescence spectra. Conditions: see Fig. A4.9. Excitation wavelength: see legend; instrumental set-up: see Fig. A4.9.

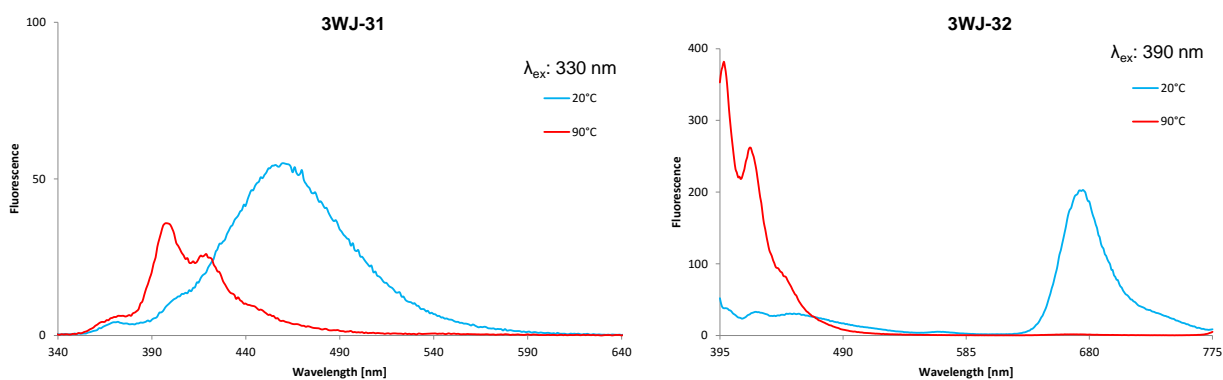


Fig. A4.14. Fluorescence spectra. Conditions: see Fig. A4.9. Excitation wavelength: see legend; instrumental set-up: see Fig. A4.9.

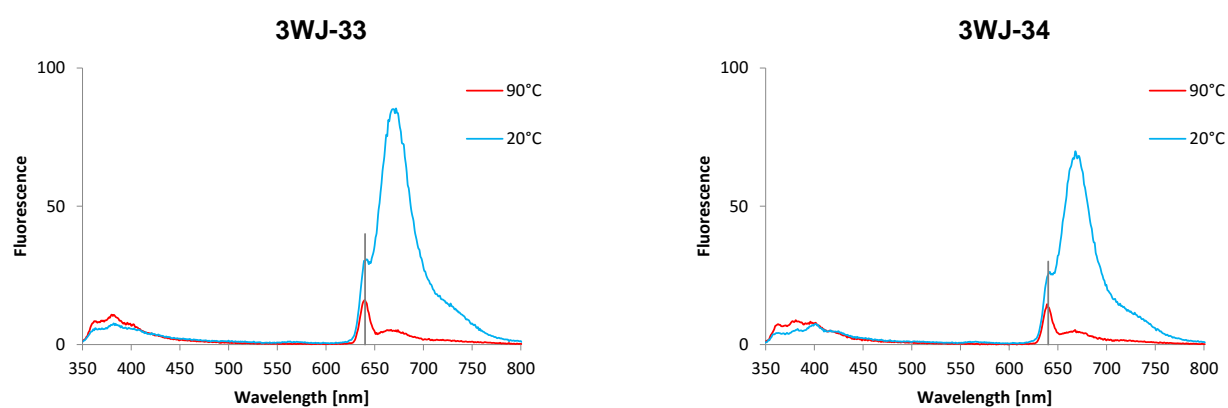


Fig. A4.15. Fluorescence spectra. Conditions: see Fig. A4.9. Excitation wavelength: 320 nm; instrumental set-up: see Fig. A4.9.

Appendix B

Synthetic and analytical procedure

Oligonucleotide-synthesis was performed by an automated oligonucleotide synthesis on a 394-DNA/RNA synthesizer (*Applied Biosystems*), based on phosphoramidite chemistry. The building blocks of the pyrene derivatives were synthesized according to previously described protocols^[1] as well as the phenanthrene^[2] and PDI^[3]. Cleavage from the solid support and final deprotection was done by an overnight treatment with 30% NH₄OH solution at 55°C. The Cy-phosphoramidite was obtained from *GlenResearch* (Sterling, USA), incorporation, cleavage and deprotection followed the *UltraMILD* procedure (*GlenResearch*). All unmodified strands were commercially obtained from *Microsynth* (Balgach, Switzerland).

Reversed-phase HPLC purification of the modified oligonucleotides was carried out on a LC-20AT system (*Shimadzu*, Kyoto, Japan) using a LiChrospher 100 RP18, 5 μ m column (*Dr. Maisch GmbH*, Ammerbuch, Germany) and a gradient consisting of eluent A (0.1 M triethylamine / acetic acid) and B (acetonitrile) with 5-50% B within 20 minutes.

Molecular mass of the synthesized oligonucleotides was determined by LC-MS (LC-20AT, SPD-M20A, LCMS-2010EV, all *Shimadzu*), with a C18 3.5 μ m 2.1x100 mm column (XTerra MS, *Waters*, Milford, USA) and an applied gradient of 100% A (50 mM ammonium formate) to 50% B (acetonitrile) over 10 minutes.

UV-Vis spectra were collected on a Varian Cary-100 Bio-UV / Visible spectrophotometer equipped with a Varian Cary-block temperature controller, 1 cm quartz cuvettes and processed with Varian WinUV software. Experiments were performed with samples prepared from 1 μ M single strand concentration in *Milli-Q* H₂O containing 100 mM NaCl and 10 mM sodium phosphate buffer (pH 7.0).

Thermal denaturation curves were recorded on the same device (same conditions), the absorption at 260 nm was monitored for three ramps (cooling-heating-cooling cycles in the temperature range of 20°C – 90°C; gradient of 0.5°C/min). The melting temperatures (T_m) were calculated on the basis of: the temperature at which the ΔAbs between two data points is the highest within each ramp. The average temperature of all three ramps was determined.

[1] H. Bittermann, D. Siegemund, V. L. Malinovskii, R. Häner. *J. Am. Chem. Soc.*, **2008**, 130, 15285-15287.

S. M. Langenegger, R. Häner. *Chem. Commun.*, **2004**, 2792-2793.

[2] S. M. Langenegger, R. Häner. *Helv. Chim. Acta*, **2002**, 3414-3421.

S. M. Langenegger, R. Häner. *ChemBioChem*, **2005**, 6, 848-851.

[3] N. Rahe, C. Rinn, T. Carell. *Chem. Commun.*, **2003**, 2119-2121.

Fluorescence spectra were acquired on a Varian Cary Eclipse fluorescence spectrophotometer equipped with a Varian Cary-block temperature controller with 1 cm x 1 cm quartz cuvettes and Varian Eclipse software. Instrumental setups for fluorescence emission and excitation spectra were: $\lambda_{ex} / \lambda_{em}$: according to description in the corresponding figure; excitation slit width: 5 nm; emission slit width: 5 nm; PMT voltage: 580 V. Samples treated as mentioned above.

Polyacrylamide gel electrophoresis (PAGE) was performed using a 10% stacking gel on top of a 20% resolving gel. 8 μ L of each sample mixture (1 μ M single strand concentration; 15% glycerol; 90 mM Tris-borate buffer, pH 8.0) were loaded onto the gel. The gel ran for 2h in a closed chamber at 4°C (180V / 5mA / 2W). Staining was done with Stains-all reagent dissolved in a buffered formamide solution.

Investigated oligonucleotides and masses

Table A5.1: Sequences, molecular formula, masses and epsilons of **ON1** to **ON7**.

ID:	Sequence (5'-3')	molecular formula	calcd. avg. mass	found avg. mass	calcd. ϵ_{260} [$\text{dm}^3 \text{mol}^{-1} \text{cm}^{-1}$]
ON1	GAA GGA ACG TPP PPP ACA CTC GCA G	C305H358N94O143P24	8372.1	8370.9	366800
ON2	CTG CGA GTG TPP PPP AGC GTG GAA C	C306H360N90O148P24	8410.1	8408.9	354900
ON3	GTT CCA CGC TSA CGT TCC TTC	C216H271N65O129P20	6461.4	6460.0	196500
ON4	GTT CCA CGC TXA CGT TCC TTC	C216H265N63O127P20	6395.3	6393.9	207900
ON5	GTT CCA CGC TEA CGT TCC TTC	C222H269N65O131P20	6563.4	6560.2	213600
ON6	GTT CCA CGC TCyA CGT TCC TTC	C223H286N65O127P20	6528.5	6530.6	197900
ON7	GTT CCA CGC TYA CGT TCC TTC	C216H265N63O127P20	6395.3	6393.1	217900

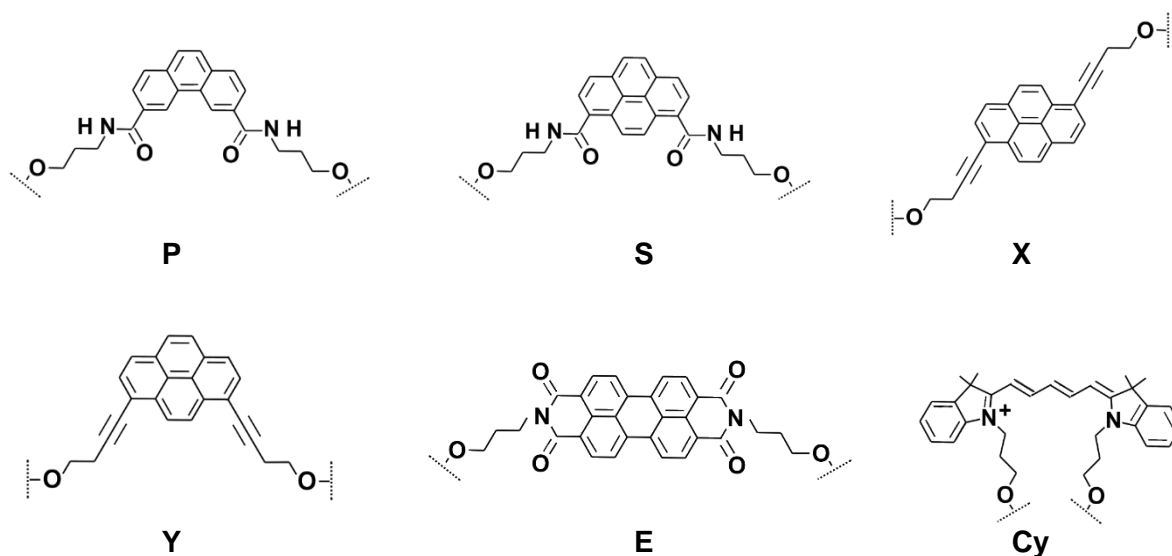


Fig. A5.1 : Structures of the non-nucleosidic building blocks.

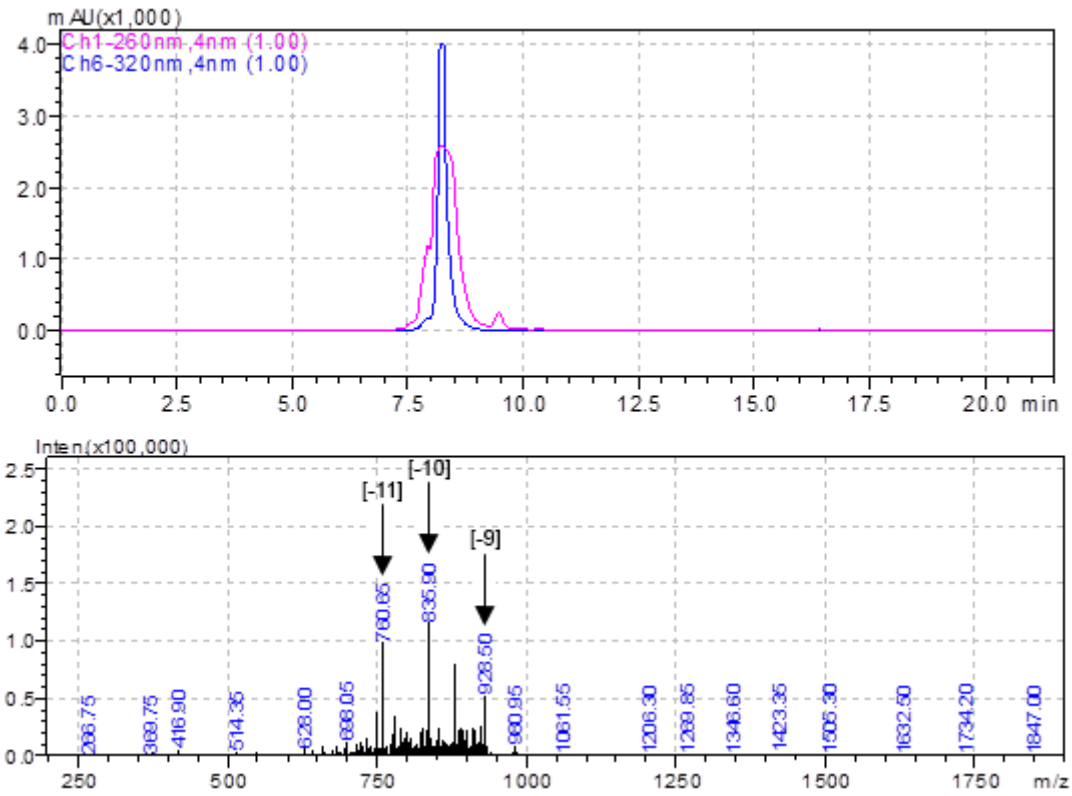


Fig. A5.2: PDA trace (top) and ESI mass spectrum (bottom) of ON1.

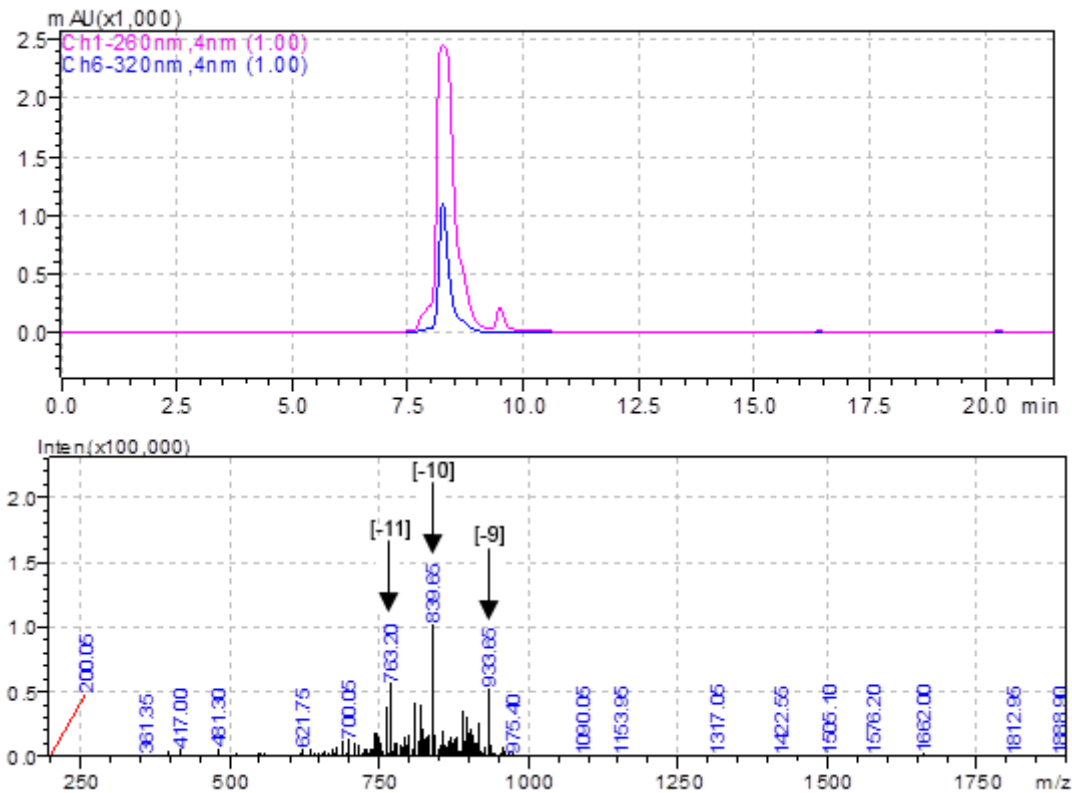


Fig. A5.3: PDA trace (top) and ESI mass spectrum (bottom) of ON2.

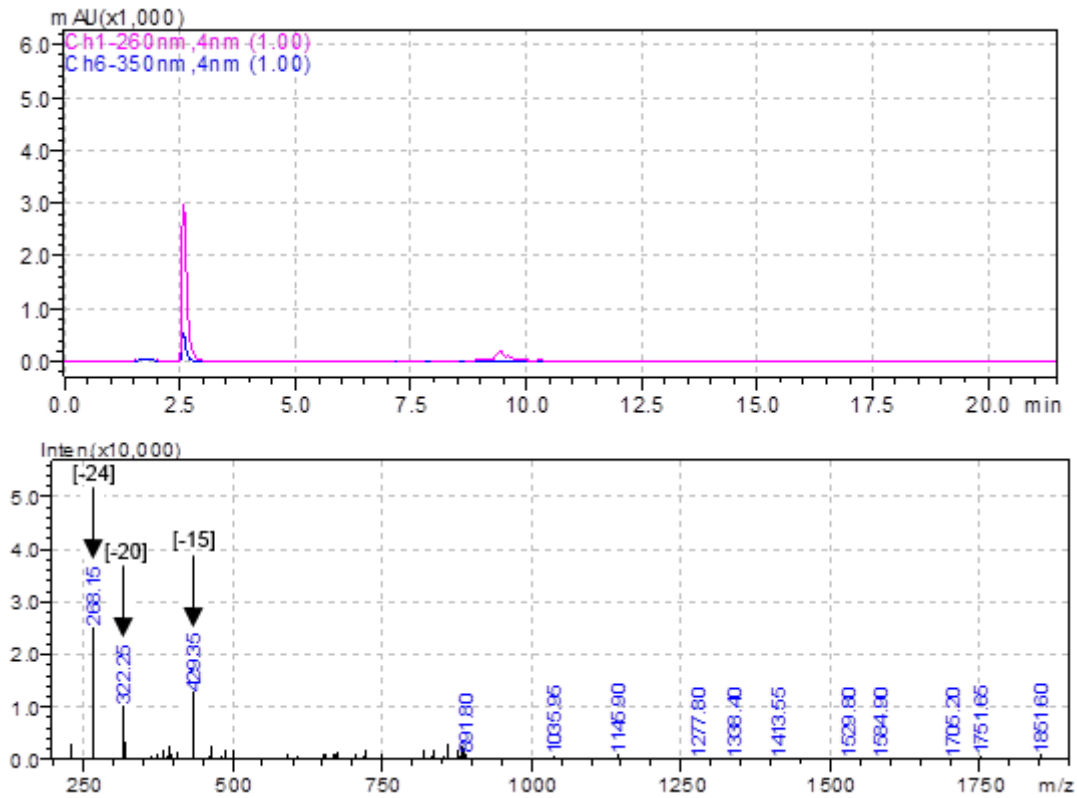


Fig. A5.4: PDA trace (top) and ESI mass spectrum (bottom) of **ON3**.

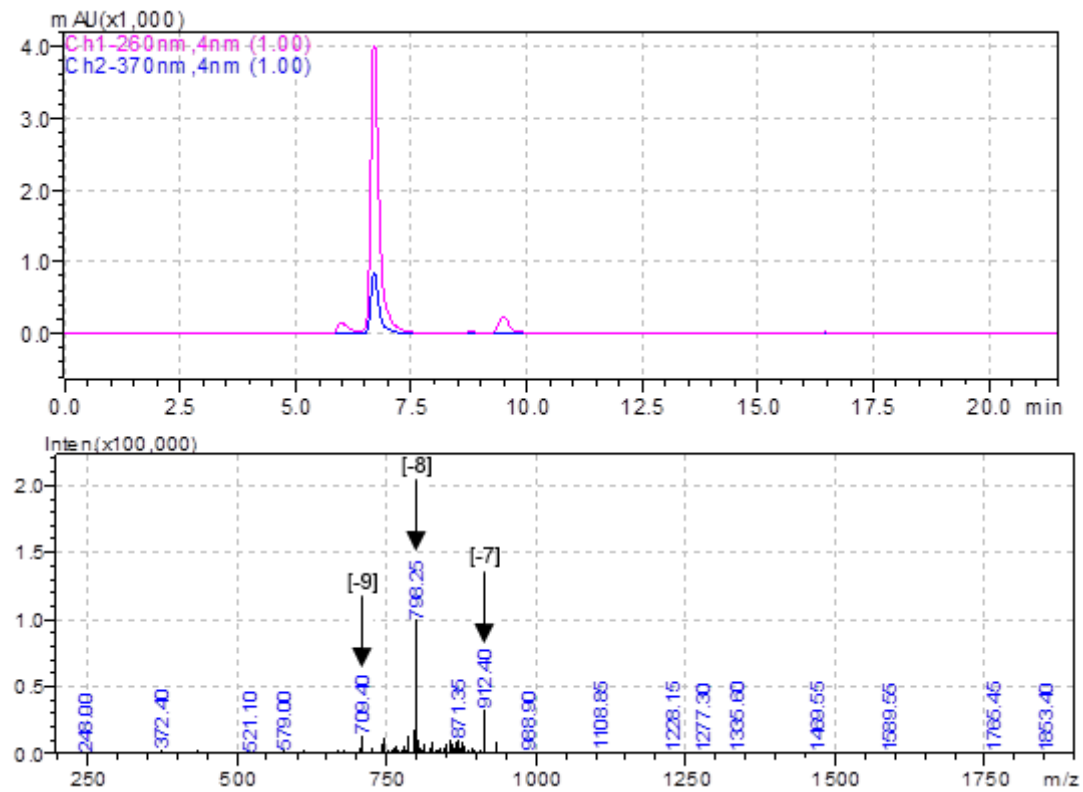


Fig. A5.5: PDA trace (top) and ESI mass spectrum (bottom) of **ON4**.

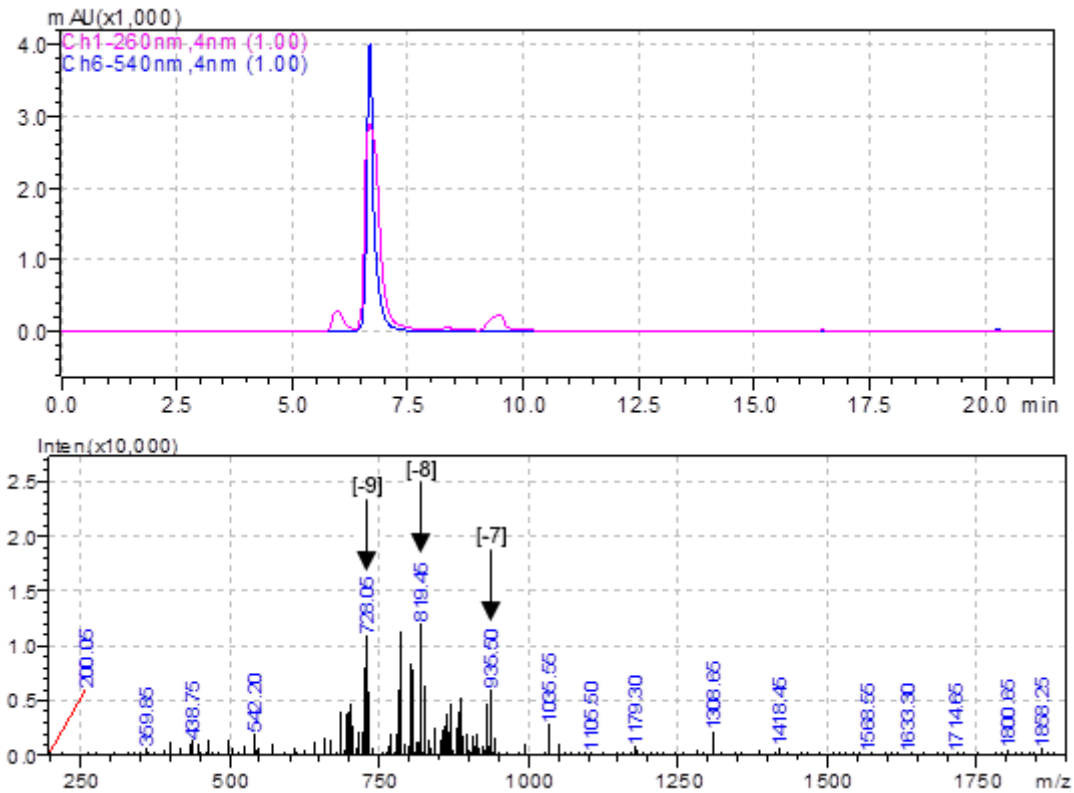


Fig. A5.6: PDA trace (top) and ESI mass spectrum (bottom) of ON5.

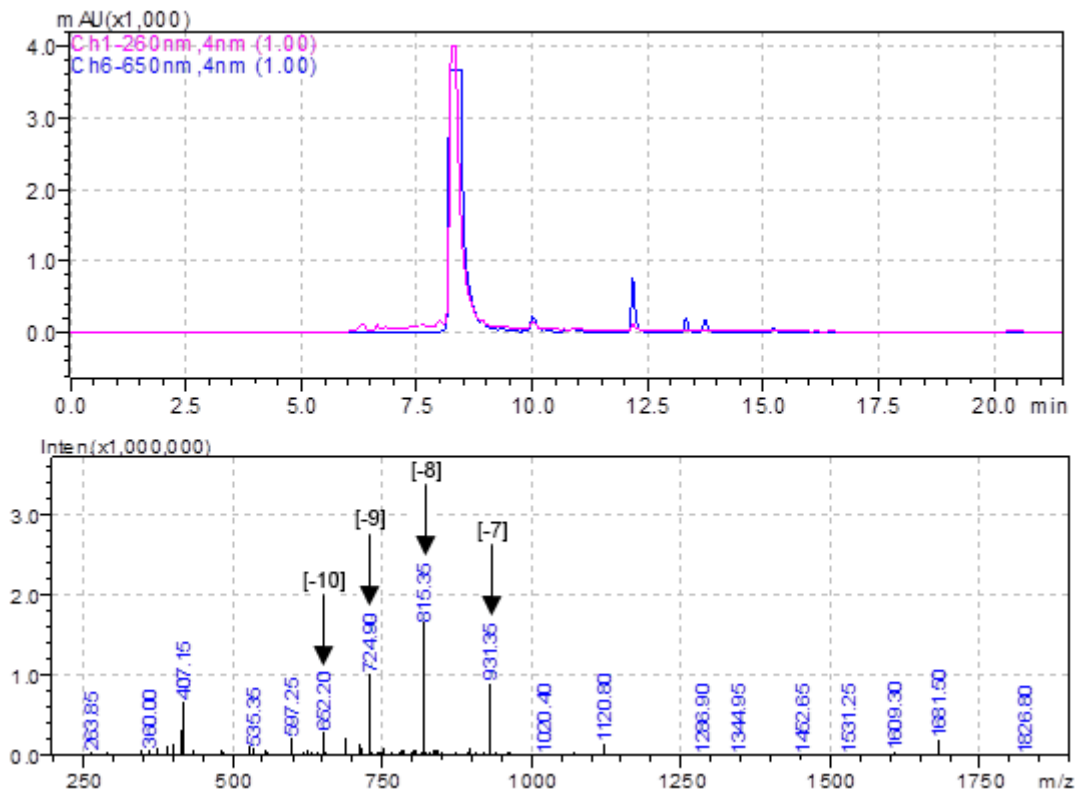


Fig. A5.7: PDA trace (top) and ESI mass spectrum (bottom) of ON6.

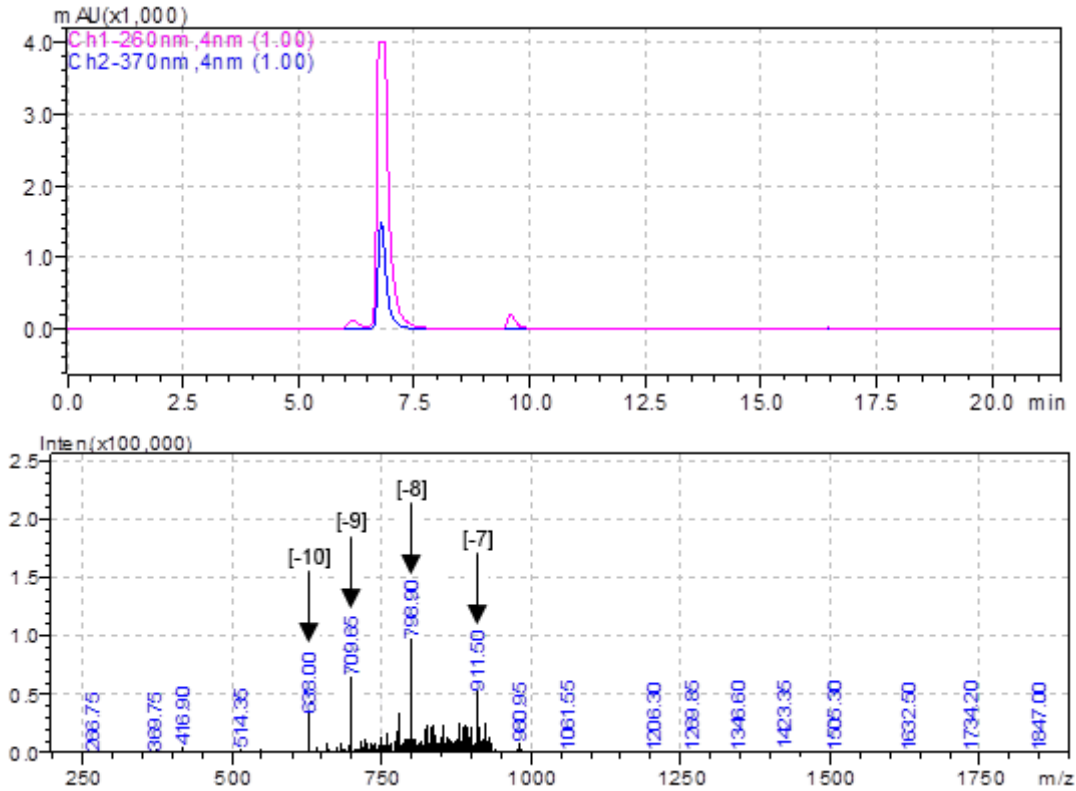


Fig. A5.8: PDA trace (top) and ESI mass spectrum (bottom) of ON7.

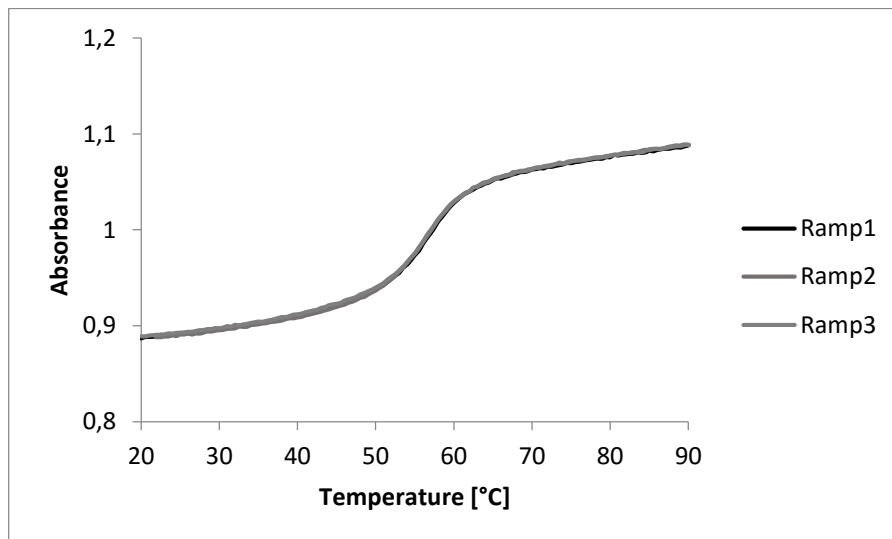
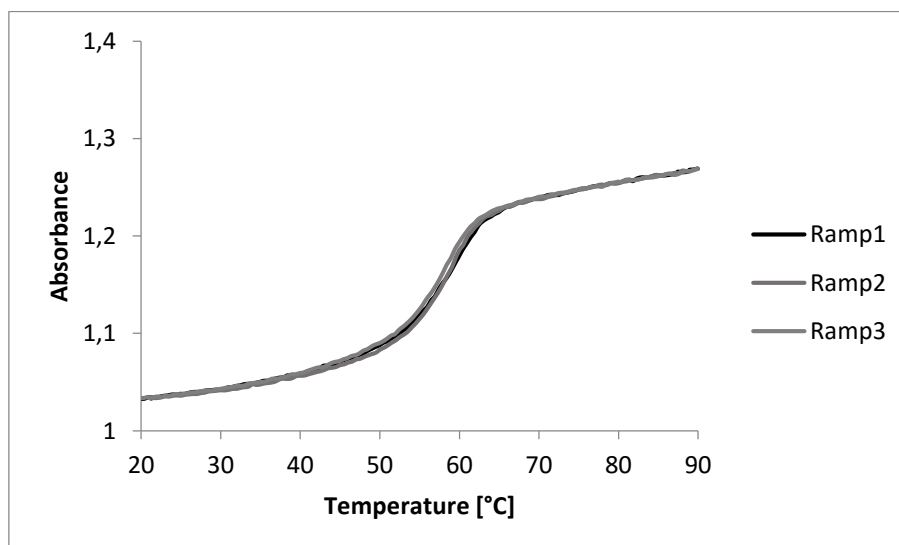
Table A5.2: Overview of all the 3WJs and the sequences that were used.

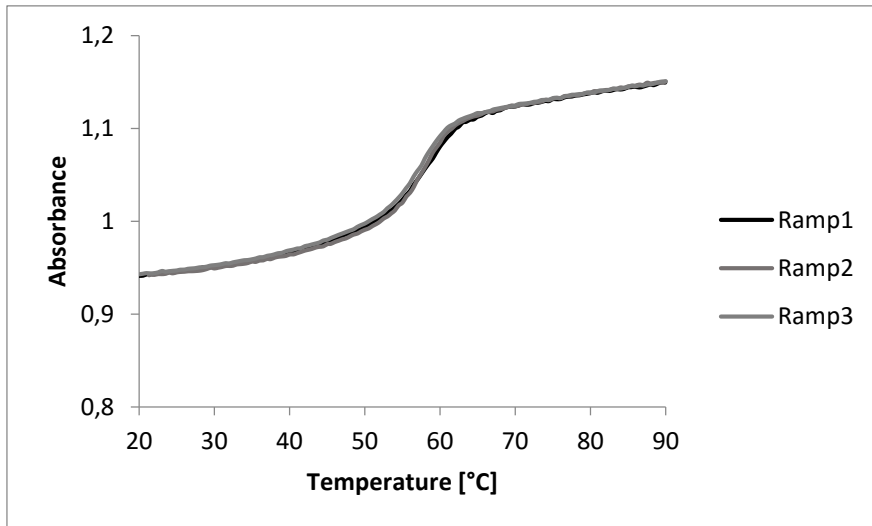
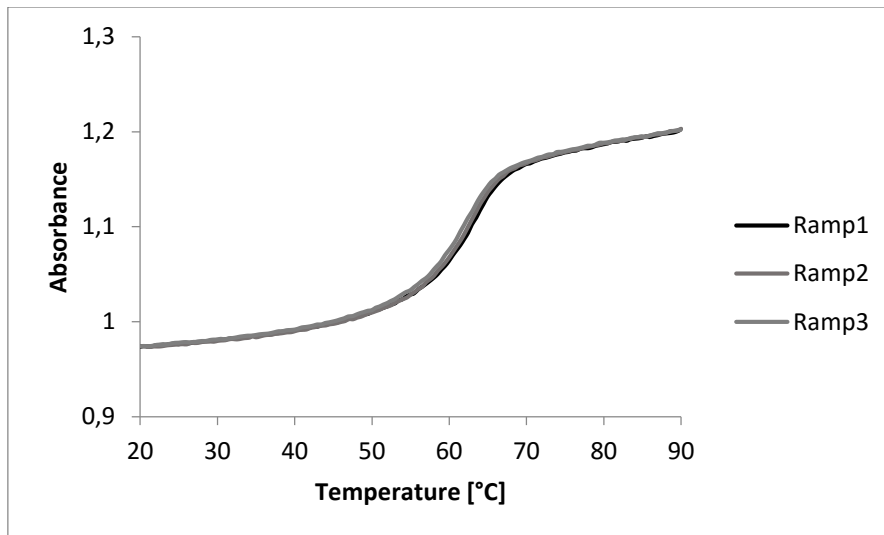
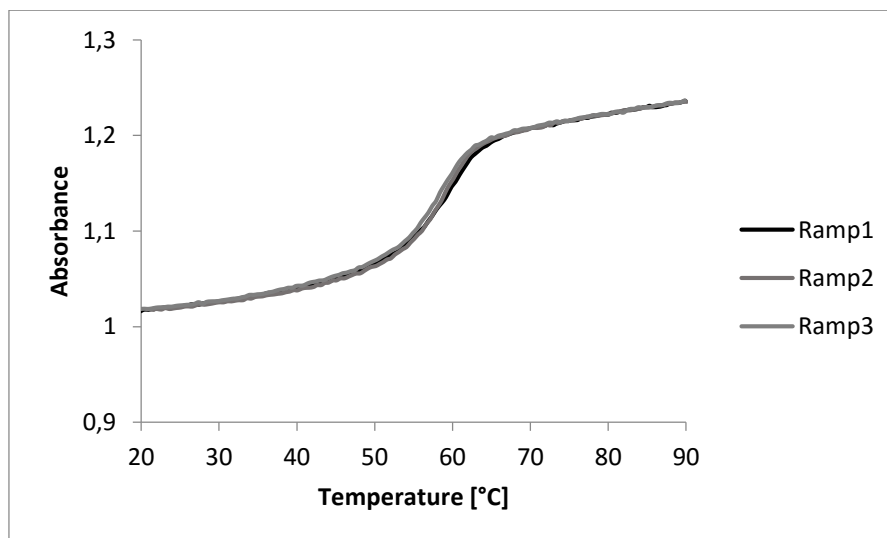
Name	Sequences (5'-3')	Name	Sequences (5'-3')
3WJ-1	GAA GGA ACG TPP PPP ACA CTC GCA G	3WJ-7	GAA GGA ACG T-A CAC TCG CAG
	CTG CGA GTG TPP PPP AGC GTG GAA C		CTG CGA GTG T-A GCG TGG AAC
	GTT CCA CGC T-A CGT TCC TTC		GTT CCA CGC TS A CGT TCC TTC
3WJ-2	GAA GGA ACG TPP PPP ACA CTC GCA G	3WJ-8	GAA GGA ACG T-A CAC TCG CAG
	CTG CGA GTG TPP PPP AGC GTG GAA C		CTG CGA GTG T-A GCG TGG AAC
	GTT CCA CGC TS A CGT TCC TTC		GTT CCA CGC TX A CGT TCC TTC
3WJ-3	GAA GGA ACG TPP PPP ACA CTC GCA G	3WJ-9	GAA GGA ACG T-A CAC TCG CAG
	CTG CGA GTG TPP PPP AGC GTG GAA C		CTG CGA GTG T-A GCG TGG AAC
	GTT CCA CGC TX A CGT TCC TTC		GTT CCA CGC TCy A CGT TCC TTC
3WJ-4	GAA GGA ACG TPP PPP ACA CTC GCA G	3WJ-10	GAA GGA ACG T-A CAC TCG CAG
	CTG CGA GTG TPP PPP AGC GTG GAA C		CTG CGA GTG T-A GCG TGG AAC
	GTT CCA CGC TE A CGT TCC TTC		GTT CCA CGC TE A CGT TCC TTC
3WJ-5	GAA GGA ACG TPP PPP ACA CTC GCA G	3WJ-11	GAA GGA ACG T-A CAC TCG CAG
	CTG CGA GTG TPP PPP AGC GTG GAA C		CTG CGA GTG T-A GCG TGG AAC
	GTT CCA CGC TCy A CGT TCC TTC		GTT CCA CGC TY A CGT TCC TTC
3WJ-6	GAA GGA ACG TPP PPP ACA CTC GCA G		
	CTG CGA GTG TPP PPP AGC GTG GAA C		
	GTT CCA CGC TY A CGT TCC TTC		

T_m values and thermal denaturation profiles**Table A5.3:** T_m of the individual three-way junctions.

Name	T _m	Name	T _m
3WJ-1	57°C	3WJ-7	47°C
3WJ-2	59°C	3WJ-8	49°C
3WJ-3	58°C	3WJ-9	49°C
3WJ-4	63°C	3WJ-10	47°C
3WJ-5	59°C	3WJ-11	44°C
3WJ-6	57°C		

Thermal denaturation profiles (Ramp1: 90°C → 20°C, Ramp2: 20°C → 90°C and Ramp3: 90°C → 20°C):

**Fig. A5.9:** Melting profile of 3WJ-1.**Fig. A5.10:** Melting profile of 3WJ-2.

**Fig. A5.11:** Melting profile of 3WJ-3.**Fig. A5.12:** Melting profile of 3WJ-4.**Fig. A5.13:** Melting profile of 3WJ-5.

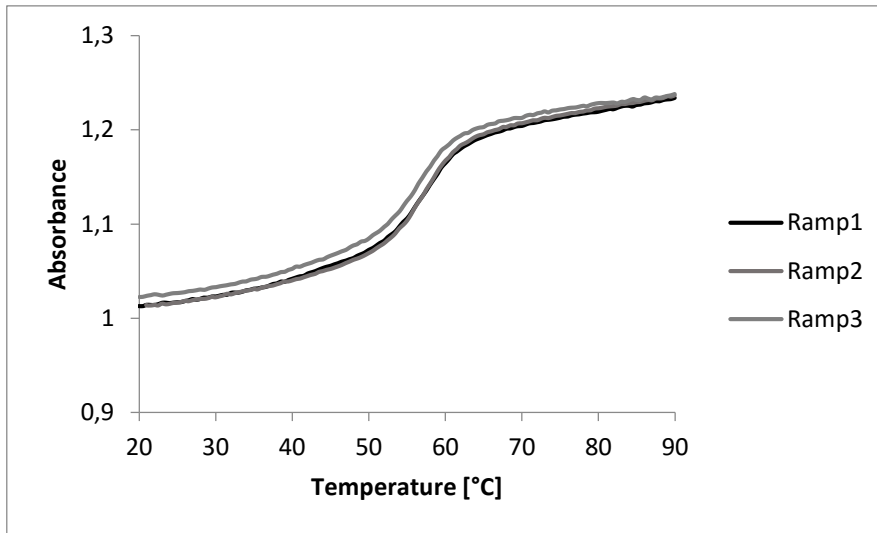


Fig. A5.14: Melting profile of 3WJ-6.

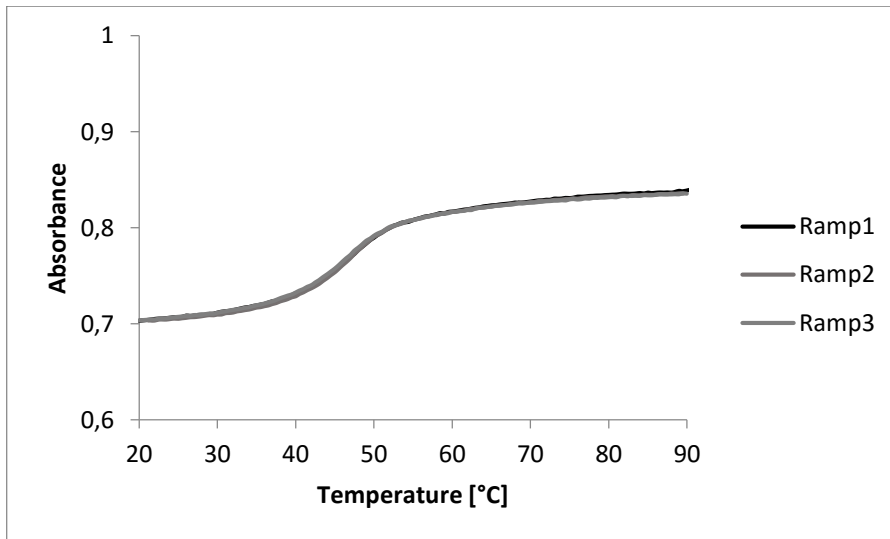


Fig. A5.15: Melting profile of 3WJ-7.

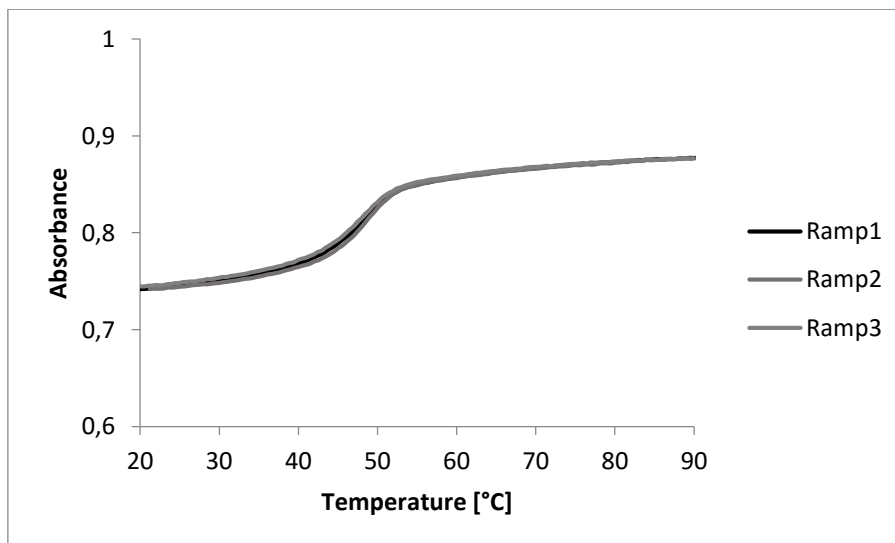


Fig. A5.16: Melting profile of 3WJ-8.

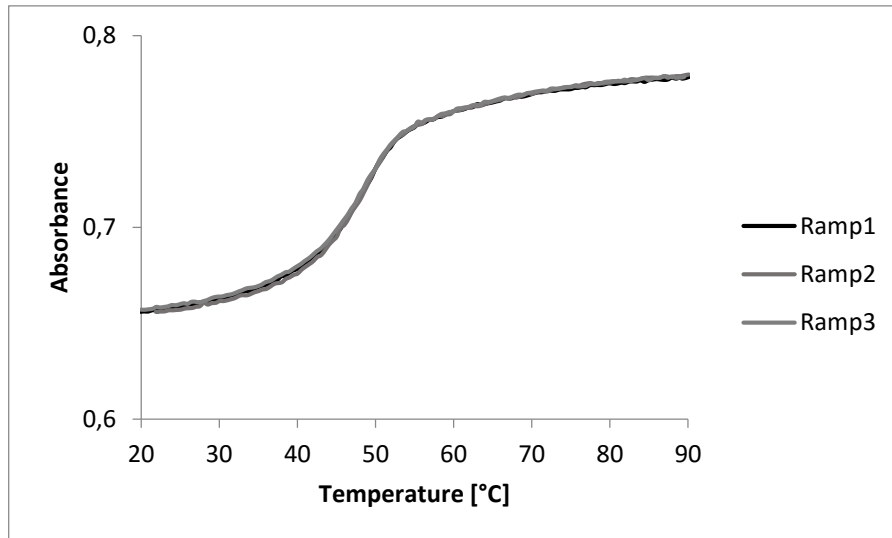


Fig. A5.17: Melting profile of 3WJ-9.

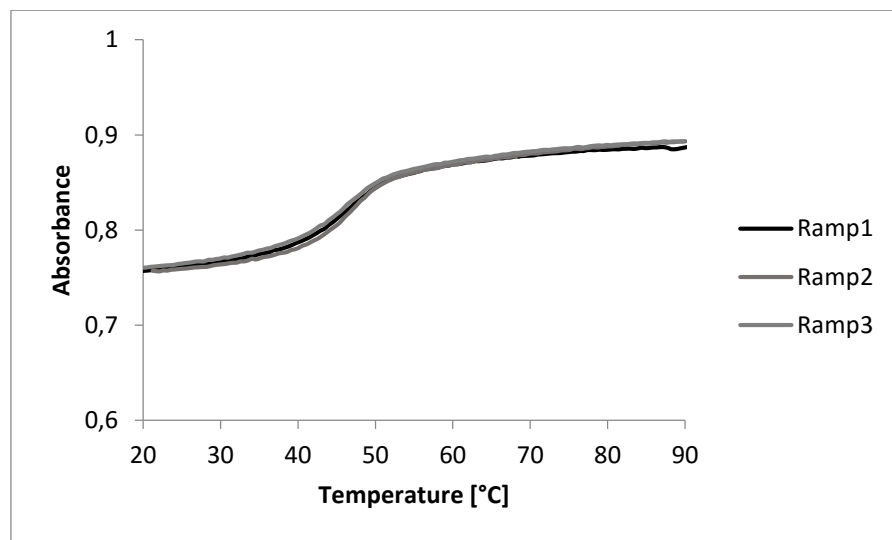


Fig. A5.18: Melting profile of 3WJ-10.

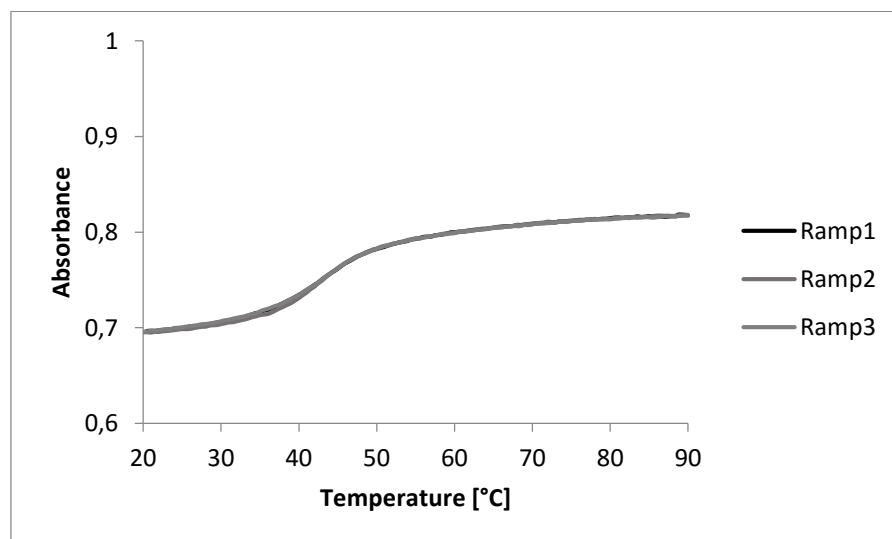


Fig. A5.19: Melting profile of 3WJ-11.

UV/Vis spectra

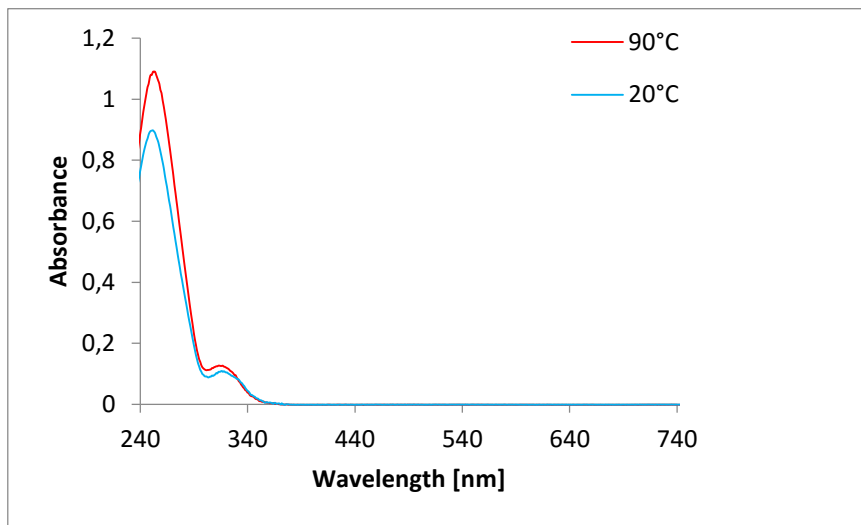


Fig. A5.20: Temperature-dependent UV/Vis spectra of **3WJ-1**.

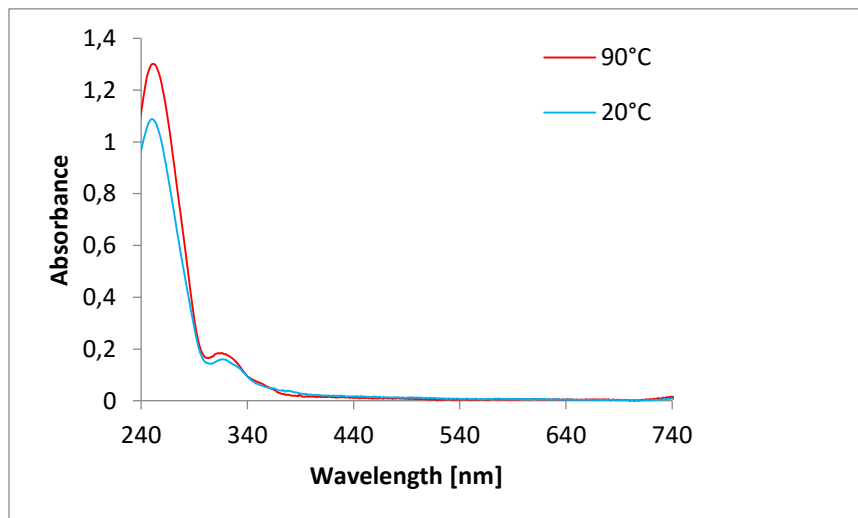


Fig. A5.21: Temperature-dependent UV/Vis spectra of **3WJ-2**.

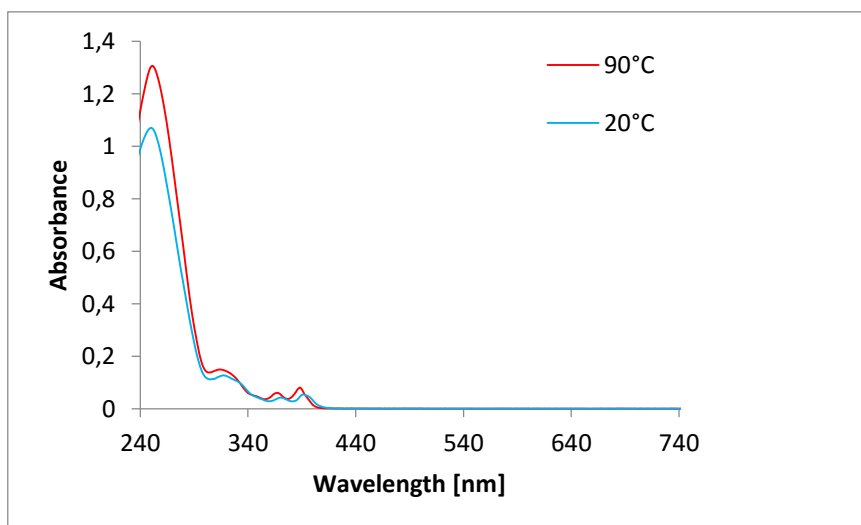


Fig. A5.22: Temperature-dependent UV/Vis spectra of **3WJ-3**.

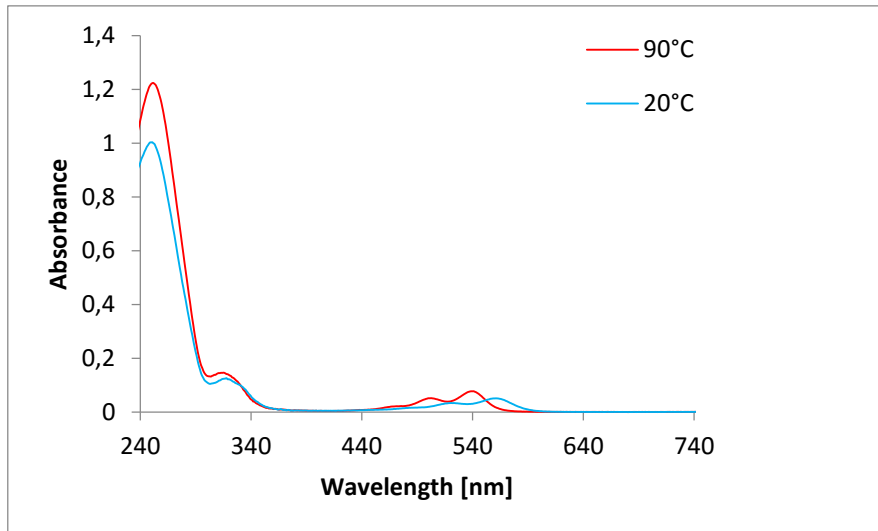


Fig. A5.23: Temperature-dependent UV/Vis spectra of **3WJ-4**.

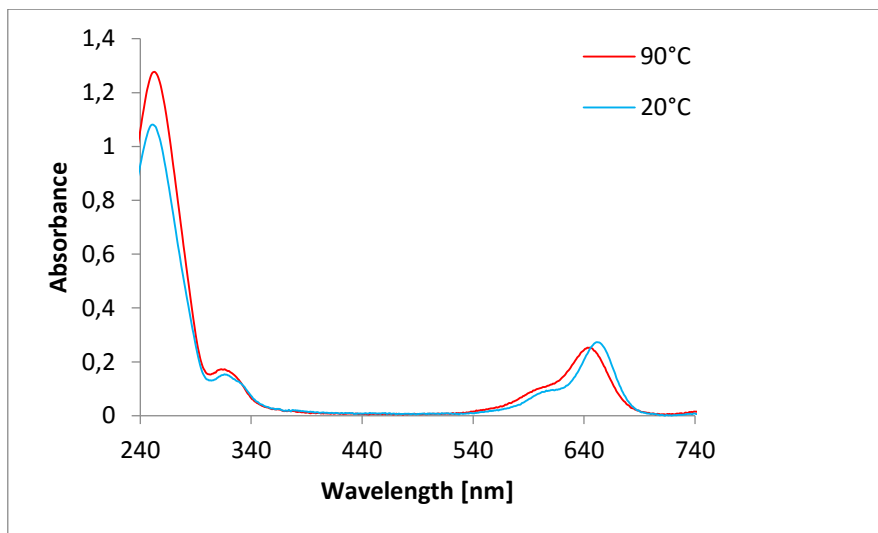


Fig. A5.24: Temperature-dependent UV/Vis spectra of **3WJ-5**.

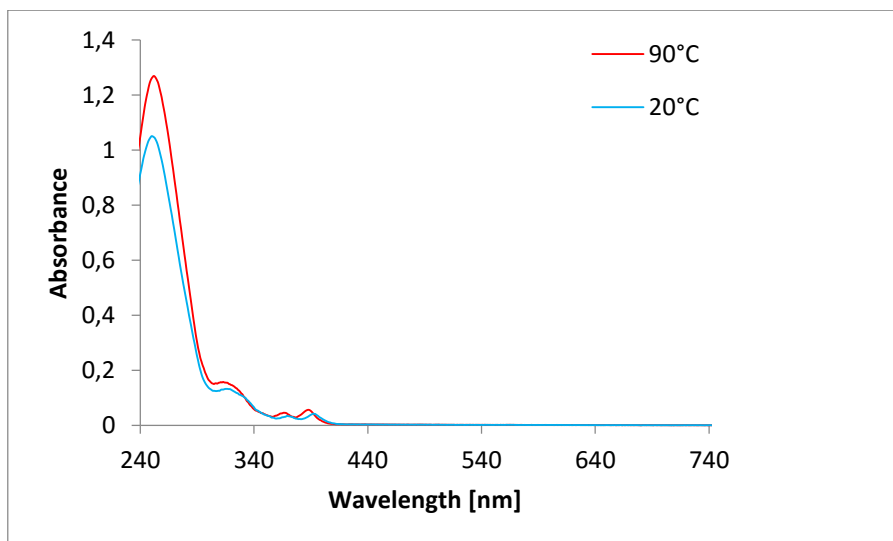


Fig. A5.25: Temperature-dependent UV/Vis spectra of **3WJ-6**.

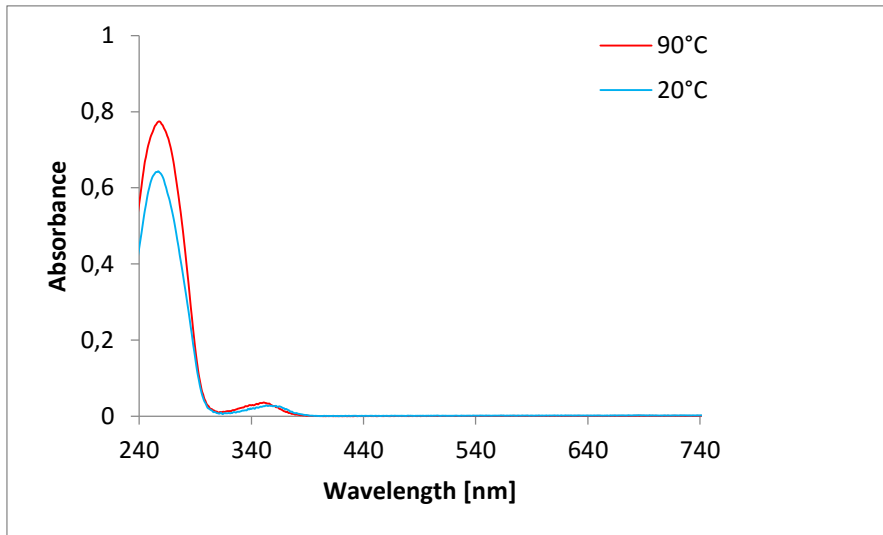


Fig. A5.26: Temperature-dependent UV/Vis spectra of **3WJ-7**.

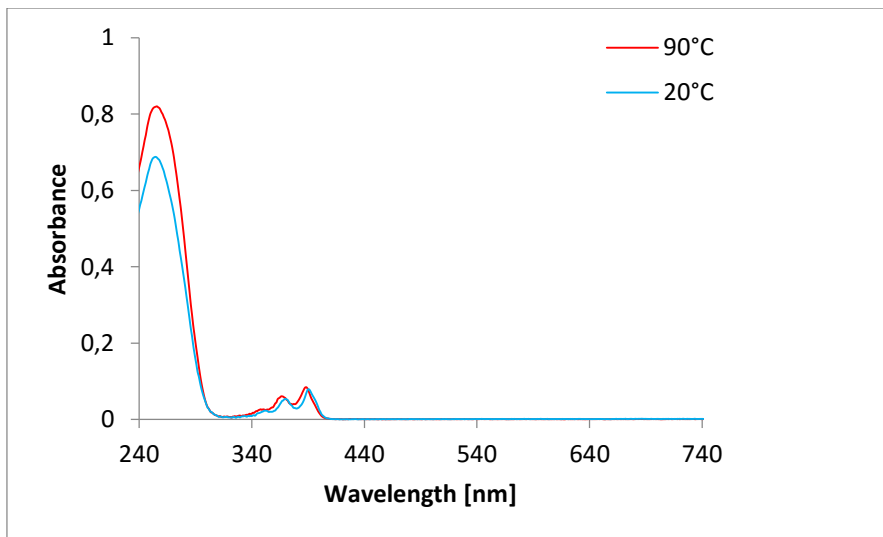


Fig. A5.27: Temperature-dependent UV/Vis spectra of **3WJ-8**.

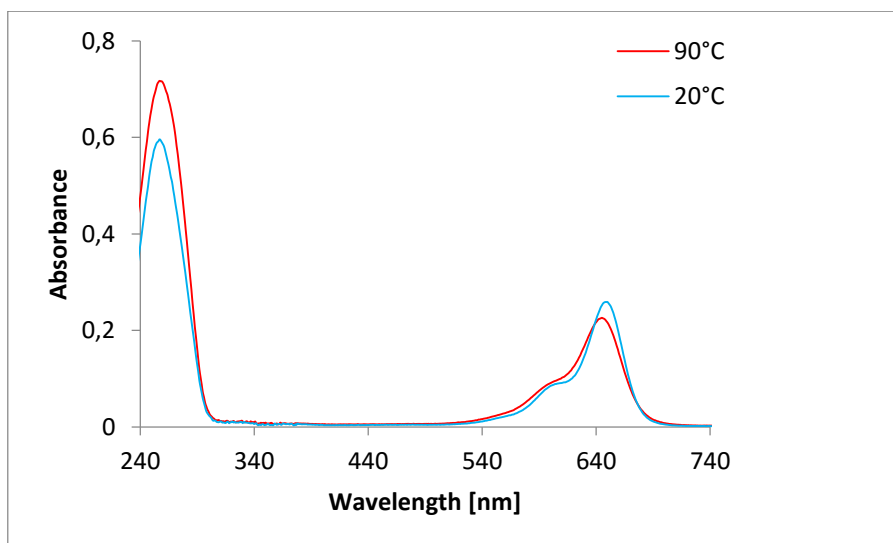


Fig. A5.28: Temperature-dependent UV/Vis spectra of **3WJ-9**.

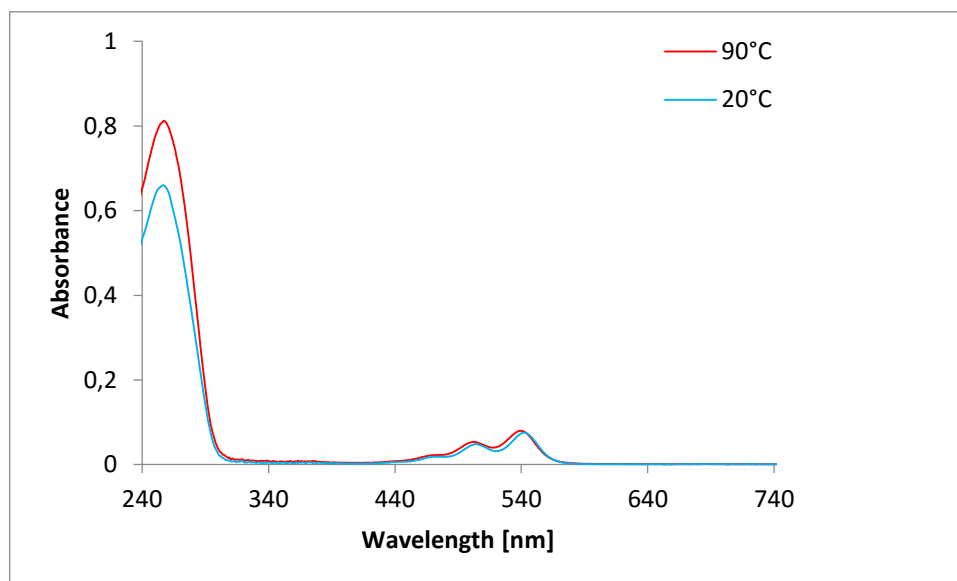


Fig. A5.29: Temperature-dependent UV/Vis spectra of **3WJ-10**.

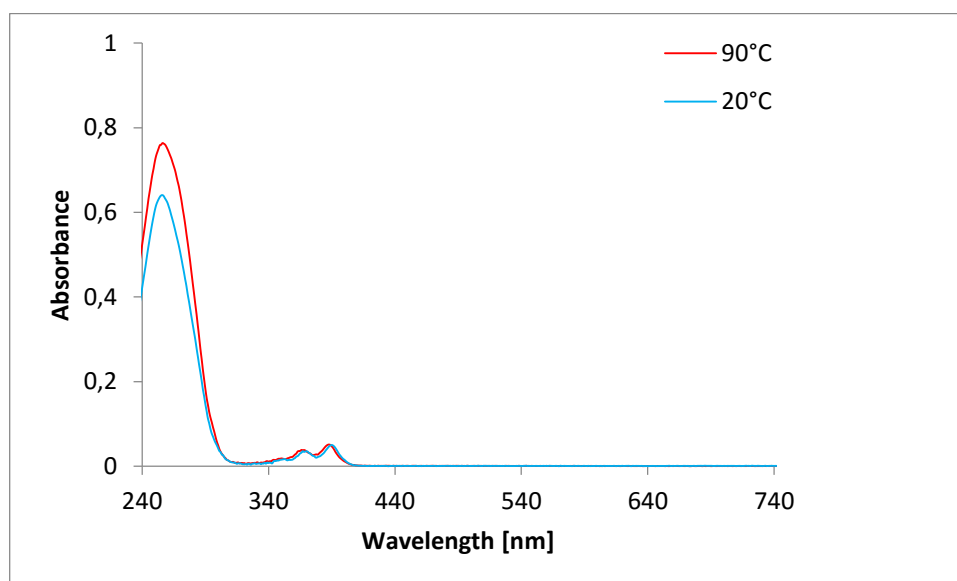


Fig. A5.30: Temperature-dependent UV/Vis spectra of **3WJ-11**.

Fluorescence spectra

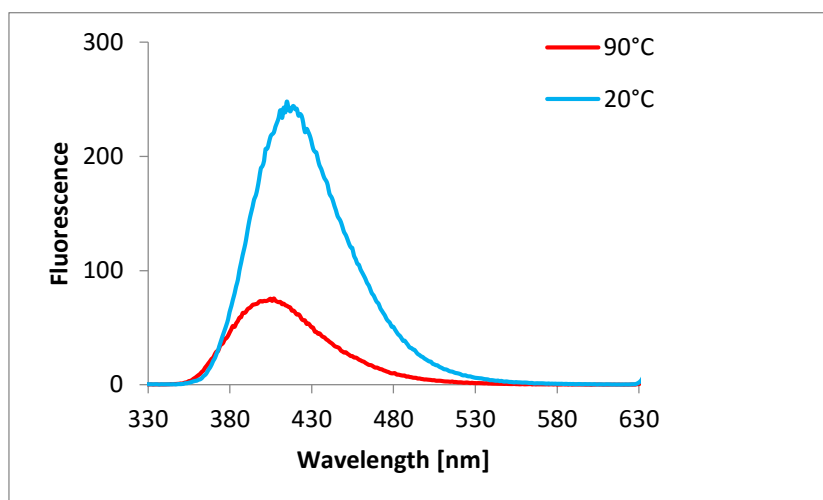


Fig. A5.31: Temperature-dependent fluorescence emission spectra (λ_{ex} : 320 nm) of **3WJ-1**. Max. Intensity for 20°C at 415 nm; Max. Intensity for 90°C at 407 nm.

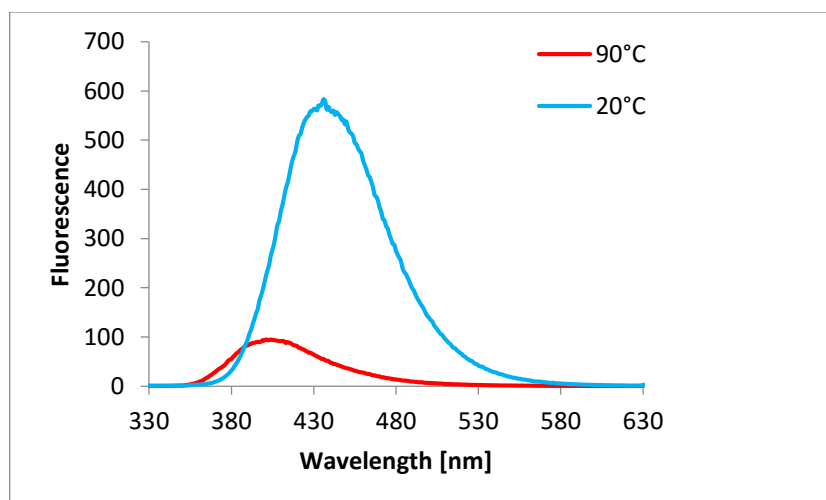


Fig. A5.32: Temperature-dependent fluorescence emission spectra (λ_{ex} : 320 nm) of **3WJ-2**. Max. Intensity for 20°C at 436 nm; Max. Intensity for 90°C at 401 nm.

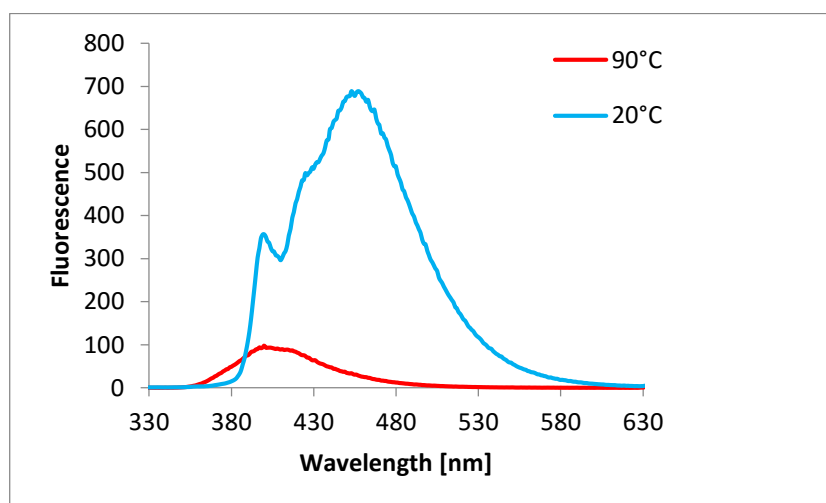


Fig. A5.33: Temperature-dependent fluorescence emission spectra (λ_{ex} : 320 nm) of **3WJ-3**.

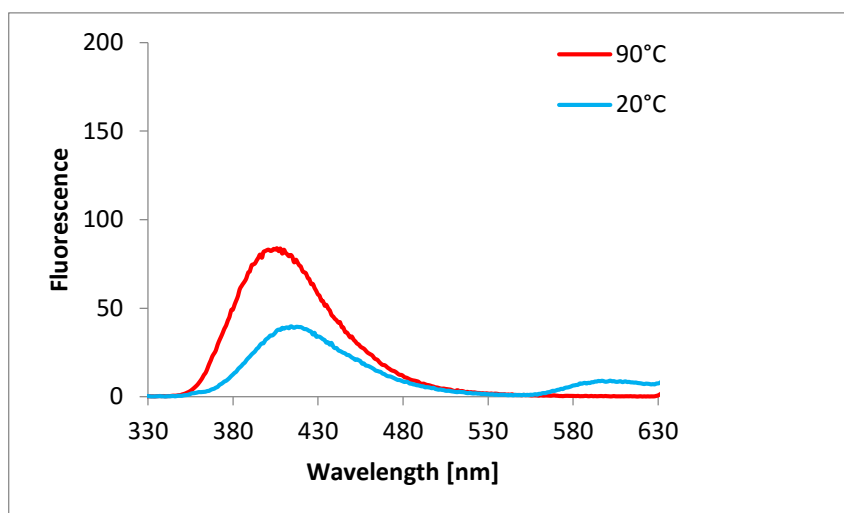


Fig. A5.34: Temperature-dependent fluorescence emission spectra (λ_{ex} : 320 nm) of **3WJ-4**.

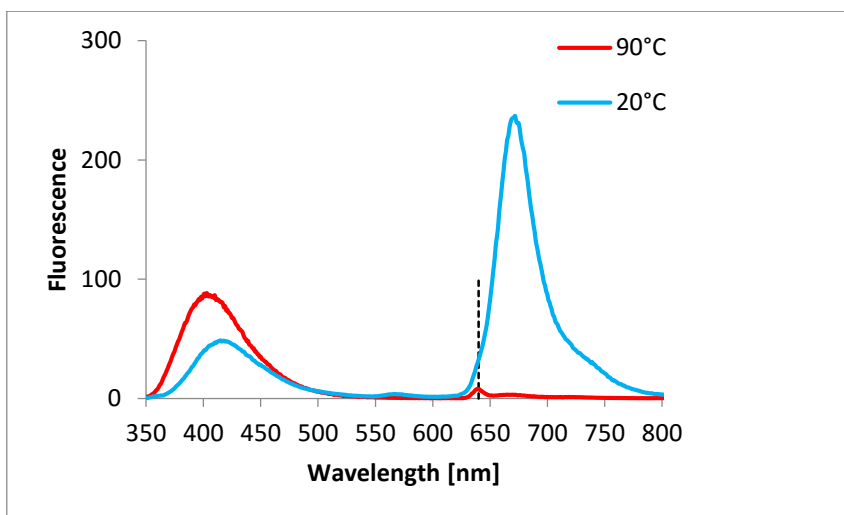


Fig. A5.35: Temperature-dependent fluorescence emission spectra (λ_{ex} : 320 nm) of **3WJ-5**.
First max. Intensity for 20°C at 415 nm; Max. Intensity for 90°C at 403 nm.

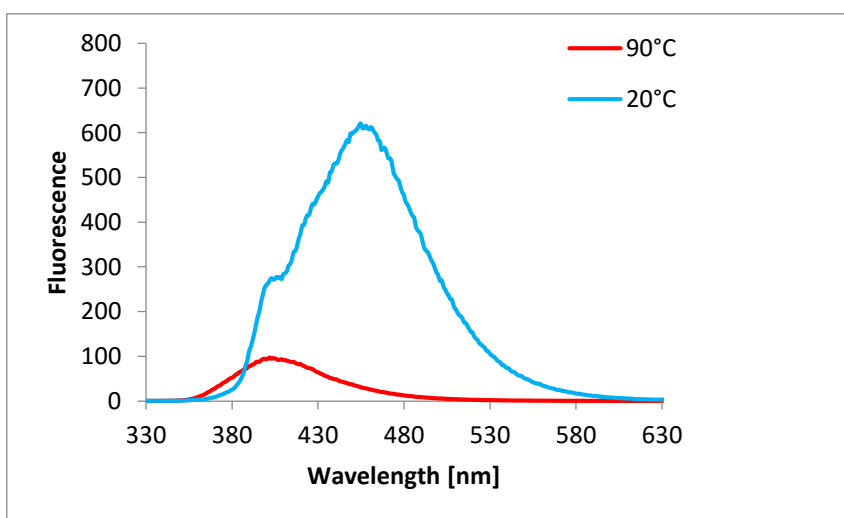


Fig. A5.36: Temperature-dependent fluorescence emission spectra (λ_{ex} : 320 nm) of **3WJ-6**.

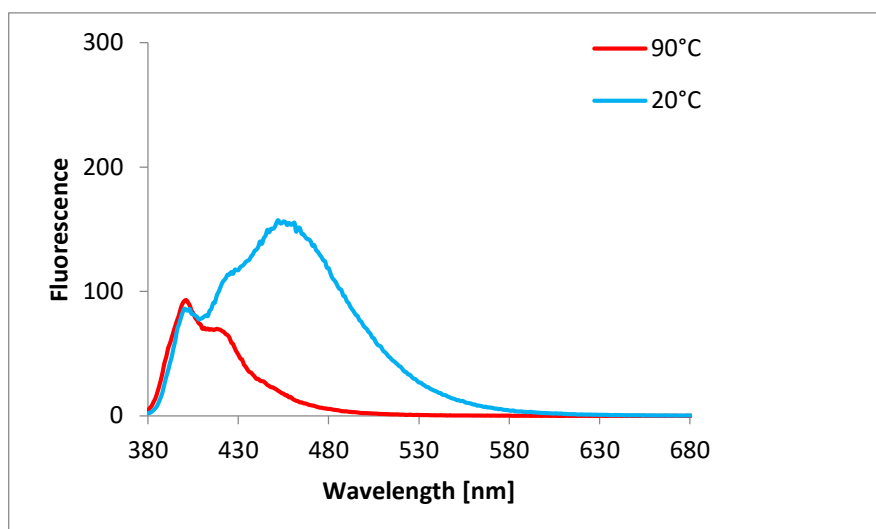


Fig. A5.37: Temperature-dependent fluorescence emission spectra (λ_{ex} : 370 nm) of **3WJ-6**.

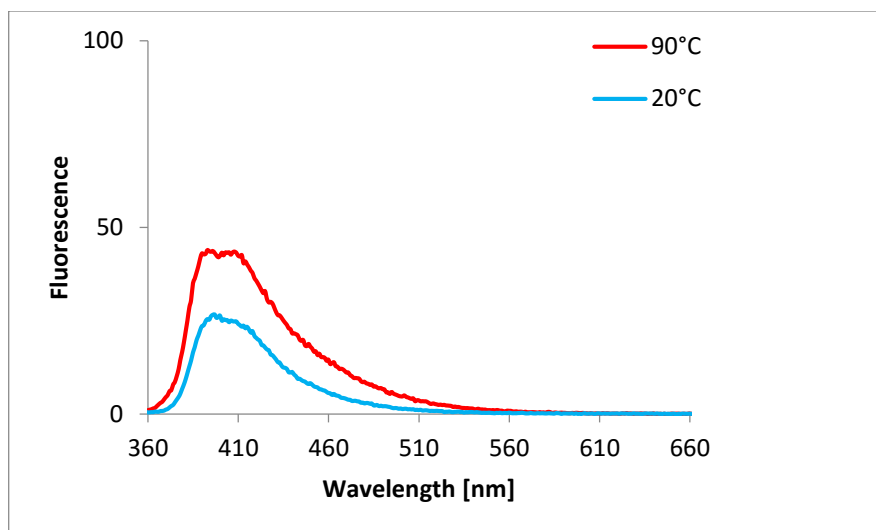


Fig. A5.38: Temperature-dependent fluorescence emission spectra (λ_{ex} : 350 nm) of **3WJ-7**.

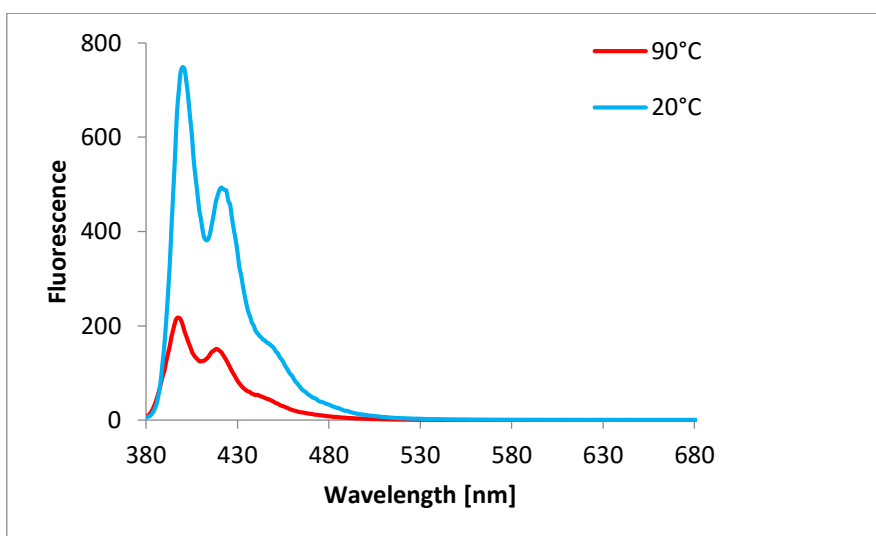


Fig. A5.39: Temperature-dependent fluorescence emission spectra (λ_{ex} : 370 nm) of **3WJ-8**.

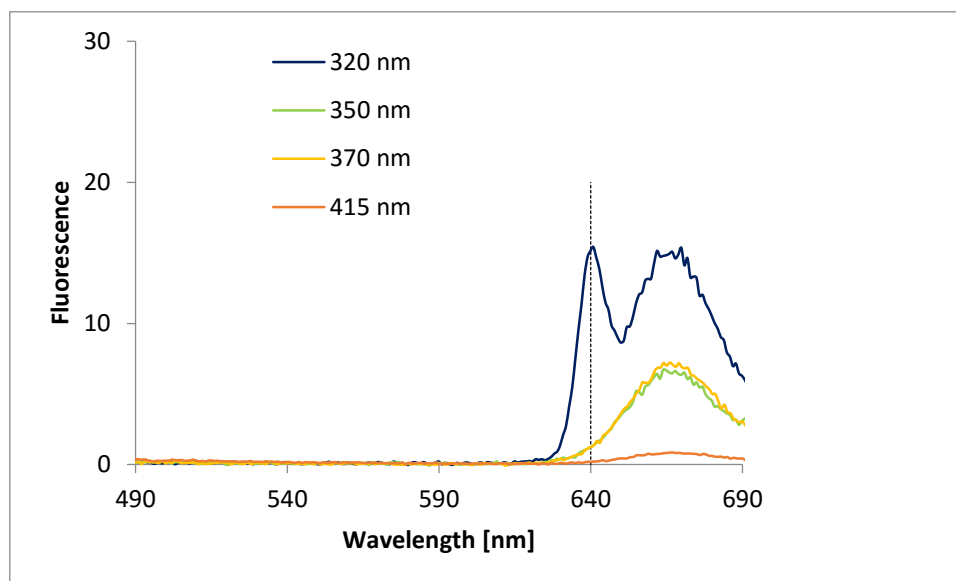


Fig. A5.40: Fluorescence emission spectra (λ_{ex} : see legend) of 3WJ-9.

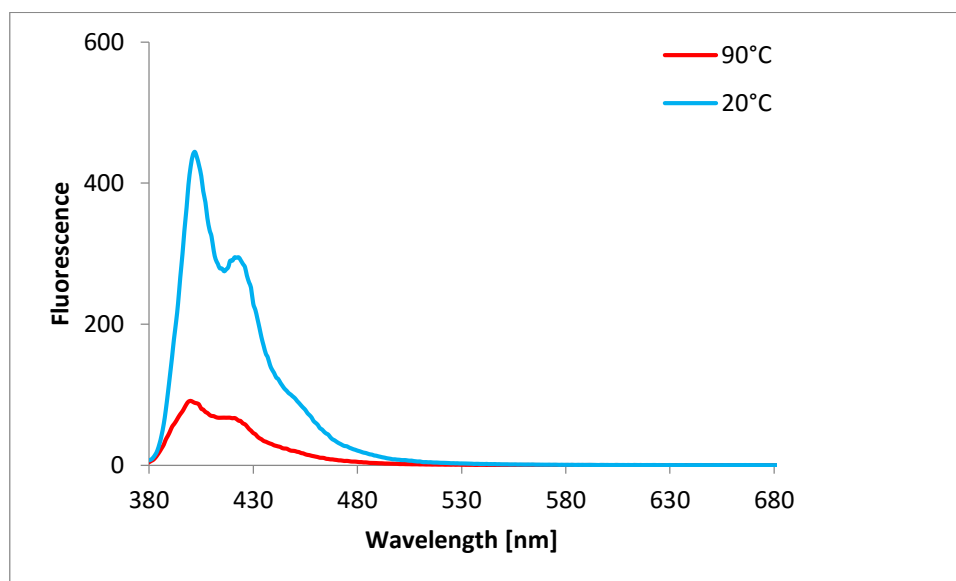


Fig. A5.41: Temperature-dependent fluorescence emission spectra (λ_{ex} : 370 nm) of 3WJ-11.

Excitation spectra

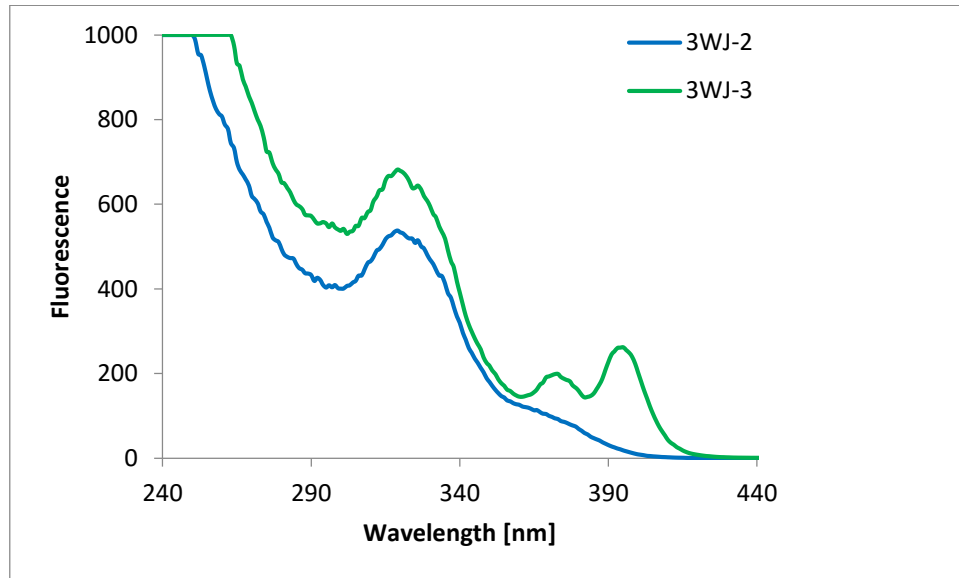


Fig. A5.42: Excitation spectra (λ_{em} : 450 nm) of **3WJ-2** and **3WJ-3**.

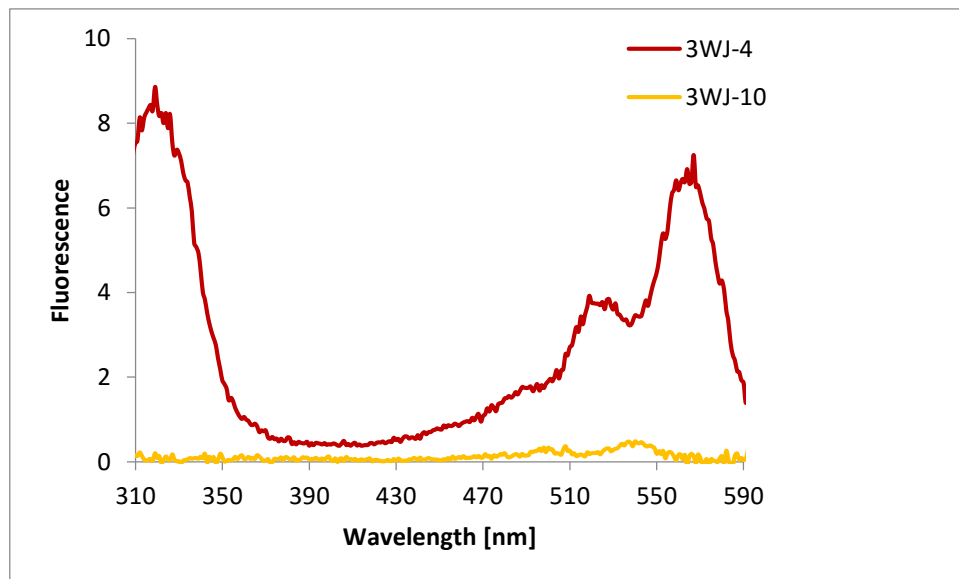


Fig. A5.43: Excitation spectra (λ_{em} : 600 nm) of **3WJ-4** and **3WJ-10**.

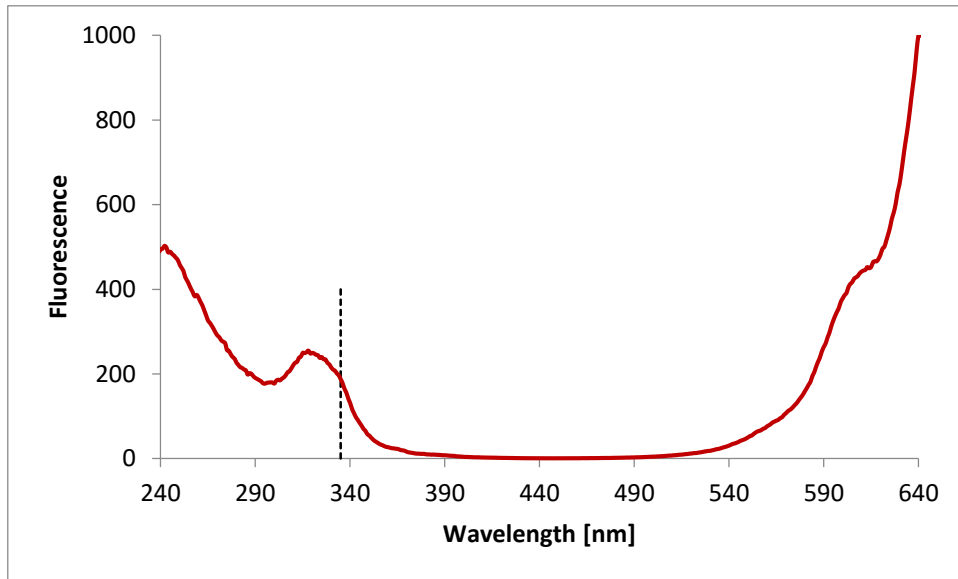


Fig. A5.44: Excitation spectra (λ_{em} : 670 nm) of 3WJ-5.

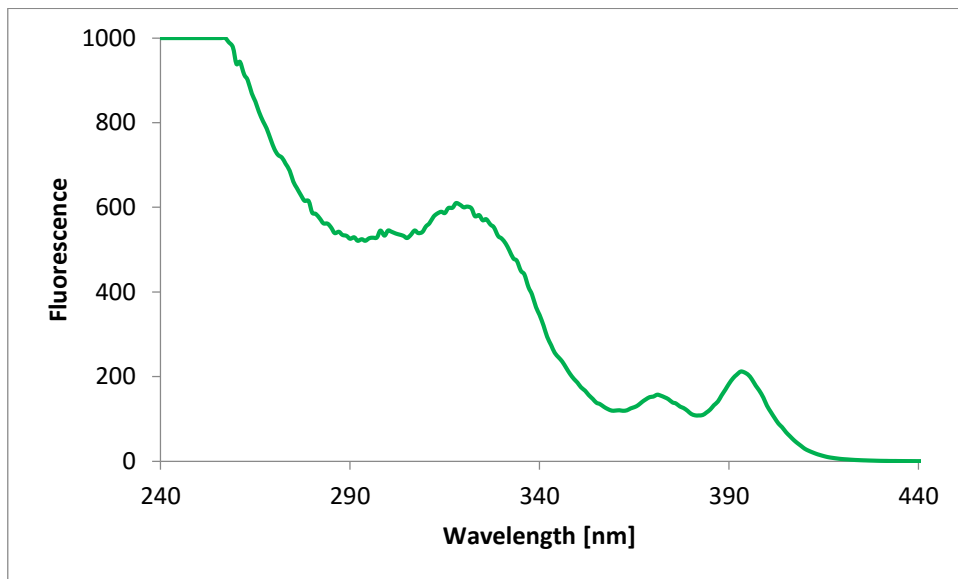


Fig. A5.45: Excitation spectra (λ_{em} : 450 nm) of 3WJ-6.

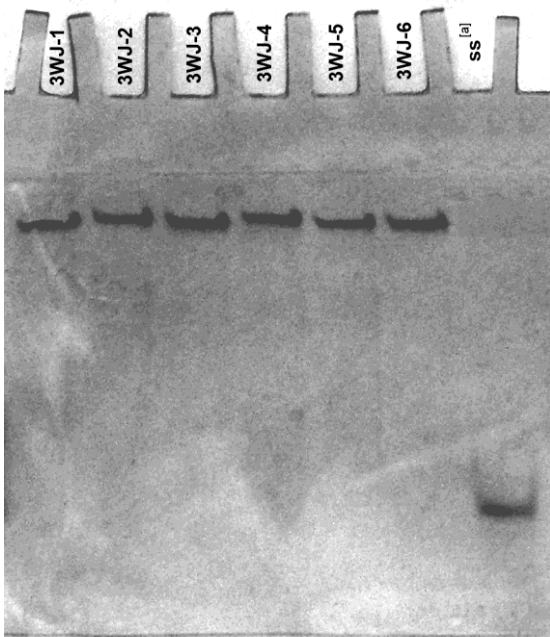
Polyacrylamide gels

Fig. A5.46: Non-denaturing polyacrylamide gel of 3WJs 1 to 6. [a] For control an unmodified single strand with the length of 20 bp and a final concentration of 3 μ M was chosen.

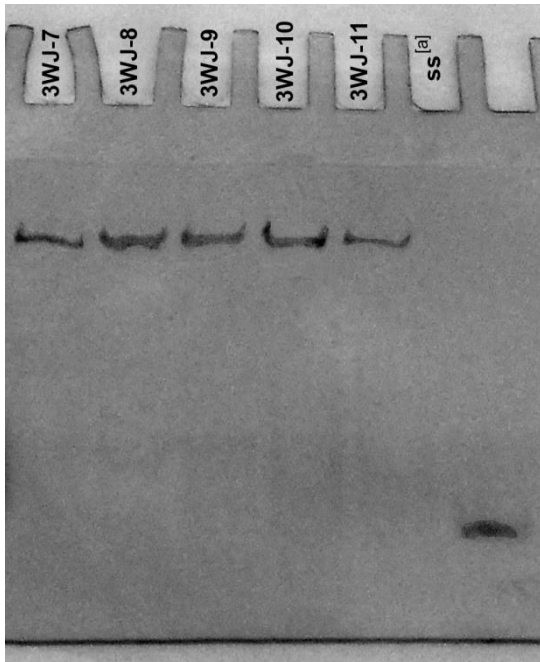


Fig. A5.47: Non-denaturing polyacrylamide gel of 3WJs 7 to 11. [a] For control an unmodified single strand with the length of 20 bp and a final concentration of 3 μ M was chosen.

Quantum yield determination

Table A5.4: Quantum yields were determined using 2-aminopyridine as standard. Area under the curve was obtained from fluorescence emission spectra (320 nm at 20°C). Same settings and conditions as for fluorescence measurements were applied. Absorption (Abs) was measured at 320 nm using the data received from UV/Vis spectra at 20°C. The values for Φ_F were calculated according to:

$$\Phi = \Phi_{\text{Ref.}} \cdot \frac{\text{Area}}{\text{Area}_{\text{Ref.}}} \cdot \frac{\text{Abs}_{\text{Ref.}}}{\text{Abs}}$$

	2-aminopyridine	3WJ-1	3WJ-2	3WJ-3	3WJ-4	3WJ-5	3WJ-6
Area:	35631	17272	45746	62858	3435	14982	56111
Abs:	0.034	0.107	0.138	0.125	0.122	0.149	0.130
Quantum yield Φ_F :	0.66 ^[1]	0.10	0.21	0.32	0.02	0.06	0.27

Table A5.5: Quantum yields were determined using Quinine sulfate as standard. Area under the curve was obtained from fluorescence emission spectra (370 nm at 20°C). Same settings and conditions as for fluorescence measurements were applied. Absorption (Abs) was measured at 370 nm using the data received from UV/Vis spectra at 20°C. Calculations: see equation above.

	quinine sulfate	3WJ-2	3WJ-3	3WJ-6
Area:	55176	8418	18981	14575
Abs:	0.087	0.019	0.043	0.034
Quantum yield Φ_F :	0.53 ^[1]	0.36	0.37	0.36

[1] *Pure Appl. Chem.*, Vol. 83, No. 12, pp. 2213–2228, 2011.

Calculation of Förster radius (phenanthrene excimer – Cy)

Calculations were done by using the protocol to calculate the Förster radius of a FRET pair (<http://www.photobiology.info/Experiments/Biolum-Expt.html>). The emission spectrum of **3WJ-1** and the absorption spectrum **3WJ-9** were used for the calculations.

Extinction coefficient acceptor at λ_{\max} ($M^{-1}cm^{-1}$)
250000

Dipole orientation factor (-)
0.666666

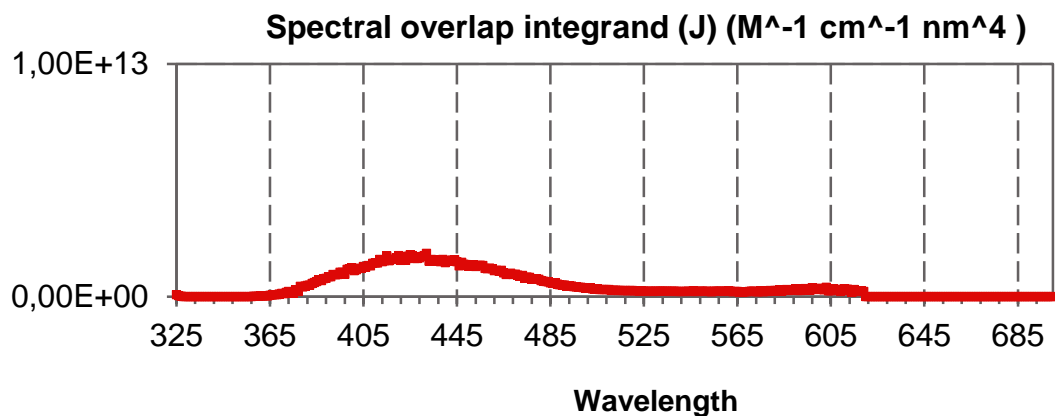
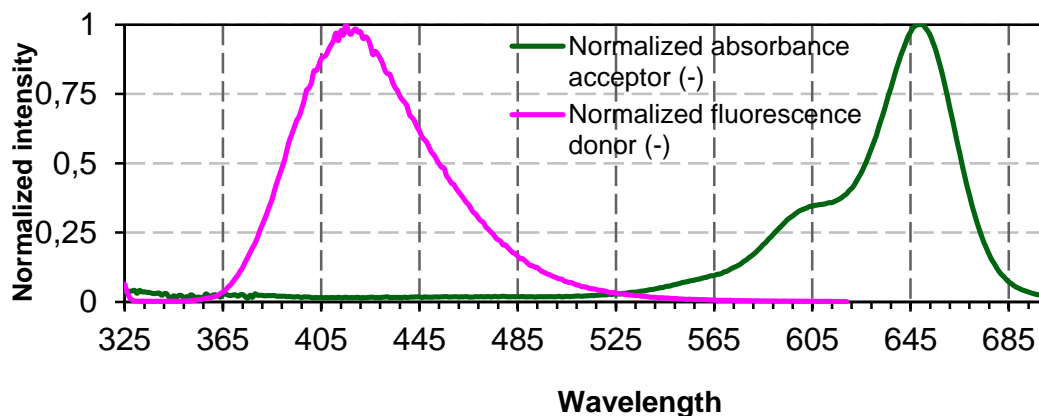
Refractive index medium
1.33

Quantum yield donor
0.1

Cumulative normalization factor ($\int F_{\text{donor}}(\lambda) d\lambda$)
69.72

Spectral overlap integral J ($M^{-1} cm^{-1} nm^4$)
1.70E+14

Calculated critical distance R_0 (Å)
26.12



Appendix C

Synthetic and analytical procedure

The synthesis of the building blocks is described: **α** (alkynylphenanthrene),^[1] **E** (perylene-diimide, PDI),^[2] **Cy3** and **Cy5** (commercially available, see below).

Oligonucleotide-synthesis was performed by an automated oligonucleotide synthesis on a 394-DNA/RNA synthesizer (*Applied Biosystems*), based on phosphoramidite chemistry. The building blocks were synthesized and incorporated according to previously described protocols (see above). Cleavage from the solid support and final deprotection was done by an overnight treatment with 30% NH₄OH solution at 55°C. The Cy-phosphoramidites were obtained from *GlenResearch* (Sterling, USA), incorporation, cleavage and deprotection followed the *UltraMILD* procedure (*GlenResearch*). All unmodified strands were commercially obtained from *Microsynth* (Balgach, Switzerland).

Reversed-phase HPLC purification of the modified oligonucleotides was carried out on a LC-10ADvp system (*Shimadzu*, Kyoto, Japan) using a LiChrospher 100 RP18, 5 μm column (*Dr. Maisch GmbH*, Ammerbuch, Germany) and a gradient consisting of eluent A (0.1 M triethylamine / acetic acid) and B (acetonitrile) with 5-50% B within 20 minutes. The temperature of the column was set to 40°C in a CTO-10ASvp oven (*Shimadzu*).

Molecular mass of the synthesized oligonucleotides was determined by LC-MS (NSI neg) on a LTQ Orbitrap XL with nano ESI (*Thermo*).

UV-Vis spectra were collected on a Varian Cary-100 Bio-UV / Visible spectrophotometer or a Varian Cary 300 Scan UV-Visible Spectrophotometer equipped with a Varian Cary-block temperature controller, 1 cm quartz cuvettes and processed with Varian WinUV software. Experiments were performed with samples prepared from 1 μM single strand concentration in *Milli-Q* H₂O containing 100 mM NaCl and 10 mM sodium phosphate buffer (pH 7.0).

Thermal denaturation curves were recorded on the same device (same conditions), the absorption at 260 nm was monitored for three ramps (cooling-heating-cooling cycles in the temperature range of 20°C – 90°C; gradient of 0.5°C/min).

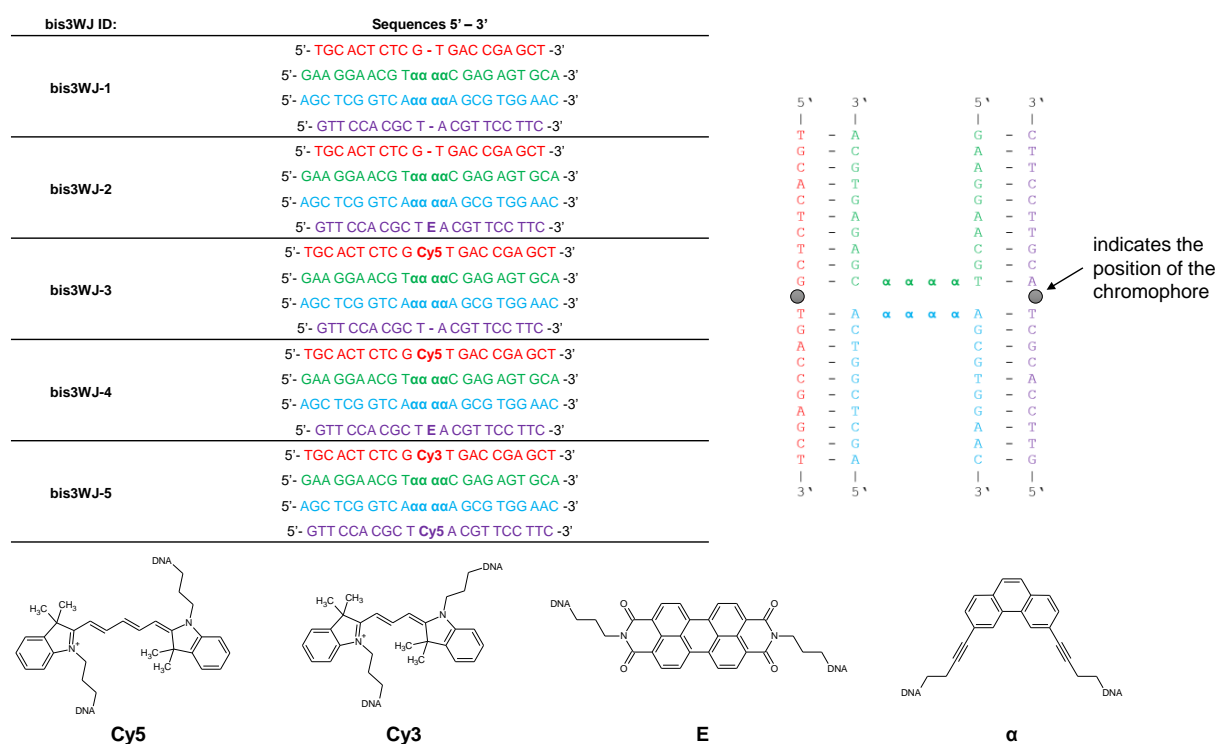
[1] C. B. Winiger, S. Li, G. R. Kumar, S. M. Langenegger, R. Häner. *Angew. Chem. Int. Ed.*, **2014**, 53, 13609-13613.

[2] N. Rahe, C. Rinn and T. Carell. *Chem. Commun.*, **2003**, 2119–2121.

Fluorescence spectra were acquired on a Varian Cary Eclipse fluorescence spectrophotometer equipped with a Varian Cary-block temperature controller with 1 cm x 1 cm quartz cuvettes and Varian Eclipse software. Instrumental setups for fluorescence emission spectra were: λ_{ex} according to description in the corresponding figure; excitation slit width: 5 nm; emission slit width: 5 nm; PMT voltage: 600 V. Samples treated as mentioned above.

Polyacrylamide gel electrophoresis (PAGE) was performed using a 20% gel. 12 μ L of each sample mixture (final concentration of 4 μ M per single strand; 10% glycerol; 90 mM Tris-borate buffer, pH 8.0; 0.01% (w/v) Orange G dye) were loaded onto the gel. The gel ran for 1h 50min in a closed chamber at 4°C (180V / 30mA / 5W). Staining was done with Stains-all reagent dissolved in a buffered formamide solution.

Overview three-way junctions



Scheme A6.1. Overview of all the bis3WJs, the sequences and the non-nucleosidic building blocks.

UV/Vis spectra

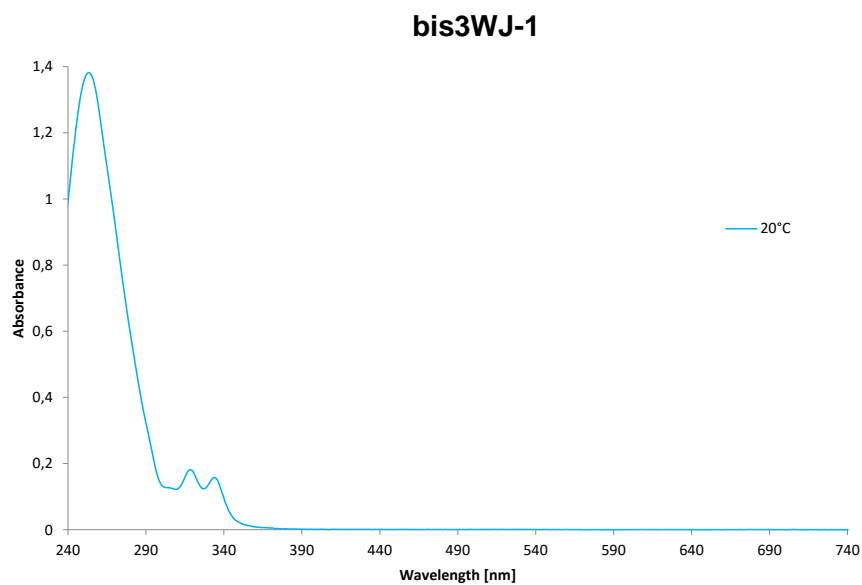


Fig. A6.1. UV/Vis spectrum of **bis3WJ-1** at 20°C. Conditions: see above.

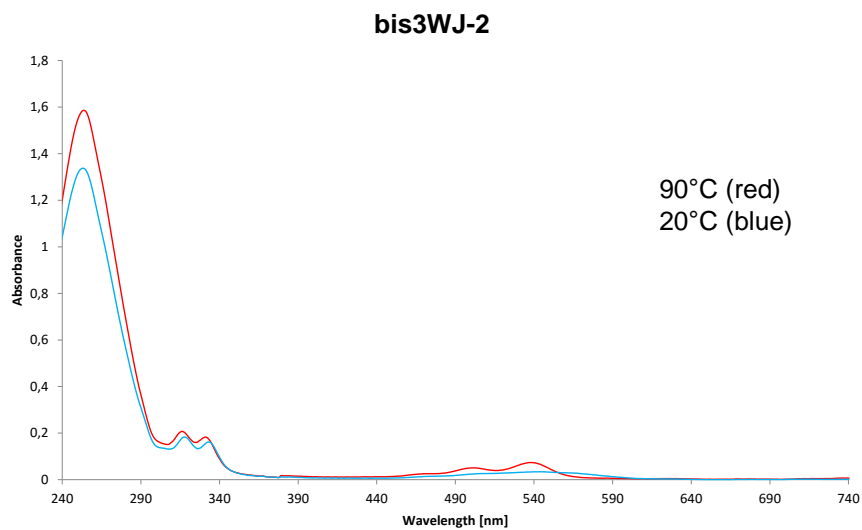


Fig. A6.2. UV/Vis spectra of **bis3WJ-2**. Conditions: see above.

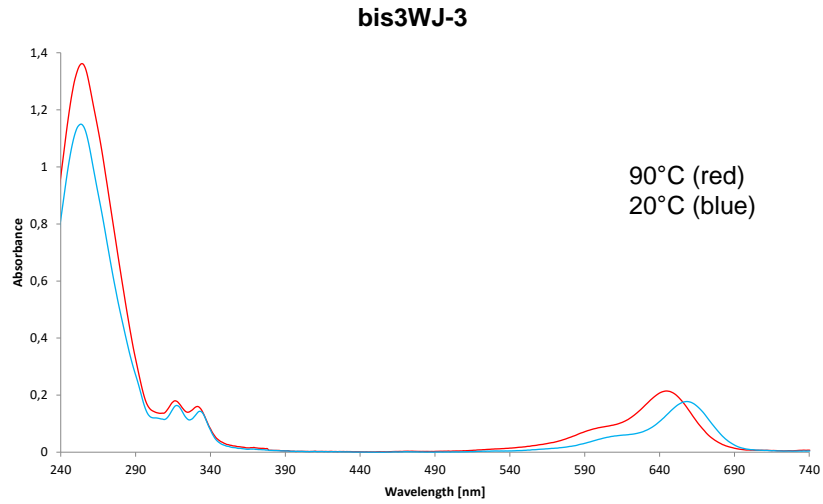


Fig. A6.3. UV/Vis spectra of **bis3WJ-3**. Conditions: see above.

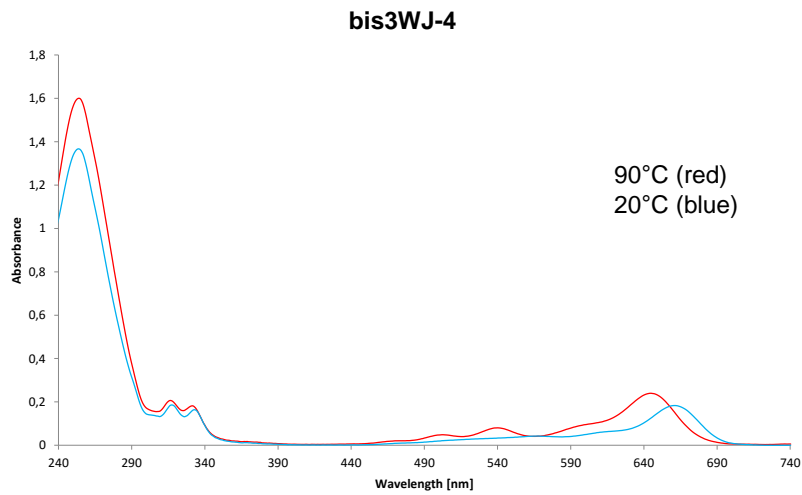


Fig. A6.4. UV/Vis spectra of **bis3WJ-4**. Conditions: see above.

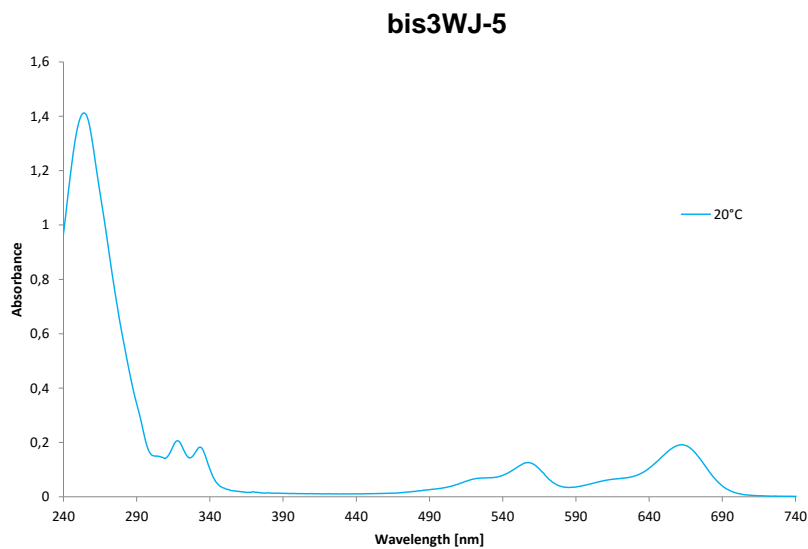


Fig. A6.5. UV/Vis spectrum of **bis3WJ-5** at 20°C. Conditions: see above.

Fluorescence spectra

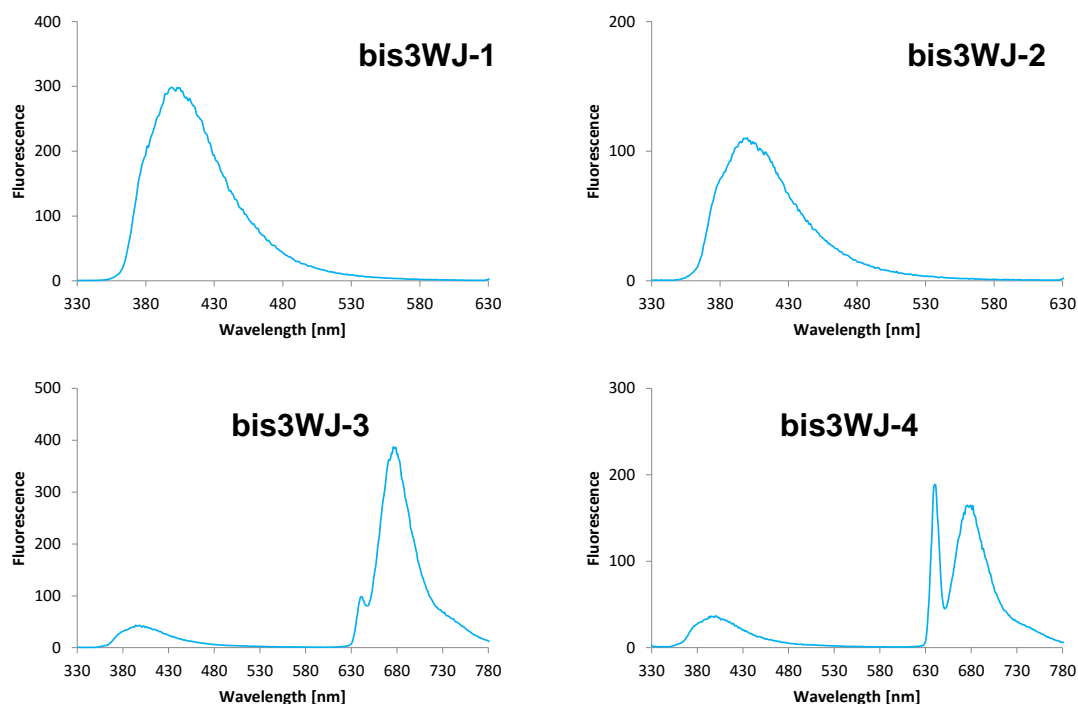


Fig. A6.6. Fluorescence spectra of **bis3WJ-1** to **bis3WJ-4** at 20°C and an excitation wavelength of 320 nm. Other conditions / instrumental set-up: see above. Sharp peak at 640 nm (in spectra of **bis3WJ-3** and **bis3WJ-4**) indicates artefacts caused by the second order transmission of the monochromator.

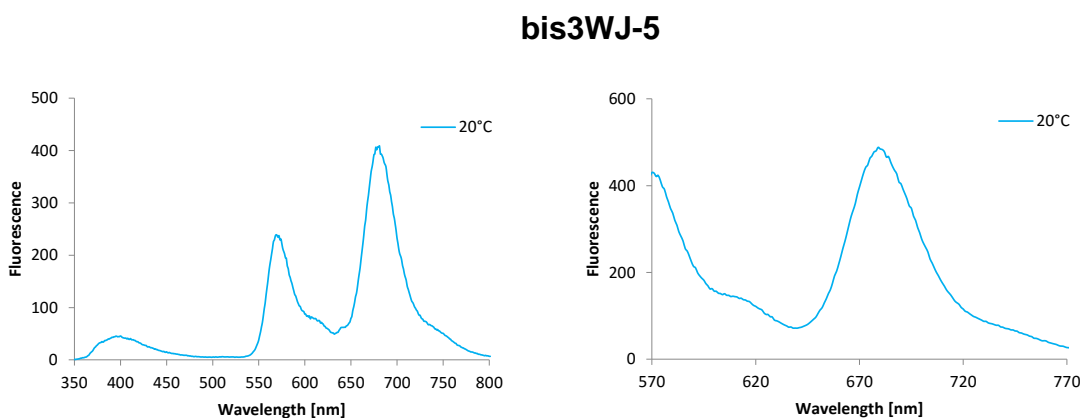


Fig. A6.7. Fluorescence spectra of **bis3WJ-5** at 20°C and an excitation wavelength of 320 nm (left) and 560 nm (right). Other conditions / instrumental set-up: see above.

T_m values and thermal denaturation profiles

Thermal denaturation profiles (Ramp1: 90°C → 20°C, Ramp2: 20°C → 90°C and Ramp3: 90°C → 20°C):

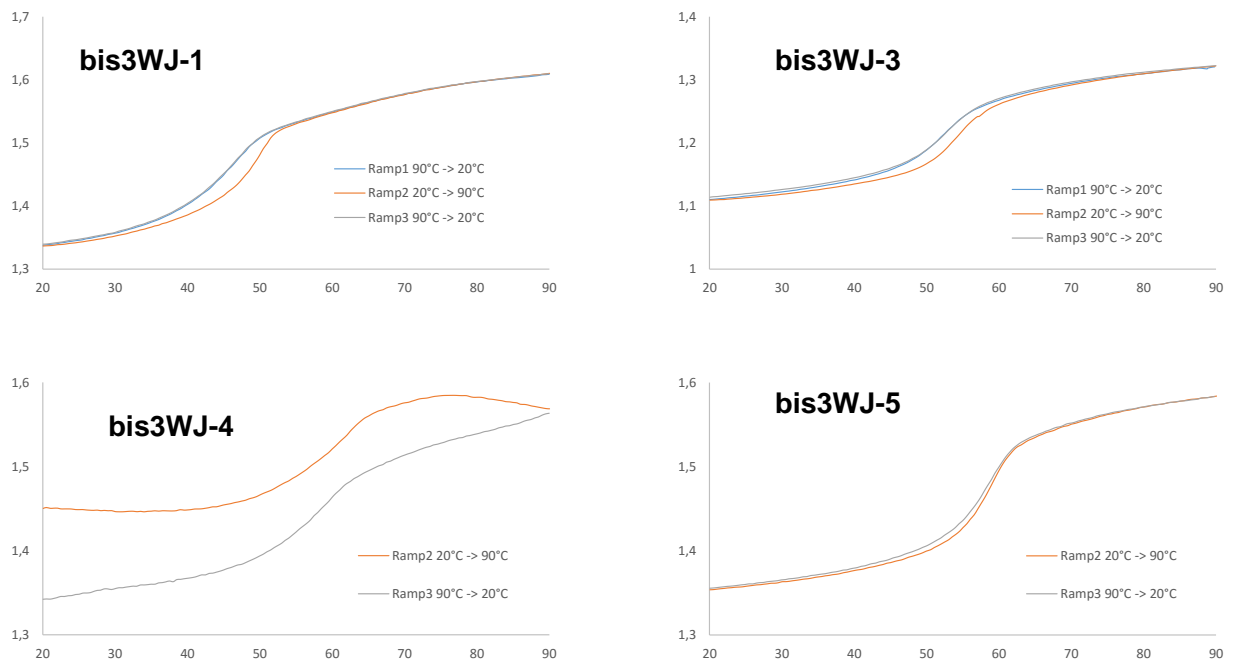


Fig. A6.8. Melting profiles of **bis3WJ-1**, **bis3WJ-3** to **bis3WJ-5**. The following melting temperatures were determined: for **bis3WJ-1**: 48°C; **bis3WJ-3**: 52°C; **bis3WJ-4**: 61°C; **bis3WJ-5**: 59°C.

Polyacrylamide gels

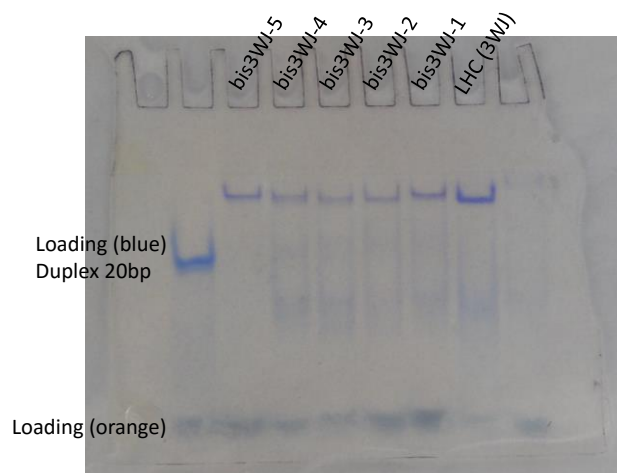


Fig. A6.9. Non-denaturing polyacrylamide gel of **bis3WJ-1** to **bis3WJ-5**. As a control a DNA duplex (20bp) was chosen and a modified DNA 3WJ (LHC from Chapter 5) for comparison.

Erklärung

Erklärung

gemäss Art. 28 Abs. 2 RSL 05

Name/Vorname: **Probst Markus**
.....

Matrikelnummer: **05-122-874**
.....

Studiengang: **Chemie und Molekulare Wissenschaften**
.....

Bachelor Master Dissertation

Titel der Arbeit: **Functional and Structural Studies of DNA**
Assembled Oligochromophores.
.....
.....

LeiterIn der Arbeit: **Prof. Dr. Robert Häner**
.....
.....

Ich erkläre hiermit, dass ich diese Arbeit selbständig verfasst und keine anderen als die angegebenen Quellen benutzt habe. Alle Stellen, die wörtlich oder sinngemäss aus Quellen entnommen wurden, habe ich als solche gekennzeichnet. Mir ist bekannt, dass andernfalls der Senat gemäss Artikel 36 Absatz 1 Buchstabe o des Gesetzes vom 5. September 1996 über die Universität zum Entzug des auf Grund dieser Arbeit verliehenen Titels berechtigt ist.

Bern, 01. April 2016
.....

Ort/Datum

.....
Unterschrift

Lebenslauf

Persönliche Angaben:

Markus Probst,

geboren am **14.06.1985**

mit Heimatort Langnau i.E.

Studium und Ausbildung:

- 2012 – 2016** ***Doktorat Chemie und Molekulare Wissenschaften,***

Universität Bern.

Titel der Arbeit: „Functional and Structural Studies of DNA Assembled Oligochromophores“, Leiter der Arbeit: Prof. Dr. R. Häner.
- 2010 – 2012** ***Masterstudium „Biochemistry and Chemical Biology“,***

Universität Bern.

Titel der Masterarbeit: “The DNA three-way junction as a mould for tripartite chromophore assembly“, Leiter der Arbeit: Prof. Dr. R. Häner.
- 2006 – 2010** ***Bachelorstudium „Biochemistry and Molecular Biology“,*** Universität Bern.

Titel der Bachelorarbeit: “Changing the substrate specificity of alpha-TTP by model-inspired site-directed mutagenesis“, Leiter der Arbeit: Prof. Dr. A. Stocker.
- 2001 – 2004** Eidgenössische Maturität am Gymnasium Langenthal mit Schwerpunktfach Biologie und Chemie.

Publikationen:

Probst Markus, Aeschimann Walter, Chau Thi-Thu-Hang, Langenegger Simon Matthias, Stocker Achim and Häner Robert. „Crystal structure of pyrene- and phenanthrene-modified DNA in complex with the BpuJ1 endonuclease binding domain“, *Nucleic Acids Research*, **2016**, script in preparation.

O. Khorev, C. Bösch, M. Probst, R. Häner. „Observation of the Rare Chrysenone Excimer“, *Chem. Sci.*, **2014**, 5, 1506 – 1512.

M. Probst, S. M. Langenegger, R. Häner. „A modular LHC built on the DNA three-way junction“, *Chem. Commun.*, **2014**, 50, 159 – 161.

M. Probst, D. Wenger, S. M. Biner and R. Häner. „The DNA three-way junction as a mould for tripartite chromophore assembly“, *Organic & Biomolecular Chemistry*, **2012**, 10, 755 – 759.